



EUMETSAT

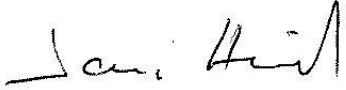
AC SAF

**ATMOSPHERIC COMPOSITION
MONITORING**

OPERATIONS REPORT

Issue 1/2025 rev. 1

Reporting period: January – June 2025

Authors			
Prepared by			
NAME	INSTITUTE		
Jari Hovila	FMI		
Contributions			
NAME	INSTITUTE		
Jari Hovila, Jukka Kujanpää, Kaisa Lakkala	FMI		
Axel Schmidt, Matthias Hofmann, Birgit Wunschheim	DLR		
Olaf Tuinder, Robert van Versendaal	KNMI		
Helge Jønych-Sørensen	DMI		
Katerina Garane, MariLiza Koukouli, Konstantinos Michailidis	AUTH		
Jeroen van Gent, José Granville, Jean-Christopher Lambert, Bavo Langerock, Gaia Pardini, Tijn Verhoelst	BIRA-IASB		
Andy Delcloo	KMI		
Peggy Tesche-Achtert	DWD		
Anne Boynard, Cathy Clerbaux, Maya George, Camille Viatte	LATMOS		
Rosa Astoreca, Pierre-François Coheur, Daniel Hurtmans, Catherine Wespes	ULB		
Carlos Vicente	EUMETSAT		
Approved by			
AC SAF Technical Manager	Jari Hovila / FMI	26/11/2025	 <i>Signature</i>



EUMETSAT

ACSAF

REFERENCE: **SAF/AC/FMI/OPS/RP/001**

ISSUE: 1/2025 rev. 1

DATE: 26/11/2025

PAGES: 168

Document change log

Revision	Date	Description of change
1	26/11/2025	Initial revision

List of abbreviations

AC SAF	Satellite Application Facility on Atmospheric Composition Monitoring
ARP	Absorbing Aerosol Index from PMDs data product
ARP-A	Absorbing Aerosol Index from PMDs data product from Metop-A
ARP-B	Absorbing Aerosol Index from PMDs data product from Metop-B
ARP-C	Absorbing Aerosol Index from PMDs data product from Metop-C
ARS	Absorbing Aerosol Height data product
ARS-A	Absorbing Aerosol Height data product from Metop-A
ARS-B	Absorbing Aerosol Height data product from Metop-B
ARS-C	Absorbing Aerosol Height data product from Metop-C
ATMOS	Atmospheric Parameters Measured by in-Orbit Spectroscopy (DLR data service)
ATO	Assimilated Total Ozone
AUTH	Aristotle University of Thessaloniki
BIRA-IASB	Belgian Institute for Space Aeronomy
BrO	Bromine Oxide
CDOP	Continuous Development and Operations phase
CDR	Climate Data Record
CO	Carbon Monoxide
DLR	German Aerospace Center
DMI	Danish Meteorological Institute
DWD	German Weather Service
ECMWF	European Centre for Medium-Range Weather Forecasts
EDC	EUMETSAT Data Centre
EDD	Erythemat Daily Dose
EUMETCast	EUMETSAT's primary dissemination mechanism for the near real-time delivery of satellite data and products
EUMETSAT	European Organisation for the Exploitation of Meteorological Satellites
FMI	Finnish Meteorological Institute
GOME	Global Ozone Monitoring Experiment
H ₂ O	Water Vapour
HCHO	Formaldehyde
HNO ₃	Nitric acid
HR	High resolution
KMI	Royal Meteorological Institute of Belgium
KNMI	Royal Netherlands Meteorological Institute
L1b	Level 1b data product
L1c	Level 1c data product
L2	Level 2 data product
L3	Level 3 data product



LATMOS	Laboratoire Atmosphères, Milieux, Observations Spatiales
LER	Lambertian-equivalent reflectivity data record
NHP	Near Real-time High-resolution Ozone Profile data product
NO2	Nitrogen Dioxide
NRT	Near Real-time
NTO	Near Real-time Total Column data product
NUV	Near Real-time UV index data product
O3	Ozone
O3M SAF	Satellite Application Facility on Ozone and Atmospheric Chemistry Monitoring
OHP	Offline High-resolution Ozone Profile data product
OHP-A	Offline High-resolution Ozone Profile data product from Metop-A
OHP-B	Offline High-resolution Ozone Profile data product from Metop-B
OHP-C	Offline High-resolution Ozone Profile data product from Metop-C
OEM	Optimal Estimation Method
OPERA	Ozone Profile Retrieval Algorithm
OTO	Offline Total Column data product
OUV	Offline Surface UV data product
OUV-A	Offline Surface UV data product from Metop-A
OUV-AB	Offline Surface UV data product from Metop-A and Metop-B
OUV-B	Offline Surface UV data product from Metop-B
OUV-BC	Offline Surface UV data product from Metop-B and Metop-C
PDU	Product Dissemination Unit
PGE	Product Generation Element
PMD	Polarisation Measurement Device
RD	Reference Document
RMS	Root Mean Square
RMSE	Root Mean Square Error
SACS	Support to Aviation Control Service
SCD	Slant Column Density
SO2	Sulphur Dioxide
TOC	Total Ozone Column data product
TrOC	Global Tropospheric Ozone Column data product
TTrOC	Tropical Tropospheric Ozone Column data product
ULB	Université libre de Bruxelles
UTC	Coordinated Universal Time

TABLE OF CONTENTS

1.	INTRODUCTION	8
1.1.	Scope	8
1.2.	Reporting period	8
1.2.1.	<i>Highlights</i>	8
1.3.	Reference documents	8
1.4.	Definition of terms	11
1.5.	Accuracy requirements of AC SAF products	12
2.	PROCESSING CENTRE: FMI	19
2.1.	Offline surface UV radiation	19
2.1.1.	<i>Availability</i>	19
2.1.2.	<i>Timeliness</i>	19
2.2.	Services, main events and anomalies	20
3.	PROCESSING CENTRE: DLR	23
3.1.	NRT and offline total/tropospheric trace gas columns, tropical tropospheric ozone	23
3.1.1.	<i>Availability</i>	23
3.1.2.	<i>Timeliness</i>	25
3.2.	Services, main events and anomalies	27
4.	PROCESSING CENTRE: KNMI	29
4.1.	NRT and offline ozone profiles, absorbing aerosol height and index, global tropospheric ozone	29
4.1.1.	<i>Availability</i>	29
4.1.2.	<i>Timeliness</i>	30
4.2.	Services, main events and anomalies	32
5.	PROCESSING CENTRE: DMI	34
5.1.	NRT clear-sky and cloud-corrected UV index / Global 1-day UV index forecast	34
5.1.1.	<i>Availability</i>	34
5.1.2.	<i>Timeliness</i>	34
5.2.	Services, main events and anomalies	35
6.	PROCESSING CENTRE: EUMETSAT	37
6.1.	NRT IASI CO, SO ₂ , HNO ₃ and ozone profile	37
6.1.1.	<i>Availability</i>	37
6.1.2.	<i>Timeliness</i>	38
6.2.	Services, main events and anomalies	39
7.	VALIDATION AND QUALITY MONITORING	41
7.1.	GOME-2 total ozone column products	41
7.1.1.	<i>Total ozone column validation</i>	41
7.1.2.	<i>Validation website</i>	47
7.1.3.	<i>Online quality monitoring</i>	49
7.2.	GOME-2 tropospheric ozone products	50
7.3.	GOME-2 trace gas products	53
7.3.1.	<i>Online quality monitoring</i>	78
7.4.	GOME-2 ozone profile products	82
7.4.1.	<i>Online quality monitoring</i>	85
7.5.	GOME-2 aerosol products	87
7.5.1.	<i>Online quality monitoring</i>	91
7.6.	GOME-2 UV products	92

7.6.1.	Online quality monitoring.....	92
7.7.	IASI NRT products.....	94
8.	LIST OF AC SAF USERS.....	121
8.1.	FMI archive	121
8.2.	DLR archive	134
8.3.	DMI (NUV product via FTP)	145
8.4.	KNMI (unofficial NRT AAI via FTP).....	145
8.5.	Known international projects that use EUMETCast or WMO/GTS	146
8.6.	EUMETCast	147
9.	UPDATES DURING THE REPORTING PERIOD.....	148
9.1.	Software updates.....	148
9.2.	Hardware updates	148
9.3.	Documentation updates	148
10.	CHANGES IN APPEARANCE AND CONTENT OF THE WEB PORTAL.....	149
	APPENDIX 1.....	150
	APPENDIX 2.....	168

1. Introduction

1.1. Scope

The scope of this document is to summarise the operational activities concerning the products in operation and the associated services during the reporting period to see that the general requirements applicable to these services and products of the AC SAF [RD1, RD2, RD3] are fulfilled. Intended readers of this document are the members of AC SAF project team, Review Board of the annual Operations Review, AC SAF Steering Group and EUMETSAT OPS/WG as well as the users of the AC SAF products.

Operations Reports include information about product availability/timeliness, quality assurance, website usage, and delivery statistics. Main events, major anomalies and software/hardware updates are reported also. AC SAF Operations Report is published twice a year.

1.2. Reporting period

This Operations Report covers the period January – June 2025.

1.2.1. Highlights

New products

- 5 February: Demonstrational daily IASI dust optical depth product available
- 14 March: LER v4.1 released
- 6 May: Global 1-day UV index forecast replaced NUV products

1.3. Reference documents

Table 1.1. Operations Report reference documents

Reference	Title	Issued	Reporting period
RD1	Product Requirements Document (SAF/AC/FMI/RQ/PRD/001)	20/12/2023	N/A
RD2	Service Specification (SAF/AC/FMI/RQ/SESP/001)	26/02/2025	N/A
RD3	EUMETSAT Operational Services Specification (EUM/OPS/SPE/20/109969)	16/02/2023	N/A
RD4	O3M SAF Validation Report for NRT, offline and reprocessed total ozone columns	11/12/2015	January 2007 – December 2014
RD5	AC SAF Validation Report for NRT, offline, reprocessed and level 3 total/tropospheric NO ₂ columns	10/11/2017	Metop-A: January 2007 – July 2015 Metop-B: January 2013 – July 2015

Reference	Title	Issued	Reporting period
RD6	O3M SAF Validation Report for Metop-A NRT and offline coarse/high-resolution ozone profiles	20/02/2012	January 2007 – May 2011
RD7	O3M SAF Validation Report for Metop-B NRT and offline coarse/high-resolution ozone profiles	30/06/2013	December 2012 – April 2013
RD8	AC SAF Validation Report for Global 1-day UV Index Forecast	07/02/2025	January 2016 – December 2019
RD9	O3M SAF Validation Report for NRT, offline and reprocessed total SO ₂ columns	09/12/2015	January 2007 – December 2014
RD10	O3M SAF Validation Report for offline and reprocessed total BrO columns	09/12/2015	January 2007 – December 2014
RD11	O3M SAF Validation Report for NRT, offline and reprocessed total HCHO columns	30/10/2015	January 2007 – July 2015
RD12	O3M SAF Validation Report for offline and reprocessed total H ₂ O columns	30/10/2015	January 2007 – August 2015
RD13	O3M SAF Validation Report for NRT and offline aerosol products	25/06/2013	January 2007 – May 2013
RD14	O3M SAF Validation Report for Metop-B offline UV products	03/02/2015	June 2012 – May 2013
RD15	AC SAF Validation Report for GOME-2 surface LER product	27/03/2019	MSC: February 2007 – June 2018 PMD: April 2008 – June 2018
RD16	O3M SAF Validation Report for offline tropospheric ozone columns (cloud slicing)	03/07/2015	January 2007 – December 2014
RD17	O3M SAF Validation Report for NRT and offline tropospheric ozone columns (ozone profiles)	09/09/2015	January 2007 – December 2014
RD18	O3M SAF Validation Report for NRT IASI CO	17/11/2015	September 2015 – November 2015
RD19	AC SAF Validation Report for NRT IASI SO ₂	17/11/2017	Metop-A: January 2007 – December 2013 June 2017 – October 2017 Metop-B: June 2017 – December 2017

Reference	Title	Issued	Reporting period
RD20	AC SAF Validation Report for Metop-C offline tropical tropospheric ozone columns	05/06/2020	February – December 2019
RD21	AC SAF Validation Report for Metop-C NRT and offline global tropospheric ozone columns	05/06/2020	February – December 2019
RD22	AC SAF Validation Report for Metop-C NRT and offline high-resolution ozone profiles	05/06/2020	February – December 2019
RD23	AC SAF Validation Report for Metop-C NRT and offline total ozone columns	25/05/2020	February – July 2019
RD24	AC SAF Validation Report for Metop-C NRT and offline total/tropospheric nitrogen dioxide columns	25/11/2019	February – July 2019
RD25	AC SAF Validation Report for Metop-C NRT and offline total formaldehyde columns	19/05/2020	February – July 2019
RD26	AC SAF Validation Report for Metop-C offline total bromine monoxide columns	19/05/2020	February – July 2019
RD27	AC SAF Validation Report for Metop-C offline total water vapour columns	30/03/2020	February – July 2019
RD28	AC SAF Validation Report for NRT, offline and reprocessed absorbing aerosol height products	03/07/2020	2007-2019
RD29	AC SAF Validation Report for Metop-C NRT and offline absorbing aerosol index from PMDs products	09/10/2019	January – October 2019
RD30	AC SAF Validation Report for Metop-C NRT and offline total sulphur dioxide products	21/01/2021	February – July 2019
RD31	AC SAF Validation Report for NRT IASI total O ₃ and O ₃ profiles	28/02/2022	December 2019 – November 2020
RD32	AC SAF Validation Report for NRT IASI HNO ₃	26/04/2022	December 2019 – December 2021

Online documents:

[Service Specification](#), [Validation Reports](#)

1.4. Definition of terms

Availability is based on the definition in the EUMETSAT Operational Services Specification [RD3].

Product-specific clarifications:

- For NRT products, the monthly availability limit is 97.5 %. The availability is calculated as a “worst case scenario”:

$$\frac{\text{in time processed and disseminated L2 PDUs}}{\text{received L1b PDUs} + \text{missed L1b PDUs marked as “reception confirmed” in the EUMETCast sendlist}}$$

- For offline products, the monthly availability limit is 95.5 %. The availability is defined by the ratio of the number of in time processed, archived and quality-approved L2 products to the number of orbits for which L1b PDUs have been received per month.
- NUV and OUV are daily L3 products, and availability is defined as the fraction of days in a month with products fulfilling the timeliness requirements
- TTrOC is a monthly L3 product and availability is 100 % or 0 % depending on whether the product fulfills the timeliness requirement or not

Timeliness defines whether the product is near real time (NRT) product which is disseminated or ready for download in three hours from sensing at the latest or offline product which is available for download in two weeks after sensing at the latest, during system availability. System unavailability will in most cases not lead to loss of data but to delays with respect to the specified timeliness. In practice, timeliness of a product is determined by calculating the time from sensing to EUMETCast or archive upload. In the Operations Reports, the timeliness is presented as monthly average, minimum and maximum values.

Accuracy of a satellite product is defined as a comparison of the mean/median bias (absolute and/or relative differences) of the product against ground-based and/or satellite-based reference data. Precision around the accuracy is given as a spread around the averaged bias (either through standard deviation or other robust metrics).

1.5. Accuracy requirements of AC SAF products

The following table lists all operational AC SAF products and their accuracy requirements as defined in [RD2]. Also results of the semi-annual online quality assessment are reported.

Table 1.2. Accuracy requirements and validation results of AC SAF products

Product identifier	Product name	Threshold accuracy	Target accuracy	Optimal accuracy	Achieved accuracy according to online quality assessment (Section 7)
O3M-41.1	NRT total O3	20 %	4 % (SZA < 80°) 6 % (SZA > 80°)	1.5 %	w.r.t. Brewer ground reference: For SZA ≤ 80°: Mean rel. bias: +0.6 % Max rel. bias (SZA=75° – 80°): +2.4 % For SZA > 80°: Mean rel. bias: +1.0 %
O3M-300					w.r.t. Brewer ground reference: For SZA ≤ 80°: Mean rel. bias: +1.6 % Max rel. bias (SZA=70° – 75°): +3.0 % For SZA > 80°: Mean rel. bias: +2.7 %
O3M-50.1	NRT total NO2	20 % of annual mean	8 – 15 % of annual mean	4 – 8 % of annual mean	Abs. bias of -0.25×10^{15} molec/cm ² (GOME-2B) and -0.15×10^{15} molec/cm ² (GOME-2C) w.r.t. NDACC ZLS-DOAS. This corresponds to target accuracy reached.
O3M-338					
O3M-52.1	NRT tropospheric NO2	50 %	30 %	20 %	Between optimal and threshold accuracy depending on the pollution levels (for the O3M-341 MAX-DOAS station subset tested here).
O3M-341					

EUMETSAT Satellite Application Facility on Atmospheric Composition Monitoring

OPERATIONS REPORT 1/2025 rev. 1

Product identifier	Product name	Threshold accuracy	Target accuracy	Optimal accuracy	Achieved accuracy according to online quality assessment (Section 7)
O3M-55.1	NRT total SO ₂	100 %	50 % (SZA < 70°)	30 %	50 % (SZA < 70°)
O3M-374					
O3M-177	NRT total HCHO	100 %	50 % (polluted)	30 %	
O3M-344					
O3M-47.1	NRT high-resolution ozone profile	30 % in stratosphere 70 % in troposphere	15 % in stratosphere 30 % in troposphere	10 % in stratosphere 25 % in troposphere	
O3M-311					
O3M-78	NRT absorbing aerosol height	3 km (layer height < 10 km) 4 km (layer height > 10 km)	2 km (layer height < 10 km) 3 km (layer height > 10 km)	1 km (layer height < 10 km) 2 km (layer height > 10 km)	No on-going monitoring available
O3M-364					
O3M-72.1	NRT absorbing aerosol index from PMDs	1.0 index points	0.5 index points	0.2 index points	0.5 index points, based on monitoring of global trends
O3M-362					
O3M-409	NRT UV index, clear-sky	20 %	10 %	5 %	Deviation of the global average UV index for January – April 2025 from the preceding 8 years average was -2.7 % for NUV/CLEAR and 0.9 % for NUV/CLOUD
O3M-410	NRT UV index, cloud-corrected				
O3M-410.1	Global 1-day UV index forecast	Absolute deviation: 2	1	0.5	Deviation for the locations included in the most recent validation report (RD 8) was -3.0 %. Target accuracy was achieved.
O3M-172	NRT global tropospheric ozone	50 %	20 %	15 %	
O3M-174					Same as for NRT high-resolution ozone profile
O3M-304					

EUMETSAT Satellite Application Facility on Atmospheric Composition Monitoring

OPERATIONS REPORT 1/2025 rev. 1

Product identifier	Product name	Threshold accuracy	Target accuracy	Optimal accuracy	Achieved accuracy according to online quality assessment (Section 7)
O3M-80	NRT IASI CO	25 % (normal conditions) 50 % (high pollution or low signal)	12 % (normal conditions) 20 % (high pollution or low signal)	5 % (normal conditions) 10 % (high pollution or low signal)	Accuracy is estimated at 7 % for the entire NDACC network. During local winter months with high solar zenith angle measurements the target accuracy can be exceeded but remains below the threshold accuracy of 25 %. For high latitude sites the biases fall within the target accuracy of 20 %. For the high pollution site Xianghe (near Beijing), the accuracy is estimated at 12 %.
O3M-352					
O3M-57	NRT IASI SO2	200 % (below 10 km) 100 % (above 10 km)	100 % (below 10 km) 35 % (above 10 km)	50 % (below 10 km) 20 % (above 10 km)	
O3M-377					
O3M-81	NRT IASI HNO3	50 %	35 %	10 %	Accuracy is estimated at 14 % for the entire NDACC network. Higher biases reaching 20 % are observed at tropical NDACC sites and in the southern hemisphere (Lauder and Wollongong). Lower relative biases below 10 % at high latitude sites.
O3M-336					
O3M-44	NRT IASI total O3	10 %	5 %	1 %	
O3M-306					
O3M-49	NRT IASI ozone profile	30 % in stratosphere 50 % in troposphere	15 % in stratosphere 30 % in troposphere	5 % in stratosphere 10 % in troposphere	
O3M-315					
O3M-06.1	Offline total O3	20 %	4 % (SZA < 80°) 6 % (SZA > 80°)	1.5 %	
O3M-42.1					Same as for NRT total O3
O3M-301					

EUMETSAT Satellite Application Facility on Atmospheric Composition Monitoring

OPERATIONS REPORT 1/2025 rev. 1

Product identifier	Product name	Threshold accuracy	Target accuracy	Optimal accuracy	Achieved accuracy according to online quality assessment (Section 7)
O3M-07.1	Offline total NO ₂	20 % of annual mean	8 – 15 % of annual mean	4 – 8 % of annual mean	
O3M-51.1					Same as for NRT total NO ₂
O3M-339					
O3M-37.1	Offline tropospheric NO ₂	50 %	30 %	20 %	
O3M-53.1					Same as for NRT tropospheric NO ₂
O3M-342					
O3M-09.1	Offline total SO ₂	100 %	50 % (SZA < 70°)	30 %	
O3M-56.1					Same as for NRT total SO ₂
O3M-375					
O3M-08.1	Offline total BrO	50 %	30 %	15 %	Generally within the target requirements for the S5p comparisons, within optimal accuracy for comparisons to Harestua ZSLDOAS.
O3M-82.1					
O3M-317					
O3M-10.1	Offline total HCHO	100 %	50 % (polluted cond.)	30 %	
O3M-58.1					Same as for NRT total HCHO
O3M-345					
O3M-12.1	Offline total H ₂ O	25 %	10 %	5 %	
O3M-86.1					
O3M-386					

Product identifier	Product name	Threshold accuracy	Target accuracy	Optimal accuracy	Achieved accuracy according to online quality assessment (Section 7)
O3M-35	Offline tropical tropospheric ozone	50 %	25 %	15 %	
O3M-43					
O3M-302					
O3M-303	Offline L3 daily averaged total O3	20 %	4 % (SZA < 80°) 6 % (SZA > 80°)	1.5 %	Same as for the offline L2 total O3
O3M-388	Offline L3 monthly averaged total O3				
O3M-340	Offline L3 daily averaged total NO2	20 %	8 %	5 %	Same as for the offline L2 total NO2
O3M-389	Offline L3 monthly averaged total NO2				
O3M-343	Offline L3 daily averaged tropospheric NO2	50 %	30 %	20 %	Same as for the offline L2 tropospheric NO2
O3M-390	Offline L3 monthly averaged tropospheric NO2				
O3M-376	Offline L3 daily averaged total SO2	100 %	50 % (SZA < 70°)	30 %	Same as for the offline L2 total SO2
O3M-397	Offline L3 monthly averaged total SO2				
O3M-318	Offline L3 daily averaged total BrO	50 %	30 %	15 %	Same as for the offline L2 total BrO
O3M-391	Offline L3 monthly averaged total BrO				
O3M-387	Offline L3 daily averaged total H2O	25 %	10 %	5 %	Same as for the offline L2 total H2O
O3M-393	Offline L3 monthly averaged total H2O				

Product identifier	Product name	Threshold accuracy	Target accuracy	Optimal accuracy	Achieved accuracy according to online quality assessment (Section 7)
O3M-346	Offline L3 daily averaged total HCHO	100 % (polluted cond.)	50 % (polluted cond.)	30 % (polluted cond.)	Same as for the offline L2 total HCHO
O3M-394	Offline L3 monthly averaged total HCHO				
O3M-39.1	Offline high-resolution ozone profile	30 % in stratosphere 70 % in troposphere	15 % in stratosphere 30 % in troposphere	10 % in stratosphere 25 % in troposphere	
O3M-48.1					Same as for NRT high-resolution ozone profile
O3M-312					
O3M-172	NRT global tropospheric ozone	50 %	20 %	15 %	
O3M-174					Same as for NRT product
O3M-304					
O3M-173	Offline global tropospheric ozone	50 %	20 %	15 %	
O3M-175					Same as for NRT product
O3M-305					
O3M-69	Offline absorbing aerosol height	3 km (layer height < 10 km) 4 km (layer height > 10 km)	2 km (layer height < 10 km) 3 km (layer height > 10 km)	1 km (layer height < 10 km) 2 km (layer height > 10 km)	
O3M-79					GOME2 – EARLINET: 40.0 % (< 1 km) 64.2 % (< 2 km) 82.7 % (< 3 km)
O3M-365					
O3M-63.1	Offline absorbing aerosol index from PMDs	1.0 index points	0.5 index points	0.2 index points	
O3M-73.1					Same as for NRT AAI
O3M-363					

Product identifier	Product name	Threshold accuracy	Target accuracy	Optimal accuracy	Achieved accuracy according to online quality assessment (Section 7)
O3M-450 – O3M-464	Offline surface UV	50 %	20 %	10 %	Average value of the global erythemal daily dose during the reporting period deviated -0.97 % from the long-term average. See Figure 7.28.

Latest validation reports for all pre-operational and operational AC SAF products are listed in Section 1.3.

2. Processing centre: FMI

2.1. Offline surface UV radiation

Offline surface UV radiation (OUV) product is a L3 multi-mission (Metop-B+C) product consisting of 15 sub-products which are listed in Table 2.1. Since they are all archived in the same file, single entries in the tables in the following sections represent them all.

Table 2.1. OUV sub-products

Product Identifier	Product Name	Product Acronym
O3M-450	Offline UV daily dose, erythemat (CIE) weighting	MM-O-UV_DD_CIE
O3M-451	Offline UV daily dose, plant response weighting	MM-O-UV_DD_PLANT
O3M-452	Offline UV daily dose, DNA damage weighting	MM-O-UV_DD_DNA
O3M-453	Offline UV daily dose, UVA range (315-400 nm)	MM-O-UV_DD_UVA
O3M-454	Offline UV daily dose, UVB range (280-315 nm)	MM-O-UV_DD_UVB
O3M-455	Offline UV daily maximum dose rate, erythemat (CIE) weighting	MM-O-UV_MDSR_CIE
O3M-456	Offline UV daily maximum dose rate, plant response weighting	MM-O-UV_MDSR_PLANT
O3M-457	Offline UV daily maximum dose rate, DNA damage weighting	MM-O-UV_MDSR_DNA
O3M-458	Offline UV daily maximum dose rate, UVA range (315-400 nm)	MM-O-UV_MDSR_UVA
O3M-459	Offline UV daily maximum dose rate, UVB range (280-315 nm)	MM-O-UV_MDSR_UVB
O3M-460	Offline UV solar noon UV index	MM-O-UV_NOON_UVI
O3M-461	Offline UV daily maximum ozone photolysis rate	MM-O-UV_MPHR_O3
O3M-462	Offline daily maximum nitrogen dioxide photolysis rate	M-O-UV_MPHR_NO2
O3M-463	Offline UV daily dose, vitamin D weighting	MM-O-UV_DD_VITD
O3M-464	Offline UV daily maximum dose rate, vitamin D weighting	MM-O-UV_MDSR_VITD

2.1.1. Availability

Availability requirement for OUV has been defined in Section 1.4. The availability statistics of FMI products are presented in Table 2.2. If the availability requirement has been violated, those values are marked with red colour, identified by numbers and reported in Table 2.7.

Table 2.2. Availability of OUV product during the reporting period

1/2025	2/2025	3/2025	4/2025	5/2025	6/2025
100 %	100 %	100 %	100 %	100 %	100 %

2.1.2. Timeliness

Timeliness indicates the elapsed time between sensing and product dissemination. Timeliness requirement is 15 days for offline products. If the requirement has been violated, those values are

marked with red colour. In addition, the violations are identified by numbers and reported in Table 2.7 if they have caused the availability values to drop below the allowed limits.

Note: timeliness violations are not listed as anomalies if the availability is above the limit.

The values in Table 2.3 indicate the elapsed times (days, hours and minutes in the format [ddT]hh:mm) from sensing to archive upload. In each cell, the values from top to bottom represent observed monthly average, minimum and maximum times.

Table 2.3. Timeliness of OUV product during the reporting period

1/2025	2/2025	3/2025	4/2025	5/2025	6/2025
avg: 04T01:03 min: 04T00:27 max: 04T01:27	avg: 04T01:14 min: 04T00:32 max: 04T01:32	avg: 04T01:18 min: 04T00:32 max: 04T01:32	avg: 04T01:19 min: 04T00:37 max: 04T01:37	avg: 04T01:13 min: 04T00:37 max: 04T01:42	avg: 04T01:12 min: 04T00:42 max: 04T01:42

2.2. Services, main events and anomalies

Table 2.4. FMI service statistics related to product archiving, ordering and AC SAF Helpdesk

Description of service / event	1/2025	2/2025	3/2025	4/2025	5/2025	6/2025
Product ordering ¹						
Number of users (cumulative)	725	729	742	747	753	757
Number of orders	7	7	45	12	49	74
Number of ordered products	OHP: 1 ARP: 1 OUV subset: 366 OUV time-series: 25692	ARS: 4318 OUV time-series: 2191 LER: 4	OHP: 1512 OUV subset: 5497 OUV time-series: 9126	OHP: 38 ARP: 1915 OUV subset: 31 OUV time-series: 2373	ARS: 10268 OUV subset: 52 OUV time-series: 163574 LER: 2	OHP: 172 ARS: 960 ARP: 380 OUV subset: 75 OUV time-series: 334098
Ordered data volume	OHP: 253 MB ARP: 6.85 MB OUV subset: 10.9 MB OUV time-series: 5.93 MB	ARS: 4.44 GB OUV time-series: 687 kB LER: 8.06 GB	OHP: 454 GB OUV subset: 4.84 GB OUV time-series: 786 kB	OHP: 9.55 GB ARP: 14.0 GB OUV subset: 952 kB OUV time-series: 664 kB	ARS: 10.6 GB OUV subset: 37.9 MB OUV time-series: 16.7 MB LER: 4.07 GB	OHP: 43.3 GB ARS: 999 MB ARP: 2.75 GB OUV subset: 92.3 MB OUV time-series: 21.0 MB
Number of failed orders ²	0	0	0	0	0	0
Archive statistics ³						
Number of archived products (Metop-B)	OHP: 439 ARS: 439 ARP: 439	OHP: 397 ARS: 397 ARP: 397	OHP: 439 ARS: 439 ARP: 439	OHP: 426 ARS: 426 ARP: 426	OHP: 439 ARS: 439 ARP: 439	OHP: 423 ARS: 423 ARP: 423
Size of archived products (Metop-B)	OHP: 110 GB ARS: 451 MB ARP: 3.18 GB	OHP: 100 GB ARS: 407 MB ARP: 2.89 GB	OHP: 110 GB ARS: 451 MB ARP: 3.20 GB	OHP: 107 GB ARS: 440 MB ARP: 3.09 GB	OHP: 110 GB ARS: 455 MB ARP: 3.17 GB	OHP: 106 GB ARS: 439 MB ARP: 3.05 GB
Number of archived products (Metop-C)	OHP: 439 ARS: 439 ARP: 439	OHP: 396 ARS: 396 ARP: 396	OHP: 439 ARS: 439 ARP: 439	OHP: 423 ARS: 423 ARP: 423	OHP: 440 ARS: 440 ARP: 440	OHP: 425 ARS: 425 ARP: 425

Size of archived products (Metop-C)	OHP: 110 GB ARS: 455 MB ARP: 3.21 GB	OHP: 99.5 GB ARS: 409 MB ARP: 2.90 GB	OHP: 110 GB ARS: 454 MB ARP: 3.22 GB	OHP: 105 GB ARS: 438 MB ARP: 3.07 GB	OHP: 110 GB ARS: 459 MB ARP: 3.19 GB	OHP: 106 GB ARS: 443 MB ARP: 3.07 GB
Number of archived multi-mission products	OUV: 31	OUV: 28	OUV: 31	OUV: 30	OUV: 31	OUV: 30
Size of archived multi-mission products	OUV: 565 MB	OUV: 537 MB	OUV: 579 MB	OUV: 532 MB	OUV: 542 MB	OUV: 507 MB
GOME-2 L1b PDU rolling archive statistics ⁴						
PDUs archived / PDUs “reception confirmed” (Metop-B)	14862/13558 110 %	13440/12561 107 %	14879/14802 101 %	14395/14384 100 %	14880/14880 100 %	14261/14383 99.2 % (1)
PDUs archived / PDUs “reception confirmed” (Metop-C)	14879/13438 110 %	13440/12566 107 %	14870/14787 101 %	14359/14359 100 %	14880/14880 100 %	14257/14365 99.2 % (1)
Helpdesk statistics						
Number of emails	0	2	4	9	2	2
Number of email threads	0	1	3	3	2	1
Average response time ([ddT]hh:mm)	-	00:38	17:56	01T04:23	05T18:04 ⁵	01T20:54

¹ More detailed information about the orders is available in Appendix 1

² Failed orders are detailed in Appendix 2

³ Based on sensing start time

⁴ For Level 1b products, the availability is defined as the number of archived L1b PDUs divided by the number of L1b PDUs with status “reception confirmed” in the EUMETCast sendlist. PDUs received via EUMETCast Terrestrial may increase the ratio above 100 %.

⁵ Helpdesk operator was on an extended sick leave

Data archive statistics since 2008 are illustrated in Figure 2.1.

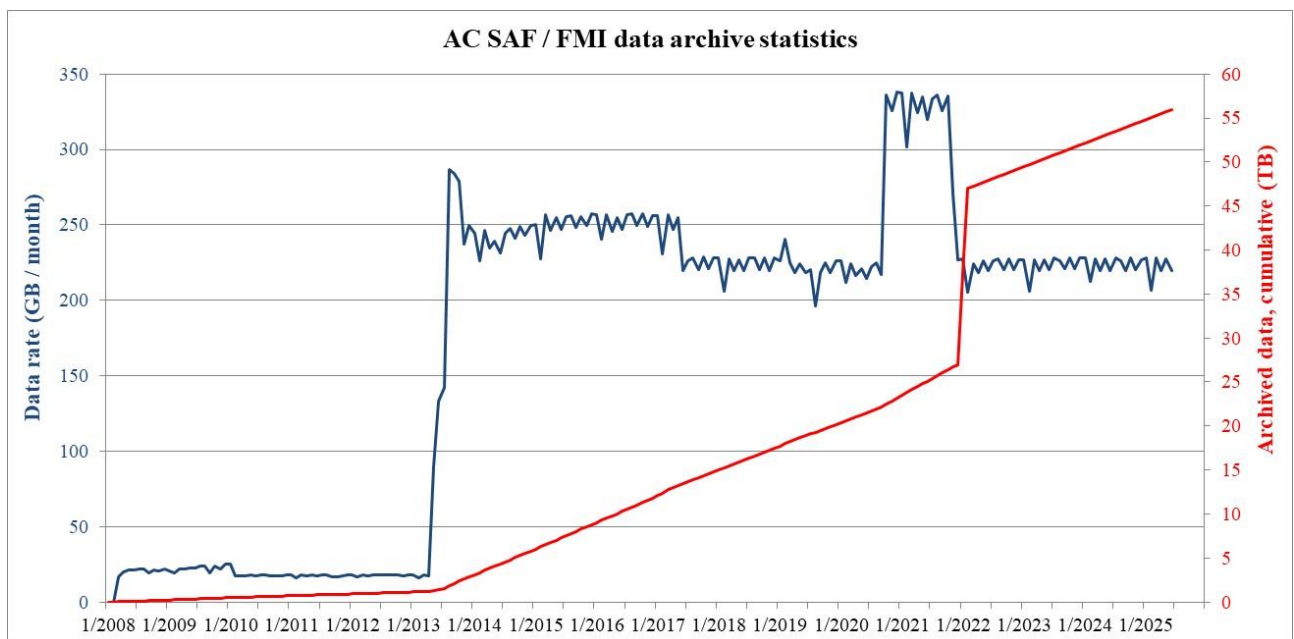


Figure 2.1. FMI data archive statistics: data rate and cumulative amount of data

Sudden increase in the cumulative amount of archived data in January – February 2022 is due to archiving of Metop-A/B high-resolution ozone profile data record R1.

Events affecting the data rate are presented in Table 2.5.

Table 2.5. Events affecting the FMI archive data rate

Date	Event	Data rate (GB/month)
03/2008	Archiving of OOP-A started	19.1 – 22.2
06/2009	Archiving of OUV-A started	19.2 – 23.8
11/2009	Archiving of ARS-A started	25.3
02/2010	Compression of OOP-A started	16.2 – 18.3
05/2013	Archiving of OHP-A started	133 – 142
08/2013	Archiving of OOP-B, OHP-B and ARS-B started	279 – 284
11/2013	Archiving of ARP-A and ARP-B started. KNMI implements shuffling algorithm in the hdf5 compression	226 – 250
03/2014	Archiving of OUV-A discontinued, archiving of OUV-B started	227 – 250
02/2015	OPERA algorithm update, tropospheric integrated profiles added	247 – 257
06/2017	Archiving of OOP-A and OOP-B discontinued	206 – 229
10/2020	Archiving of ARS-C, ARP-C and OHP-C started	302 – 338
11/2021	Archiving of OHP-A, ARS-A and ARP-A discontinued	206 – 228
01/2023	Archiving of IASI-B/C L3 CO started	206 – 228

Table 2.6 lists the main events (product/service/hardware/software updates etc.) at FMI during the reporting period.

Table 2.6. Main events at FMI during the reporting period

Date	Description
	<i>Nothing to report.</i>

Table 2.7 lists the main local and external anomalies during the reporting period. Corrective and preventive actions should be provided also when applicable.

Table 2.7. Main local and external anomalies affecting FMI systems and performance during the reporting period

ID	Time period	Description
1	1 – 2 June	Timeouts when connecting to the FMI FTP server

3. Processing centre: DLR

3.1. NRT and offline total/tropospheric trace gas columns, tropical tropospheric ozone

This section reports availability and timeliness of the operational NRT and offline L2 and L3 products processed for GOME-2 on Metop-B and Metop-C.

3.1.1. Availability

For Level 1b products, the availability is defined as the number of L1b PDUs with status “reception confirmed”, i.e. EUMETSAT received these L1b PDUs through its EUMETCast reference receiving station, divided by the total number of L1b PDUs listed in the EUMETCast sendlist.

Availability for offline L2 and L3 products has been defined in Section 1.4. The availability statistics of DLR products are presented in Table 3.1 and Table 3.2. If the availability requirements have been violated, those values are marked with red colour, identified by numbers and reported in Table 3.7.

Table 3.1. Availability of Metop-B total and tropospheric trace gas column products during the reporting period

Product Identifier	Product Name	1/2025	2/2025	3/2025	4/2025	5/2025	6/2025
L1b	PDUs received / PDUs “reception confirmed”	14857/13547 110 %*	13440/12561 107 %*	14879/14802 101 %*	14384/14322 100 %	14880/13250 112 %*	14383/14383 100 %
O3M-41.1	NRT total O3	99.9 %	100 %	99.9 %	100 %	100 %	100 %
O3M-50.1	NRT total NO2						
O3M-52.1	NRT tropospheric NO2						
O3M-55.1	NRT total SO2						
O3M-177.0	NRT total HCHO						
O3M-42.1	Offline total O3	98.9 %	99.3 %	99.8 %	99.8 %	89.1 % (1)	99.3 %
O3M-51.1	Offline total NO2						
O3M-53.1	Offline tropospheric NO2						
O3M-56.1	Offline total SO2						
O3M-58.1	Offline total HCHO						
O3M-82.1	Offline total BrO						
O3M-86.1	Offline total H2O						
O3M-43	Offline tropical tropospheric ozone	100 %	100 %	100 %	100 %	100 %	100 %

* The values higher than 100 % are a result of single missing sendlist files or partially available content within the sendlist files

Table 3.2. Availability of Metop-C total and tropospheric trace gas column products during the reporting period

Product Identifier	Product Name	1/2025	2/2025	3/2025	4/2025	5/2025	6/2025
L1b	PDUs received / PDUs "reception confirmed"	14865/14787 110 %*	13437/12566 107 %*	14865/14787 101 %*	14338/14275 100 %*	14877/13274 112 %*	14356/14365 99.9 %
O3M-300	NRT total O3	99.9 %	100 %	99.9 %	100 %	99.9 %	100 %
O3M-338	NRT total NO2						
O3M-341	NRT tropospheric NO2						
O3M-374	NRT total SO2						
O3M-344	NRT total HCHO						
O3M-301	Offline total O3	98.0 %	99.5 %	99.6 %	99.3 %	87.4 % (1)	99.5 %
O3M-339	Offline total NO2						
O3M-342	Offline tropospheric NO2						
O3M-375	Offline total SO2						
O3M-345	Offline total HCHO						
O3M-317	Offline total BrO						
O3M-386	Offline total H2O						
O3M-302	Offline tropical tropospheric ozone	100 %	100 %	100 %	100 %	100 %	100 %

* The values higher than 100 % are a result of single missing sendlist files or partially available content within the sendlist files

3.1.2. Timeliness

Timeliness indicates the elapsed time between sensing and product dissemination. Timeliness requirements are 3 hours for NRT products, 14 days for the offline tropical tropospheric ozone product and 15 days for the other offline products. If the requirements have been violated, those values are marked with red colour. In addition, the violations are identified by numbers and reported in Table 3.7 if they have caused the availability values to drop below the allowed limits.

Note: timeliness violations are not listed as anomalies if the availability is above the limit.

The values in Table 3.3 and Table 3.4 indicate the elapsed times (days, hours and minutes in the format [ddT]hh:mm) from sensing to EUMETCast (NRT) or AC SAF FTP site (offline) upload. For the offline tropical tropospheric ozone product, however, the values indicate the elapsed time from the end of the preceding month to product upload to the AC SAF FTP site. Timeliness requirement for those products is currently 14 days.

In each cell, the values from top to bottom represent observed monthly average, minimum and maximum times.

Table 3.3. Timeliness of Metop-B total and tropospheric trace gas column products during the reporting period

Product Identifier	Product Name	1/2025	2/2025	3/2025	4/2025	5/2025	6/2025
O3M-41.1	NRT total O3	avg: 00:53 min: 00:35 max: 02:27	avg: 00:53 min: 00:28 max: 01:43	avg: 00:58 min: 00:29 max: 01:47	avg: 00:56 min: 00:29 max: 02:14	avg: 00:55 min: 00:30 max: 01:47	avg: 00:55 min: 00:30 max: 01:51
O3M-50.1	NRT total NO2						
O3M-52.1	NRT tropospheric NO2						
O3M-55.1	NRT total SO2						
O3M-177.0	NRT total HCHO						
O3M-42.1	Offline total O3	avg: 01T01:57 min: 01T01:03 max: 02T10:43	avg: 01T01:27 min: 01T01:04 max: 01T19:15	avg: 01T02:09 min: 01T01:01 max: 01T15:43	avg: 01T01:08 min: 01T01:00 max: 01T01:52	avg: 02T04:44 min: 01T01:02 max: 16T10:49 (1)	avg: 01T16:33 min: 01T01:01 max: 10T16:49
O3M-51.1	Offline total NO2						
O3M-53.1	Offline tropospheric NO2						
O3M-56.1	Offline total SO2						
O3M-58.1	Offline total HCHO						
O3M-82.1	Offline total BrO						
O3M-86.1	Offline total H2O						
O3M-43	Offline tropical tropospheric ozone	26T17:32 (2)	13T19:45	07T10:32	19T13:32 (2)	37T09:26 (2)	92T10:45 (2)

Table 3.4. Timeliness of Metop-C total and tropospheric trace gas column products during the reporting period

Product Identifier	Product Name	1/2025	2/2025	3/2025	4/2025	5/2025	6/2025
O3M-300	NRT total O3	avg: 01:38 min: 01:11 max: 02:04	avg: 01:38 min: 00:43 max: 01:51	avg: 01:43 min: 00:32 max: 02:08	avg: 01:39 min: 00:33 max: 02:26	avg: 01:38 min: 00:34 max: 06:05 (1)	avg: 01:36 min: 00:34 max: 02:12
O3M-338	NRT total NO2						
O3M-341	NRT tropospheric NO2						
O3M-374	NRT total SO2						
O3M-344	NRT total HCHO						
O3M-301	Offline total O3	avg: 01T02:32 min: 01T01:04 max: 03T10:37	avg: 01T01:25 min: 01T01:04 max: 01T08:34	avg: 01T02:13 min: 01T01:01 max: 01T14:50	avg: 01T01:21 min: 01T00:50 max: 01T11:19	avg: 01T02:27 min: 01T01:02 max: 01T01:13	avg: 01T05:16 min: 01T00:58 max: 07T01:48
O3M-339	Offline total NO2						
O3M-342	Offline tropospheric NO2						
O3M-375	Offline total SO2						
O3M-345	Offline total HCHO						
O3M-317	Offline total BrO						
O3M-386	Offline total H2O						
O3M-302	Offline tropical tropospheric ozone	26T17:33 (2)	13T19:45	07T10:33	19T13:32 (2)	37T09:26 (2)	92T08:45 (2)

3.2. Services, main events and anomalies

Table 3.5. DLR service statistics related to product archiving and ordering

Description of service / event	1/2025	2/2025	3/2025	4/2025	5/2025	6/2025
Archive statistics ²						
Number of archived products (cumulative) – according to product insertion time	557008	557800	58680	559531	560362	561256
Size of archived products (TB, cumulative) ⁴	15.74	15.78	15.83	15.88	15.91	15.96
Number of missing orbit products – according to sensing time	0	0	0	0	0	0
Number of archived products with good/poor/error ³ quality assessed per month – according to product insertion time	858/0/7	789/2/2	874/0/6	845/0/5	827/1/5	883/2/8
Online Access ¹						
Number of FTP (ATMOS/VELA) subscribers	656	660	672	678	680	684
Number of FTP (ATMOS/VELA) downloads	(*)	132731	33520	48421	90496	148128
Downloaded data volume (GB)	(*)	116.5	192.4	116.5	165.0	1262.0

¹ NTO product and OTO product is stored at the DLR for external search and download

² O3MOTO product (collection GOME.TC, Metop missions) is archived and available to non-NRT users

³ good: max. 2 PDUs missing, poor/error: more than 2 PDUs missing

⁴ GOME.TC.AGG products have been deleted, which explains less products in 01/2025 compared to 12/2024

(*) Due to a server upgrade, the respective log information for retrieving the number of FTP downloads from 08/2024 up to including 01/2025 is irrecoverably lost; preventive action: incorporation of log file availability into monitoring system.

Table 3.6 lists the main events (product/service/hardware/software updates etc.) at DLR during the reporting period.

Table 3.6. Main events at DLR during the reporting period

Date	Event
	<i>Nothing to report.</i>

Table 3.7 lists the main and external local anomalies at DLR during the reporting period. Corrective and preventive actions should be provided also when applicable.

Table 3.7. Main local and external anomalies affecting DLR systems and performance during the reporting period

ID	Time period	Description
1	24 – 25 May	<p>The availability of offline products is below the threshold value for both Metop-B and Metop-C. This is due to the fact, that for two consecutive days there was a problem within the archiving system, which resulted in a logical error in the communication of our systems. Manual corrections in the database were conducted, but this didn't activate the triggers for the product publishing.</p> <p>Corrective action: Manual corrections in the database were conducted to resolve the situation. The missing products have been provided (outside of the timeliness of the products) on the publishing end point.</p> <p>Preventive action: Update of operations procedures to include measures and check actions for exactly this (or very similar) issue type.</p>
2	January, April – June	<p>The timeliness of ≤ 2 weeks as specified in the currently applicable version (2.1) of the AC SAF Service Specification has been violated consistently (except for 02/2025 and 03/2025 for both missions Metop-B and Metop-C) in the reporting period. The generation of the tropospheric ozone products is triggered manually after a certain and not fully fixed time period after all L2 data covering the respective month plus its nominal 14 days timeliness have passed.</p> <p>Corrective action: None</p> <p>Preventive action: A discussion about the potential adaption of the timeliness requirement for this product type (O3M-43) has been held in the Operations Review 16 in January 2025. During the Operations Review a final check on the user needs with regards to the product availability has been suggested by the project team. DLR clarified the user needs. However, final feedback towards the project team and clarification is pending.</p>

4. Processing centre: KNMI

4.1. NRT and offline ozone profiles, absorbing aerosol height and index, global tropospheric ozone

4.1.1. Availability

For Level 1b products, the availability is defined as the number of unique L1b PDUs received either via EUMETCast Satellite or EUMETCast Terrestrial (demonstrational dissemination service), divided by the number of L1b PDUs not marked as “not sent” in the EUMETCast Satellite sendlist. This approximation presumes that all PDUs marked as “sent not confirmed” are still available via EUMETCast Terrestrial. Availability is higher than 100 % if there are more PDUs received from Terrestrial than is indicated by the Satellite sendlists.

Availability for offline L2 products has been defined in Section 1.4. The availability statistics of KNMI products are presented in Table 4.1 and Table 4.2. If the availability requirements have been violated, those values are marked with red colour, identified by numbers and reported in Table 4.9.

Tropospheric ozone products are included in the ozone profile products and have the same statistics. The same applies to scattering aerosol index products which are included in the absorbing aerosol index products.

Table 4.1. Availability of Metop-B L1b PDUs, ozone profile products and aerosol products during the reporting period

Product Identifier	Product Name	1/2025	2/2025	3/2025	4/2025	5/2025	6/2025
EUMETCast							
L1b	PDUs received / sent	14862/13547 110 %	13440/12561 107 %	14879/14802 101 %	14395/14322 101 %	14880/13250 112 %	14383/14383 100 %
O3M-47.1	NRT high-resolution ozone profile	100 %	100 %	100 %	100 %	100 %	100 %
O3M-78	NRT absorbing aerosol height	100 %	100 %	100 %	100 %	100 %	100 %
O3M-72.1	NRT absorbing aerosol index from PMDs	100 %	100 %	100 %	100 %	100 %	100 %
WMO/GTS							
O3M-47.1	NRT high-resolution ozone profile	100 %	100 %	100 %	100 %	100 %	100 %
FMI archive							
O3M-48.1	Offline high-resolution ozone profile	100 %	100 %	100 %	100 %	100 %	100 %
O3M-79	Offline absorbing aerosol height	100 %	100 %	100 %	100 %	100 %	100 %
O3M-73.1	Offline absorbing aerosol index from PMDs	100 %	100 %	100 %	100 %	100 %	100 %

Table 4.2. Availability of Metop-C L1b PDUs, ozone profile products and aerosol products during the reporting period

Product Identifier	Product Name	1/2025	2/2025	3/2025	4/2025	5/2025	6/2025
EUMETCast							
L1b	PDUs received / sent	14879/13438 110 %	13440/12566 107 %	14870/14787 101 %	14359/14275 101 %	14880/13274 112 %	14365/14365 100 %
O3M-311	NRT high-resolution ozone profile	100 %	100 %	100 %	100 %	100 %	100 %
O3M-364	NRT absorbing aerosol height	100 %	100 %	100 %	100 %	100 %	100 %
O3M-362	NRT absorbing aerosol index from PMDs	100 %	100 %	100 %	100 %	100 %	100 %
WMO/GTS							
O3M-311	NRT high-resolution ozone profile	100 %	100 %	100 %	100 %	100 %	100 %
FMI archive							
O3M-312	Offline high-resolution ozone profile	100 %	100 %	100 %	100 %	100 %	100 %
O3M-365	Offline absorbing aerosol height	100 %	100 %	100 %	100 %	100 %	100 %
O3M-363	Offline absorbing aerosol index from PMDs	100 %	100 %	100 %	100 %	100 %	100 %

4.1.2. Timeliness

Timeliness indicates the elapsed time between sensing and product dissemination. Timeliness requirements are 3 hours for NRT products and 15 days for offline products. If the requirements have been violated, those values are marked with red colour. In addition, the violations are identified by numbers and reported in Table 4.9 if they have caused the availability values to drop below the allowed limits.

Note: timeliness violations are not listed as anomalies if the availability is above the limit.

The values in Table 4.3 and Table 4.4 indicate elapsed times (days, hours and minutes in the format [ddT]hh:mm) from sensing to EUMETCast and WMO/GTS (NRT) or archive upload (offline). In each cell, the values from top to bottom represent observed monthly average, minimum and maximum times.

Tropospheric ozone products are included in the ozone profile products and have the same statistics.

Table 4.3. Timeliness of Metop-B ozone profile and aerosol products during the reporting period

Product Identifier	Product Name	1/2025	2/2025	3/2025	4/2025	5/2025	6/2025
EUMETCast							
O3M-47.1	NRT high-resolution ozone profile	avg: 01:15 min: 00:29 max: 02:23	avg: 01:06 min: 00:29 max: 02:17	avg: 01:09 min: 00:29 max: 02:05	avg: 01:07 min: 00:30 max: 02:41	avg: 01:07 min: 00:32 max: 02:07	avg: 01:07 min: 00:33 max: 02:11
O3M-78	NRT absorbing aerosol height	avg: 00:53 min: 00:29 max: 02:05	avg: 00:54 min: 00:29 max: 01:46	avg: 00:56 min: 00:29 max: 01:47	avg: 00:54 min: 00:29 max: 02:19	avg: 00:54 min: 00:30 max: 01:46	avg: 00:54 min: 00:30 max: 01:50
O3M-72.1	NRT absorbing aerosol index from PMDs	avg: 00:53 min: 00:29 max: 02:07	avg: 00:54 min: 00:29 max: 01:46	avg: 00:56 min: 00:29 max: 01:50	avg: 00:54 min: 00:29 max: 02:19	avg: 00:54 min: 00:30 max: 01:46	avg: 00:54 min: 00:30 max: 01:50
WMO/GTS							
O3M-47.1	NRT high-resolution ozone profile	avg: 01:06 min: 00:30 max: 02:23	avg: 01:07 min: 00:30 max: 02:20	avg: 01:10 min: 00:30 max: 02:09	avg: 01:48 min: 00:35 max: 02:50	avg: 01:08 min: 00:33 max: 02:07	avg: 01:07 min: 00:34 max: 02:11
FMI archive							
O3M-48.1	Offline high-resolution ozone profile	avg: 07:40 min: 06:51 max: 02T02:15	avg: 07:37 min: 06:54 max: 02T02:18	avg: 07:41 min: 06:57 max: 02T02:21	avg: 07:51 min: 06:47 max: 02T02:47	avg: 10:19 min: 06:50 max: 02T03:05	avg: 10:41 min: 06:42 max: 02T02:56
O3M-79	Offline absorbing aerosol height	avg: 07:39 min: 06:52 max: 02T02:52	avg: 07:35 min: 06:52 max: 02T02:13	avg: 07:37 min: 06:55 max: 02T02:16	avg: 07:47 min: 06:37 max: 02T02:37	avg: 10:18 min: 06:46 max: 02T03:01	avg: 10:39 min: 06:37 max: 02T02:58
O3M-73.1	Offline absorbing aerosol index from PMDs	avg: 07:37 min: 06:46 max: 02T02:40	avg: 07:33 min: 06:52 max: 02T02:43	avg: 07:36 min: 06:46 max: 02T02:46	avg: 07:45 min: 06:37 max: 02T02:12	avg: 10:15 min: 06:46 max: 02T03:09	avg: 10:37 min: 06:43 max: 02T02:57

Table 4.4. Timeliness of Metop-C ozone profile and aerosol products during the reporting period

Product Identifier	Product Name	1/2025	2/2025	3/2025	4/2025	5/2025	6/2025
EUMETCast							
O3M-311	NRT high-resolution ozone profile	avg: 01:49 min: 00:39 max: 02:41	avg: 01:49 min: 00:42 max: 02:25	avg: 01:52 min: 00:32 max: 02:41	avg: 01:47 min: 00:34 max: 02:49	avg: 01:47 min: 00:33 max: 02:21	avg: 01:45 min: 00:38 max: 02:23
O3M-364	NRT absorbing aerosol height	avg: 01:38 min: 00:39 max: 02:22	avg: 01:38 min: 00:41 max: 01:56	avg: 01:40 min: 00:32 max: 02:35	avg: 01:36 min: 00:34 max: 02:26	avg: 01:35 min: 00:33 max: 02:02	avg: 01:33 min: 00:34 max: 02:12
O3M-362	NRT absorbing aerosol index from PMDs	avg: 01:38 min: 00:39 max: 02:22	avg: 01:38 min: 00:41 max: 01:56	avg: 01:40 min: 00:32 max: 02:35	avg: 01:36 min: 00:33 max: 02:26	avg: 01:35 min: 00:33 max: 02:01	avg: 01:33 min: 00:34 max: 02:12

Product Identifier	Product Name	1/2025	2/2025	3/2025	4/2025	5/2025	6/2025
WMO/GTS							
O3M-311	NRT high-resolution ozone profile	avg: 01:50 min: 00:39 max: 02:42	avg: 01:50 min: 00:42 max: 02:26	avg: 01:52 min: 00:34 max: 02:54	avg: 01:48 min: 00:35 max: 02:50	avg: 01:47 min: 00:37 max: 02:21	avg: 01:46 min: 00:38 max: 02:24
FMI archive							
O3M-312	Offline high-resolution ozone profile	avg: 08:03 min: 07:15 max: 02T02:47	avg: 08:01 min: 07:18 max: 08:39	avg: 08:24 min: 07:27 max: 02T03:09	avg: 12:20 min: 07:30 max: 02T03:41	avg: 15:56 min: 07:35 max: 02T03:47	avg: 16:36 min: 07:35 max: 02T03:50
O3M-365	Offline absorbing aerosol height	avg: 08:02 min: 07:19 max: 02T02:37	avg: 08:00 min: 07:13 max: 08:34	avg: 08:25 min: 07:22 max: 02T03:04	avg: 12:16 min: 07:31 max: 02T03:40	avg: 15:53 min: 07:34 max: 02T03:43	avg: 16:32 min: 07:31 max: 02T03:46
O3M-363	Offline absorbing aerosol index from PMDs	avg: 08:01 min: 07:19 max: 02T03:12	avg: 07:58 min: 07:22 max: 08:33	avg: 08:23 min: 07:22 max: 02T03:21	avg: 12:16 min: 07:25 max: 02T03:36	avg: 15:52 min: 07:34 max: 02T03:40	avg: 16:31 min: 07:10 max: 02T03:42

4.2. Services, main events and anomalies

Tropospheric ozone products are included in the ozone profile products and have the same statistics.

Table 4.5. Number of products sent to FMI archive¹

Product Identifier	Product Name	Metop satellite	1/2025	2/2025	3/2025	4/2025	5/2025	6/2025
O3M-48.1	Offline high-resolution ozone profile	B	439	397	439	426	439	423
O3M-312		C	439	396	439	423	440	425
O3M-79	Offline absorbing aerosol height	B	439	397	439	426	439	423
O3M-365		C	439	396	439	423	440	425
O3M-73.1	Offline absorbing aerosol index from PMDs	B	439	397	439	426	439	423
O3M-363		C	439	396	439	423	440	425

Table 4.6. Number of products stored locally at KNMI²

Product Identifier	Product Name	Metop satellite	1/2025	2/2025	3/2025	4/2025	5/2025	6/2025
O3M-47.1	NRT high-resolution ozone profile	B	8846	8012	8836	8496	8686	8339
O3M-311		C	8782	7960	8758	8328	8584	8285
O3M-78	NRT absorbing aerosol height	B	8846	8012	8836	8496	8686	8339
O3M-364		C	8782	7960	8758	8328	8584	8285

Product Identifier	Product Name	Metop satellite	1/2025	2/2025	3/2025	4/2025	5/2025	6/2025
O3M-72.1	NRT absorbing aerosol index from PMDs	B	8846	8012	8836	8496	8686	8339
O3M-362		C	8782	7960	8758	8328	8584	8285
O3M-48.1	Offline high-resolution ozone profile	B	439	397	439	426	439	423
O3M-312		C	439	396	439	423	440	425
O3M-79	Offline absorbing aerosol height	B	439	397	439	426	439	423
O3M-365		C	439	396	439	423	440	425
O3M-73.1	Offline absorbing aerosol index from PMDs	B	439	397	439	426	439	423
O3M-363		C	439	396	439	423	440	425

Table 4.7. EUMETCast and WMO/GTS uploads³

Product Identifier	Product Name	Metop satellite	1/2025	2/2025	3/2025	4/2025	5/2025	6/2025
O3M-47.1	NRT high-resolution ozone profile	B	8846/8846	8012/8012	8836/8836	8496/8485	8686/8686	8339/8339
O3M-311		C	8782/8782	7960/7960	8758/8758	8328/8328	8584/8584	8285/8285
O3M-78	NRT absorbing aerosol height	B	8846	8012	8836	8496	8686	8339
O3M-364		C	8782	7960	8758	8328	8584	8285
O3M-72.1	NRT absorbing aerosol index from PMDs	B	8846	8012	8836	8496	8686	8339
O3M-362		C	8782	7960	8758	8328	8584	8285

¹ Products are archived in HDF5 format.

² Products are stored for 3 years (in HDF5 and BUFR formats).

³ NRT high-resolution ozone profile is disseminated via EUMETCast and WMO/GTS in BUFR format. NRT absorbing aerosol index and NRT absorbing aerosol index from PMDs are disseminated only via EUMETCast (in HDF5 and BUFR formats).

Table 4.8 lists the main events (product/service/hardware/software updates etc.) at KNMI during the reporting period.

Table 4.8. Main events at KNMI during the reporting period

Date	Description
	<i>Nothing to report.</i>

Table 4.9 lists the main local and external anomalies at KNMI during the reporting period. Corrective and preventive actions should be provided also when applicable.

Table 4.9. Main local and external anomalies affecting KNMI systems and performance during the reporting period

ID	Time period	Description
		<i>Nothing to report.</i>

5. Processing centre: DMI

5.1. NRT clear-sky and cloud-corrected UV index / Global 1-day UV index forecast

New NUV product “Global 1-day UV index forecast” (O3M-410.1) was declared operational 6 May 2025. This product replaces the two previous products “NRT UV index, clear-sky” (O3M-409) and “NRT UV index cloud-corrected” (O3M-410). Transition is reflected in the tables below. The requirements on availability and timeliness remain the same.

5.1.1. Availability

NUV product is required to be produced every day, either based on new GOME ATO input or in the case of ATO delivery failure based on back-up total ozone data (ECMWF or climatology).

Availability requirement for NUV has been defined in Section 1.4. The availability statistics of DMI products are presented in Table 5.1. If the requirement is violated, those values are marked with red colour, identified by numbers and reported in Table 5.5.

Table 5.1. Availability of NRT UV products during the reporting period

Product Identifier	Product Name	1/2025	2/2025	3/2025	4/2025	5/2025	6/2025
O3M-409	NRT UV index, clear-sky	90.3 %	100 %	100 %	100 %		
O3M-410	NRT UV index, cloud-corrected						
O3M-410.1	Global 1-day UV index forecast					100 %	96.7 %

5.1.2. Timeliness

Timeliness requirement for NUV says that the final NUV product is to be delivered to users no later than 04:00 UTC. The timeliness reported in Table 5.2 is calculated as the time difference (hours and minutes in format hh:mm) between 04:00 UTC and the time when the NUV products are available to users. Thus, **positive** values refer to situations where the timeliness requirement is violated and marked in red colour. In addition, the violations are identified by numbers and reported in Table 5.5 if they have caused the availability values to drop below the allowed limits.

Days where no products are produced or could be delivered to users (as indicated in Table 5.1) are not included in Table 5.2.

From top to bottom, the values in Table 5.2 represent observed monthly average, minimum and maximum time differences.

Table 5.2. Timeliness of NRT UV products during the reporting period

Product Identifier	Product Name	1/2025	2/2025	3/2025	4/2025	5/2025	6/2025
O3M-409	NRT UV index, clear-sky	avg: -00:49 min: -00:54 max: +01:10 (1,2)	avg: -00:54 min: -00:54 max: -00:53	avg: -00:53 min: -00:54 max: -00:53	avg: -00:53 min: -00:54 max: -00:53		
O3M-410	NRT UV index, cloud-corrected						
O3M-410.1	Global 1-day UV index forecast					avg: -00:53 min: -00:54 max: -00:52	avg: -00:44 min: -00:53 max: +01:46 (3)

5.2. Services, main events and anomalies

Table 5.3. Number of products stored locally at DMI¹

Description of service / event	1/2025	2/2025	3/2025	4/2025	5/2025	6/2025
Storage statistics						
Number of stored products (NRT UV index, clear-sky)	31	28	31	30		
Number of stored products (NRT UV index, cloud-corrected)	31	28	31	30		
Total size of stored products (MB)	248	224	248	240		
Number of stored products (Global 1-day UV index forecast)					31	30
Total size of stored products (GB)					2.73	2.64

¹ NUV products are stored at the DMI at least until the end of the Metop programs.

Table 5.4 lists the main events (product/service/hardware/software updates etc.) at DMI during the reporting period.

Table 5.4. Main events at DMI during the reporting period

Date	Event
6 May	Global 1-day UV index forecast declared operational
28 June	Operational delivery of data for a new user “Municipality of Aarhus” begins

Table 5.5 lists the main local and external anomalies at DMI during the reporting period. Corrective and preventive actions should be provided also when applicable.

Table 5.5. Main local and external anomalies affecting DMI systems and performance during the reporting period

ID	Time period	Description
1	31 December 2024 – 3 January 2025	<p>An end-of-year diagnostic tool was for unknown reasons running in endless loop and caused the transfer of NUV product to the web server to fail. The product was produced and archived but not transferred to users. The problem was solved 3 January and product delivered with a 70-minute delay.</p> <p>Corrective action: The failed diagnostic tool was stopped</p> <p>Preventive action: In the future, the tool shall only be manually executed during daytime</p>
2	5 January	<p>The DMI web server was full, caused by other applications. NUV was produced but not available for users.</p> <p>Corrective action: IT cleaned space on the web server</p> <p>Preventive action: Some applications were moved to other sites and automatic clean-up procedure was initiated</p>
3	14 June	<p>The crontab file for the NUV operator was gone, so no jobs were executed. Crontab file was restored and products delivered with a 1h 45min delay.</p> <p>Corrective action: Crontab table restored from backup and processing performed manually</p> <p>Preventive action: The cause of the loss of the crontab file has not been understood and never seen before. Thus, no preventive action could be taken.</p>

6. Processing centre: EUMETSAT

6.1. NRT IASI CO, SO₂, HNO₃ and ozone profile

6.1.1. Availability

For Level 1c products, the availability is defined as the number of available PDUs divided by the number of maximum expected PDUs.

For NRT products, the availability requirement is 97.5 % and it is defined by the ratio of the number of in time processed and disseminated products to the number of maximum expected input products (L1c PDUs) per month.

The availability statistics of EUMETSAT products are presented in Table 6.1 and Table 6.2. If the availability requirements have been violated, those values are marked with **red** colour, identified by numbers and reported in Table 6.7 and/or Table 6.8.

Note that in the frame of this product processing centre being the EUMETSAT HQ in Darmstadt, the L1c data is directly available to the L2+ algorithm, i.e., its availability is not dependable of EUMETCast dissemination, which can sometimes be translated into higher L2+ availability than the applicable L1c, depending on the data which has been successfully disseminated. Furthermore, since there is no relay of information from *Satellite* processing centres, the L2 product availability in the following tables concern the end-to-end availability as they were recorded in the EUMETSAT Reference Receiving Stations.

Table 6.1. Availability of Metop-B L1c PDUs and IASI NRT products during the reporting period

Product Identifier	Product Name	1/2025	2/2025	3/2025	4/2025	5/2025	6/2025
L1c	PDUs available / PDUs expected	14738/14880	13361/13440	14872/14880	14304/14400	14880/14880	14304/14400
L1c	Availability	99.1 %	99.4 %	100 %	99.3 %	100 %	99.3 %
O3M-80	NRT IASI CO	99.0 %	99.4 %	100 %	99.1 %	100 %	99.3 %
O3M-57	NRT IASI SO ₂	99.0 %	99.4 %	100 %	99.1 %	100 %	99.3 %
O3M-81	NRT IASI HNO ₃	99.0 %	99.4 %	100 %	99.1 %	100 %	99.3 %
O3M-49	NRT IASI ozone profile	99.0 %	99.4 %	100 %	99.1 %	100 %	99.3 %

Table 6.2. Availability of Metop-C L1c PDUs and IASI NRT products during the reporting period

Product Identifier	Product Name	1/2025	2/2025	3/2025	4/2025	5/2025	6/2025
L1c	PDUs available / PDUs expected	14625/14880	13438/13440	14717/14880	14202/14400	14799/14880	14362/14400
L1c	Availability	98.3 %	100 %	98.9 %	98.6 %	99.5 %	99.7 %
O3M-352	NRT IASI CO	98.3 %	99.9 %	98.9 %	98.6 %	99.5 %	99.7 %
O3M-377	NRT IASI SO2	98.3 %	99.9 %	98.9 %	98.6 %	99.5 %	99.7 %
O3M-336	NRT IASI HNO3	98.3 %	99.9 %	98.9 %	98.6 %	99.5 %	99.7 %
O3M-315	NRT IASI ozone profile	98.3 %	99.9 %	98.9 %	98.6 %	99.5 %	99.7 %

6.1.2. Timeliness

Timeliness indicates the elapsed time between sensing and product dissemination. Timeliness requirement is 3 hours for NRT products. If the requirements have been violated, those values are marked with red colour. In addition, the violations are identified by numbers and reported in Table 6.8 if they have caused the availability values to drop below the allowed limits.

Note: timeliness violations are not listed as anomalies if the availability is above the limit.

The values in Table 6.3 and Table 6.4 indicate elapsed times (hours and minutes in the format hh:mm) from sensing to EUMETCast Reference Receiving Station, i.e., end-to-end timeliness. In each cell, the values from top to bottom represent observed monthly average, minimum and maximum times.

Table 6.3. Timeliness of Metop-B IASI NRT products during the reporting period

Product Identifier	Product Name	1/2025	2/2025	3/2025	4/2025	5/2025	6/2025
O3M-80	NRT IASI CO	avg: 01:02 min: 00:35 max: 02:51	avg: 01:04 min: 00:35 max: 01:49	avg: 01:06 min: 00:36 max: 01:51	avg: 01:00 min: 00:33 max: 02:55	avg: 01:00 min: 00:31 max: 01:49	avg: 01:00 min: 00:31 max: 02:10
O3M-57	NRT IASI SO2	avg: 01:02 min: 00:35 max: 02:52	avg: 01:04 min: 00:35 max: 01:49	avg: 01:06 min: 00:36 max: 01:51	avg: 01:00 min: 00:33 max: 02:55	avg: 01:00 min: 00:31 max: 01:49	avg: 01:00 min: 00:31 max: 02:10
O3M-81	NRT IASI HNO3	avg: 01:02 min: 00:35 max: 02:52	avg: 01:04 min: 00:35 max: 01:49	avg: 01:06 min: 00:36 max: 01:51	avg: 01:00 min: 00:33 max: 02:55	avg: 01:00 min: 00:31 max: 01:49	avg: 01:00 min: 00:31 max: 02:10
O3M-49	NRT IASI ozone profile	avg: 01:02 min: 00:35 max: 02:52	avg: 01:04 min: 00:35 max: 01:49	avg: 01:06 min: 00:36 max: 01:51	avg: 01:00 min: 00:33 max: 02:56	avg: 01:00 min: 00:31 max: 01:49	avg: 01:00 min: 00:31 max: 02:10

Table 6.4. Timeliness of Metop-C IASI NRT products during the reporting period

Product Identifier	Product Name	1/2025	2/2025	3/2025	4/2025	5/2025	6/2025
O3M-352	NRT IASI CO	avg: 01:34 min: 00:55 max: 02:57	avg: 01:37 min: 00:57 max: 02:15	avg: 01:39 min: 00:57 max: 02:25	avg: 01:37 min: 00:54 max: 03:09	avg: 01:39 min: 00:45 max: 02:20	avg: 01:37 min: 00:54 max: 02:18
O3M-377	NRT IASI SO ₂	avg: 01:34 min: 00:55 max: 02:57	avg: 01:37 min: 00:57 max: 02:14	avg: 01:39 min: 00:57 max: 02:25	avg: 01:37 min: 00:54 max: 03:09	avg: 01:39 min: 00:45 max: 02:20	avg: 01:37 min: 00:54 max: 02:18
O3M-336	NRT IASI HNO ₃	avg: 01:34 min: 00:55 max: 02:57	avg: 01:37 min: 00:57 max: 02:15	avg: 01:39 min: 00:57 max: 02:25	avg: 01:37 min: 00:54 max: 03:09	avg: 01:39 min: 00:45 max: 02:20	avg: 01:37 min: 00:54 max: 02:18
O3M-315	NRT IASI ozone profile	avg: 01:34 min: 00:55 max: 02:57	avg: 01:37 min: 00:57 max: 02:14	avg: 01:39 min: 00:57 max: 02:25	avg: 01:37 min: 00:54 max: 03:09	avg: 01:39 min: 00:45 max: 02:20	avg: 01:37 min: 00:54 max: 02:18

6.2. Services, main events and anomalies

Table 6.5. Number of products stored locally at EUMETSAT¹

Product Identifier	Product Name	Metop satellite	1/2025	2/2025	3/2025	4/2025	5/2025	6/2025
O3M-80	NRT IASI CO	B	14732	13361	14873	14268	14879	14304
O3M-352		C	14626	13431	14718	14206	14798	14363
O3M-57	NRT IASI SO ₂	B	14732	13361	14874	14268	14879	14303
O3M-377		C	14626	13431	14717	14206	14798	14363
O3M-81	NRT IASI HNO ₃	B	14732	13361	14874	14268	14879	14303
O3M-336		C	14625	13430	14716	14205	14798	14362
O3M-49	NRT IASI ozone profile	B	14732	13361	14874	14268	14879	14303
O3M-315		C	14626	13431	14717	14206	14798	14363

¹ PDUs are concatenated back to orbit-based products before being stored

Table 6.6. EUMETCast uploads¹

Product Identifier	Product Name	Metop satellite	1/2025	2/2025	3/2025	4/2025	5/2025	6/2025
O3M-80	NRT IASI CO	B	14732	13361	14873	14268	14879	14304
O3M-352		C	14626	13431	14718	14206	14798	14363
O3M-57	NRT IASI SO2	B	14732	13361	14874	14268	14879	14303
O3M-377		C	14626	13431	14717	14206	14798	14363
O3M-81	NRT IASI HNO3	B	14732	13361	14874	14268	14879	14303
O3M-336		C	14625	13430	14716	14205	14798	14362
O3M-49	NRT IASI ozone profile	B	14732	13361	14874	14268	14879	14303
O3M-315		C	14626	13431	14717	14206	14798	14363

¹ NRT IASI products are disseminated via EUMETCast (in BUFR format)

Table 6.7 lists the main events (product/service/hardware/software updates etc.) at EUMETSAT during the reporting period.

Table 6.7. Main planned activities at EUMETSAT during the reporting period

ID	Date	Description
1		<i>Nothing to report.</i>

Table 6.8 lists the main local and external anomalies at EUMETSAT during the reporting period. Corrective and preventive actions should be provided also when applicable.

Table 6.8. Main local and external anomalies affecting EUMETSAT systems and performance during the reporting period

ID	Time period	Description
1		<i>Nothing to report.</i>

7. Validation and quality monitoring

This section describes the validation status and validation/quality monitoring activities of NRT and offline data products during the reporting period. Validation reports for data records are found from <https://acsaf.org/valreps.html>

Reference documents are listed in Section 1.3 and accuracy requirements in Section 1.5.

7.1. GOME-2 total ozone column products

Table 7.1. Validation status of total ozone column products

Product Identifier	Product Name	Accuracy	Reference	Validating Institute	Correlative data sources
O3M-41.1	NRT total O3	Fulfils threshold accuracy requirement	RD4	AUTH	World Ozone Mapping Centre
O3M-300			RD23		
O3M-06.1	Offline total O3	Fulfils threshold accuracy requirement	RD4	AUTH	World Ozone and Ultraviolet Radiation Data Center (WOUDC), of the World Meteorological Organization, (WMO), Global Atmosphere Watch, (GAW)
O3M-42.1			RD4		
O3M-301			RD23		

Validation results can be found in more detail on the AC SAF validation & quality assessment website at http://acsaf.physics.auth.gr/eumetsat/validation/near_real and <http://acsaf.physics.auth.gr/eumetsat/validation/offline>

7.1.1. Total ozone column validation

This summary presents the validation activities for total ozone column products (TOCs), reported by the GOME-2/Metop-B and GOME-2/Metop-C instruments (hereafter GOME-2B and GOME-2C, respectively). Members of the Laboratory of Atmospheric Physics of the Aristotle University of Thessaloniki ([LAP/AUTH](#)), Thessaloniki, Greece, involved in the validation activities include Professor, Dr. Dimitris Balis, Special Teaching Fellow & Researcher, Dr. Katerina Garane and Research Associate, Dr. MariLiza Koukouli.

During the reporting period, the operational validation of offline total ozone and NRT total ozone products continued as per previous periods.

7.1.1.1 Update of database for reference ground-based data

For the nominal validation, the ground-based TOCs from Brewer, Dobson and M-124 instruments reported to the World Ozone and Ultraviolet Radiation Data Centre ([WOUDC](#)), are employed. WOUDC is one of the World Data Centres which are part of the Global Atmosphere Watch ([GAW](#)) programme of the World Meteorological Organization ([WMO](#)). For the quality of the reference ground-based data used for the validation of the total ozone products, updated information were extracted from recent inter-comparisons and calibration records. This continuously updated selection of ground-based measurements has already been used numerous times in the validation and analysis of global total ozone records such as the inter-comparison between the OMI/Aura TOMS and OMI/Aura DOAS algorithms [Balis *et al.*, 2007a], the validation of ten years of GOME/ERS-2 ozone record [Balis *et al.*, 2007b], the validation of the updated version of the OMI/Aura TOMS algorithm [Antón *et al.*, 2009], the GOME-2/Metop-A validation [Loyola *et al.*,

2011; Koukouli *et al.*, 2012], the GOME-2B validation [Hao *et al.*, 2014] and the evaluation of the European Space Agency's Ozone Climate Change Initiative project [O₃-CCI] TOCs [Koukouli *et al.*, 2015, Garane *et al.*, 2018], as well as in TROPOMI/S5P TOCs validation [Garane *et al.*, 2019]. In all the aforementioned works, LAP/AUTH assumes the leading role in the validation efforts. The number of WOUDC ground-based stations used in the full operational periods of the two instruments, alongside the mean difference between ground- and space-based TOC estimates is given in Table 7.2.

The comparisons and validation results with respect to the M-124 instruments are available via the [validation website](#), but not shown herein for reasons of brevity.

7.1.1.2 Validation results for the offline total ozone products

GOME-2B and GOME-2C OTO data for the period December 2012 (or January 2019 for GOME-2C) to June 2025 have been downloaded, quality-assured and pre-processed in order to perform the validation strategies. The GDP-4.8 algorithm is the latest version of the GDP-4.x suite of algorithms that have been used for the operational processing of GOME-2B total ozone columns. GOME-2C is processed with GDP-4.9. The main differences between GDP-4.8 and GDP-4.9 concern the SO₂ vertical column retrieval. For ozone only minor updates have been performed, such as the optimization of the slit function, the introduction of a pseudo absorber for possible orbital variations of the resolution etc. Therefore, the ozone columns from GOME-2C can be assumed to be similar to the respective data from GOME-2B, analysed with the previous version of the algorithm.

This period's satellite-to-ground-based measurements comparisons were performed and added to the existing time series. The majority of the quality-assured ground-based Brewer and Dobson TOCs are reported to the WOUDC repository between 3 and 6 months after measurement, which accounts for the last couple of months missing from the comparative plots shown below. This is a common reporting feature, quite unavoidable.

In Figure 7.1, left column of figures, the status of GOME-2B and GOME-2C TOCs since the beginning of each individual mission is shown in the form of a monthly mean time-series of the percentage differences between each sensor and ground-based observations. Panel (a) shows the co-locations with Brewer Northern Hemisphere (NH) stations, panel (c) with Dobson NH stations and panel (e) with Dobson Southern Hemisphere (SH) stations. The plots in the right column of Figure 7.1 (panels (b), (d) and (f)) illustrate the overlapping period of operation of the GOME-2B and GOME-2C sensors, beginning in 2019 and continuing thereafter.

As expected, the seasonality in the differences between satellite and ground-based observations is more pronounced in the Dobson co-locations (panels c – f) and is a prominent feature which appears in most operational and scientific satellite TOC comparisons, see for e.g. the validation of the OMI/Aura products [Balis *et al.*, 2007a], the GOME/ERS-2 product [Balis *et al.*, 2007b] and even the recent GOME/ERS-2, SCIAMACHY/Envisat and GOME-2A ESA products [Koukouli *et al.*, 2015, Garane *et al.*, 2018]. The underlying causes stem from the methodology used to handle the variability of the stratospheric temperature and its subsequent influence on the ozone absorption coefficients used in the various algorithms [Fragkos *et al.*, 2013; Serdyuchenko *et al.*, 2014]. Hence, when the stratospheric temperature deviates strongly from what is assumed by the algorithms, which is usually the case during the winter months, the differences between ground and satellite increase. See the work of Koukouli *et al.*, 2016, and discussion therein, on this topic.

The well-known reason for the Dobson total ozone seasonality could be treated following a methodology (see Komhyr *et al.*, 1993 and Koukouli *et al.*, 2016) that is utilized by the LAP/AUTH validation chain to post-correct the Dobson ground-based measurements for their effective temperature dependence, but the correction is always dependent on the temperature dataset that is

used for its implementation. Additionally, the official repositories such as WOUDC do not provide temperature corrected data and to keep our validation analysis compatible with other studies and validation reports on various other sensors, it was chosen to use the Dobson ground-based dataset as originally provided by WOUDC.

The ranges of the monthly mean percentage differences between each sensor and their respective collocated ground-based observations are as follows:

GOME-2B

- From the beginning of the record until 2022, differences range between -1 and +3 %.
- From 2022 onward, a continuous decline is observed, reaching approximately -4 % by June 2025

GOME-2C

- During the first year of the GOME-2C operation, differences range from 0 % to +2.5 %
- After March 2020, this range shifts upward to approximately +1.5 to +4 %
- A subsequent decline is observed from mid-2023, with differences decreasing by ~ -1 to -1.5 % depending on the season and the ground-based reference

All the aforementioned ranges depend on the season and the ground-based reference.

Agreement between the two sensors

Using the ground-based measurements as a common reference, Figure 7.1 reveals a noticeable difference in the agreement levels between the two sensors in the NH, with a clear shift occurring around spring 2020:

- Before that point, the deviation between the two sensors was minimal, ranging from ~ 0 – 1 %. During that time, GOME-2C reported higher TOCs than GOME-2B, particularly in the summer months, with differences reaching up to ~0.8 %.
- From March 2020 until mid-2023, the deviation between the two sensors gradually increased, reaching levels up to ~4 %. This difference is especially pronounced during summer months. Throughout this period, GOME-2B continuously reported lower TOCs than GOME-2C and their deviation shows a seasonal dependence:
 - It is lower during winter months (e.g. ~0.5 % in January 2020 going up to ~3 % in December 2024), and
 - higher during summer months (e.g. ~1.6 % in June 2020 and up to ~4 % in July 2024)

A similar pattern is observed in the SH (panels c and f), starting also since March or April 2020:

- This increased deviation between the two sensors is especially pronounced during the local spring-summer months, going up to ~3.5 % in December 2024, and
- as in the NH, GOME-2B continuously reports lower TOCs than GOME-2C, during this period

The observation that GOME-2B total ozone retrievals have been continuously decreasing since early 2020 is also supported by direct satellite-to-satellite comparisons (not shown here) and is currently under investigation by the algorithm team. In parallel, the team is assessing a potentially evolving pattern in the GOME-2C total ozone retrievals.

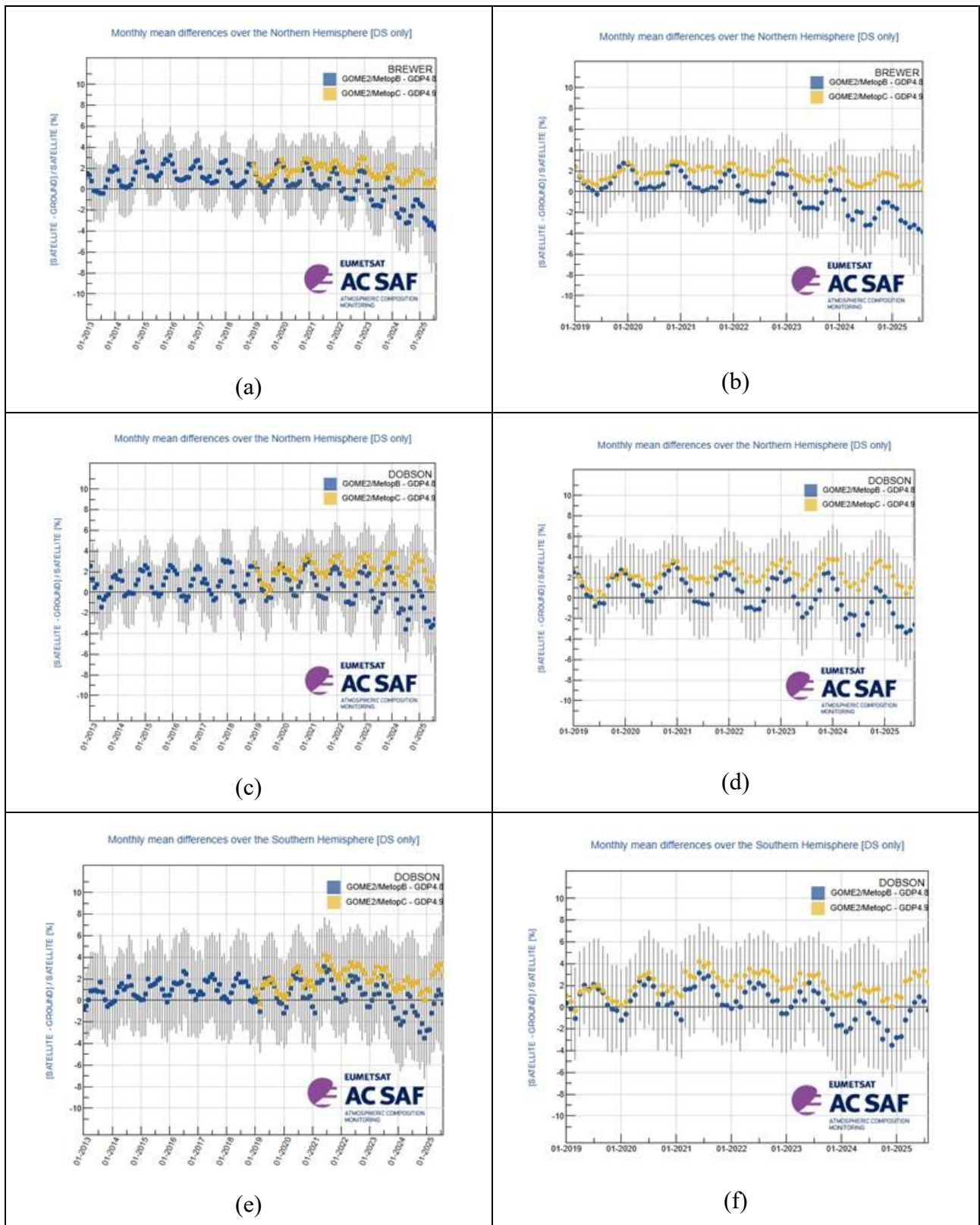


Figure 7.1. Hemispherical time-series of the monthly mean percentage differences between GOME-2B GDP-4.8 (blue symbols) and GOME-2C GDP-4.9 (orange symbols) total ozone products against ground-based observations. Panels a – d: Northern Hemisphere, panels e and f: Southern Hemisphere. Brewer co-locations are shown in panels a and b (Northern Hemisphere only). Dobson co-locations are

shown in panels c – f. The difference between the left and the right column of figures is the time period covered.

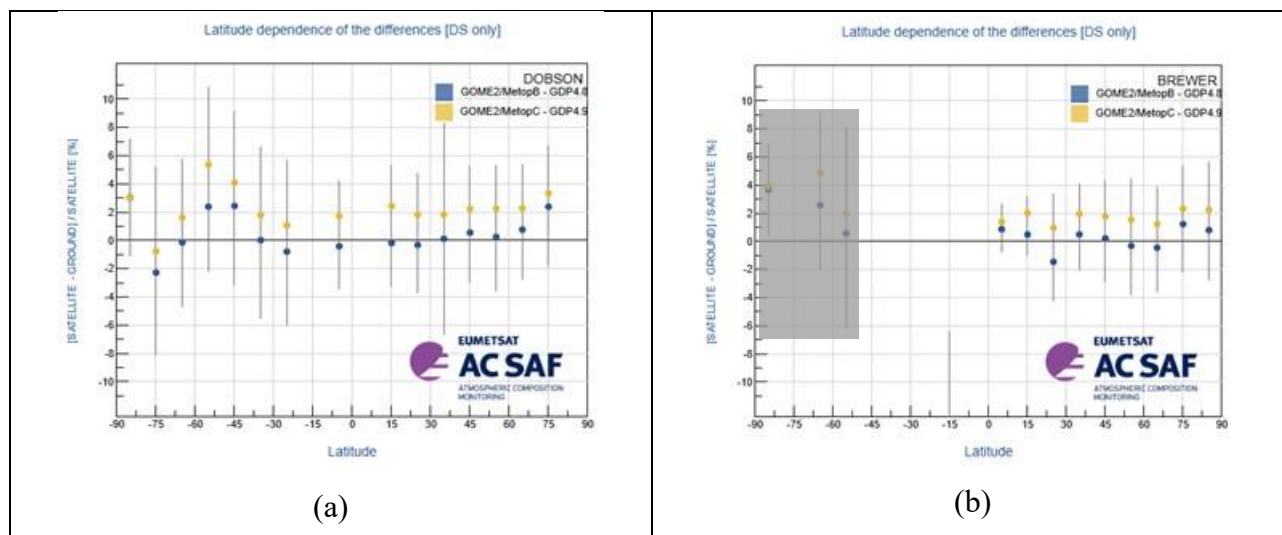


Figure 7.2. The latitudinal dependency of the differences for the Dobson (panel a) and the Brewer network (panel b). The Brewer SH mean biases are greyed out because the limited number of stations in this part of the Earth cannot provide reliable validation results.

The detected drift between the two GOME-2 instruments is likely caused by the degradation of the L1 data. For the ozone slant column density (SCD) fit, the algorithm team incorporated two pseudo absorbers into the non-operational DOAS retrieval, which improved the observed drift in the SCDs between the two instruments. A large-scale test within the official testing environment is being prepared, which will also include the AMF component. Once a reasonable amount of data has been processed, they will be provided to AUTH for comparison to ground based observations. Based on a successful validation phase, the updated dataset will be released as operational product.

In the latitudinal plot (Figure 7.2), it is shown that the overall agreement of both sensors to the ground-based measurements is within 0 – 2 % in the tropics and mid-latitudes. Additionally, it is noticeable that the comparisons of GOME-2C with respect to ground-based measurements have almost no dependency on latitude, having a very stable relative mean bias of ~2 % for the NH stations and for co-locations northwards ~40°S. The TOC underestimation of GOME-2B with respect to GOME-2C is also shown to be global, but it appears to be more evident for the mid-latitudes and the tropics, where GOME-2B reports lower TOCs by about 1 – 2 % with respect to GOME-2C.

It should be noted that the co-locations used in Figure 7.2 cover the time-period of the two sensors operating in tandem, since January 2019. The respective latitudinal plot made with co-locations covering only 2024 and 2025 (not shown here), when the divergence between the two sensors is stronger, indicates that these recently increased differences between the GOME-2B and GOME-2C total ozone observations result almost equally from all latitude belts.

7.1.1.3 Tables of statistics

In Table 7.2, the summary statistics for the GOME-2B and GOME-2C comparisons against co-located total ozone observations from the Dobson and Brewer stations presented in the previous section, are enumerated. The number of individual daily common observations for the Dobsons apply to the entire globe, whereas the Brewer comparisons depict only the NH.

The relative differences between GOME-2B and the Brewer and Dobson stations are notably stable, exhibiting an average mean difference of about $+0.5 \pm 4.5$ %. GOME-2C shows a higher mean relative bias with respect to ground-based measurements, ranging from $+1.6$ to $+2.1 \pm 4.6$ %. Nonetheless, **both total ozone products remain well within the product accuracy requirements (4 % for SZA < 80° and 8 % for SZA > 80°).**

Table 7.2. Summary statistics for the respective time period of operation of each sensor, based on GOME-2B and GOME-2C OTO data compared to WOUDC Brewer & Dobson observations

		Brewer	Dobson
GOME-2B 01/2013 – 06/2025	# stations:	70	64
	# obs:	199 400	137 300
	Mean Rel. Bias (%):	0.3 ± 4.4	0.6 ± 4.9
	Compliance with the product requirements:		
	Mean Rel. Bias for SZA ≤ 80°:	0.6 %	0.6 %
	Mean Rel. Bias for SZA > 80°:	1.0 %	1.9 %
GOME-2C 01/2019 – 06/2025	# stations:	57	52
	# obs:	92 310	61 650
	Mean Rel. Bias (%):	1.3 ± 4.2	2.3 ± 5.0
	Compliance with the product requirements:		
	Mean Rel. Bias for SZA ≤ 80°:	1.6 %	2.1 %
	Mean Rel. Bias for SZA > 80°:	2.7 %	3.4 %

7.1.1.4 Validation results for the NRT total ozone products

The GOME-2B and GOME-2C NRT total ozone products are continuously validated against Brewer and Dobson TOCs routinely deposited in the World Meteorological Organisation (WMO) [Ozone Mapping Centre](#), also hosted by the Laboratory of Atmospheric Physics, AUTH. The comparative datasets that cover the last two-three years of observations, are updated weekly and they are operationally available by the [online quality monitoring tool operated by AUTH](#). Some indicative plots are shown in Figure 7.3.

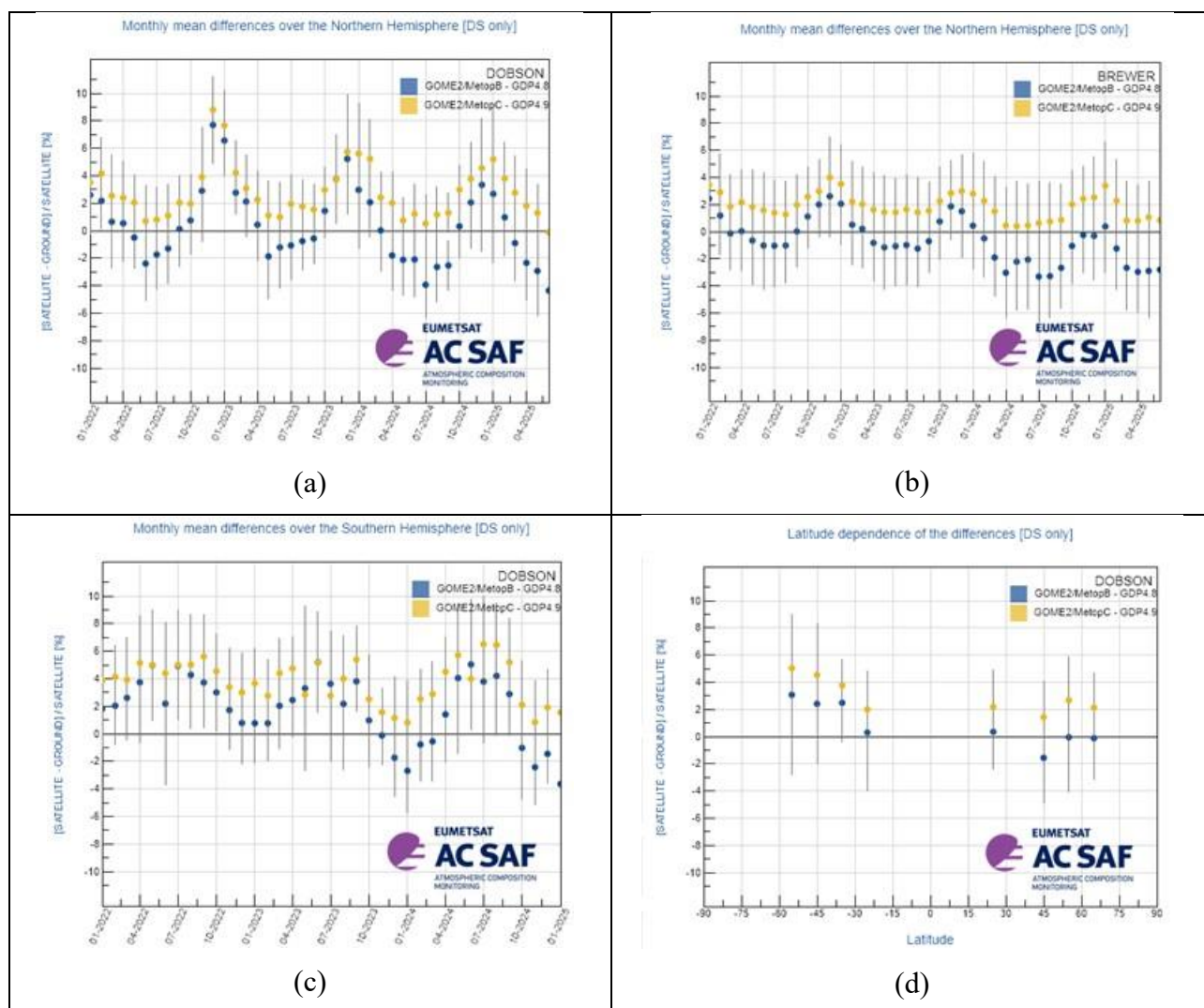


Figure 7.3. The percentage differences of the GOME-2B (blue) and GOME-2C (orange) NRT total ozone observations against the Dobson (panels a, c, and d) and Brewer (panel b) ground-based co-located measurements. Panels (a) and (c) show the Dobson NH (panel a) and SH (panel c) monthly mean time-series. Panel (b) shows the Brewer NH monthly mean time-series. The Dobson latitudinal dependency plot is shown in panel (d), made with co-locations since January 2022.

7.1.2. Validation website

The [AC SAF Ozone Validation & Quality Assessment](#) was launched on the initiation of the project's CDOP 2 phase in 2013. The validation webpages host the validation results of GOME-2A GDP-4.8, GOME-2B GDP4.8 and GOME-2C GDP4.9 near real-time and offline total ozone data. Currently, the validation results are available until September 2025 (NRT ground-based dataset).

The validation website will soon include validation results for the IASI CDR total ozone dataset, processed and were made available by EUMETSAT in early September 2025. Currently, the adjustment of the validation chain to ingest IASI is in progress.

The website and the processing algorithms that run behind it are routinely inspected and quality controlled. All the necessary actions, needed to keep it at its current good state, are taken by the LAP/AUTH team.

References:

Antón, M., Loyola, D., López, M., Vilaplana, J. M., Bañón, M., Zimmer, W., and Serrano, A.: Comparison of GOME-2/MetOpA total ozone data with Brewer spectroradiometer data over the Iberian Peninsula, *Annales Geophysicae*, 27, 1377–1386, 2009.

<https://doi.org/10.5194/angeo-27-1377-2009>

Balis, D., Kroon M., Koukouli, M.E., Brinksma, E. J., Labow, G., Veeffkind, J. P., and McPeters, R. D.: Validation of Ozone Monitoring Instrument total ozone column measurements using Brewer and Dobson spectrophotometer ground-based observations, *J. Geophys. Res.*, 112, D24S46, 2007a.

<https://doi.org/10.1029/2007JD008796>

Balis, D., Lambert, J.-C., Van Roozendaal, M., Spurr, R., Loyola, D., Livschitz, Y., Valks, P., Amiridis, V., Gerard, P., Granville, J., and Zehner, C.: Ten years of GOME/ERS-2 total ozone data – The new GOME data processor (GDP) version 4: 2. Ground-based validation and comparisons with TOMS V7/V8, *J. Geophys. Res.*, vol. 112, D07307, 2007b.

<https://doi.org/10.1029/2005JD006376>

Fragkos, K., Bais, A. F., Balis, D., Meleti, C., and Koukouli, M. E.: The effect of three different absorption cross-sections and their temperature dependence on total ozone measured by a mid-latitude Brewer spectrophotometer, *Atmos. Ocean*, 53, 2015.

<https://doi.org/10.1080/07055900.2013.847816>

Hao, N., Koukouli, M. E., Inness, A., Valks, P., Loyola, D. G., Zimmer, W., Balis, D. S., Zyrichidou, I., Van Roozendaal, M., Lerot, C., and Spurr, R. J. D.: GOME-2 total ozone columns from MetOp-A/MetOp-B and assimilation in the MACC system, *Atmos. Meas. Tech.*, 7, 2937–2951, 2014.

<https://doi.org/10.5194/amt-7-2937-2014>

Koukouli, M. E., Balis, D. S., Loyola, D., Valks, P., Zimmer, W., Hao, N., Lambert, J.-C., Van Roozendaal, M., Lerot, C., and Spurr, R. J. D.: Geophysical validation and long-term consistency between GOME-2/MetOp-A total ozone column and measurements from the sensors GOME/ERS-2, SCIAMACHY/ENVISAT and OMI/Aura, *Atmos. Meas. Tech.*, 5, 2169–2181, 2012.

<https://doi.org/10.5194/amt-5-2169-2012>

Koukouli, M. E., Lerot, C., Granville, J., Goutail, F., Lambert, J.-C., Pommereau, J.-P., Balis, D., Zyrichidou, I., Van Roozendaal, M., Coldewey-Egbers, M., Loyola, D., Labow, G., Frith, S., Spurr, S., and Zehner, C.: Evaluating a new homogeneous total ozone climate data record from GOME/ERS-2, SCIAMACHY/Envisat and GOME-2/MetOp-A, *J. Geophys. Res. Atmos.*, 120, 12296–12312, 2015.

<https://doi.org/10.1002/2015JD023699>

Koukouli, M. E., Zara, M., Lerot, C., Fragkos, K., Balis, D., van Roozendaal, M., Allart, M. A. F., and van der A, R. J.: The impact of the ozone effective temperature on satellite validation using the Dobson spectrophotometer network, *Atmos. Meas. Tech.*, 9, 2055–2065, 2016.

<https://doi.org/10.5194/amt-9-2055-2016>

Loyola, D. G., Koukouli, M. E., Valks, P., Balis, D. S., Hao, N., Van Roozendaal, M., Spurr, R. J. D., Zimmer, W., Kiemle, S., Lerot, C., and Lambert, J.-C.: The GOME-2 total column ozone product: Retrieval algorithm and ground-based validation, *J. Geophys. Res.*, 116, 2011.

<https://doi.org/10.1029/2010JD014675>

Serdyuchenko, A., Gorshelev, V., Weber, M., Chehade, W., and Burrows, J. P.: High spectral resolution ozone absorption cross-sections – Part 2: Temperature dependence, *Atmos. Meas. Tech.*, 7, 625–636, 2014.

<https://doi.org/10.5194/amt-7-625-2014>

Garane, K., Lerot, C., Coldewey-Egbers, M., Verhoelst, T., Koukouli, M. E., Zyrichidou, I., Balis, D. S., Danckaert, T., Goutail, F., Granville, J., Hubert, D., Keppens, A., Lambert, J.-C., Loyola, D., Pommereau, J.-P., Van Roozendael, M., and Zehner, C.: Quality assessment of the Ozone_cci Climate Research Data Package (release 2017) – Part 1: Ground-based validation of total ozone column data products, *Atmos. Meas. Tech.*, 11, 1385-1402, 2018.

<https://doi.org/10.5194/amt-11-1385-2018>

Garane, K., Koukouli, M.-E., Verhoelst, T., Lerot, C., Heue, K.-P., Fioletov, V., Balis, D., Bais, A., Bazureau, A., Dehn, A., Goutail, F., Granville, J., Griffin, D., Hubert, D., Keppens, A., Lambert, J.-C., Loyola, D., McLinden, C., Pazmino, A., Pommereau, J.-P., Redondas, A., Romahn, F., Valks, P., Van Roozendael, M., Xu, J., Zehner, C., Zerefos, C., and Zimmer, W.: TROPOMI/S5P total ozone column data: global ground-based validation and consistency with other satellite missions, *Atmos. Meas. Tech.*, 12, 5263–5287, 2019.

<https://doi.org/10.5194/amt-12-5263-2019>

7.1.3. Online quality monitoring

The online quality monitoring tool is operational and consists of the continuous generation of plots showing the slant column density (SCD) distribution, the vertical column density (VCD) distribution as well as the root mean square (RMS) as histograms per sensing day as well as time series per sensing month. These plots are generated for three different geographic regions, the Pacific ocean (25-15S, 210-250E), the Sahara desert (20-30N, 0-30E) and global, in order to represent typical extremes of ground reflectivity and atmospheric conditions as well as the global mean. The plots are generated per sensing instrument (GOME-2B, GOME-2C) and per product (O₃, NO₂, BrO, HCHO, SO₂, H₂O).

The online quality monitoring plots are published in PDF format on the DLR AC SAF FTP server (acsaf.eoc.dlr.de) using the following directory schemes:

```
/oq/GOME-2[BC]/[O3 NO2 BrO HCHO SO2 H2O]/daily/YYYY/MM/DD/[global sahara  
pacific]/*. [vcd scd rms]_hist.pdf
```

```
/oq/GOME-2[BC]/[O3 NO2 BrO HCHO SO2 H2O]/monthly/YYYY/MM/[global sahara pacific]/  
*. [vcd scd rms]_series.pdf
```

In addition, the quality of the GOME_2 data can also be visually inspected from the DLR-trace calendar: <https://atmos.eoc.dlr.de/app/missions/gome2> shows the most recent results. Previous results can be found at <https://atmos.eoc.dlr.de/app/calendar> (please make sure you selected the right instrument). For some users the calendar seems to be the more convenient or reliable status information. So, in the near future we will discontinue the online quality tool and provide the calendar only.

More information about quality monitoring of the operational GOME-2 total ozone columns by other AC SAF and external partners is available at the following websites:

<https://acsaf.org> → Validation & QA → QM websites

http://acsaf.physics.auth.gr/eumetsat/validation/near_real

<http://acsaf.physics.auth.gr/eumetsat/validation/offline>

<https://www.temis.nl/acsaf/vod.php>

7.2. GOME-2 tropospheric ozone products

Table 7.3. Validation status of tropospheric ozone products

Product Identifier	Product Name	Accuracy	Reference	Validating Institute	Correlative data sources
O3M-35	Offline tropical tropospheric ozone	Fulfils target accuracy requirement	RD16	KMI	Ozonesonde data from SHADOZ , NDACC , NILU and WOUDC
O3M-43					
O3M-302			RD20		
O3M-174	NRT global tropospheric ozone	Fulfils target accuracy requirement	RD17	KMI	Ozonesonde data from SHADOZ , NDACC , NILU and WOUDC
O3M-304			RD21		
O3M-173	Offline global tropospheric ozone	Fulfils target accuracy requirement	RD17	KMI	Ozonesonde data from SHADOZ , NDACC , NILU and WOUDC
O3M-175					
O3M-305			RD21		

Validation activities summary for global tropospheric ozone:

This summary contains validation results of the GOME-2B and GOME-2C high resolution (HR) global tropospheric ozone column (TrOC) products, retrieved by the Ozone Profile Retrieval Algorithm (OPERA) at KNMI. It covers the time period July 2024 – June 2025. Validation results are shown from two TrOC products, i.e. the tropopause related product and a fixed altitude TrOC product. The TrOC products are derived from the daily operational ozone profile product.

Since these TrOC products are derived from the OPERA ozone profile product, OPERA averaging kernel smoothing has been applied to the ground-based reference profiles before calculating comparison statistics. This AVK smoothing is expected to reduce the vertical smoothing difference error between satellite and ground-based measurements. The outcome is summarized at the end of this section.

The global tropospheric ozone column (TrOC) product has the following user requirements:

- Threshold accuracy: within 50 %
- Target accuracy: within 20 %
- Optimal accuracy: within 15 %

This summary was made available by Dr. Andy Delcloo from KMI. More information on how these values are extracted is available in the [validation report](#). The collocation data used are the same as for the ozone profiles (Figure 7.23).

The statistics on the accuracy of the GOME-2B and GOME-2C HR tropospheric ozone column products (tropopause related) for different latitude belts, validated against $X_{AVK-sonde}$, are shown in Table 7.4 and Table 7.5.

Table 7.4. Relative differences (RD) and standard deviation (STDEV) are shown (in percent) together with the absolute difference (DU) on the accuracy of the GOME-2B HR tropospheric ozone column products (tropopause related) for five different latitude belts, validated against X_{AVK-sonde}

July 2024 – June 2025	GOME-2B HR			
	RD (%)	STDEV (%)	AD (DU)	STDEV (DU)
Northern Polar Region	-5.79	25.9	-1.01	7.14
Northern Mid-Latitudes	12.0	33.0	3.69	9.35
Tropical region	46.0	56.7	10.5	11.4
Southern Mid-Latitudes	3.91	30.1	0.81	6.10
Southern Polar Region	9.76	66.5	-0.71	6.75

Table 7.5. Relative differences (RD) and standard deviation (STDEV) are shown (in percent) together with the absolute difference (DU) on the accuracy of the GOME-2C HR tropospheric ozone column products (tropopause related) for five different latitude belts, validated against X_{AVK-sonde}

July 2024 – June 2025	GOME-2C HR			
	RD (%)	STDEV (%)	AD (DU)	STDEV (DU)
Northern Polar Region	-4.39	15.6	-0.90	5.76
Northern Mid-Latitudes	3.63	18.4	1.00	5.30
Tropical region	49.8	41.5	10.9	8.63
Southern Mid-Latitudes	-6.83	16.1	-1.24	3.75
Southern Polar Region	-26.4	27.5	-3.38	4.24

The statistics on the accuracy of the GOME-2B and GOME-2C HR tropospheric ozone column products (fixed altitude) for different latitude belts, validated against X_{AVK-sonde}, are shown in Table 7.6 and Table 7.7.

Table 7.6. Relative differences (RD) and standard deviation (STDEV) are shown (in percent) together with the absolute difference (DU) on the accuracy of the GOME-2B HR tropospheric ozone column products (fixed altitude) for five different latitude belts, validated against X_{AVK-sonde}

July 2024 – June 2025	GOME-2B HR			
	RD (%)	STDEV (%)	AD (DU)	STDEV (DU)
Northern Polar Region	-4.16	15.0	-0.71	2.62
Northern Mid-Latitudes	4.05	16.1	0.77	2.73
Tropical region	32.7	46.4	3.89	5.41
Southern Mid-Latitudes	0.25	15.0	-0.10	1.58
Southern Polar Region	-9.00	16.8	-0.75	1.19

Table 7.7. Relative differences (RD) and standard deviation (STDEV) are shown (in percent) together with the absolute difference (DU) on the accuracy of the GOME-2C HR tropospheric ozone column products (fixed altitude) for five different latitude belts, validated against X_{AVK-sonde}

July 2024 – June 2025	GOME-2C HR			
	RD (%)	STDEV (%)	AD (DU)	STDEV (DU)
Northern Polar Region	-2.74	8.38	-0.42	1.43
Northern Mid-Latitudes	0.61	9.30	0.08	1.57
Tropical region	32.3	33.2	3.70	3.75
Southern Mid-Latitudes	-5.01	8.14	-0.58	0.96
Southern Polar Region	-14.9	14.1	-0.85	1.04

For the GOME-2B and GOME-2C TrOC products, most of these products comply with the target accuracy requirement. Only for the tropical region (GOME-2B/C), this is obviously not the case. Between all sensors, there is a clear offset visible in the results. Also here, a degradation correction will be necessary to correct for this offset.

Validation activities summary for tropical tropospheric ozone:

This summary contains validation results of the GOME-2B and GOME-2C tropical tropospheric ozone column (TTrOC) products, using the cloud slicing method. The tropospheric ozone retrieval is based on the GOME-2 ozone columns as derived by the GOME Data Processor (GDP, version 4.8) and covers the tropical latitude belt (20S – 20N). This product is available on a monthly basis and has a resolution of 1.25° latitude x 2.5° longitude.

The tropical tropospheric ozone column product has the following user requirements:

- Threshold accuracy: within 50 %
- Target accuracy: within 25 %
- Optimal accuracy: within 15 %

This summary was made available by Dr. Andy Delcloo from KMI. More information on how these values are extracted is available in the [validation report](#). The collocation data used are the same as for the ozone profiles (Figure 7.23).

The time period considered is from January 2021 until December 2022 for the GOME-2B and GOME-2C offline TTrOC products.

In Table 7.8 and Table 7.9, the statistics on the accuracy of the GOME-2B/C tropical tropospheric ozone column products for different stations under consideration are shown, showing some general statistics for both datasets.

For GOME-2B, there is an issue with the cloud data, the low cloud fractions are systematically overestimated. Therefore, every month, less data is available. For this reason, Table 7.8 only shows statistics on the time period 2021 – 2022. The production team should be contacted how to proceed. Since there is no significant improvement possible, according to the developers, we suggest stopping this product for GOME-2B.

Table 7.8. Relative Differences (RD), standard deviation (STDEV), correlation, bias and RMSE are shown on the accuracy of the GOME-2B TTrOC product for the time period January 2021 – December 2022

Station	RD (%)	STDEV (%)	Correlation	Bias (DU)	RMSE (DU)
Paramaribu	3.61	28.2	0.43	0.59	5.32
Samoa	20.1	28.8	0.56	2.82	5.18
Ascension Island	4.04	13.0	0.83	1.10	3.44
Kuala Lumpur	-6.62	12.1	0.73	-1.47	2.98
Nairobi	15.9	12.1	0.67	2.66	3.09
Natal	6.44	21.5	0.80	1.93	5.47

Table 7.9. Relative Differences (RD), standard deviation (STDEV), correlation, bias and RMSE are shown on the accuracy of the GOME-2C TTrOC product for the time period January 2022 – December 2023

Station	RD (%)	STDEV (%)	Correlation	Bias (DU)	RMSE (DU)
Paramaribu	10.8	19.3	0.64	1.95	3.95
Samoa	17.8	27.3	0.60	2.30	4.11
Ascension Island	3.16	27.0	0.50	0.80	7.80
Kuala Lumpur	9.85	18.7	0.35	1.32	2.94
Nairobi	20.9	22.8	0.50	3.34	4.65
Natal	8.66	27.9	0.65	1.75	5.58

It is shown that for GOME-2C, most of the stations are within the target accuracy (20 %), except for Nairobi. The correlation varies between 0.4 and 0.7 with a rmse between 1.3 and 3.3 DU. These TTrOC products still fulfill the user requirements. Also here we observe a degradation of the product (less data available).

7.3. GOME-2 trace gas products

Table 7.10. Validation status of trace gas products

Product Identifier	Product Name	Accuracy	Reference	Validating Institute	Correlative data sources
O3M-50.1	NRT total NO2	Fulfils threshold accuracy requirement	RD5	BIRA-IASB	NDACC zenithSky measurements
O3M-338			RD24		
O3M-52.1	NRT tropospheric NO2	Fulfils threshold accuracy requirement	RD5	BIRA-IASB	BIRA-IASB and other MAXDOAS stations
O3M-341			RD24		
O3M-55.1	NRT total SO2	Fulfils threshold accuracy requirement	RD9	AUTH	
O3M-374			RD30		

Product Identifier	Product Name	Accuracy	Reference	Validating Institute	Correlative data sources
O3M-177	NRT total HCHO	Fulfil threshold accuracy requirement	RD11	BIRA-IASB	BIRA-IASB and other MAXDOAS stations
O3M-344			RD25		
O3M-51.1	Offline total NO ₂	Fulfil threshold accuracy requirement	RD5	BIRA-IASB	NDACC zenithSky measurements
O3M-339			RD24		
O3M-37.1	Offline tropospheric NO ₂	Fulfil threshold accuracy requirement	RD5	BIRA-IASB	BIRA-IASB and other MAXDOAS stations
O3M-53.1			RD24		
O3M-342					
O3M-09.1	Offline total SO ₂	Fulfil threshold accuracy requirement	RD9	AUTH	
O3M-56.1			RD30		
O3M-375					
O3M-08.1	Offline total BrO	Fulfil threshold accuracy requirement	RD10	BIRA-IASB	BIRA-IASB Harestua zenithSky station and satellite comparisons
O3M-82.1			RD26		
O3M-317					
O3M-10.1	Offline total HCHO	Fulfil target accuracy requirement	RD11	BIRA-IASB	BIRA-IASB and other MAXDOAS stations
O3M-58.1			RD25		
O3M-345					
O3M-12.1	Offline total H ₂ O	Fulfil threshold accuracy requirement	RD12	FMI, DLR	IGRA , COSMIC-SuomiNet , SSM/I
O3M-86.1			RD27		Comparison against GOME-2B water vapour data
O3M-386					

Validation activities summary:

This summary presents validation activities for offline total and tropospheric NO₂, total HCHO, and total BrO data products of GOME-2B/C as performed at BIRA-IASB and SO₂ data as performed at AUTH.

The authors of this summary are Gaia Pinaridi (for tropospheric NO₂ and HCHO validation), Jean-Christopher Lambert, José Granville and Tijnl Verhoelst (for total/stratospheric NO₂ validation), Jeroen van Gent (for BrO validation) and Jeroen van Gent and MariLiza Koukouli (for quality assessment).

Validation exercises are performed following the protocols described in the original Metop-A, Metop-B and Metop-C [validation reports](#) and updated in Pinaridi *et al.* (AMT 2020) and Verhoelst *et al.* (AMT 2021), and the results presented in this report are based on updates of the correlative datasets with the last available – and sometimes improved – versions. While illustrations at a few stations are included in this report, all the updated figures are reported on the [BIRA-IASB trace gases validation server](#).

Update of database for reference data

For this report, the validation database was updated with ground-based NDACC UVVIS ZenithSky NO₂ data (as usual) and MAXDOAS NO₂ and HCHO data from BIRA, KNMI and IUPB (as collected for the NIDFORVAL S5p validation project and already used in Pinardi *et al.* (AMT 2020), Verhoelst *et al.* (AMT 2021) and De Smedt *et al.* (ACP 2021), in order to cover as much as possible the period until mid of 2025. BIRA-IASB ZenithSky BrO data at Harestua could not be updated for this report, due to BIRA-IASB change of personnel and only the comparisons of GOME-2 to TROPOMI BrO VCD are updated.

ZenithSky NO₂ total columns are collected from the NDACC Data Host Facility (to where the data have to be uploaded by instrument Pis within 1 year after data acquisition) and from the SAOZ rapid delivery operational facility operated by LATMOS. The SAOZ at Bauru (Brazil) is unfortunately no longer operational. The ground-based data are then quality assessed and post-processed at BIRA-IASB in preparation for the data comparisons. This preparation includes calculation of the effective ground-based airmasses with which GOME-2 data co-locations will be sought.

The BIRA-IASB MAXDOAS ground-based dataset are automatically retrieved with the FRM4DOAS analysis chain. The FRM4DOAS (Fiducial Reference Measurements for Ground-Based DOAS Air-Quality Observations) is an ESA activity aiming at the development of the first centralised NRT processing system for MAX-DOAS instruments operated within the international Network for the Detection of Atmospheric Composition Change (NDACC). It includes the launch of the NDACC MAX-DOAS Processing Service in a demonstration mode, focusing on tropospheric and stratospheric NO₂ vertical profiles, total O₃ columns, and tropospheric HCHO profiles as target MAX-DOAS products for the first phase of the project (July 2016 – August 2021), see <https://frm4doas.aeronomie.be/>. The lower tropospheric profiles and vertical columns processing chain rely on parallel runs of optimal estimation based MMF (Friedrich *et al.*, 2019) and parametrized approach MAPA (Beirle *et al.*, 2019) algorithms and testings of their results coherence. The service is running in a best-effort mode at the time of writing for a limited number of stations belonging to the project partners, and only tropospheric NO₂ and total O₃ are to the NDACC RD database. More details can be found in Van Roozendaal *et al.* 2024.

IUPB and KNMI sites are retrieved respectively with the QA4ECV database approach (https://uv-vis.aeronomie.be/groundbased/QA4ECV_MAXDOAS/index.php), as discussed and used in Pinardi *et al.* (AMT 2020) and Verhoelst *et al.* (AMT 2021) for NO₂ and De Smedt *et al.* (ACP 2021) for HCHO. This approach only provides VCD columns, and profiles are not retrieved. These datasets are also used for the online validation of S5p (<https://mpc-vdaf-server.tropomi.eu/no2/no2-offl-maxdoas> and <https://mpc-vdaf-server.tropomi.eu/hcho/hcho-offl-maxdoas>).

The NO₂ and HCHO datasets include the following ground-based stations:

- OHP (from June 2007 to July 2014 with the geometrical approximation, and since August 2014 to March 2017 with the bePRO profiling tool)
- Uccle (from April 2011 to March 2016 with a miniMAXDOAS instrument (Uccle-miniDOAS) and from end of January 2017 to February 2020 with a scientific grade MAXDOAS: Uccle-SG)
- Bujumbura (from November 2013 to July 2017; since then, the instrument had a power failure and only limited operations and data transfer was possible)
- LePort, on Reunion Island (from April 2016 to 10 January 2018). The instrument has been reinstalled in June 2018 on the Maïdo site, and data analysis from the FRM4DOAS analysis chain was tested, but it is not adapted for tropospheric (NO₂, HCHO) gases validation at this mountainous site and is not used for this report.

- Xianghe (from March 2010 to July 2018 and from October 2019 to August 2022). Since November 2021 the retrievals in the UV are of bad quality and the UV channel broke down early 2022. SO₂ MAXDOAS profiles were also analysed for the whole time-series (2010 to Oct. 2021), although the SO₂ levels are very low now in China nowadays.
- Kinshasa (from December 2019 to May 2025). The instrument and the FRM4DOAS processing are described in Yombo Phaka et al., 2023.
- IUPB Bremen and Athens and KNMI Cabauw and De Bilt data used here covers the periods from April/May 2018 to summer 2025 for NO₂ and the KNMI also for HCHO.

Status of GOME-2B and GOME-2C tropospheric NO₂

Comparisons with ground-based MAXDOAS instruments is performed similarly as in previous [validation report](#). In Pinaridi *et al.* (2020) it is shown that best results are achieved by filtering out the largest pixels and selecting only pixels covering the stations. For GOME-2, the selection includes keeping only pixels with a size of less than 100 km, while selecting pixels over the station, only slightly changes the results, as generally pixels with their center within 50 km, are covering the station. This improvement of the biases comes at the expenses of a strongly reduced number of pixels (see AC SAF Operations Report 1/2020).

Only BIRA MAXDOAS station from Kinshasa can be used in the first part of 2025, and we also used some available MAXDOAS data from KNMI and IUPB, as presented above.

Figure 7.4 shows example of results for GOME-2B and GOME-2C for Kinshasa. Monthly mean differences are calculated for every year and for the whole time-series in order to see the evolution in time of the bias. Table 7.11 reports the median differences and the spread (half the percentile 68) at the stations, with and without the smoothing, and the figures for all the stations can be found on the [BIRA-IASB validation web server](#).

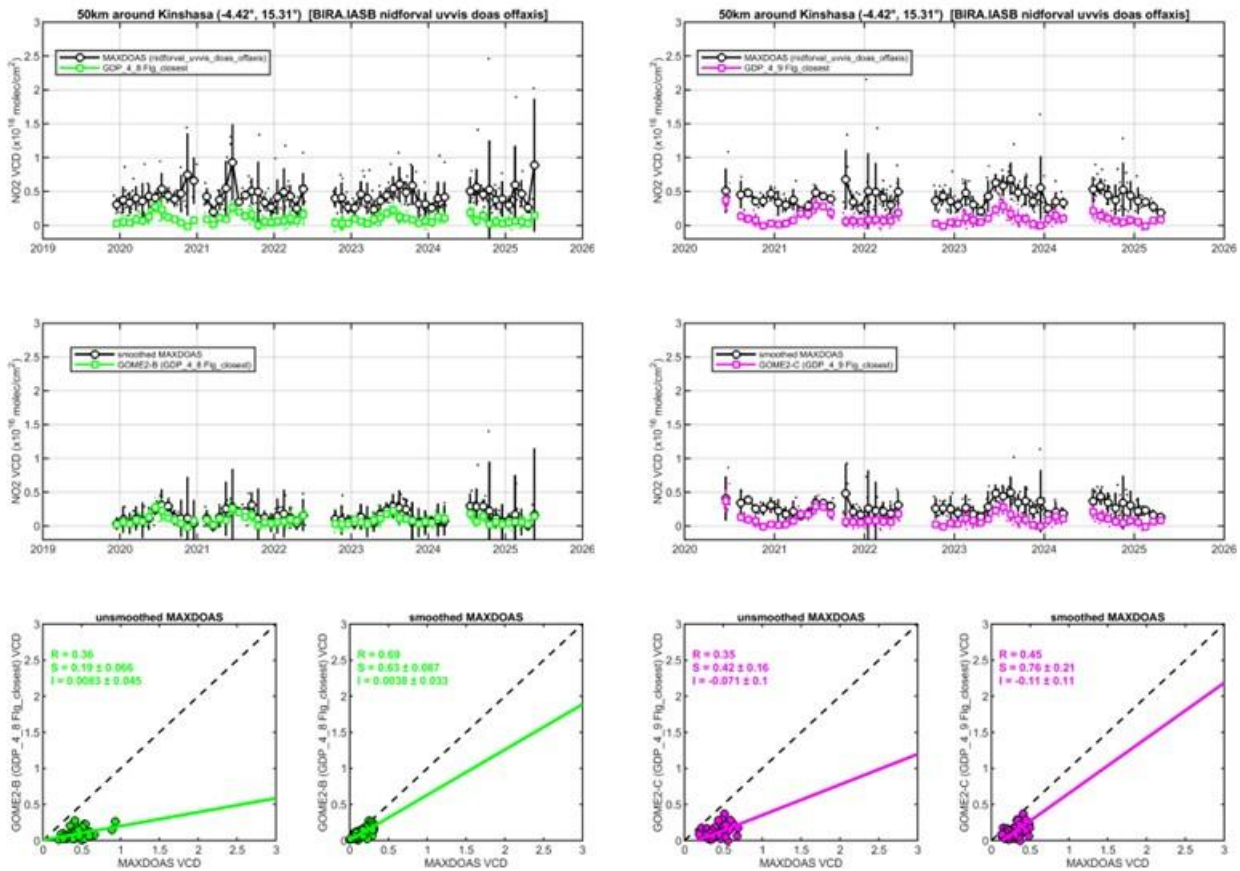


Figure 7.4. Illustration for the Kinshasa MAXDOAS versus GOME-2B GDP-4.8 (left) and GOME-2C GDP-4.9 (right) tropospheric NO₂ comparisons.

Table 7.11. Median Absolute Differences (AD=SAT-GB, in 10¹⁵ molec/cm²), Relative Differences (RD, in %) and spread (0.5*IP68) on the accuracy of GOME-2B and GOME-2C tropospheric NO₂ products when comparing to MAXDOAS data (NOT cloud filtered). Values for the last 12 months are given, and the values for the whole time-series are reported in brackets for comparison. Results for both the original comparisons (pixels over the station, for pixels smaller than 100 km side) and for the smoothed comparisons are reported. Only the first rows are stations with recent data (in bold below), the others are given as examples of past results.

	GOME-2B			GOME-2C		
	AD (×10 ¹⁵)	RD (%)	SPREAD (%)	AD (×10 ¹⁵)	RD (%)	SPREAD (%)
Bremen (IUPB) Last 12 months: 10/2024 – 9/2025 [whole period: since 04/2018]	-2.2 [-2.2]	-51 [-41]	77 [59]	-1.2 [-1.9]	-32 [-41]	46 [45]
Athens (IUPB) Last 12 months: 8/2024 – 7/2025 [whole period: since 05/2018]	-1.7 [-1.9]	-36 [-38]	26 [37]	-2.4 [-2.1]	-44 [-41]	23 [28]
Cabauw (KNMI) Last 12 months: 6/2024 – 5/2025	0.8 [0.25]	20 [3.829]	29 [34]	-0.3 [-0.3]	-6 [-5.4]	39 [30]

	GOME-2B			GOME-2C		
[whole period: since 04/2018]						
De Bilt (KNMI) Last 12 months: 6/2024 – 5/2025 [whole period: since 04/2018]	0.6 [0.1]	9 [1.5]	29 [38]	0.5 [-0.1]	8 [-1.2]	40 [39]
Kinshasa * last 12 months: 6/2024 – 05/2025 [whole period: 12/2019 – 05/2025]	-3.6 [-3.2]	-88 [-82]	28 [30]	-3.3 [-3.2]	-79 [-78]	26.5 [27.7]
Kinshasa smoothed *	-0.55 [-0.3]	-47 [-28]	53 [58]	-2.1 [-1.6]	-72 [-67]	34 [37.5]
Uccle SG last 12 months: 03/2019 – 02/2020 [whole period: 02/2017 – 02/2020]	-1.2 [-1.4]	-16 [-20]	33 [36]	-	-	-
Uccle SG smoothed	-2.5 [-2.7]	-26 [-29]	38 [36]	-	-	-
Reunion Maido (last 12 months: 12/2018 – 11/2019) [whole period: 06/2018 – 11/2019]	-0.02 [-0.02]	-4.2 [-4.3]	76 [93]	-	-	-
Reunion Maido smoothed	-0.03 [-0.01]	-1.4 [-9]	85 [115]	-	-	-
Xianghe (last 12 months: 12/2020 – 07/2022) [whole period: 03/2010 – 07/2022]	0.9 [-0.8]	-4.9 [-4.4]	26 [25]	-0.3 [-0.8]	-1.2 [-9]	23 [21]
Xianghe smoothed	-2.2 [-3.8]	-17 [-18]	28 [36]	-2.1 [-2.4]	-13 [-21]	29 [36]
Bujumbura (last 12 months: 07/2016 – 07/2017) [whole period: 11/2013 – 07/2017]	-3.4 [-3.2]	-83 [-81]	42 [28]	-	-	-
Bujumbura smoothed	-2 [-1.8]	-70 [-74]	21 [35]	-	-	-
OHP (last 12 months: 03/2016 – 03/2017) [whole period: 08/2014 – 03/2017]	-0.7 [-0.6]	-37 [-28]	34 [36]	-	-	-

	GOME-2B			GOME-2C		
OHP smoothed	-0.5 [-0.4]	-36 [-24]	41 [39]	-	-	-
Reunion LePort Last 12 months: 12/2016 – 12/2017) [whole period: 04/2016 – 12/2017]	-1.4 [-1.4]	-83 [-84]	25 [25]	-	-	-
Reunion LePort smoothed	-0.41 [-0.42]	-59 [-60]	22 [25]	-	-	-
Uccle minDOAS (last 12 months: 03/2015 – 03/2016) [whole period: 04/2011 – 03/2016]	-2.6 [-3]	-26 [-31]	25 [24]	-	-	-
Uccle minDOAS smoothed	-3.6 [-3.3]	-29 [-33]	20 [30]	-	-	-

* The Kinshasa site had to be processed with a different satellite pixels selection (closest valid flagged pixel instead of valid pixel over the site) to have enough daily coincidences and allow meaningful comparisons.

From Figure 7.4 it can be seen, that GOME-2C scatter plot is similar to what obtained with GOME-2B (confirming past results from Xianghe), although the statistics are slightly different, probably due to the presence in GOME-2B period of a few larger NO₂ columns (between $1 - 2 \times 10^{15}$ molec/cm²) that strongly influence the regression analysis (Pinardi *et al.*, 2020). There are some differences in the absolute and relative differences for GOME-2B and GOME-2C and for the last 12 months compared to the whole period. These depend from one station to the other (ie. -6 % bias for GOME-2C compared to 20 % for GOME-2B in Cabauw, -32 % compared to -51 % for Bremen and 8 % compared to 9 % for De Bilt).

The biases results are usually within or close to the requirements (target accuracy requirement of 30 % in polluted conditions and optimal accuracy of 20 %), as it was the case for the other sensors for Xianghe and Uccle in the past. Kinshasa, Cabauw and De Bilt sites are remote sites, with low levels of NO₂ pollution and low biases, while Bremen and Athens are more urban polluted sites, with biases around the -40 % levels, with a spatial comparison mismatch (horizontal dilution component) as highlighted in Pinardi *et al.* (2020) and also seen for other BIRA-IASB sites in the past. Beijing and OHP report about 50 % biases, while larger values are found for Bujumbura and Reunion, as previously (Pinardi *et al.*, 2014; NO₂ Validation Report 2015; Pinardi *et al.*, 2020). As before, smoothing the MAXDOAS profiles with the satellite averaging kernels is not always reducing the mean comparison differences, with an impact of ~10 – 20 % depending on the station (AC SAF Operations Report 1/2018, PT meeting of May 2018). The comparison improvement for Kinshasa is clear in Figure 7.4.

In terms of stability most of the stations report differences over time up to 15 % for both GOME-2B and GOME-2C, which is also about the level of difference between GOME-2B and GOME-2C (10 to 15 %, except Cabauw and Bremen in this case), and the levels we had in the past between GOME-2A and GOME-2B. These biases could be partly reduced in the future with the improved GDP-4.9 GOME-2 algorithm (Liu *et al.*, 2019).

Status of GOME-2B and GOME-2C total (stratospheric) NO₂

Quality monitoring of the GOME-2 NO₂ total (stratospheric) column data is regularly carried out using correlative ground-based measurements collected from about 20 Zenith-Scattered-Light DOAS UV-visible (ZSL-DOAS) instruments affiliated with the Network for the Detection of Atmospheric Composition Change (NDACC). The NO₂ column validation protocol has already been described in previous AC SAF validation reports with its latest updates published in Verhoelst *et al.* (AMT 2021). This protocol includes the selection of GOME-2/NDACC co-located data pairs based on the air-mass matching technique, a model-based photochemical correction compensating for significant solar local time differences between GOME-2 mid-morning and NDACC twilight observations in polar summer, and a cloud-based filtering of NO₂ data over polluted stations aiming at the removal of pollution-affected pixels. At some stations, real-time processing of the ground-based observations still uses NO₂ absorption cross-sections at room temperature instead of stratospheric temperature. As a result, the retrieved total NO₂ column is affected by a negative systematic bias of 15 – 20 % with a seasonal component. Such data are removed. Thanks to this strict protocol, data comparisons can be carried out within a residual uncertainty of about $2 - 3 \times 10^{14}$ molec/cm² combining both the ground-based data uncertainty and comparison errors. This uncertainty is indicated by the shaded area on the pole-to-pole graphs. Drift estimates are performed using both a strict linear regression (but reporting on the autocorrelation ϕ in the residuals) and a regression including annual and semi-annual terms. The latter can for instance absorb the seasonally varying bias due to the fixed assumed effective temperature in the ZSL-DOAS retrievals.

Figure 7.5 shows the comparison of NO₂ column data at the NDACC Antarctic station of Dumont d'Urville, a station located on the polar circle, in a pristine environment without any known source of tropospheric NO₂. Comparison results at this station are representative of the validation of purely stratospheric data series, at moderate and large solar zenith angle, and over the full range of NO₂ stratospheric column values from winter lows of about 1×10^{14} molec/cm² (wintertime denoxification episodes) up to summer highs of 7×10^{15} molec/cm² (complete depletion of N₂O₅ into NO₂ due to polar midnight Sun). On a monthly median basis, and over the 16 years covered by the three satellites, the target bias of $3 - 5 \times 10^{14}$ molec/cm² hasn't often been exceeded, except occasionally in October when the station is overpassed frequently by the border of the polar vortex, thus when atmospheric variability contributes significant co-location mismatch noise and bias to the difference in stratospheric NO₂. The ground dataset shown in this figure is a composite dataset consisting of the NDACC reprocessed dataset extended through the last year by the near-real-time dataset (latmos_rt).

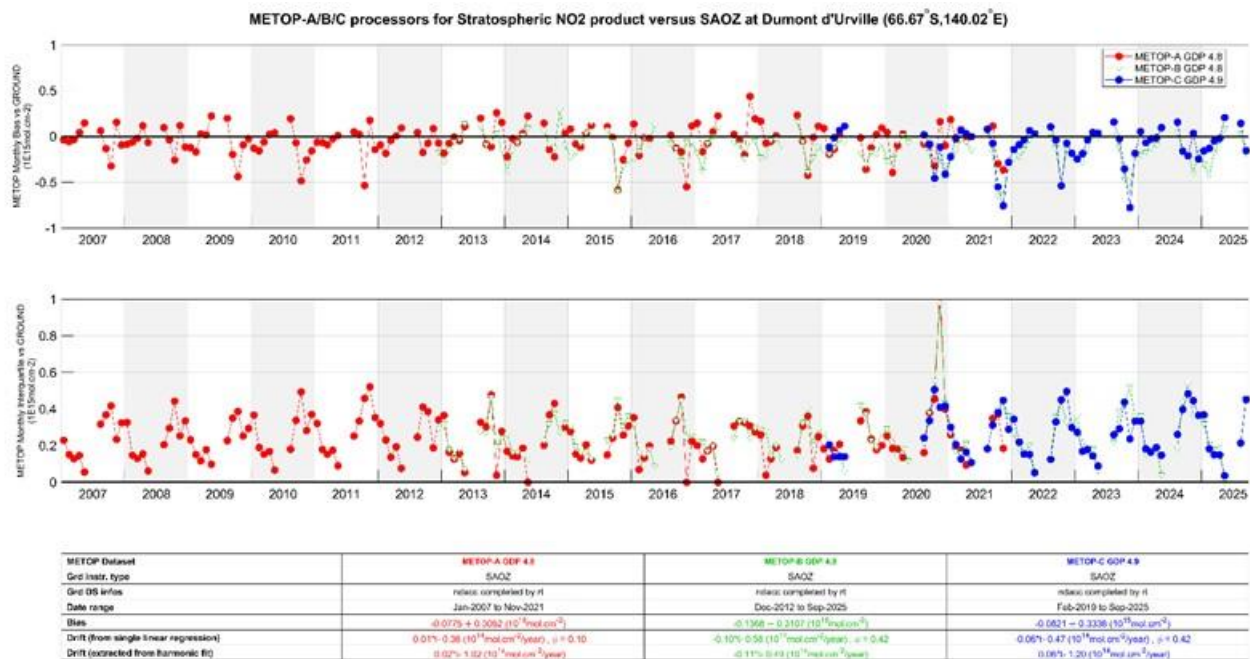


Figure 7.5. Comparison of NO₂ column data measured at the NDACC Antarctic station of Dumont d'Urville (by the GOME-2 instruments) and by the CNRS/LATMOS ZSL-DOAS spectrometer. Top: time-series of the median NO₂ column difference per month; centre: time-series of the dispersion of the NO₂ column difference per month; bottom (table): summary statistics.

Figure 7.6 and Figure 7.7 display similar results obtained at the NDACC station of Izaña on Tenerife (Canary Islands) and the NDACC Southern Tropic station of Saint-Denis de la Réunion, thus in occasional presence of pollution and over a wider range of solar zenith angle. Again, the target bias of $3 - 5 \times 10^{14}$ molec/cm² has rarely been exceeded, except in very few cases.

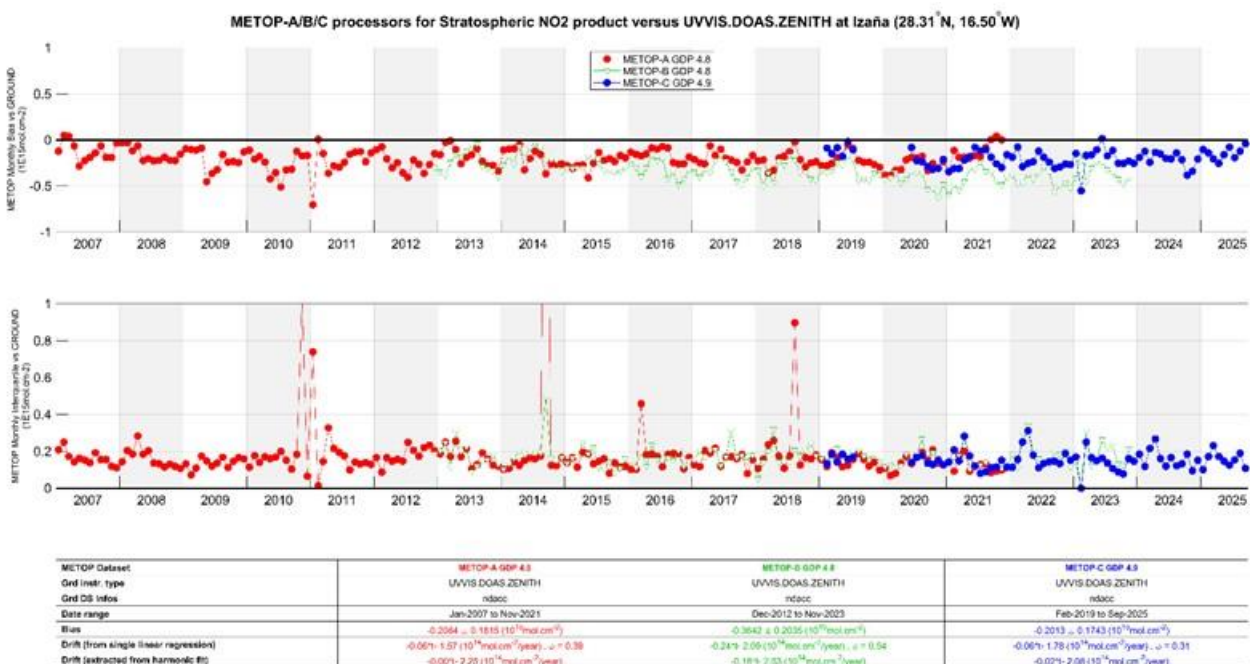


Figure 7.6. Same as Figure 7.5 but at the NDACC station of Izaña on Tenerife (Canary Islands).

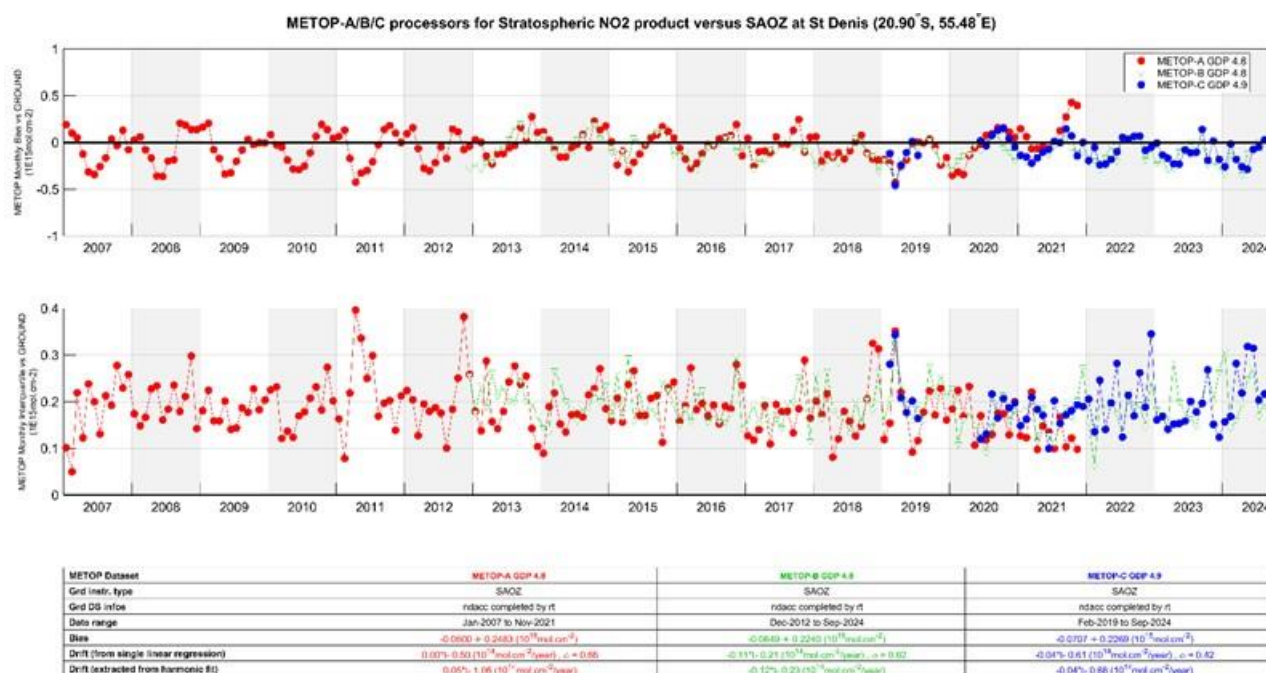


Figure 7.7. Same as Figure 7.5, but at the NDACC Southern Tropical station of Saint-Denis de la Reunion.

Figure 7.8 reports from pole to pole the median value and the dispersion of the differences between GOME-2 and NDACC ZSL-DOAS data, while Figure 7.9 displays, again from pole to pole, the linear drift between GOME-2A/B/C and NDACC data. Those graphs show the good long-term stability of the satellite NO₂ column data with respect to NDACC ZSL-DOAS data at all stations.

They also show that the target bias of $3 - 5 \times 10^{14}$ molec/cm² in unpolluted conditions is achieved at virtually all sites for all three satellites. Figure 7.7 also confirms the slight difference already noticed in previous validation reports between the biases observed respectively in the Southern and Northern hemispheres. Averaging median differences separately over the Northern and Southern Hemispheres concludes to an inter-hemispheric bias of about $2 - 3 \times 10^{14}$ molec/cm². GOME-2C NO₂ column data present a slightly more positive bias across all latitudes. Drift estimates show a bit more scatter for GOME-2C, in particular at high Northern latitudes, but the mission lifetime of GOME-2C is still relatively short for stable drift determination.

Note that for these global statistics visualized in Figure 7.8 and Figure 7.9, only ground instruments yielding co-locations with all 3 satellite instruments (on Metop-A/B/C) were used so as to limit selection biases between sounders.

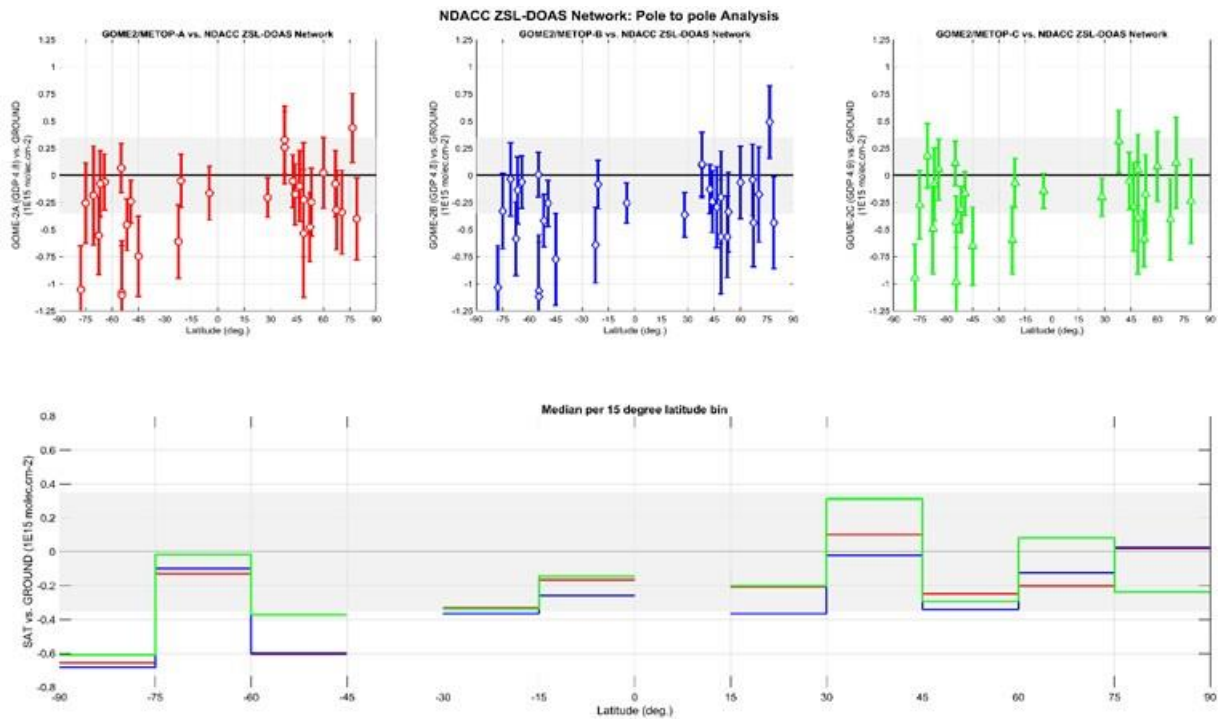


Figure 7.8. From pole to pole, median difference between the NO₂ column data reported by GOME-2A/B/C (red/blue/green) GDP-4.8 (GDP 4.9 for GOME-2C) and by ground-based ZSL-DOAS spectrometers at about 20 NDACC stations, calculated over 2007 – November 2021 for GOME-2A, 2012 – September 2025 for GOME-2B and 2019 – September 2025 for GOME-2C. Top: median difference at individual stations. Bottom: median difference averaged over 15° latitude bins.

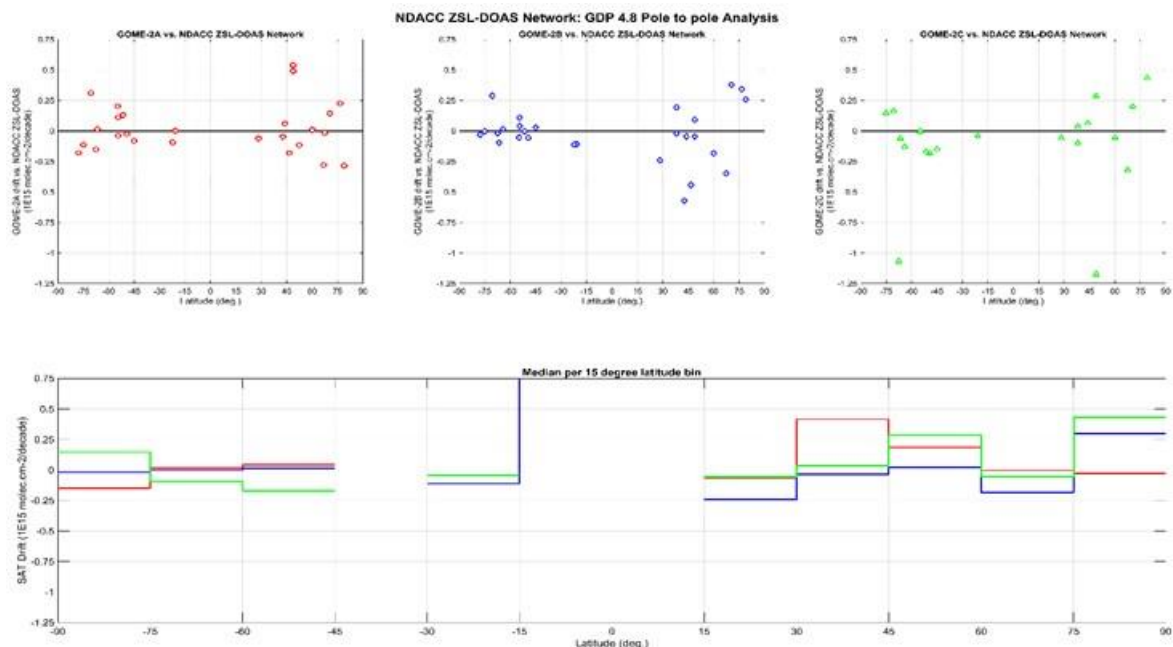


Figure 7.9. From pole to pole, linear drift from a regression model including annual and semi-annual harmonic terms of the difference between the NO₂ column data reported by GOME 2A/B/C (red/ blue/ green) GDP 4.8 (GDP 4.9 for GOME-2C) and by ground-based ZSL-DOAS spectrometers at about 20 NDACC stations, calculated over 2007 – November 2021 for GOME-2A, 2012 – September 2025 for GOME-2B and 2019 – September 2025 for GOME-2C. Top: linear drift estimates at individual stations. Bottom: same linear drift estimates but averaged over 15° latitude bins.

Status of GOME-2B and GOME-2C total HCHO

This validation exercise is an extension of what is presented in the [HCHO GDP-4.8 validation report](#), relying on correlative observations from MAX-DOAS instruments operated by BIRA-IASB at Xianghe, Bujumbura, Uccle (miniDOAS and SG), OHP and Reunion (Le Port and Maito). As discussed above, the only update possible from BIRA-IASB stations is the Kinshasa site, so the KNMI Cabauw and De Bilt sites are also included in this report. An illustration of the comparisons for De Bilt are presented in Figure 7.10, past figures can be found on the [BIRA validation web server](#) and a summary is presented in Table 7.12.

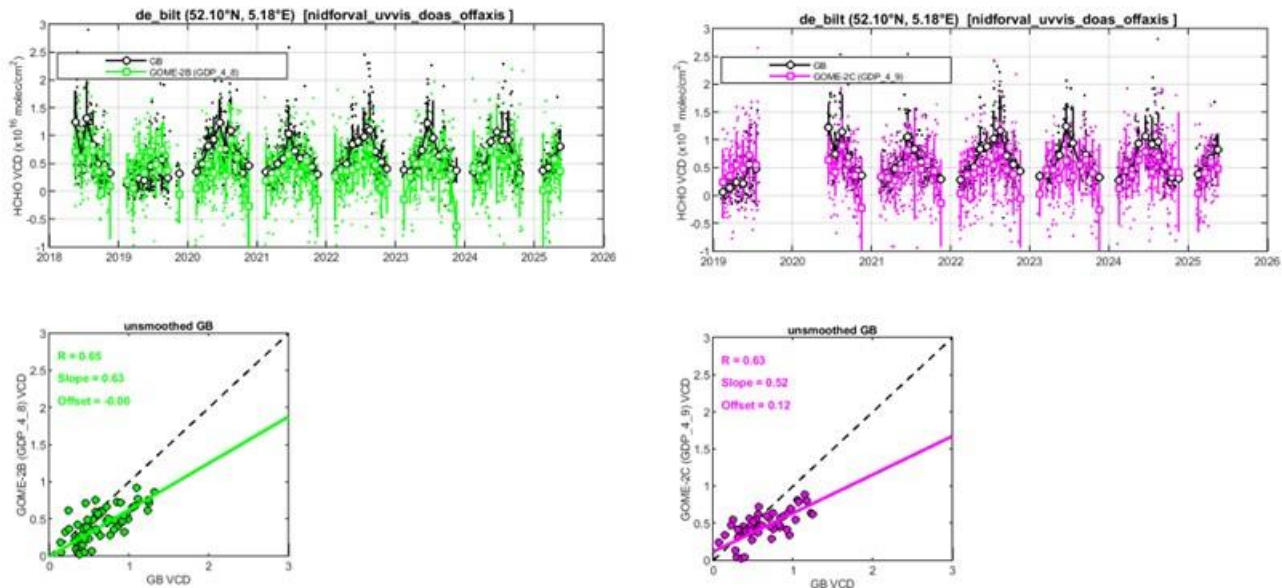


Figure 7.10. Illustration for the De Bilt MAXDOAS versus GOME-2B GDP-4.8 (left) and GOME-2C GDP-4.9 (right) HCHO comparisons.

Table 7.12. Summary of the mean biases (SAT-GB, in 10^{15} molec/cm²) between GOME-2B/C and MAX-DOAS HCHO VCDs. The values in parentheses correspond to the mean relative biases (in %) and R is the correlation coefficients and S the slope of the linear regression of the monthly mean points. Only the first two rows are stations with recent data (Cabauw, De Bilt and Kinshasa), the others are given as examples of past results.

	GOME-2B	GOME-2C
CABAUW (51.97°N, 4.93°E) (whole period: 04/2018 – 5/2025)	-1.8 ± 2 (-31 ± 44) R = 0.62, S = 0.62	-1.4 ± 2 (-24 ± 44) R = 0.63, S = 0.56
DE BILT (52.10°N, 5.18°E) (whole period: 05/2018 – 5/2025)	-2.3 ± 2.4 (-38 ± 55) R = 0.65, S = 0.63	-1.7 ± 2.4 (-28 ± 68) R = 0.63, S = 0.52
KINSHASA (4.42°S, 15.31°E) (whole period: 12/2019 – 5/2025)	-0.3 ± 3 (-2.6 ± 22) R = 0.78, S = 1.00	0.6 ± 3.2 (0.43 ± 23) R = 0.75, S = 0.74
UCCLE-SG (50.8°N, 4.3°E) (whole period: 02/2017 – 12/2019)	0.3 ± 1.6 (7 ± 52) R = 0.75, S = 0.96	-
With smoothing	1.6 ± 1.7 (49 ± 75) R = 0.76, S = 1.34	-
REUNION MAIDO (20.9°S, 55.3°E) (whole period: 06/2018 – 11/2019)	2.1 ± 0.8 (94 ± 54) R = 0.84, S = 1.17	-
With smoothing	1.7 ± 0.8 (68 ± 43) R = 0.69, S = 1.29	-
XIANGHE (39.7°N, 117.0°E) (whole period: 03/2010 – 12/2021)	-6.4 ± 2.7 (-48 ± 16) R = 0.88, S = 0.67	-8.9 ± 2.6 (-60 ± 21) R = 0.82, S = 0.76
With smoothing	0.59 ± 2.2 (-8 ± 31) R = 0.88, S = 1.19	-2.4 ± 2.7 (-29 ± 37) R = 0.79, S = 1.40
BUJUMBURA (3.0°S, 29.0°E) (whole period: 11/2013 – 07/2017)	-4.4 ± 2.2 (-32 ± 10) R = 0.88, S = 0.52	-
With smoothing	0.3 ± 2.0 (3.2 ± 25) R = 0.72, S = 0.65	-
OHP (whole period: 08/2014 – 03/2017)	0.3 ± 1.1 (4.2 ± 21) R = 0.90, S = 0.75	-
With smoothing	103.51 ± 1.0 (17 ± 22) R = 0.86, S = 1.01	-
REUNION LEPORT (20.9°S, 55.3°E) (whole period: 04/2016 – 12/2017)	103.51 ± 0.8 (39 ± 26) R = 0.80, S = 1.56	-

With smoothing	2.6 ± 0.1 (180 ± 56) R = 0.78, S = 2.83	-
UCCLE-miniDOAS (50.8°N, 4.3°E) (whole period: 04/2011 – 05/2015)	-0.6 ± 1.6 (-9.4 ± 29) R = 0.76, S = 0.89	-
With smoothing	-0.4 ± 1.7 (7.1 ± 34) R = 0.73, S = 0.88	-

Results obtained at Cabauw, De Bilt and Kinshasa confirm that both satellite instruments capture well the HCHO VCD seasonality. Results for GOME-2B and GOME-2C are similar (as shown also in the past for Xianghe), to within 10 %. Results for the whole period (shown here) and for the last 12 months generally show differences up to 15 % (not shown here, see the different figures for each station on the BIRA validation web server). In Reunion the signal is very small (less than $\sim 0.5 \times 10^{16}$ molec/cm²) and is more difficult to have firm conclusions.

A significant bias exists between GOME-2B/C and MAX-DOAS observations at the some of the stations (up to 50 %), but as already shown in the GDP-4.8 validation report, for some stations this bias can be significantly reduced when smoothing the MAX-DOAS profiles with the satellite column averaging kernels (see also values with smoothing in Table 7.12).

Status of GOME-2B and GOME-2C total BrO

GOME-2B/C total columns of BrO from GDP-4.8 (4.9 in the case of GOME-2C) operational product are usually compared to ground-based UV-visible zenith-sky measurements at Harestua, Norway (60°N, 11°E), as done in previous validation reports. The ground-based columns are derived from the vertical profiles retrieved by applying an OEM (Optimal Estimation Method) – based profiling technique to zenith-sky measurements at sunrise (Hendrick *et al.*, 2007).

Unfortunately, the unavailability of the Harestua data due to personnel-issues persists.

As a replacement, first introduced in the 2/2023 report, a comparison of total BrO columns from GOME-2B (GDP 4.8 product) and GOME-2C (GDP 4.9 product) on one hand and S5P/TROPOMI on the other hand is made below. The TROPOMI data derives from the total BrO retrieval algorithm TCBRO, developed at BIRA-IASB, that is currently running in the so-called pre-operational environment of the ESA S5P-PAL system (<https://data-portal.s5p-pal.com/>). For this, we use the high resolution (0.022°) TROPOMI BrO L3 monthly-averaged data from S5P-PAL.

For the satellite-satellite comparison, monthly average BrO VCD values over the first six months of 2025 have been derived over a 150 km area around 12 well known ground stations, ranging in latitude from the northern to the southern polar region. The geographic locations of these stations are shown in Figure 7.11.

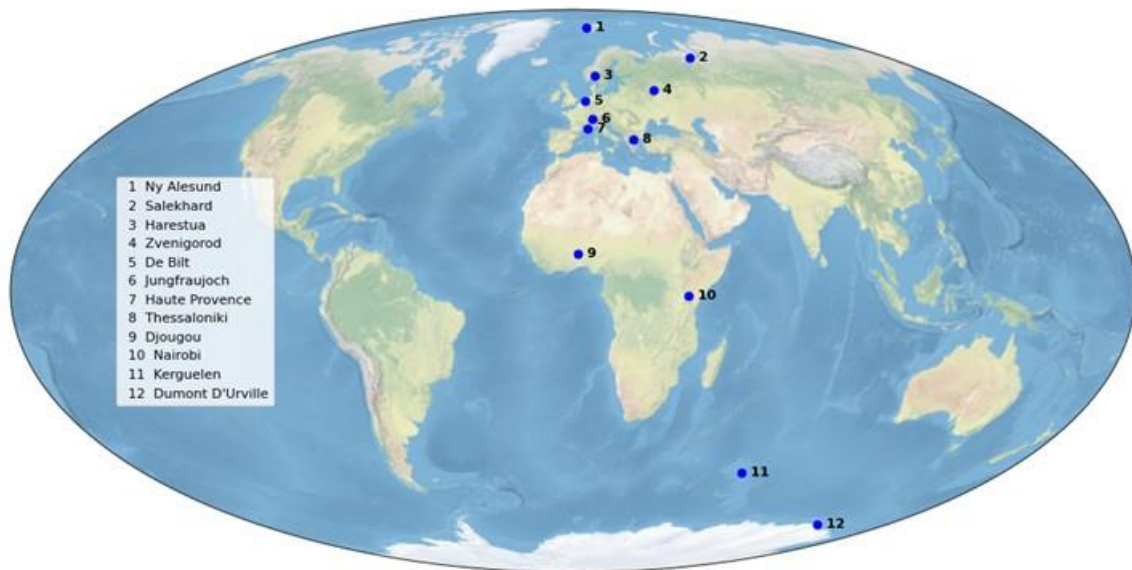
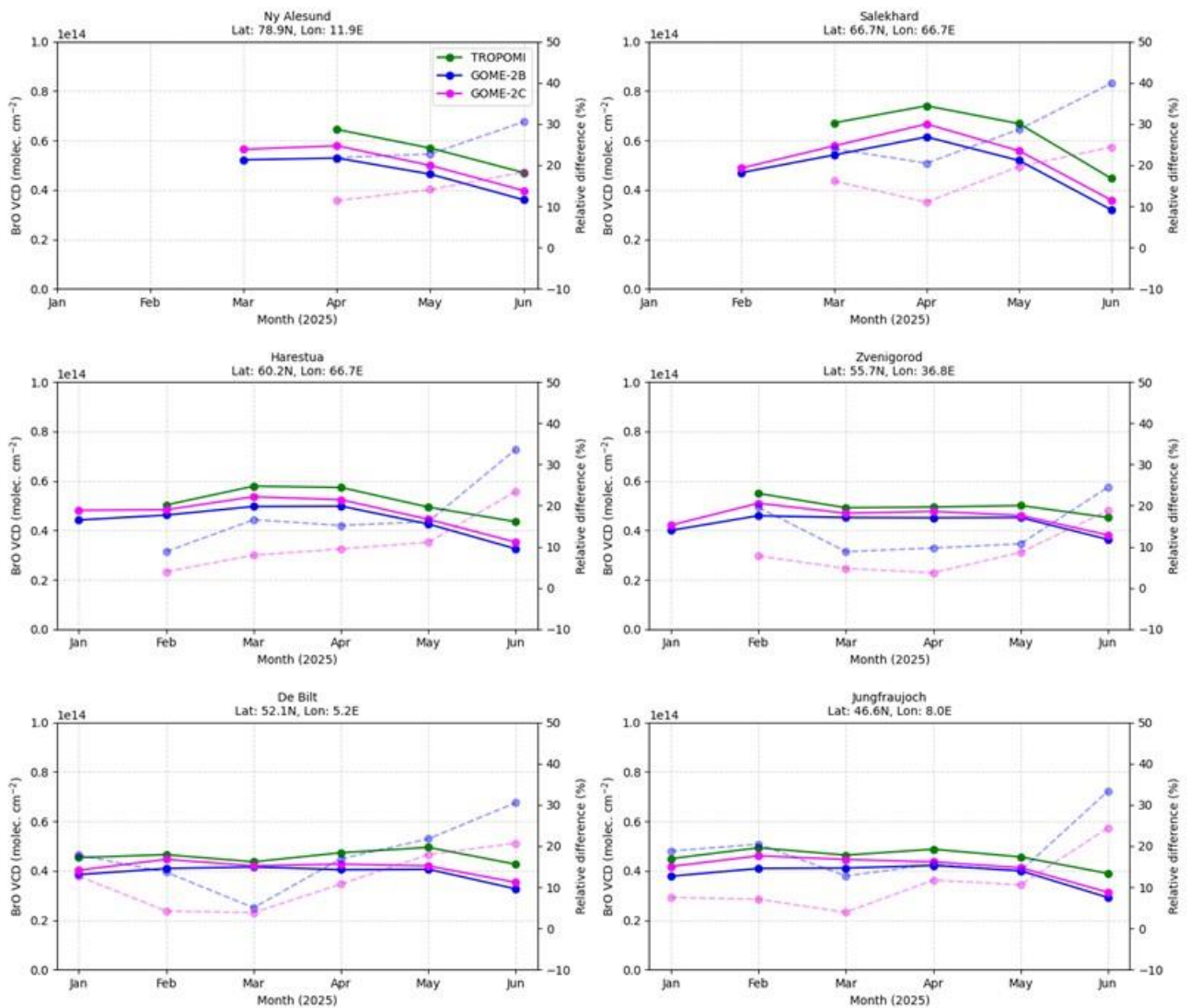


Figure 7.11. Location of the 12 stations for which overpass BrO VCD values were determined for the three sensors GOME-2B and GOME-2C and TROPOMI. VCD values were determined as average values over an area with a radius of 150 km from the station.



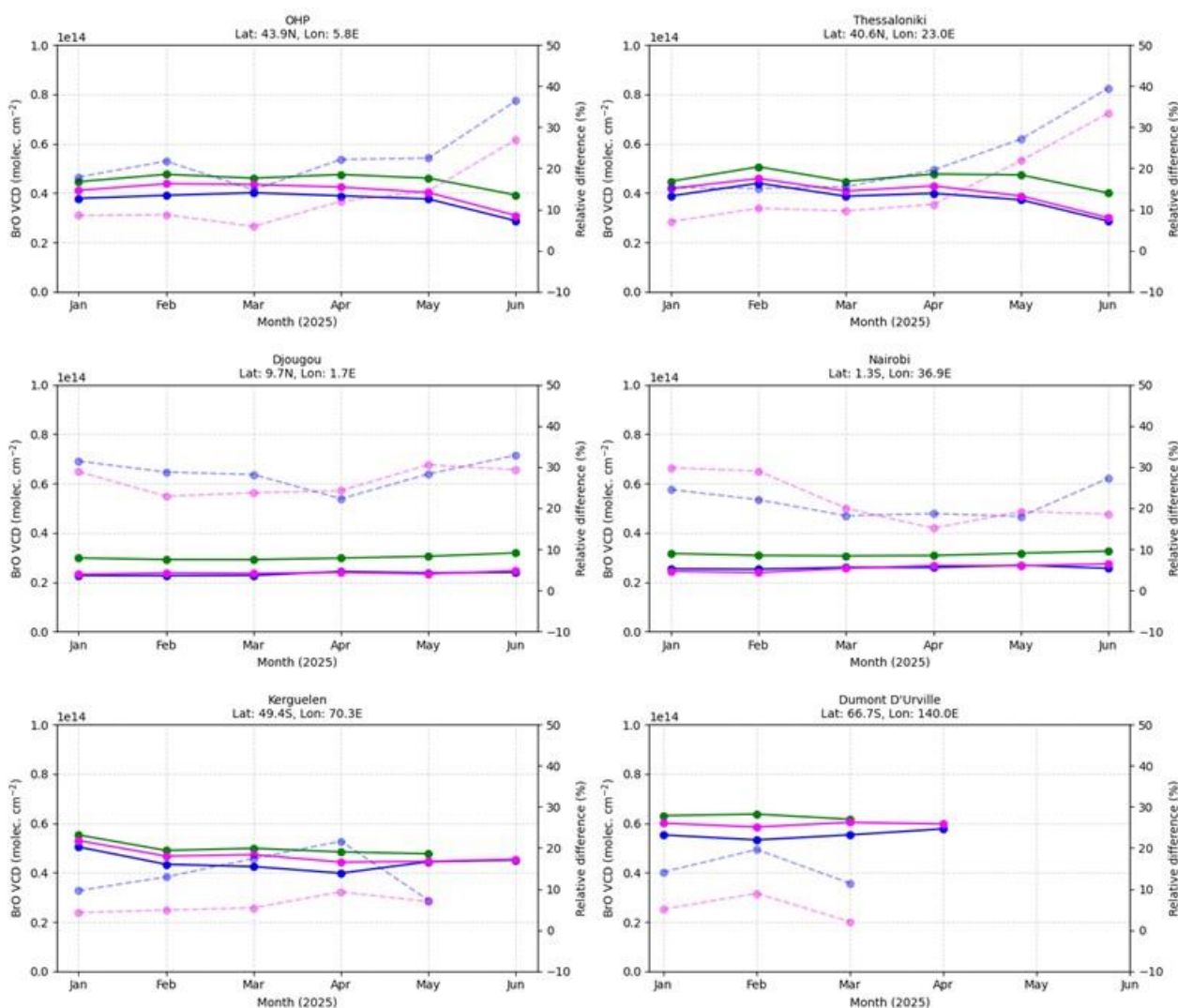


Figure 7.12. Comparison of monthly average total BrO VCD over 12 ground stations for the sensors GOME-2 B/C and TROPOMI, from January until June 2025. Solid lines indicate absolute VCD values; the solid lines display the relative differences of the TROPOMI VCD and that of the GOME-2 instruments.

The actual comparison of the BrO VCD values for the three instruments is depicted in Figure 7.12.

Overall, the two GOME-2 instruments (solid pink and blue lines) closely agree with each other. Although not always, the TROPOMI VCD values (green) tend to be higher than the GOME-2 results. The results from the three instruments agree well, however, when it comes to the variation over the year.

The origin of the negative offset of the GOME-2 values with respect to TROPOMI is not clear, but may be due to simplified air-mass-factor treatment in the TROPOMI data. Comparisons of TROPOMI values with Harestua ground measurements for 2019 show a very good agreement (Van Gent and Hendrick, 2022). This agrees with the observed lower values for the GOME-2 instruments with respect to Harestua measurements, as shown in earlier editions of this report (see the results for 2022 below).

Unfortunately, the TROPOMI monthly-averaged data obtained from S5P-PAL seems to show more missing data points than when calculating those values manually. This is quite likely due to the fact

that the S5P-PAL data is filtered for qa value > 0.5 , which, for example, eliminates pixels with large cloud cover or large solar angles. The data suffice, however for the intend of the comparison.

The dashed lines in the plots indicate relative differences. Overall, the deviation of the GOME-2 VCD's with respect to TROPOMI remains within the requirements of 30 %, although somewhat larger deviations are occasionally observed for GOME-2B in particular.

Below we repeat the results of the comparison of the GOME-2 VCDs with those from Harestua ground measurements of the Operations Report 1/2022.

The sensitivity of these measurements to the troposphere is increased by using a fixed reference spectrum corresponding to clear-sky noon summer conditions for the spectral analysis. In order to ensure the photochemical matching between satellite and ground-based observations, sunrise ground-based columns have been photochemically converted to the satellite overpass SZAs using a stacked box photochemical model (Hendrick *et al.*, 2007 and 2008).

Comparison results (150 km overpasses) for GOME-2B and GOME-2C are shown in Figure 7.13 and Figure 7.14, respectively.

Mean biases values between GOME-2B/C and ground-based data are of -15 ± 11 % and -9 ± 10 %. GOME-2B/C BrO columns are thus all within the target accuracy of 30 % and also within the optimal accuracy of 15 %, except GOME-2B which is slightly above the required optimal accuracy threshold.

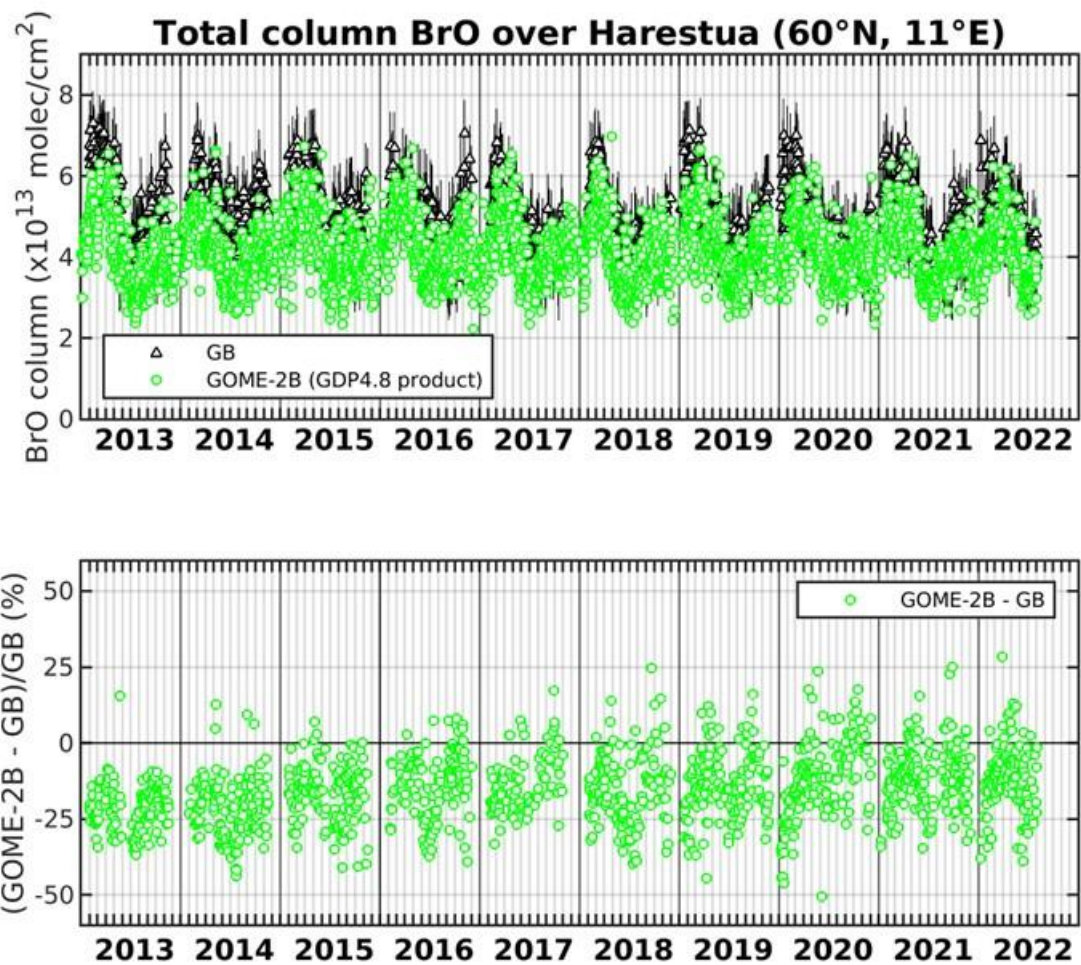


Figure 7.13. Comparison between GOME-2B GDP-4.8 and ground-based total BrO columns at Harestua (60°N, 11°E). The relative differences appear in the lower plot.

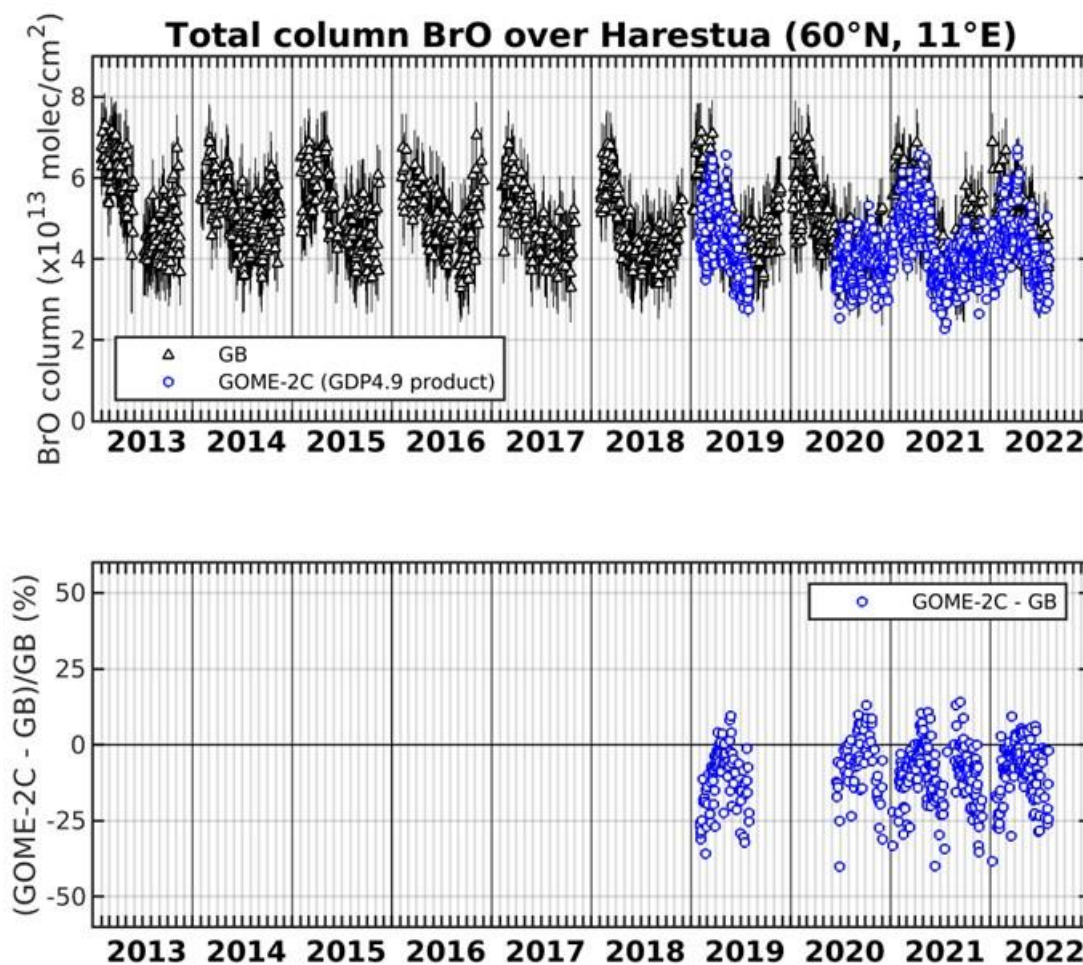


Figure 7.14. Comparison between GOME-2C GDP-4.9 and ground-based total BrO columns at Harestua (60°N, 11°E). The relative differences appear in the lower plot.

Status of GOME-2B and GOME-2C SO₂

GOME-2 SO₂ GDP-4.8 continues to be used for the near-real-time observation of volcanic activity within the [SACS](#) service. The Support to Aviation Control Service (SACS) hosted by the Royal Belgian Institute for Space Aeronomy (BIRA-IASB) aims at supporting the Volcanic Ash Advisory Centres, like Toulouse VAAC and London VAAC. This is achieved by delivering near real-time data of SO₂ and aerosols derived from satellite measurements regarding volcanic emissions by UV-VIS (OMI, GOME-2A and GOME-2B composite until 31 March 2021 and GOME-2B and GOME-2C composite since then, OMPS, TROPOMI) and infrared (AIRS, IASI-A, IASI-B) instruments. In case of volcanic eruptions over the locations of known volcanoes, shown in Figure 7.15, notifications are sent out by email to interested parties. The SACS notification archive service gathers all the notifications; the results can be found [here](#).

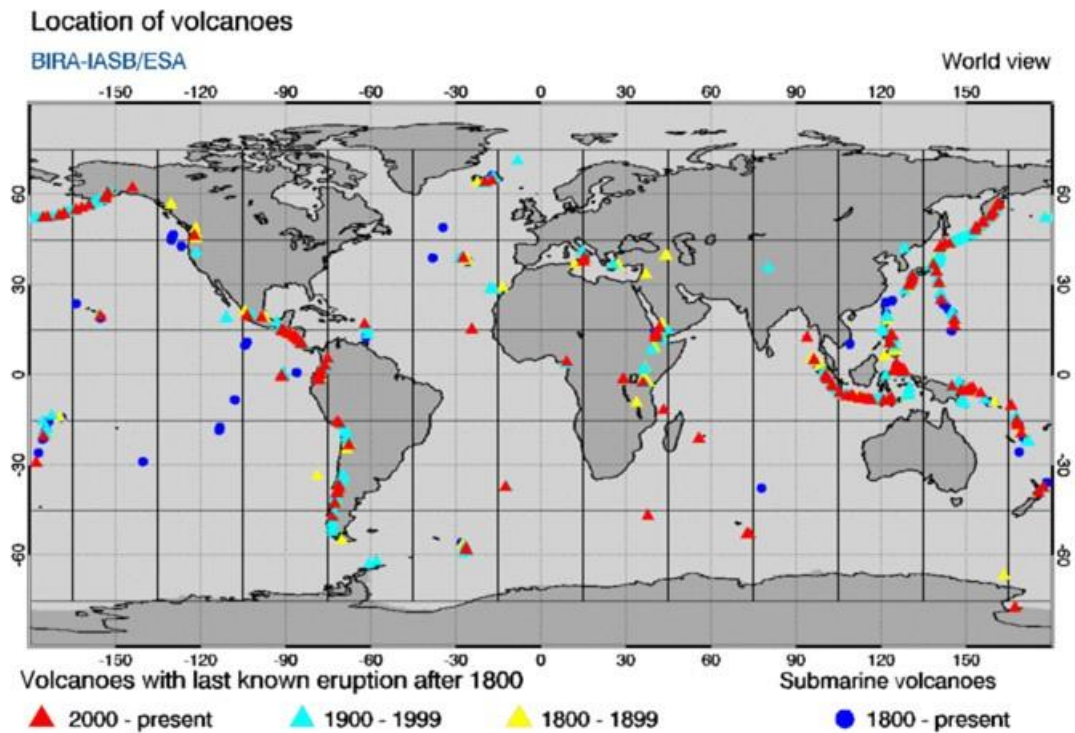


Figure 7.15. The global locations of known volcanoes with eruptions after 1800.

In the first half of 2025, SACS reported a mild level of volcanic activity throughout, with only two days holding events reporting more than 20 DU in SO₂ load as shown in Figure 7.16. GOME-2B issued 178 alerts, with SO₂ loads ranging between 2 and 24.5 DU, with a mean global level of 3.9 ± 2.4 DU and median 3.2 DU. GOME-2C issued 143 alerts, with SO₂ loads ranging between 2 – 25 DU, with a mean global level of 4.4 ± 2.7 DU and median of 3.5 DU.

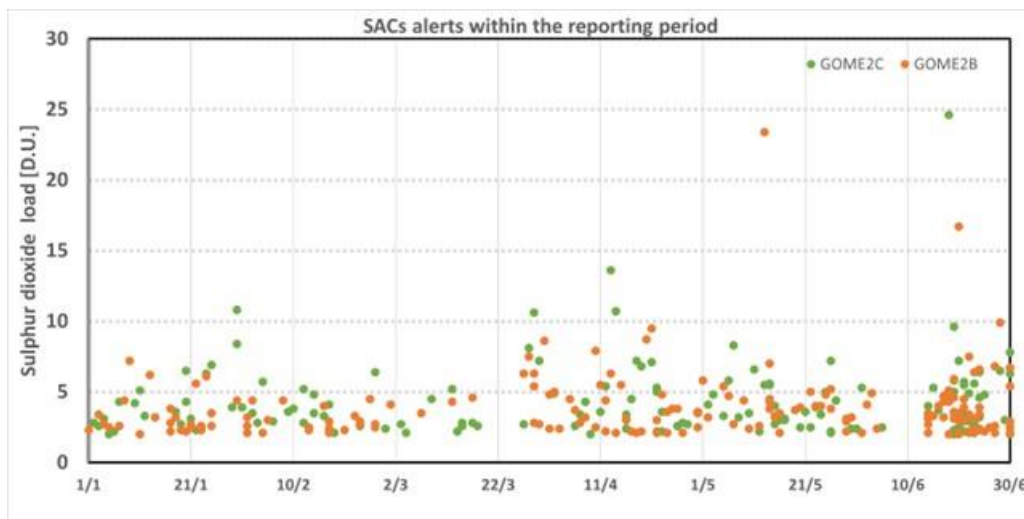


Figure 7.16. GOME-2B [orange] and GOME-2C [green] SO₂ load SACS alerts during the reporting period as time-series.

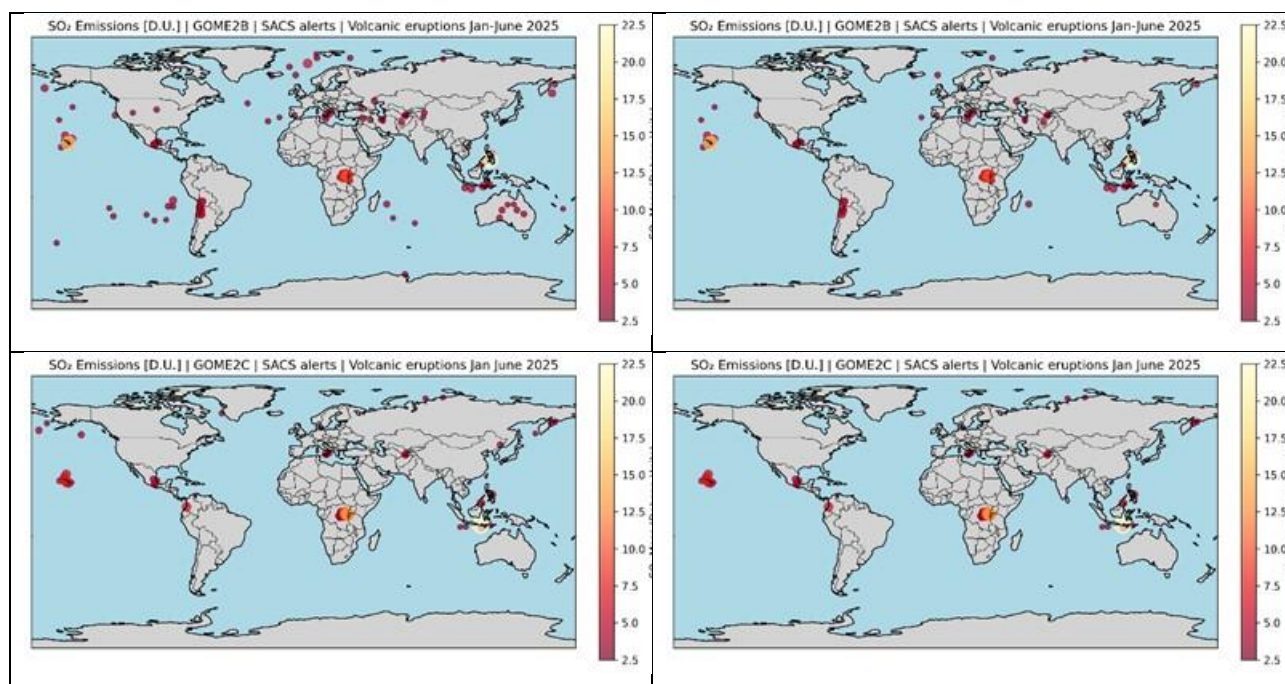


Figure 7.17. GOME-2B [upper] and GOME-2C [lower] SO₂ load SACS alerts during the reporting period with all alerts issued [left column] and filtered at < 65° SZA [right column]. The size of the markers follows the SO₂ load reported.

During the reporting period, the main eruptions/eruptive periods identified by the GOME-2B/2C observations are shown in Figure 7.17, coloured and sized according to the magnitude of the SO₂ load sensed by each instrument. While the GOME-2C alerts are reporting over known volcanic locations (shown in Figure 7.15) with and without filtering for the SZA values, the GOME-2B alerts [top left] appear to place volcanic SO₂ emissions at locations where no volcanoes exist, such as in Australia, in the United States, over the East Pacific. These mis-identifications, filtered using a cut-off for the associated SZA value, also reported by SACS, merit further investigation in the light of possible further degradation of the GOME-2B instrument as it nears its end of life.

During the reporting period, only two eruptions are moderately noteworthy:

Mount Kanlaon, Philippines | Eruption Date: May 13, 2025 | See Figure 7.18

A moderately explosive eruption occurred at the summit crater of Kanlaon Volcano at 02:55 AM local time on 13 May 2025 (19:55 UTC on May 12), generating a greyish voluminous [plume that rose approximately 4.5 kilometers](#) above the vent before drifting to the southwest. Incandescent pyroclastic density currents descended the southern slopes within approximately two kilometers of the crater based on visual and thermal camera monitoring. Thin ashfall was reported in the several localities of Negros Occidental. [Approximately 20 ktons of SO₂ were released](#) according to S5P-TROPOMI (18.5 tons according to [N20/OMPS](#))

Alert Level 3 (magmatic unrest) prevailed over Kanlaon, meaning that the volcano was in a state of magmatic unrest, with currently increased chances of short-lived moderately explosive eruptions that could generate life-threatening volcanic hazards. It was [recommended that communities within a 6-km radius from the summit crater remain evacuated](#) due to the danger of pyroclastic density currents, ballistic projectiles, ashfall, rockfall and other related hazards and also communities that experience ashfall should take precautions and use protective masks or wet cloth to prevent ash inhalation.

Mount Lewotobi (Lewotobi Laki-Laki) | Eruption Date: June 18, 2025 | See Figure 7.19

Eruptive activity continued at Lewotobi Laki-laki during 18-25 June, after the explosive eruption on 17 June at 9:35 UTC (17:35 local time) that sent a dense gray ash column [approximately 11 km](#) above the crater and release a little over 30 ktons of SO₂ ([N20/OMPS](#)) Volcanic tremors continued, indicating that the volcanic activities remained active. Six districts and two islands were impacted by volcanic ash from the eruption.

With a plume visible from a 90 to 150 km distance, [the Indonesian Center for Volcanic and Geological Disaster Mitigation escalated the volcano's alert status](#) from Level III (Alert) to Level IV (Warning), the highest level. The Alert Level remained at 4 (on a scale of 1-4) and [the public was warned to stay 7 km away from the center of Laki-laki](#) and 8 km in a semicircle clockwise from the SW to the NE. According to news reports [the number of evacuees totaled 4,954 on 19 June](#) and 4,007 as of 21 June. Finally, the eruption caused travel disruption with 12 flights at Komodo International Airport (Labuan Bajo sub-district) cancelled due to the volcanic ash.

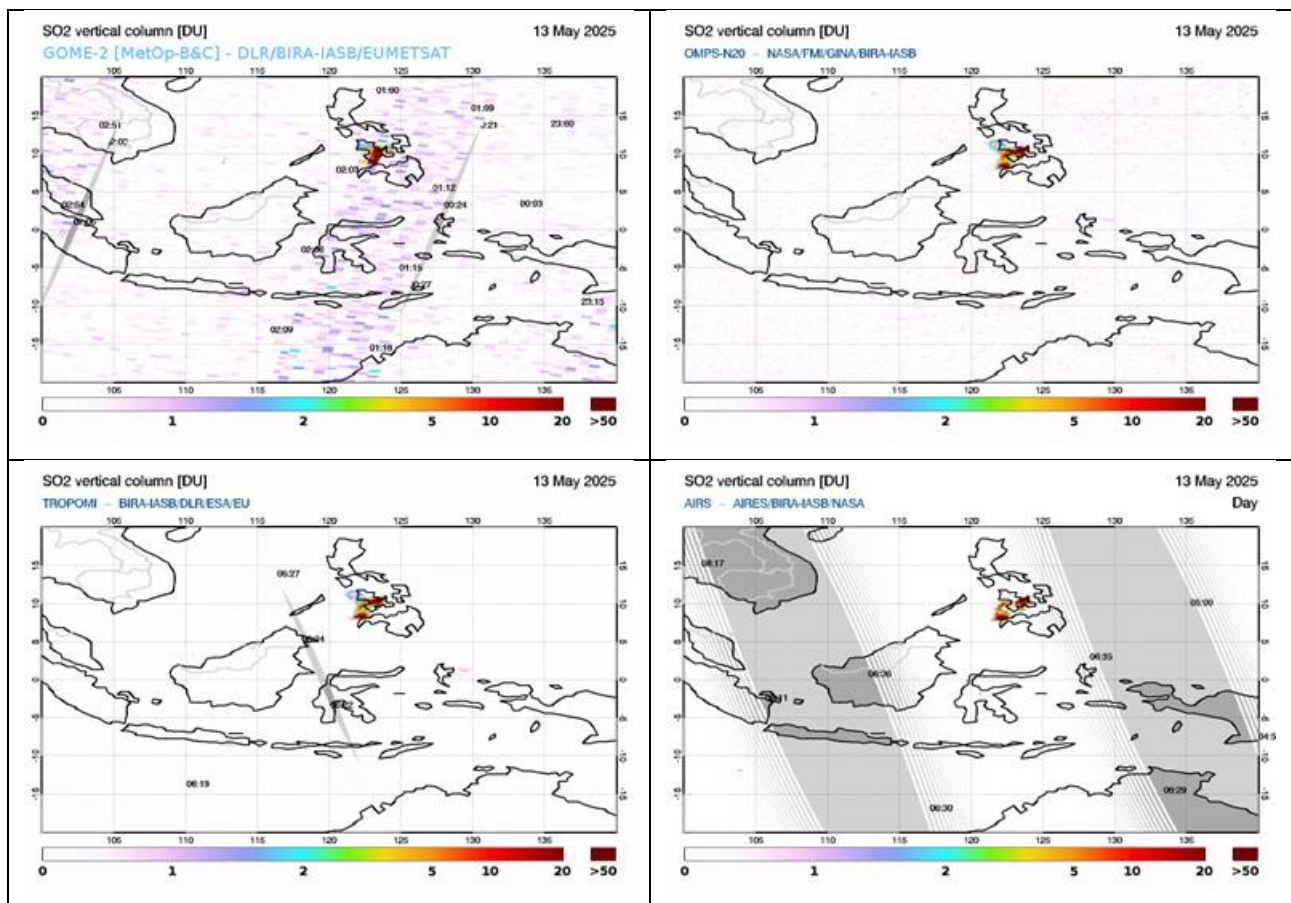


Figure 7.18. Mt. Kanlaon, Philippines, eruption, on the 13th of May 2025, sensed by GOME2-B/C [upper left], OMPS/NPP [upper right], S5P/TROPOMI [bottom left] and AIRS/Aura [bottom right] from the [SACS](#) monitoring pages.

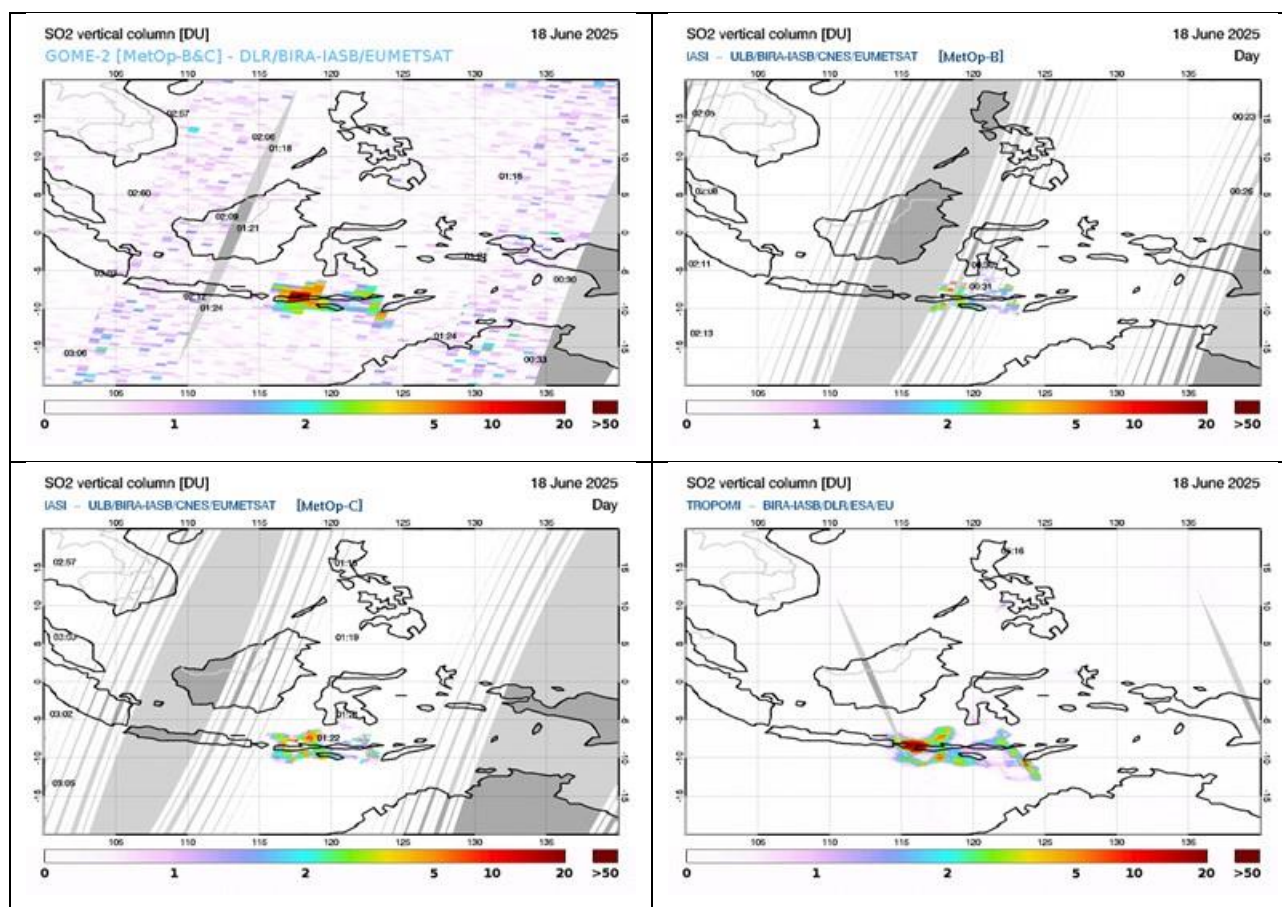


Figure 7.19. Mount Lewotobi, Indonesia, eruption, on the 18th of June 2025, sensed by GOME2-B/C [upper left], IASI-B [upper right], IASI-C [bottom left] and S5P/TROPOMI [bottom right] from the [SACS](#) monitoring pages.

The coherence of the GOME-2B/C measurements with the other morning instruments (Figure 7.18 and Figure 7.19) is quite strong and clear.

References:

Clémer, K., Van Roozendael, M., Fayt, C., Hendrick, F., Hermans, C., Pinardi, G., Spurr, R., Wang, P., and De Mazière, M.: Multiple wavelength retrieval of tropospheric aerosol optical properties from MAXDOAS measurements in Beijing, *Atmos. Meas. Tech.*, 3, 863-878, 2010.
<https://doi.org/10.5194/amt-3-863-2010>

De Smedt, I., Stavrou, T., Hendrick, F., Danckaert, T., Vlemmix, T., Pinardi, G., Theys, N., Lerot, C., Gielen, C., Vigouroux, C., Hermans, C., Fayt, C., Veeffkind, P., Müller, J.-F., and Van Roozendael, M.: Diurnal, seasonal and long-term variations of global formaldehyde columns inferred from combined OMI and GOME-2 observations, *Atmos. Chem. Phys.*, 15, 12519-12545, 2015.
<https://doi.org/10.5194/acp-15-12519-2015>

De Smedt, I., Pinardi, G., Vigouroux, C., Compernelle, S., Bais, A., Benavent, N., Boersma, F., Chan, K.-L., Donner, S., Eichmann, K.-U., Hedelt, P., Hendrick, F., Irie, H., Kumar, V., Lambert, J.-C., Langerock, B., Lerot, C., Liu, C., Loyola, D., PETERS, A., Richter, A., Rivera Cárdenas, C., Romahn, F., Ryan, R. G., Sinha, V., Theys, N., Vlietinck, J., Wagner, T., Wang, T., Yu, H., and Van Roozendael, M.: Comparative assessment of TROPOMI and OMI formaldehyde observations

and validation against MAX-DOAS network column measurements, *Atmos. Chem. Phys.*, 21, 12561–12593, 2021.

<https://doi.org/10.5194/acp-21-12561-2021>

Gielen, C., Van Roozendael, M., Hendrick, F., Pinardi, G., Vlemmix, T., De Bock, V., De Backer, H., Fayt, C., Hermans, C., Gillotay, D., and Wang, P.: A simple and versatile cloud-screening method for MAX-DOAS retrievals, *Atmos. Meas. Tech.*, 7, 3509–3527, 2014.

<https://doi.org/10.5194/amt-7-3509-2014>

Hendrick, F.M., Van Roozendael, M., Chipperfield, M.P., Dorf, M., Goutail, F., Yang, X., Fayt, C., Hermans, C., Pfeilsticker, K., Pommereau, J.-P., Pyle, J.A., Theys, N., and De Maziere, M.: Retrieval of stratospheric and tropospheric BrO profiles and columns using ground-based zenith-sky DOAS observations at Harestua, 60° N., *Atmos. Chem. Phys.*, 7, 4869–4885, 2007.

<https://doi.org/10.5194/acp-7-4869-2007>

Hendrick, F., Johnston, P.V., De Mazière, M., Fayt, C., Hermans, C., Kreher, K., Theys, N., Thomas, A., and Van Roozendael, M.: One-decade trend analysis of stratospheric BrO over Harestua (60°N) and Lauder (45°S) reveals a decline, *Geophys. Res. Letters*, 35, L14801, 2008.

<https://doi.org/10.1029/2008gl034154>

Hendrick, F., Müller, J.-F., Clémer, K., Wang, P., De Mazière, M., Fayt, C., Gielen, C., Hermans, C., Ma, J.Z., Pinardi, G., Stavrou, T., Vlemmix, T., and Van Roozendael, M.: Four years of ground-based MAX-DOAS observations of HONO and NO₂ in the Beijing area, *Atmos. Chem. Phys.*, 14, 765–781, 2014.

<https://doi.org/10.5194/acp-14-765-2014>

Pinardi, G., Van Roozendael, M., Lambert, J.-C., Granville, J., Hendrick, F., Tack, F., Yu, H., Cede, A., Kanaya, Y., Irie, I., Goutail, F., Pommereau, J.-P., Pazmino, A., Wittrock, F., Richter, A., Wagner, T., Gu, M., Remmers, J., Friess, U., Vlemmix, T., PETERS, A., Hao, N., Tiefengraber, M., Herman, J., Abuhassan, N., Bais, A., Kouremeti, N., Hovila, J., Holla, R., Chong, J., Postlyakov, O., Ma, J.: GOME-2 total and tropospheric NO₂ validation based on zenith-sky, direct-sun and multi-axis DOAS network observations, *Proceeding of the EUMETSAT conference*, 22-26 September 2014, Geneva, Switzerland.

Pinardi, G., Van Roozendael, M., Hendrick, F., Theys, N., Abuhassan, N., Bais, A., Boersma, F., Cede, A., Chong, J., Donner, S., Drosoglou, T., Frieß, U., Granville, J., Herman, J. R., Eskes, H., Holla, R., Hovila, J., Irie, H., Kanaya, Y., Karagkiozidis, D., Kouremeti, N., Lambert, J.-C., Ma, J., Peters, E., PETERS, A., Postlyakov, O., Richter, A., Remmers, J., Takashima, H., Tiefengraber, M., Valks, P., Vlemmix, T., Wagner, T., and Wittrock, F.: Validation of tropospheric NO₂ column measurements of GOME-2A and OMI using MAX-DOAS and direct sun network observations, *Atmos. Meas. Tech.*, 13, 6141–6174, 2020.

<https://doi.org/10.5194/amt-13-6141-2020>

Richter, A., Behrens, L., Hilboll, A., Munassar, S., Burrows, J.P., Pinardi, G., and Van Roozendael, M.: Cloud effects on satellite retrievals of tropospheric NO₂ over China, oral presentation at the DOAS workshop, September 2017, Yokohama, Japan.

Theys, N., De Smedt, I., Yu, H., Danckaert, T., van Gent, J., Hörmann, C., Wagner, T., Hedelt, P., Bauer, H., Romahn, F., Pedernana, M., Loyola, D., and Van Roozendael, M.: Sulfur dioxide retrievals from TROPOMI onboard Sentinel-5 Precursor: algorithm theoretical basis, *Atmos. Meas. Tech.*, 10, 119–153, 2017.

<https://doi.org/10.5194/amt-10-119-2017>

Van Gent, J. and Hendrick, F.: S5P/TROPOMI total BrO algorithm TCBRO: Validation report, issue: 1.0.0, date: 09/01/2022, https://data-portal.s5p-pal.com/product-docs/bro/S5P-L2-BIRA-VR_TCBRO_1.0.0_20220110.pdf

Verhoelst, T., Compernelle, S., Pinardi, G., Lambert, J.-C., Eskes, H. J., Eichmann, K.-U., Fjæraa, A. M., Granville, J., Niemeijer, S., Cede, A., Tiefengraber, M., Hendrick, F., Pazmiño, A., Bais, A., Bazureau, A., Boersma, K. F., Bogner, K., Dehn, A., Donner, S., Elokhov, A., Gebetsberger, M., Goutail, F., Grutter de la Mora, M., Gruzdev, A., Gratsea, M., Hansen, G. H., Irie, H., Jepsen, N., Kanaya, Y., Karagkiozidis, D., Kivi, R., Kreher, K., Levelt, P. F., Liu, C., Müller, M., Navarro Comas, M., PETERS, A. J. M., Pommereau, J.-P., Portafaix, T., Prados-Roman, C., Puentedura, O., Querel, R., Remmers, J., Richter, A., Rimmer, J., Rivera Cárdenas, C., Saavedra de Miguel, L., Sinyakov, V. P., Stremme, W., Strong, K., Van Roozendael, M., Veeffkind, J. P., Wagner, T., Wittrock, F., Yela González, M., and Zehner, C.: Ground-based validation of the Copernicus Sentinel-5P TROPOMI NO₂ measurements with the NDACC ZSL-DOAS, MAX-DOAS and Pandonia global networks, *Atmos. Meas. Tech.*, 14, 481–510, 2021.

<https://doi.org/10.5194/amt-14-481-2021>

Vlemmix, T., Hendrick, F., Pinardi, G., Smedt, I., Fayt, C., Hermans, C., PETERS, A., Wang, P., Levelt, P., and Van Roozendael, M.: MAX-DOAS observations of aerosols, formaldehyde and nitrogen dioxide in the Beijing area: comparison of two profile retrieval approaches, *Atmos. Meas. Tech.*, 2, 941–963, 2015.

<https://doi.org/10.5194/amt-8-941-2015>

Wang, T., Hendrick, F., Wang, P., Tang, G., Clémer, K., Yu, H., Fayt, C., Hermans, C., Gielen, C., Müller, J.-F., Pinardi, G., Theys, N., Brenot, H., and Van Roozendael, M.: Evaluation of tropospheric SO₂ retrieved from MAX-DOAS measurements in Xianghe, China, *Atmos. Chem. Phys.*, 14(20), 11149–11164, 2014.

<https://doi.org/10.5194/acp-14-11149-2014>

7.3.1. Online quality monitoring

Online quality monitoring plots are continuously generated at DLR and published for O₃, NO₂, BrO, HCHO, SO₂, H₂O products as described in Section 7.1.3.

BIRA-IASB provides quality assessment (QA) pages for vertical column amounts of NO₂, HCHO, BrO and SO₂ derived from GOME-2B and GOME-2C. The goal is to provide an easy tool to quickly spot anomalies and trends in the L2 data, by selecting and examining geographical regions of interest. These pages are available under <https://cdop.aeronomie.be/quality-assessment/>.

The monitored L2 is provided by DLR with processor version GDP 4.8 for GOME-2B and GDP 4.9 for GOME-2C.

System developments:

- The GOME-2 monitoring page shows time-series for Metop-B and Metop-C. Metop-A data is kept internally for comparison reasons.
- The current monitoring system, based on data storage in an SQL database, remains slow in use. As mentioned in the previous report, a new system has been under development and has shown to be much faster.

Monitoring status:

SO₂

In the case of SO₂, the available geographical regions of interest are either locations with known outgassing volcanoes or locations with strong anthropogenic sources of SO₂. The resulting graphs show a history of monthly average values over the selected region.

In Figure 7.20 and Figure 7.21, two relevant panels are presented for the time period from January to June 2025. In the upper panels, the SO₂ fitting RMS is shown, an important parameter which acts as immediate indicator to the stability of the instruments/algorithms. In the bottom panels, the total vertical SO₂ column is presented, alongside other metrics, explained in the figure caption. Both panels include smaller subpanels which show the long-term behaviour of each sensor from the beginning of the satellite mission.

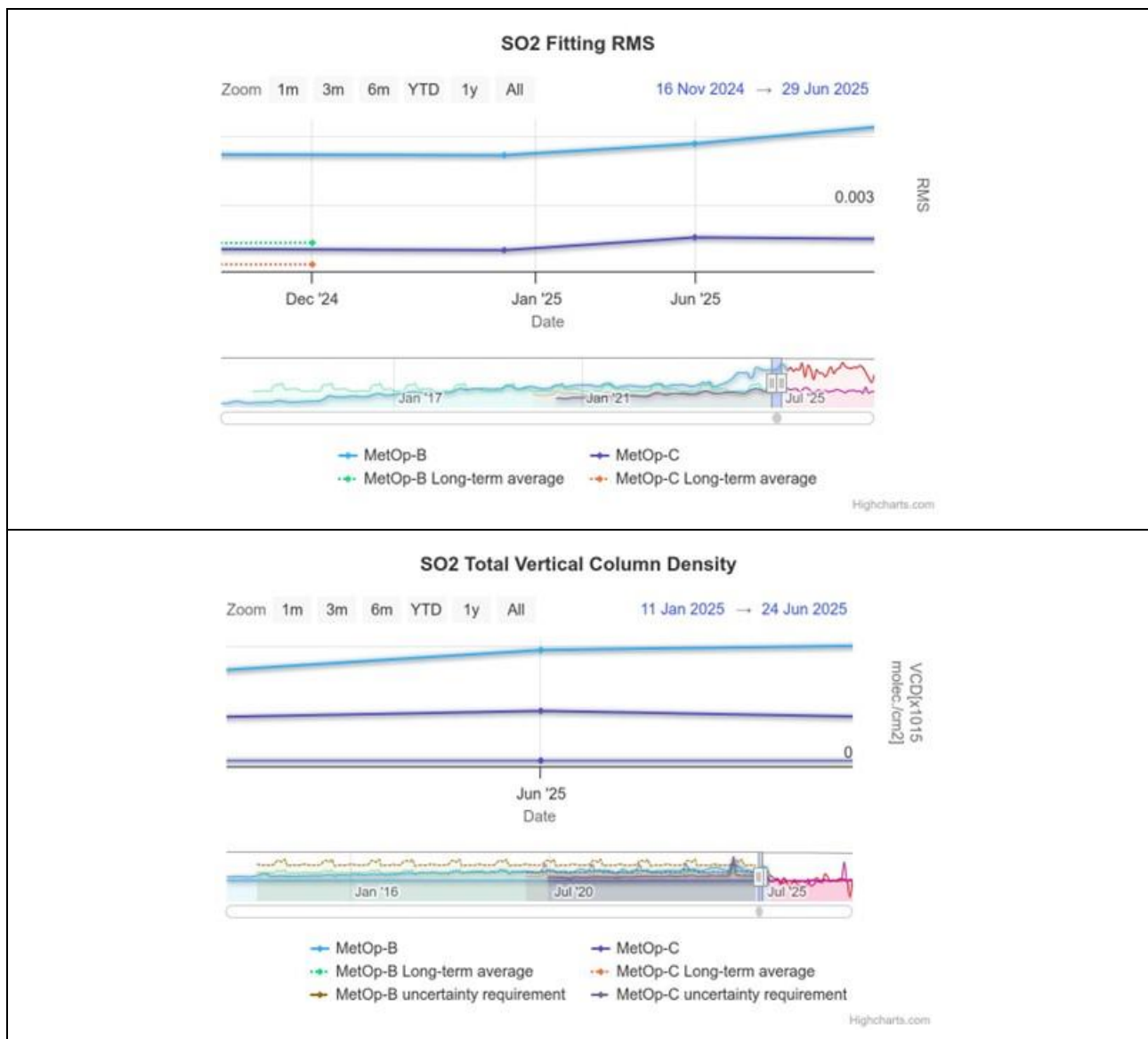


Figure 7.20. The behaviour of the GDP 4.8 GOME-2B [blue curve] and GDP 4.9 GOME-2C [black curve] 6 km plume height SO₂ products between January and June 2025 over the region of Indonesian volcanoes. Upper panel, the SO₂ fitting RMS is shown and in the bottom panel, the total vertical SO₂ column. The equivalent long-term average is also provided [see insert legend].

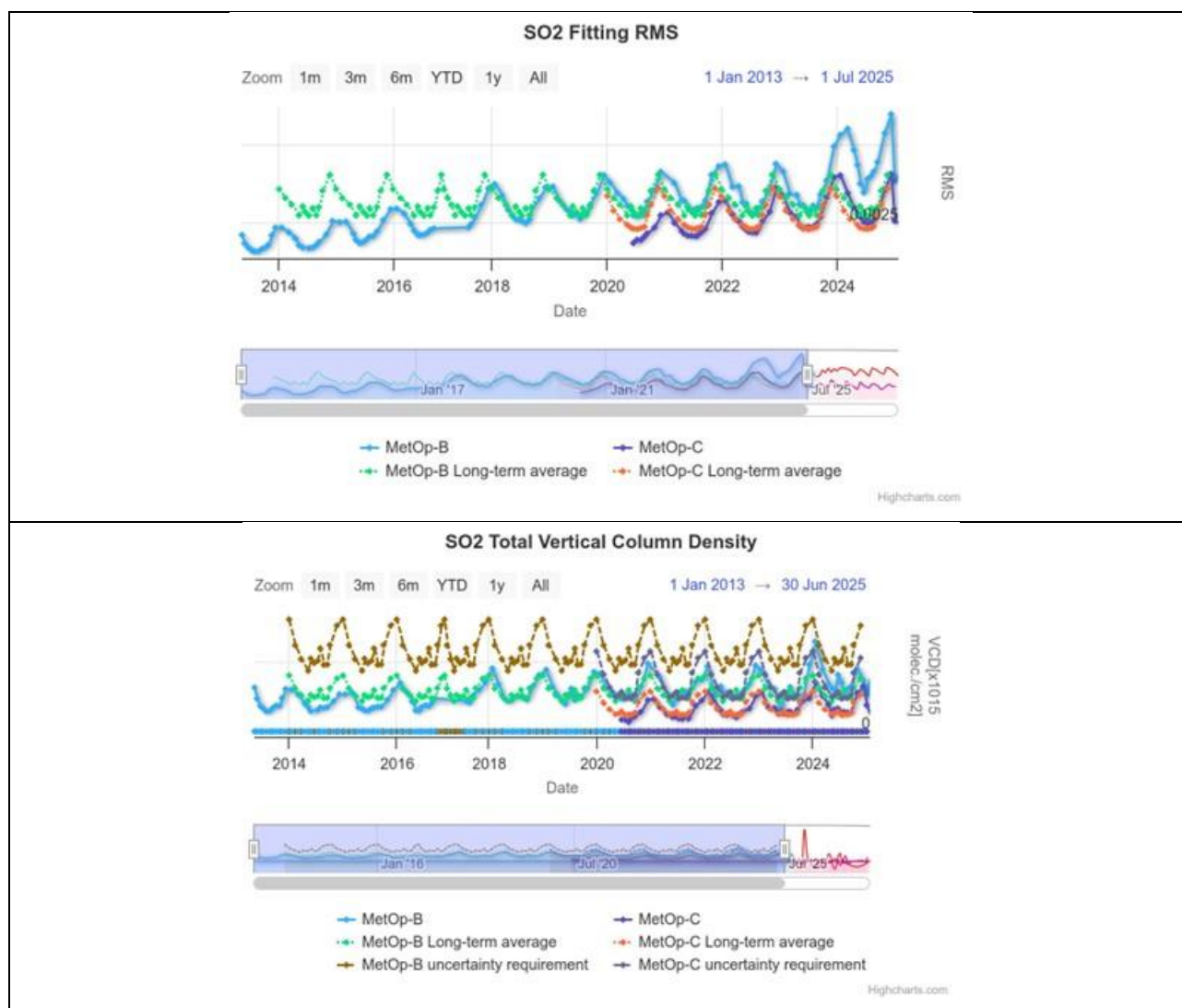


Figure 7.21. The behaviour of the GDP 4.8 GOME-2B [blue curve] and GDP 4.9 GOME-2C [black curve] 6 km plume height SO₂ products between January 2013 and July 2025, over Indonesia. Upper panel, the SO₂ fitting RMS is shown and in the bottom panel, the total vertical SO₂ column. The equivalent long-term average is also provided [see insert legend].

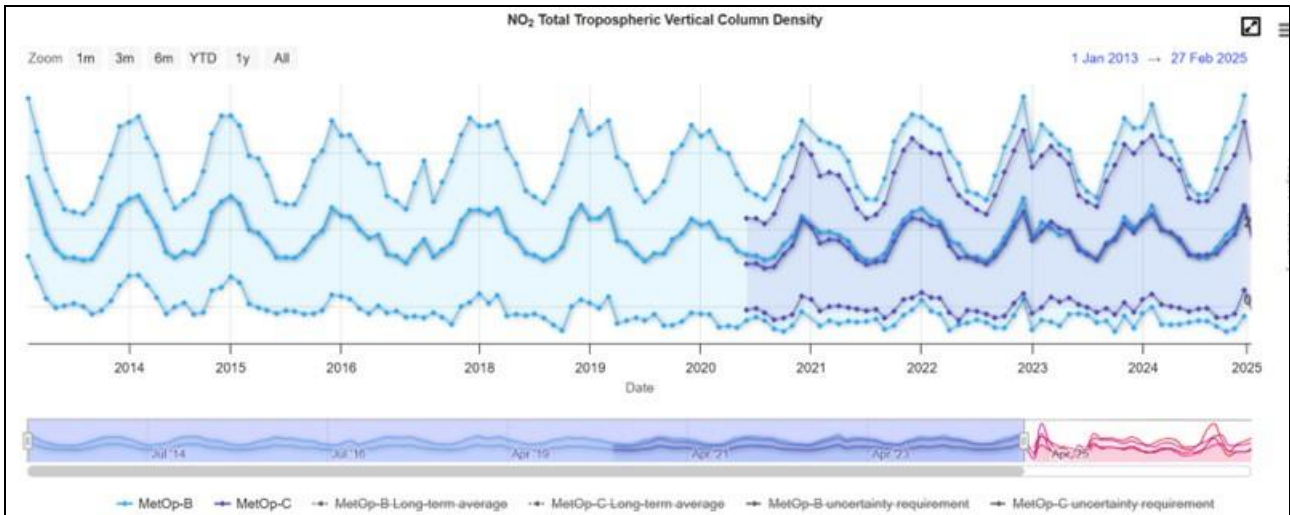
From Figure 7.20 and Figure 7.21, upper panels, no spurious jumps or artefacts are observed in the SO₂ fitting RMS during the first half of 2025, for either the anthropogenic or the volcanic locations. However, RMS continues to appear ~ 25 % larger for GOME-2B than GOME-2C and is also equally larger from its long-term average. This points to a possible degradation effect in the GOME-2B L1b data which also affects the L2 data, as shown in Figure 7.20 and Figure 7.21, lower panels. GOME-2B has provided far larger (more than 50 %) SO₂ columnar estimates than GOME-2C and ~20 – 25 % larger than the long-term average.

NO₂, HCHO, and BrO

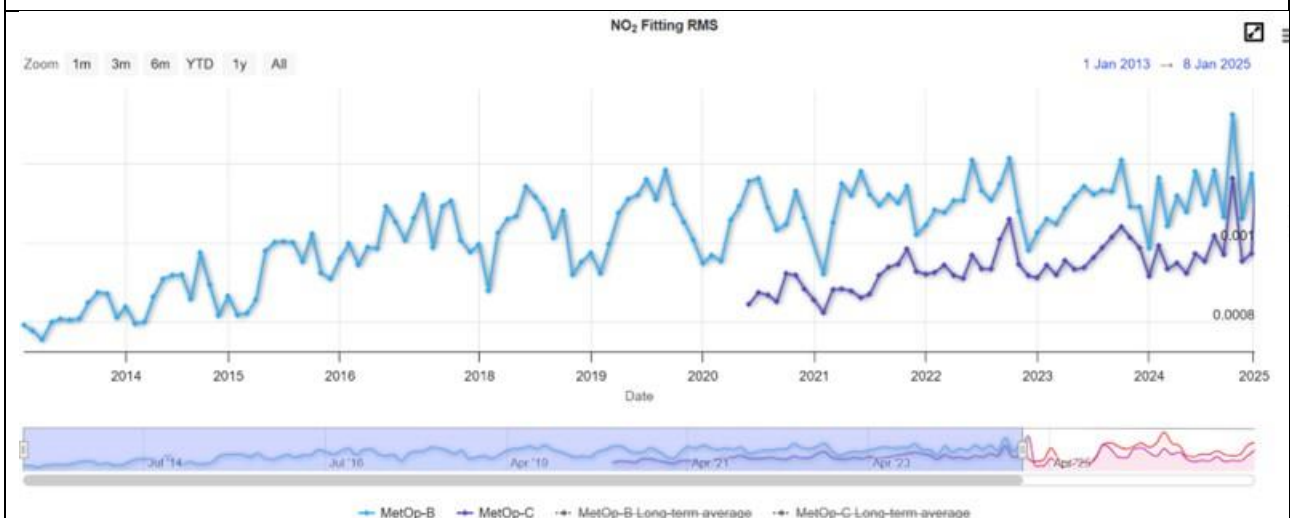
When observing the full time-series for the other monitored gases, column amounts between the two instruments agree quite well. Some examples are depicted in Figure 7.22. For NO₂, the tropospheric column amounts of both sensors show the expected annual cycle and show no systematic mutual offset (panel a, situation over the South-East US). Indications of instrumental degradation are visible in the fit residual (RMS, panel b) of both instruments. On the other hand, the

raise of GOME-2B RMS seems to have flattened out over the last few years. Similar RMS patterns are observed over other geographical regions (not shown here).

Consistent patterns of total column amounts are also observed for HCHO (panel c, Indonesia). There, however, the increase of the RMS signal for GOME-2B continues also in recent years; For BrO (panel d), a flattening of the RMS-increase is also visible, be it less pronounced than for NO₂ and depending on the observed region.



(a)



(b)

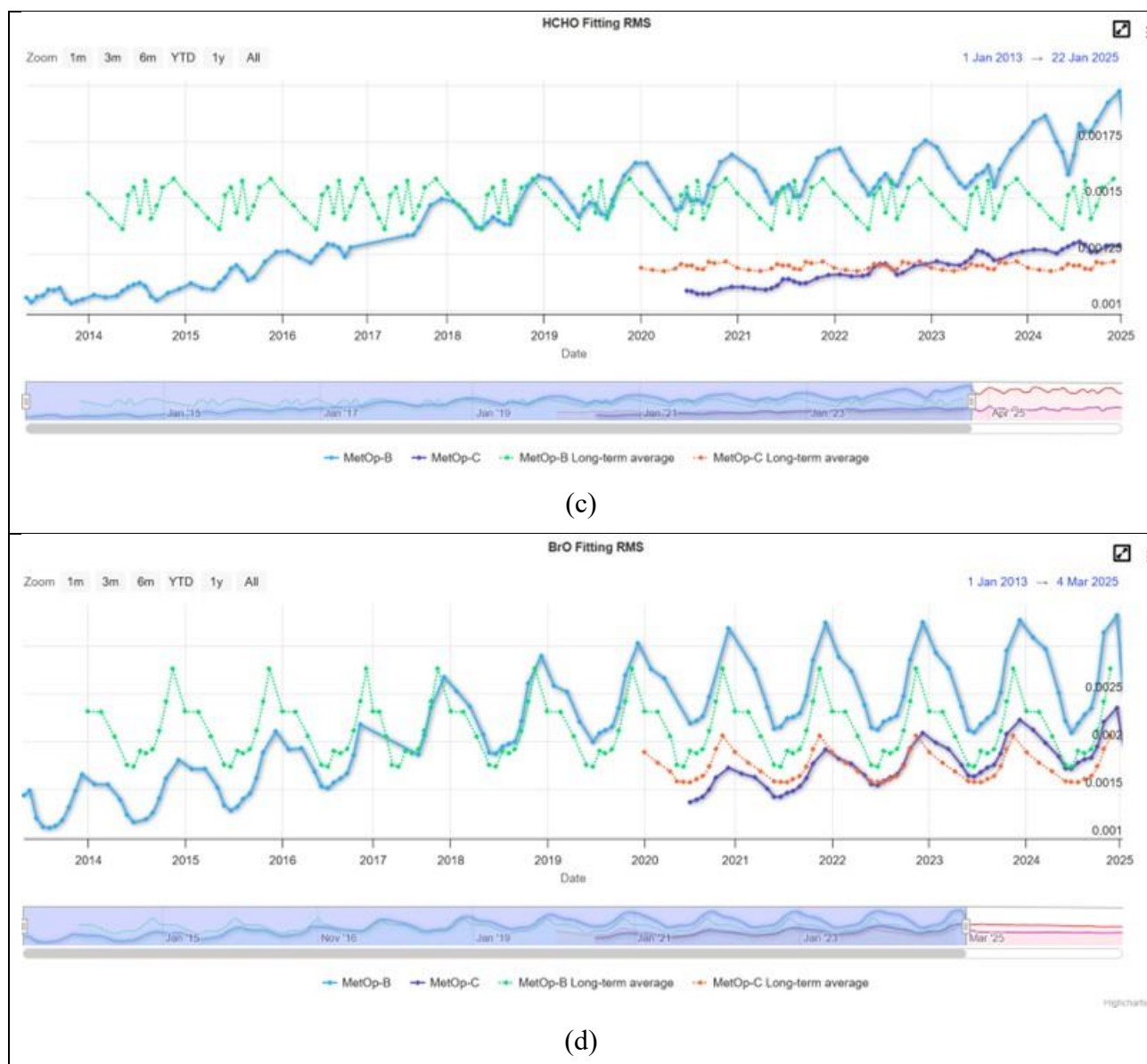


Figure 7.22. Examples of time-series from the QA monitoring page: a) NO₂ tropospheric column (plus uncertainty range) over the Southeastern US, b) NO₂ fitting RMS over S. E. US, c) HCHO fitting RMS over Indonesia, and d) Fitting RMS for BrO, averaged over the 60°-90° Arctic latitude band.

7.4. GOME-2 ozone profile products

Table 7.13. Validation status of ozone profile products

Product Identifier	Product Name	Accuracy	Reference	Validating Institute	Correlative data sources
O3M-47.1	NRT high-resolution ozone profile	Fulfils threshold accuracy requirements	RD7	KMI DWD	Ozonesonde data from SHADOZ , NDACC , NILU and WOUDC Lidar/microwave data from NDACC
O3M-311			RD22		

O3M-39	Offline high-resolution ozone profile	Fulfils threshold accuracy requirements	RD6	KMI DWD	Ozonesonde data from SHADOZ , NDACC , NILU and WOUDC Lidar/microwave data from NDACC
O3M-48			RD7		
O3M-312			RD22		

Validation results can be found in more detail on the at [AC SAF validation & quality assessment website](#).

Validation activities summary:

This summary contains validation results for the GOME-2B and GOME-2C high-resolution (HR) ozone profile products, retrieved by the Ozone Profile Retrieval Algorithm (OPERA) at KNMI. This validation section focuses on the time period July 2024 – June 2025.

The authors of this summary are Dr. Andy Delcloo from KMI and Dr. Peggy Achtert from DWD. More information on how these values are extracted is available in the [validation report](#).

There is no material difference in the content of the NRT vs. the offline vertical ozone profile data product, other than its size. The offline file is a concatenation of the NRT L2 PDUs for a particular orbit. While the validation partners are provided the L2 PDUs that were sent out in NRT for their validation, it makes no difference for the validation itself.

To report the skill scores of GOME-2 ozone profile products in a more condensed way, the statistics for the different output levels of GOME-2 are reduced to two layers: Lower Stratosphere (until an altitude of 30 km) and Upper Stratosphere (up to an altitude of 50 km).

The validation for the lower stratosphere is made with ozonesonde data, for the upper stratosphere with lidar, FTIR and/or microwave data. The stations used in this validation for the FTIR/lidar/microwave data are the Network for the Detection of Atmospheric Composition Change (NDACC) stations of Bern (microwave), Payerne (microwave), Hohenpeissenberg (lidar), Table Mountain (lidar), and Lauder (FTIR, lidar).

The collocation data used for the validation using ozonesonde data are shown in Figure 7.23.

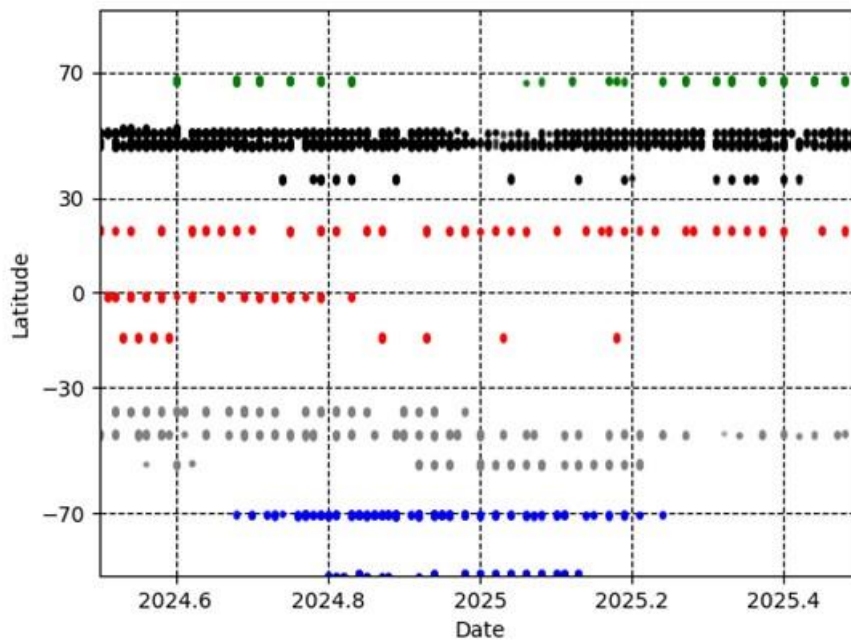


Figure 7.23. Collocation data for the validation with ozonesonde data for the time period July 2024 – June 2025.

Table 7.14 shows an overview of the obtained results for the time period July 2024 – June 2025 only for the lower and the higher stratosphere, not taking into account the tropospheric ozone column products since a dedicated product is discussed earlier in this report. The statistics for the lower stratosphere are obtained by KMI, the statistics for the higher stratosphere by DWD.

Table 7.14. Absolute Differences (AD), Relative Differences (RD) and standard deviation (STDEV) are shown on the accuracy of GOME-2B/C HR ozone profile products for the lower and the higher stratosphere for five different latitude belts for the time period July 2024 – June 2025.

GOME-2B HR						
	Lower Stratosphere			Upper Stratosphere		
	AD	RD	STDEV	AD	RD	STDEV
	(DU)	(%)	(%)	(DU)	(%)	(%)
Northern Polar Region	1.4	1.5	12.7			
Northern Mid-Latitudes	3.9	2.7	11.9	-6.9	-10.7	4.6
Tropical Region	7.9	6.0	5.40			
Southern Mid-Latitudes	15.3	7.8	10.3	-8.6	-14.9	6.4
Southern Polar Region	16.1	30.3	80.4	-	-	-
GOME-2C HR						
	Lower Stratosphere			Upper Stratosphere		
	AD	RD	STDEV	AD	RD	STDEV
	(DU)	(%)	(%)	(DU)	(%)	(%)
Northern Polar Region	0.15	1.00	9.63			
Northern Mid-Latitudes	0.21	1.70	7.95	-4.4	-6.2	2.9
Tropical Region	0.34	2.61	6.19			
Southern Mid-Latitudes	1.30	7.58	9.05	6.5	-10.1	3.8
Southern Polar Region	0.85	11.5	47.0	-	-	-

The target value (15 % accuracy) is met in both lower and upper stratosphere for all belts under consideration for Metop-B and Metop-C, except for the Southern Polar Region. The discrepancy is highest at high latitudes. For Metop-B we observed a deterioration in the upper stratosphere since the last operations report.

More detailed ozone profile validation results can also be found on the AC SAF [ozone profile validation website](#).

7.4.1. Online quality monitoring

Timeline of the vertically integrated GOME-2C ozone profile with respect to time is presented in Figure 7.24.

More information and images at the following web addresses

<https://www.temis.nl/acsaf/timeseries.php?sat=metopb>

<https://www.temis.nl/acsaf/timeseries.php?sat=metopc>

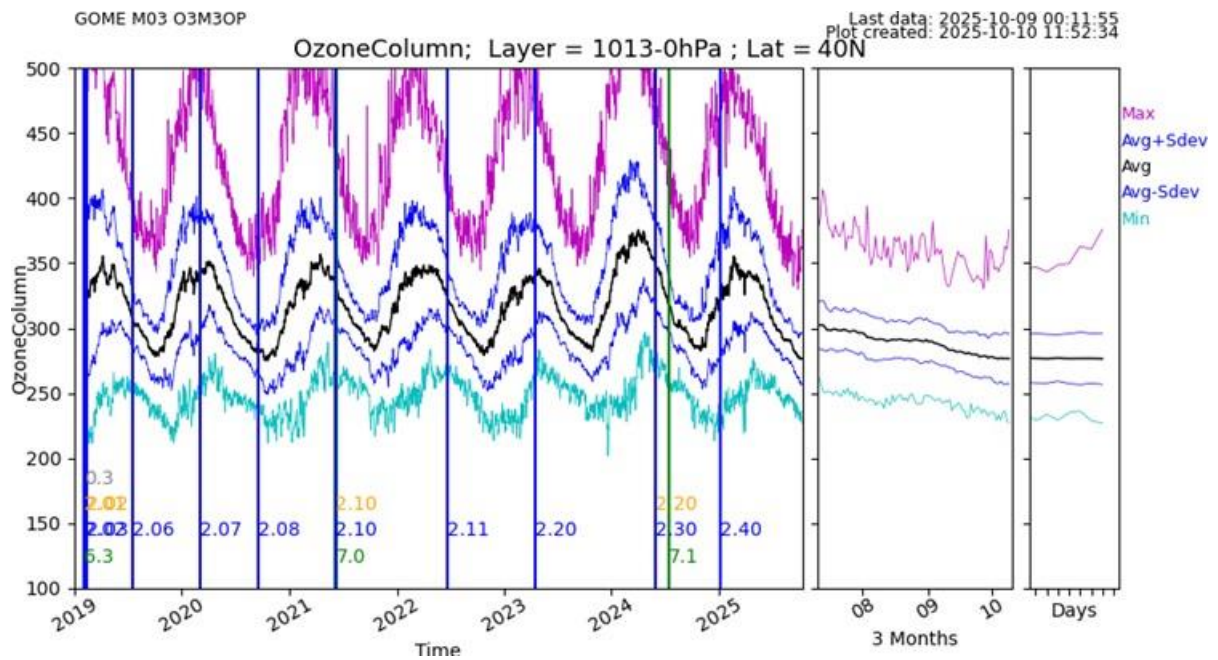


Figure 7.24. Timeline of vertically integrated GOME-2C ozone profiles (=total ozone columns) and changes in data processor (vertical lines).

Legend of the coloured vertical lines:

- Green: PPF version
- Blue: Software version (PGE)
- Orange: Algorithm version
- Grey: Config version

7.5. GOME-2 aerosol products

Table 7.15. Validation status of aerosol products

Product Identifier	Product Name	Accuracy	Reference	Validating Institute	Correlative data sources
O3M-78	NRT absorbing aerosol height	Fulfil threshold accuracy requirement	RD28	KMI, AUTH	CALIOP, EARLINET
O3M-364					
O3M-72.1	NRT absorbing aerosol index from PMDs	Fulfil threshold accuracy requirement	RD13	KNMI	Comparisons with other satellite instruments: SCIAMACHY, OMI, and intercomparison of GOME-2A with GOME-2B
O3M-362			RD29		Comparisons with the AAI products from GOME-2A and GOME-2B
O3M-69	Offline absorbing aerosol height	Fulfil threshold accuracy requirements	RD28	KMI, AUTH	CALIOP, EARLINET
O3M-79					
O3M-365					
O3M-63.1	Offline absorbing aerosol index from PMDs	Fulfil threshold accuracy requirements	RD13	KNMI	Comparisons with other satellite instruments: SCIAMACHY, OMI, and intercomparison of GOME-2A with GOME-2B
O3M-73.1			RD29		Comparisons with the AAI products from GOME-2A and GOME-2B
O3M-363					

Validation activities summary:

This summary contains validation results for the GOME-2A, GOME-2B and GOME-2C Absorbing Aerosol Height (AAH) products and is made available by the validation teams of AUTH and KMI. More information on how these values are extracted is available in the validation report [validation report](#).

AAH is a new operational AC SAF product for aerosol layer height detection, developed by KNMI within the AC SAF. It uses the AAI as an indicator to derive the actual height of the absorbing aerosol layer in the O₂-A band using the Fast Retrieval Scheme for Clouds from the Oxygen A band (FRESCO) algorithm (Wang *et al.*, 2012; Tilstra *et al.*, 2020). The AAH reported by GOME-2 onboard Metop-A, Metop-B and Metop-C, between 2007 and 2019, has been validated by AUTH against ground-based lidar data from the European Aerosol Research Lidar Network (EARLINET) database and by KMI against CALIOP aerosol layer height (De Bock, *et al.* 2020; Michailidis *et al.*, 2021).

AUTH results:

A wide choice of lidar stations (first column of Table 7.17) was made to examine the behaviour of the comparisons for different common aerosol loads around Europe. The geographical distribution

of the selected EARLINET stations depicted in Figure 7.25 indicates the domain of applicability of the validation results. All participating stations (red circles) operate high-performance multi-wavelength lidar systems. The list of stations, along with their identification codes, surface elevation, and respective references, considered for the validation of the GOME2/Metop AAH product are shown in Table 7.16.

A total of 469 carefully screened collocations between the GOME-2 retrieved Aerosol Layer Height (ALH) and EARLINET lidar measurements were identified from the beginning of the missions up to the current reporting period. The mean absolute bias (defined as *GOME-2 minus EARLINET lidar height*) was found to be equal to -0.53 ± 1.99 km, indicating a generally small systematic underestimation of the lidar-derived heights by GOME-2. The distribution of differences exhibits a near-Gaussian shape, with minimum and maximum deviations of approximately ± 5 km. When examined on a per-station basis, the mean biases for most EARLINET sites fall within the ± 1 km range, with associated standard deviations between 0.6 and 2.4 km, suggesting a consistent performance across the network with some localized variability. For the period January – June 2025, a total of 59 collocated cases were available for the validation of the GOME-2B and GOME-2C offline Aerosol Atmospheric Height (AAH) products, providing a representative sample for assessing retrieval performance during this timeframe.

Table 7.16. Locations of EARLINET lidar stations and their geographical coordinates

EARLINET Station	Code	Country	Coordinates	Elevation (m)
Antikythera	AKY	Greece	23.31E, 35.86N	193
Athens	ATZ	Greece	23.78E, 37.96N	212
Barcelona	BRC	Spain	2.12E, 41.39N	115
Bucharest	INO	Romania	26.03E, 44.34N	93
Dushanbe	DUS	Tajikistan	68.85E, 38.55N	864
Évora	EVO	Portugal	7.91W, 38.56N	293
Granada	GRA	Spain	3.60W, 37.16N	680
Lecce	SAL	Italy	18.10E, 40.33N	30
Leipzig	LEI	Germany	12.43E, 51.35N	125
Limassol ^{1,2}	LIM	Cyprus	33.04E, 34.67N	10
Minsk	MAS	Belarus	27.60E, 53.91N	200
Potenza	POT	Italy	15.72E, 40.60N	760
Sofia	SOF	Bulgaria	23.38E, 42.65N	550
Thessaloniki	THE	Greece	22.95E, 40.60N	50

¹ Cyprus University of Technology (CUT) [before Oct 2020]

² Leibniz Institute for Tropospheric Research and ERATOSTHENES Centre of Excellence [after Oct 2020]

EARLINET stations contributing to GOME2 AAH validation

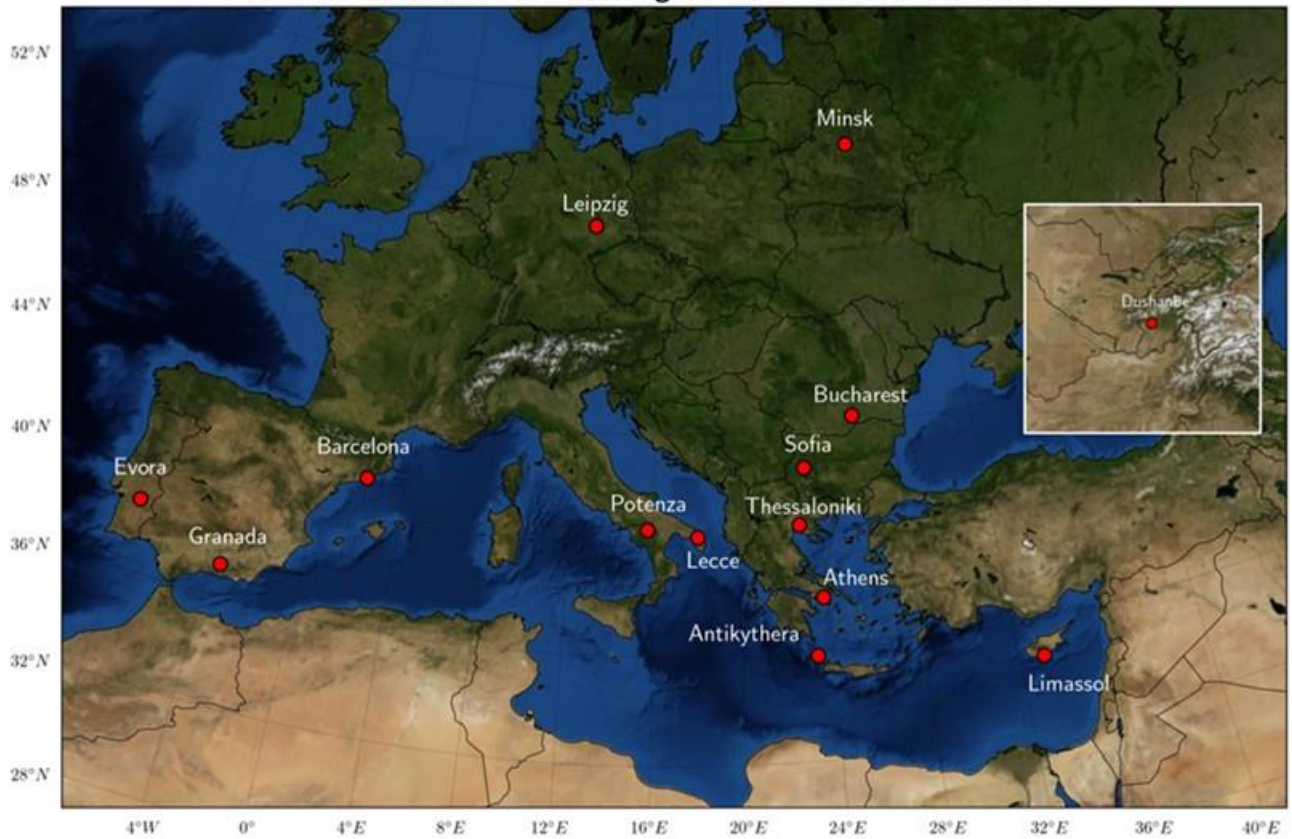


Figure 7.25. Geographical distribution of EARLINET ground-based stations for which co-locations with GOME-2 AAH data were used.

Table 7.17. Summary of statistics for the comparisons between GOME-2 AAH and LIDAR ALH for all stations

EARLINET Station	N	Statistical parameters (in km)			
		Mean absolute bias	Std	Min	Max
Athens, Greece	5	-1.98	0.78	-3.60	-1.06
Antikythera, Greece	69	-0.91	2.10	-6.77	3.84
Barcelona, Spain	36	-0.44	1.86	-4.66	2.86
Belsk, Poland	28	0.11	1.50	-3.11	3.24
Bucharest, Romania	19	-0.07	2.08	-4.81	3.37
Dushanbe, Tajikistan	36	-0.64	1.38	-3.81	1.78
Évora, Portugal	10	-0.09	1.98	-1.64	3.31
Granada, Spain	52	-0.49	2.00	-3.78	5.28
Lecce, Italy	18	-0.24	1.14	-3.47	2.05
Limassol, Cyprus	105	-1.15	2.25	-5.64	4.44
Minsk, Belarus	5	0.56	0.61	-0.05	1.51
Potenza, Italy	23	-1.25	1.68	-3.50	2.52
Thessaloniki, Greece	55	-0.12	2.07	-4.71	5.23
Warsaw, Poland	8	0.80	1.50	1.08	2.15
Summary	469	-0.53	1.99	-6.77	5.28

In Figure 7.26, the histogram of absolute differences between GOME-2 and EARLINET aerosol layer heights, calculated for all collocated cases is shown, with the associated statistics. The associated Absorbing Aerosol Index (AAI) value is color-coded. In the right panel, the scatter plot between GOME-2 AAH and aerosol layer height from EARLINET stations, for the totality of collocated cases is presented.

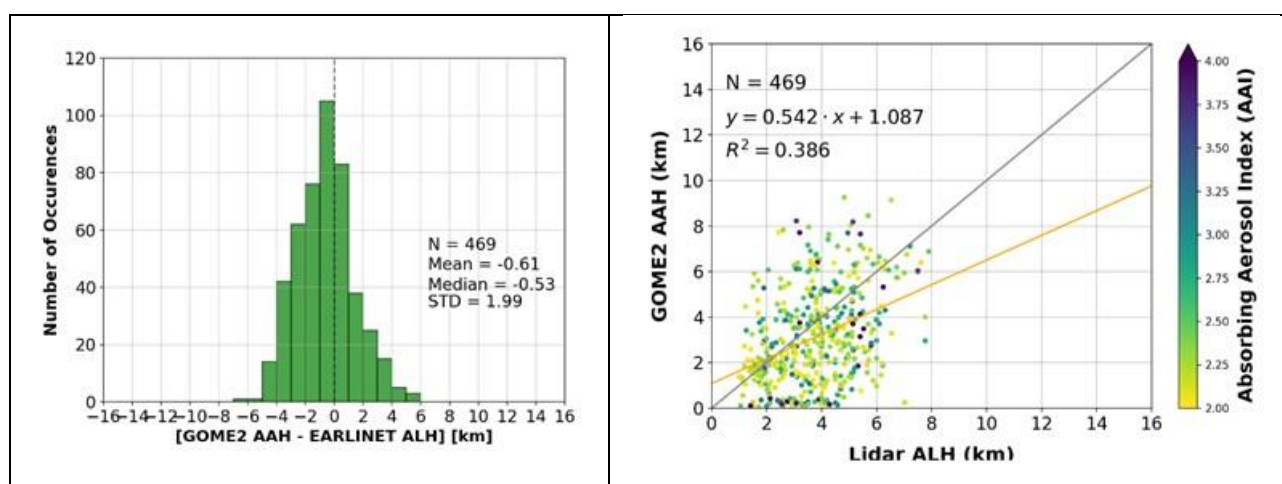


Figure 7.26. Histogram of absolute differences between GOME-2 AAH and aerosol layer height obtained from EARLINET backscatter profiles (using the WCT method), calculated for all collocated cases. The associated AAI value is color-coded. Right: Scatter plot between GOME-2 AAH and aerosol layer height from EARLINET stations, for the total of collocated cases.

Considering the possible temporal collocation mismatch and the spatial difference between the satellite pixel size and the point view of the ground-based observations, these results are quite promising and demonstrate that stable aerosol layers are well captured by the satellite sensors. The official AC SAF requirements for the accuracy of the GOME-2 AAH product state that, for heights < 10 km, the threshold accuracy is 3 km, the target accuracy is 2 km, and the optimal accuracy is 1 km. This validation effort shows that for all cases the target accuracy is met, see Table 7.18. For the different regimes, which relate to the degree of cloud cover, please refer to the [validation report](#) and Michailidis *et al.*, 2021.

Table 7.18. Percentage of collocated lidar & GOME-2 AAH cases that fulfil the optimal accuracy criteria (first row), the target criteria (second row), the threshold criteria (third row) for Regime A in the first column, Regime B in the second, Regime C in the third and the totality of the collocations in the final column. The regimes are related to the degree of cloud cover.

	Regime A (220 cases)	Regime B (211 cases)	Regime C (38 cases)	Total (469 cases)
Optimal (1 km)	28.9 %	49.2 %	47.3 %	40.0 %
Target (2 km)	52.4 %	74.8 %	73.6 %	64.2 %
Threshold (3 km)	77.3 %	87.2 %	87.2 %	82.7 %

References:

Michailidis, K., Koukouli, M.-E., Siomos, N., Balis, D., Tuinder, O., Tilstra, L. G., Mona, L., Pappalardo, G. and Bortoli, D.: First validation of GOME-2/MetOp absorbing aerosol height using EARLINET lidar observations, *Atmos. Chem. Phys.*, 21, 3193–3213, 2021.

<https://doi.org/10.5194/acp-21-3193-2021>

Tilstra, L. G., Tuinder, O., Wang, P. and Stammes, P.: ALGORITHM THEORETICAL BASIS DOCUMENT GOME-2 Absorbing Aerosol Height, SAF/AC//KNMI/ATBD/005, 1.4, Royal Netherlands Meteorological Institute, de Bilt, 2019.

https://acsaf.org/docs/atbd/Algorithm_Theoretical_Basis_Document_AA_H_Apr_2019.pdf, last access: 31 March 2021.

Wang, P., Tuinder, O. N. E., Tilstra, L. G., De Graaf, M. and Stammes, P.: Interpretation of FRESCO cloud retrievals in case of absorbing aerosol events, *Atmos. Chem. Phys.*, 12(19), 9057–9077, 2021.

<https://doi.org/10.5194/acp-12-9057-2012>

De Bock, V., A. Delcloo, K. Michailidis, M. Koukouli and D. Balis, ACSAF Absorbing Aerosol Height products validation report, SAF/AC/AUTH-RMI/VR/001, 1/2020, 3 July 2020.

https://acsaf.org/docs/vr/Validation_Report_AA_H_Jul_2020.pdf, last access: 31 March 2021.

7.5.1. Online quality monitoring

The online quality monitoring of the AAI in this section shows (left duo-plot) the radiance corrections for the PMD-AAI at 340 and 380 nm, and (right duo-plot) the uncorrected residue, and the corrected residue. The rightmost plot is the result of all the corrections and should stay more or less flat when seasonal cycles and differences are removed.

The break in the curves of the latter plot in August 2018 is caused by the introduction of a combination of the ‘End-of-Orbit’ corrections and a flattening of the AAI across the swath.

The plots can also be found at: [TEMIS website](#).

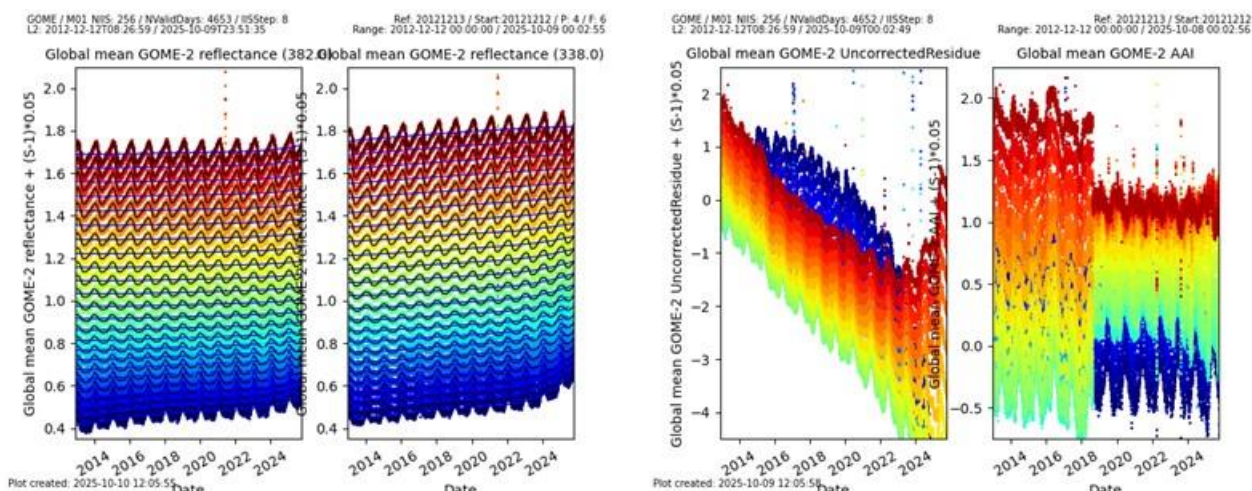


Figure 7.27. Timeline of global mean reflectances at 340 and 380 nm (left) and the uncorrected and corrected AAI from the PMDs of Metop-B.

7.6. GOME-2 UV products

Table 7.19. Validation status of UV products

Product Identifier	Product Name	Accuracy	Reference	Validating Institute	Correlative data sources
O3M-409	NRT UV index, clear-sky	Fulfils threshold accuracy requirements	RD8	DMI	WOUDC , NEUBrew , NSF
O3M-410	NRT UV index, cloud-corrected				
O3M-450 – O3M-464	Offline surface UV	Fulfils target accuracy requirements	RD14	FMI	Brewers and SUV-spectroradiometers from WOUDC , NEUBrew , NSF , NOAA , AUTH and FMI

7.6.1. Online quality monitoring

NUV:

Online quality monitoring of the NRT UV index is found on [NUV web page](#). It can be traced that the quality of the NUV products is stable since the last validation. No problems with the data quality was found in the reporting period.

OUV:

[Online quality monitoring of offline surface UV](#) has not shown any unexpected, permanent changes in the monitoring value after the latest validation, indicating that the product accuracy has remained within requirements also during the reporting period. The latest OUV validation reports were published in February 2009 covering June 2007 – May 2008 (Metop-A data) and in February 2015 covering June 2012 – May 2013 (Metop-B data).

Figure 7.28 presents the long-term monitoring graph of OUV, which illustrates seasonal variation of **global average of erythemal daily dose** (yellow markers). Any sudden changes would indicate problems with data quality. Additionally, six-month average values (January – June and July – December) are represented by red markers.

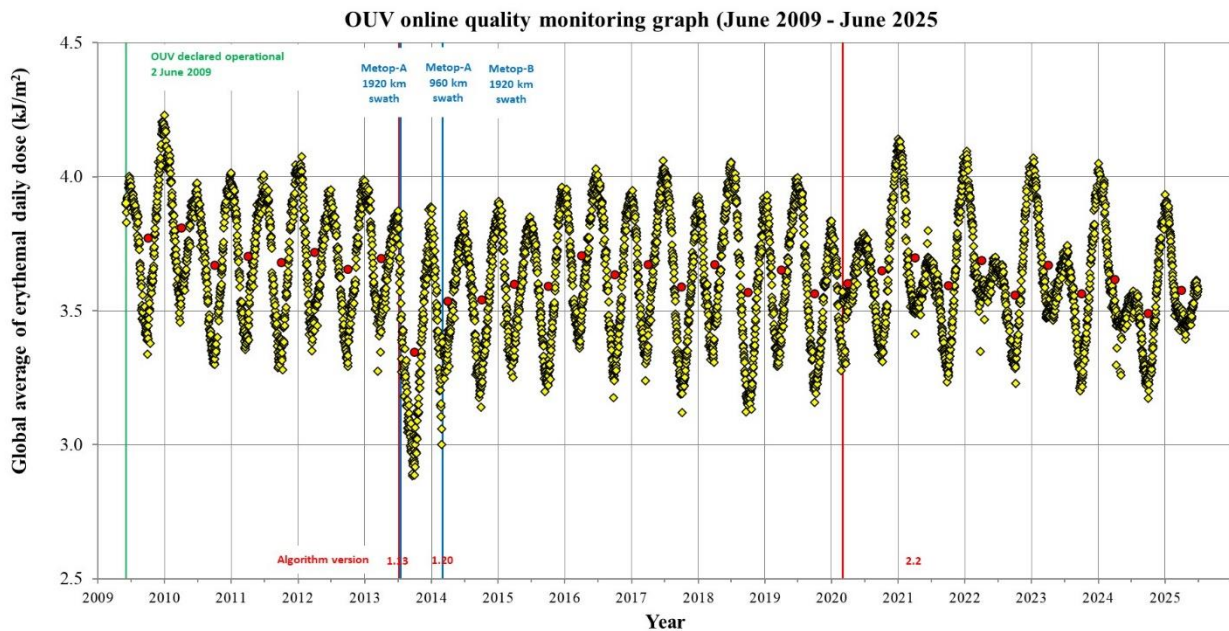


Figure 7.28. OUV long-term monitoring graph.

NOTES:

- GOME-2A was switched from nominal swath width (1920 km) to reduced swath width (960 km) 15 July 2013. The effect to OUV monitoring values can be clearly seen as more widespread global average values of erythemal daily dose. This is due to the dominance of lower EDD values in high latitudes when the satellite coverage near the equator is poor due to narrower swath width.
- OUV data processing was switched to use Metop-B data having nominal swath width of 1920 km 1 March 2014
- OUV data processing was switched to use Metop-B+C data 1 March 2020

7.7. IASI NRT products

Table 7.20. Online quality monitoring of the IASI CO, SO₂, O₃ and HNO₃ products

Product Identifier	Product Name	Accuracy	Reference	Validating Institute	Correlative data sources
O3M-80	IASI NRT CO	Fulfils threshold accuracy requirement	RD18	LATMOS	FTIR NDACC, MOPITT
O3M-57	IASI NRT SO ₂	Fulfils threshold accuracy requirement	RD19	AUTH, BIRA-IASB, LATMOS, ULB	MAXDOAS
O3M-44 O3M-49	IASI NRT O ₃	Fulfils threshold accuracy requirement	RD31	AUTH, KMI, DWD	GOME-2, balloon sonde, lidar and microwave radiometer, Brewer and Dobson
O3M-81	IASI NRT HNO ₃	Fulfils threshold accuracy requirement	RD32	BIRA-IASB	FTIR NDACC (only available in 2021)

IASI NRT O₃ and IASI NRT HNO₃ products have been released by EUMETSAT as ‘operational’ on 18 May 2022.

IASI online quality monitoring is performed at ULB and LATMOS.

IASI NRT CO online monitoring:

https://atmosphere.copernicus.eu/charts/packages/cams_monitoring/

Dissemination monitoring activities summary:

IASI CO:

The IASI NRT CO product (v6.3) has been declared operational on 2 March 2017. Here we present statistical results when comparing the EUMETSAT product disseminated by EUMETCast in BUFR format (COX) with the native product produced at ULB (FORLI-CO v20191122) for 6 days representative of 6 months: January 15th, February 15th, March 15th, April 15th, May 15th and June 15th, 2025, for Metop-B and Metop-C. This allows monitoring if any discrepancy occurs between the two, EUMETSAT and native, products. So far, the discrepancies are found within the numerical errors inherent to the use of different IT infrastructure.

CO total column and profiles are investigated. Statistics between COX data and FORLI-CO data (v20191122) are presented in Table 7.21. Profiles correlation (“Correlation”) score is computed using the discreet cross correlation integral between two profiles, normalized by the square root of the product of their auto-correlation integral. Score of 1 is expected for perfectly matching profiles, 0 for unrelated ones. Absolute and relative differences are calculated for the total columns. These tables are extracted from the Daily Reports prepared by Daniel Hurtmans at ULB.

Table 7.21. Statistics between COX data and FORLI-CO data for 6 days: January 15th, February 15th, March 15th, April 15th, May 15th and June 15th, 2025.

15/01/2025:

		IASI-c		IASI-b	
		Native	COX	Native	COX
Individual Pixels		471324	470800	574350	573452
Common Pixels		470145 (99.75%)		572545 (99.69%)	
Correlation	Mean	0.9997±0.0007		0.9997±0.0012	
	Max	1.0000		1.0000	
	Min	0.7443		0.6238	
Total Column Differences	Mean (10 ¹⁹ mol/cm ²)	0.0046±0.0042		0.0046±0.0369	
	Max (10 ¹⁹ mol/cm ²)	0.6894		2.6926	
	Min (10 ¹⁹ mol/cm ²)	-0.3307		-27.5512	
Total Column Relative Differences	Mean (%)	2.4449±1.3564		2.4729±1.5553	
	Max (%)	68.3064		85.7619	
	Min (%)	-45.8065		-256.7271	

15/02/2025:

		IASI-c		IASI-b	
		Native	COX	Native	COX
Individual Pixels		569408	568827	548483	547666
Common Pixels		567940 (99.74%)		546843 (99.70%)	
Correlation	Mean	0.9997±0.0006		0.9997±0.0007	
	Max	1.0000		1.0000	
	Min	0.8445		0.7675	
Total Column Differences	Mean (10 ¹⁹ mol/cm ²)	0.0053±0.0098		0.0053±0.0096	
	Max (10 ¹⁹ mol/cm ²)	1.1222		1.0573	
	Min (10 ¹⁹ mol/cm ²)	-0.5289		-0.6478	
Total Column Relative Differences	Mean (%)	2.4901±1.3731		2.5455±1.4006	
	Max (%)	54.3930		70.1441	
	Min (%)	-41.4536		-65.0513	

15/03/2025:

		IASI-b		IASI-c	
		Native	COX	Native	COX
Individual Pixels		586751	585353	604354	605191
Common Pixels		584376 (99.60%)		601285 (99.35%)	
Correlation	Mean	0.9997±0.0012		0.9997±0.0007	
	Max	1.0000		1.0000	
	Min	0.6035		0.8659	
Total Column Differences	Mean (10^{19} mol/cm ²)	0.0048±0.0171		0.0048±0.0037	
	Max (10^{19} mol/cm ²)	3.3465		0.2156	
	Min (10^{19} mol/cm ²)	-11.4446		-0.2149	
Total Column Relative Differences	Mean (%)	2.5191±1.5914		2.5309±1.3037	
	Max (%)	76.6288		44.9117	
	Min (%)	-296.3169		-29.8735	

15/04/2025:

		IASI-b		IASI-c	
		Native	COX	Native	COX
Individual Pixels		581816	583530	582109	583975
Common Pixels		577012 (98.88%)		577484 (98.89%)	
Correlation	Mean	0.9996±0.0009		0.9996±0.0010	
	Max	1.0000		1.0000	
	Min	0.7820		0.7607	
Total Column Differences	Mean (10^{19} mol/cm ²)	0.0051±0.0048		0.0049±0.0045	
	Max (10^{19} mol/cm ²)	1.3078		0.5693	
	Min (10^{19} mol/cm ²)	-1.2716		-1.2339	
Total Column Relative Differences	Mean (%)	2.6249±1.3569		2.6026±1.3245	
	Max (%)	71.6273		57.5917	
	Min (%)	-66.9171		-92.9423	

15/05/2025:

		IASI-b		IASI-c	
		Native	COX	Native	COX
Individual Pixels		560751	559739	570574	569615
Common Pixels		558862 (99.66%)		568759 (99.68%)	
Correlation	Mean	0.9996±0.0012		0.9996±0.0013	
	Max	1.0000		1.0000	
	Min	0.8436		0.8417	
Total Column Differences	Mean (10^{19} mol/cm ²)	0.0047±0.0047		0.0046±0.0057	
	Max (10^{19} mol/cm ²)	0.5969		2.6706	
	Min (10^{19} mol/cm ²)	-1.2794		-1.2390	
Total Column Relative Differences	Mean (%)	2.6599±1.4051		2.6224±1.3815	
	Max (%)	71.0779		81.2632	
	Min (%)	-57.0226		-79.6201	

15/06/2025:

		IASI-c		IASI-b	
		Native	COX	Native	COX
Individual Pixels		566504	565273	555842	554814
Common Pixels		564374 (99.62%)		553930 (99.66%)	
Correlation	Mean	0.9995±0.0016		0.9995±0.0016	
	Max	1.0000		1.0000	
	Min	0.6957		0.7407	
Total Column Differences	Mean (10^{19} mol/cm ²)	0.0048±0.0042		0.0048±0.0076	
	Max (10^{19} mol/cm ²)	0.6359		0.7992	
	Min (10^{19} mol/cm ²)	-0.8830		-4.5402	
Total Column Relative Differences	Mean (%)	2.6697±1.4141		2.6509±1.9542	
	Max (%)	78.1034		68.8785	
	Min (%)	-43.0413		-949.2164	

Figure 7.29 – Figure 7.34 show the correlation plots for total column between COX data and FORLI-CO for each platform. No critical deviation was found for these dates.

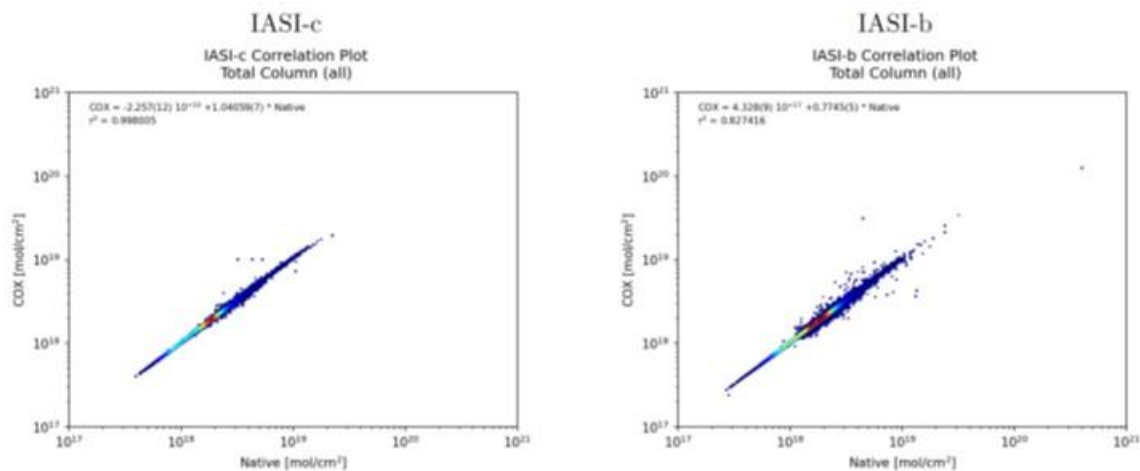


Figure 7.29. Correlation plots for total column between COX data and FORLI-CO for each platform for 15/01/2025. X-axis corresponds to native data (mol/cm²) and Y-axis corresponds to COX data (mol/cm²).

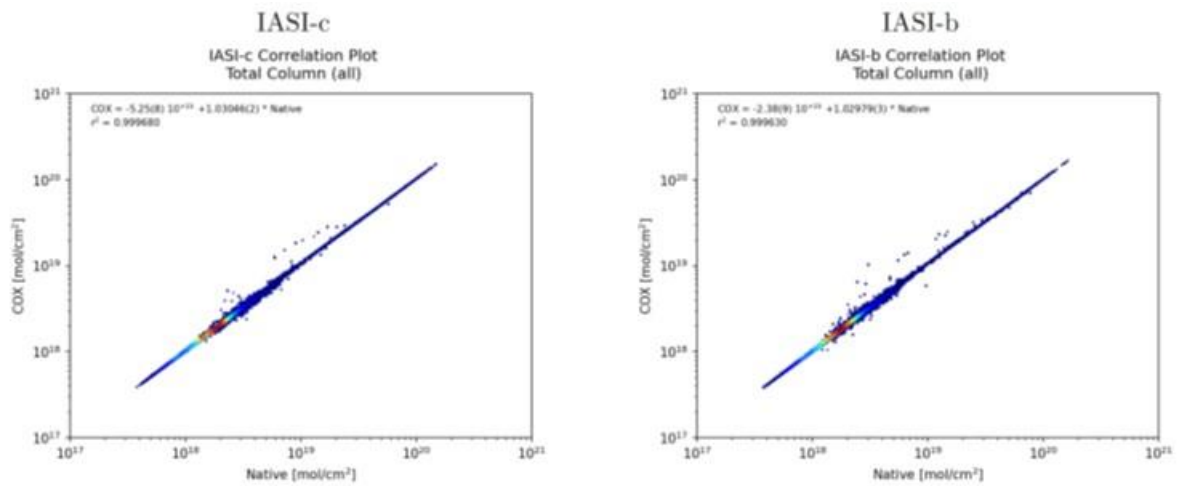


Figure 7.30. Same as Figure 7.29 but for 15/02/2025.

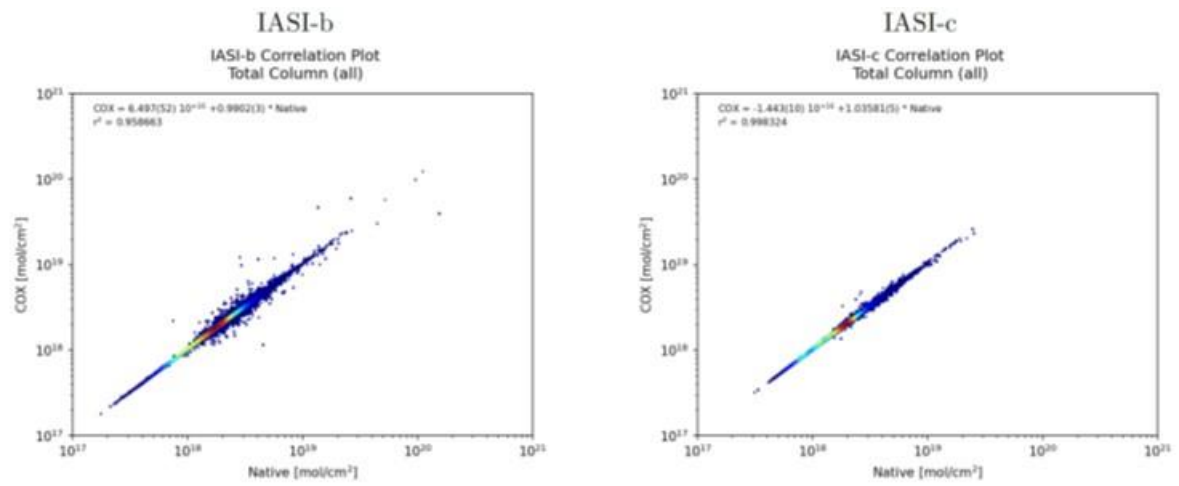


Figure 7.31. Same as Figure 7.29 but for 15/03/2025.

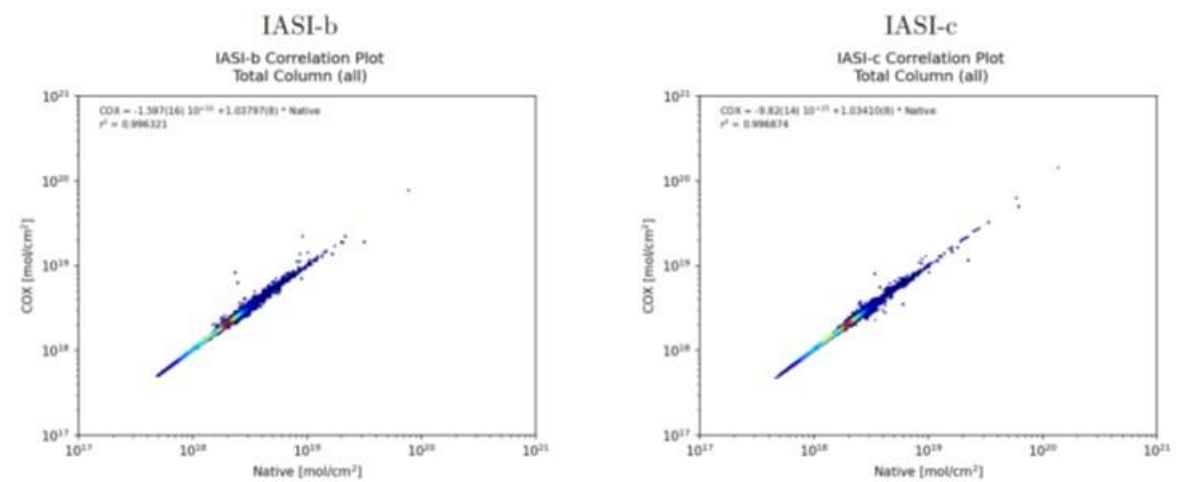


Figure 7.32. Same as Figure 7.29 but for 15/04/2025.

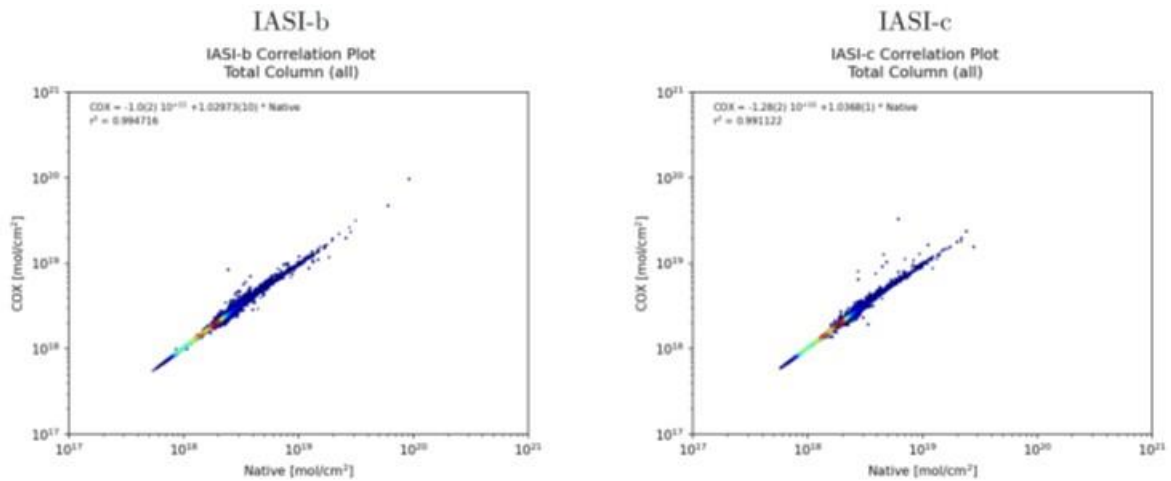


Figure 7.33. Same as Figure 7.29 but for 15/05/2025.

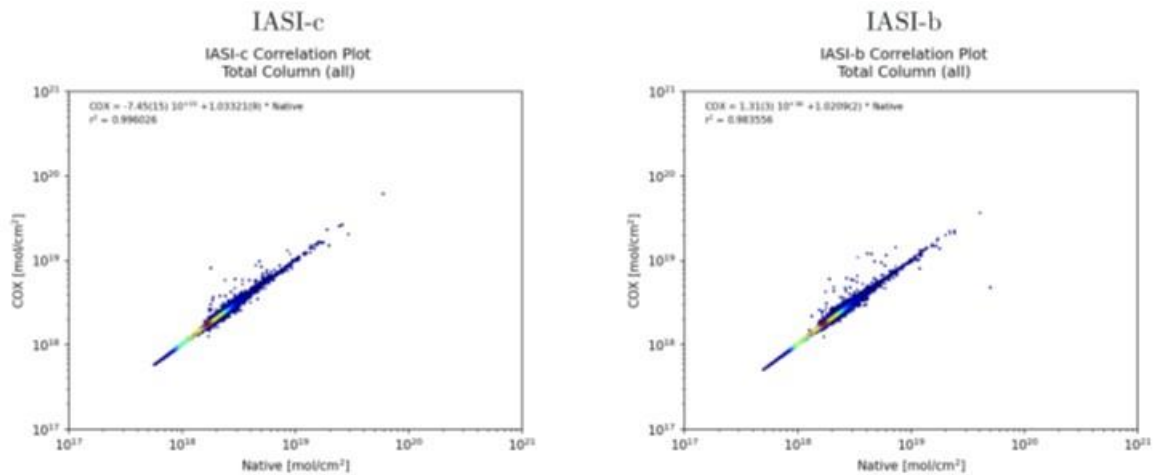


Figure 7.34. Same as Figure 7.29 but for 15/06/2025.

IASI SO₂:

The IASI BRESCIA SO₂ retrieval algorithm has been implemented in the PPF v6.3 at EUMETSAT (operational release on 18/04/2018). Here we compare the EUMETSAT product disseminated by EUMETCast in BUFR format (SO₂ EUMET) with the native product produced at ULB (SO₂ ULB) for 5 days between March and June 2025, for Metop-B and Metop-C. We choose to study 21/03/2025, 22/03/2025, 14/05/2025, 18/06/2025 and 19/06/2025.

i) Online quality monitoring for SO₂ for five estimated altitudes:

For each of the five days, scatterplots for the different estimated altitudes (7, 10, 13, 16 and 25 km) are presented (Figure 7.35 – Figure 7.39). The data have been filtered following the recommendations of the Product User Manual (Section 5.2.2, i.e. we kept the pixels in the neighbourhood (± 10 degrees) of SO₂_BT_DIFFERENCE > 1K pixels, and did not use the pixels with a SO₂_BT_DIFFERENCE < 0.4K.

We recall here that when the IASI L2 pressure and temperature profiles are not available, ECMWF forecasts (3h, interpolated in time and space) data are used in the EUMETSAT API. These pixels are flagged with SO₂_QFLAG = 11 and are not part of the comparison.

Correlation coefficients (in blue) are ~1.

So far, the discrepancies are found within the numerical errors inherent to the use of different IT infrastructure.

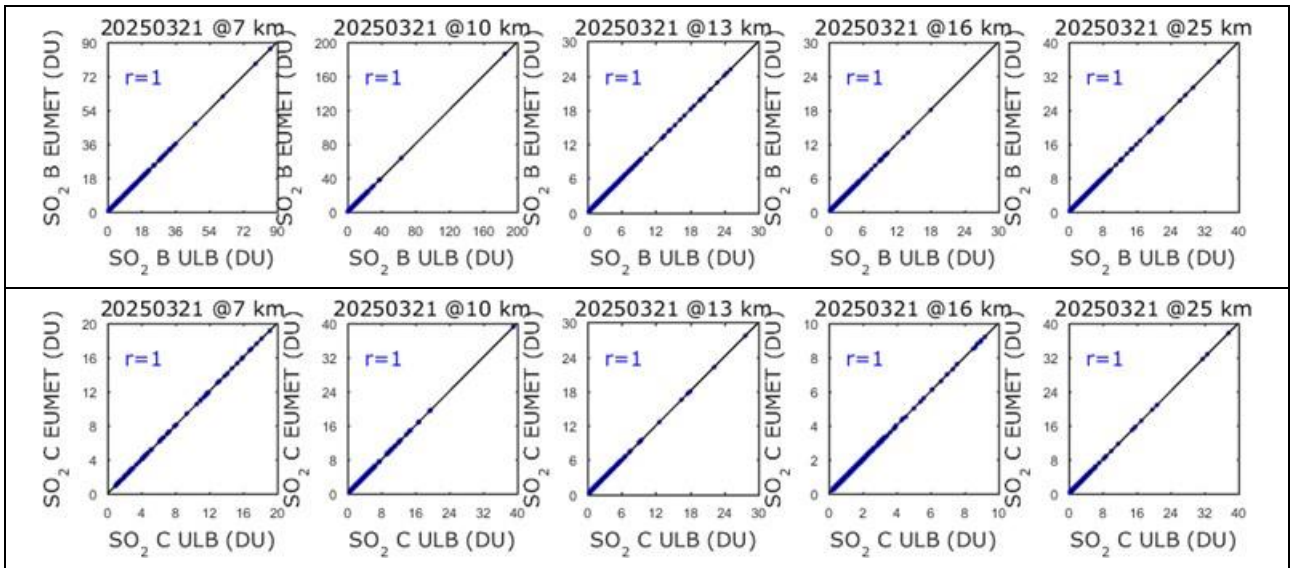


Figure 7.35. Scatterplots for Metop-B (top) and Metop-C (bottom): SO₂ EUMET versus SO₂ ULB for 21/03/2025, for the five estimated altitudes (7, 10, 13, 16 and 25 km).

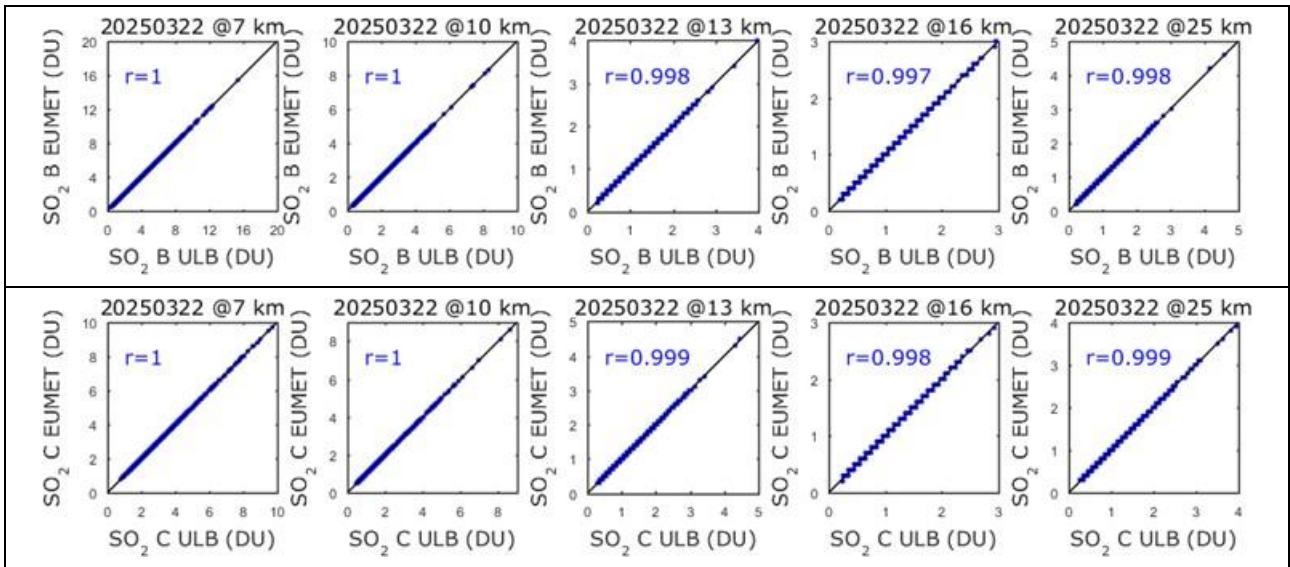
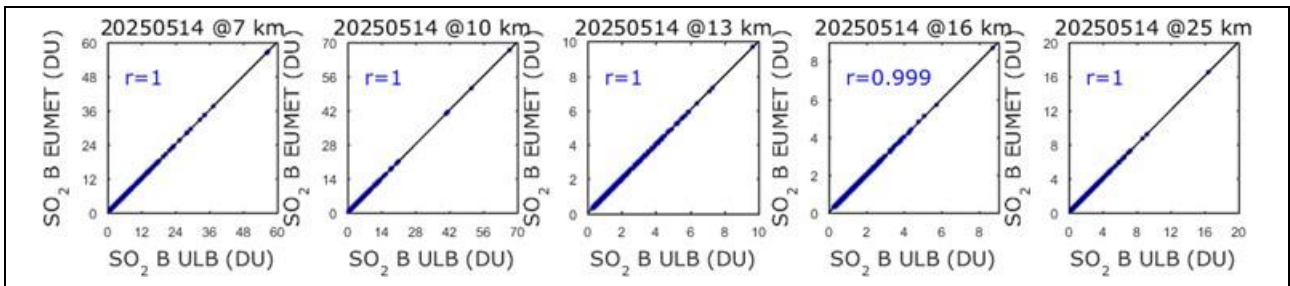


Figure 7.36. Same as Figure 7.35 but for 22/03/2025.



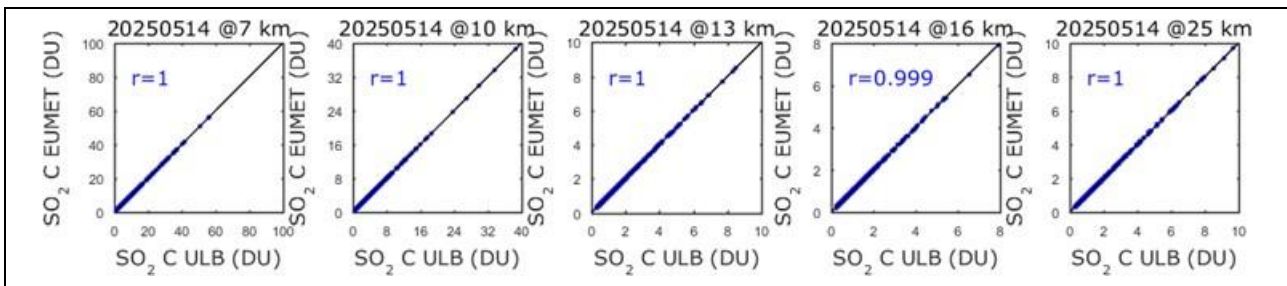


Figure 7.37. Same as Figure 7.35 but for 14/05/2025.

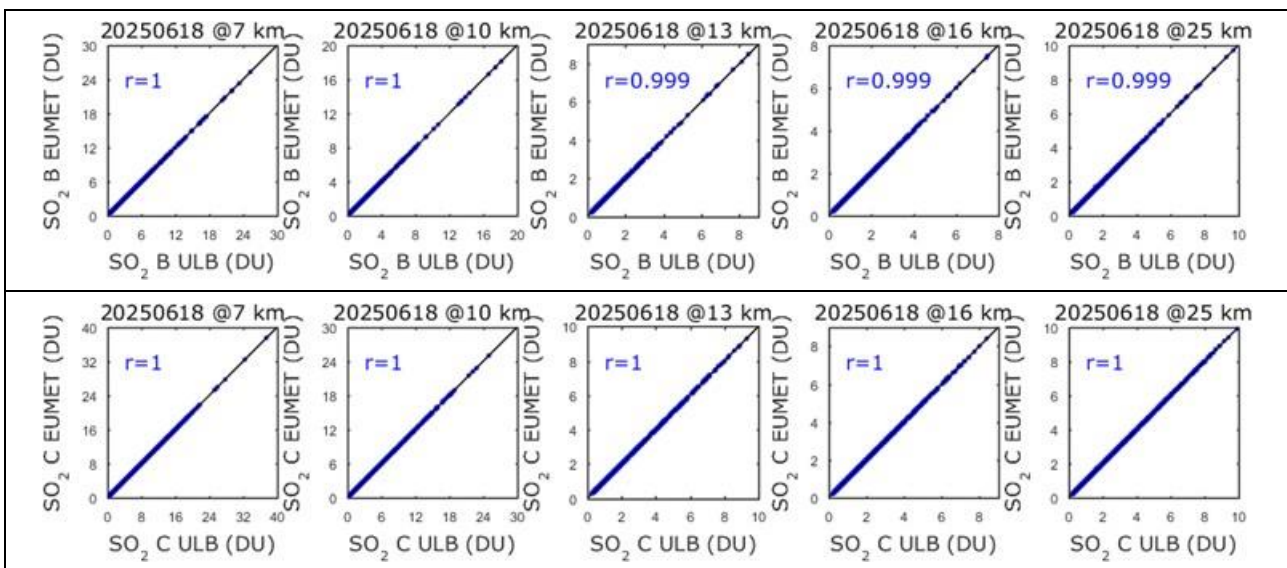


Figure 7.38. Same as Figure 7.35 but for 18/06/2025.

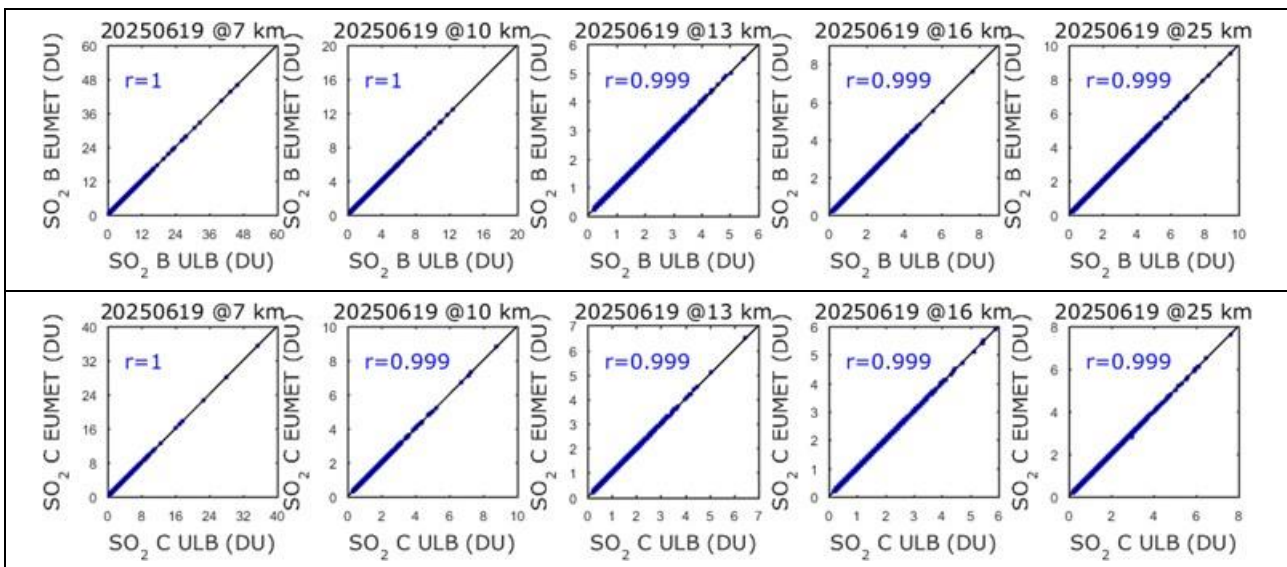


Figure 7.39. Same as Figure 7.35 but for 19/06/2025.

ii) Online quality monitoring for **SO2_ALTITUDE** and **SO2_COL**:

Although the two products **SO2_ALTITUDE** (estimated altitude of the SO₂ plume) and **SO2_COL** (SO₂ column at the estimated altitude) are operational since May 2021, **the EUMETSAT and the**

ULB algorithms versions are different, with the ULB version being the latest version of the algorithm. **As said in the previous report, the EUMETSAT and ULB products are not the same and the comparison shows differences.** Scatterplots for five dates (21/03/2025, 22/03/2025, 14/05/2025, 18/06/2025 and 19/06/2025), for Metop-B and Metop-C are shown in Figure 7.40 – Figure 7.44 to illustrate that the products do not match at all. Daniel Hurtmans provided an updated version of the Brescia algorithm (including the SO₂ altitude) for implementation to EUMETSAT, in order for the two versions to be the same. We are waiting for an update from EUMETSAT.

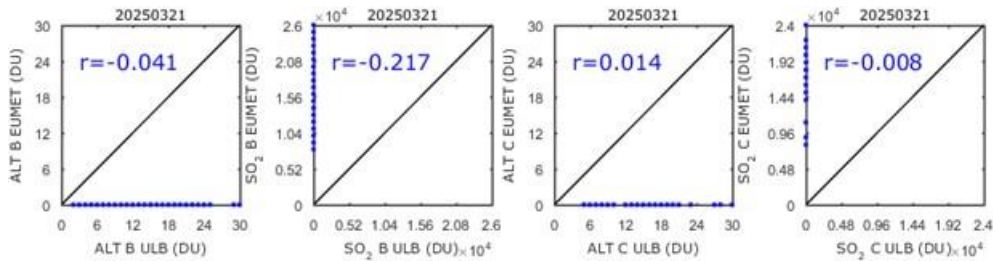


Figure 7.40. Scatter plots for Metop-B and Metop-C: SO₂_ALTITUDE EUMET versus SO₂_ALTITUDE ULB, as well as SO₂_COL EUMET versus SO₂_COL ULB, for 21/03/2025.

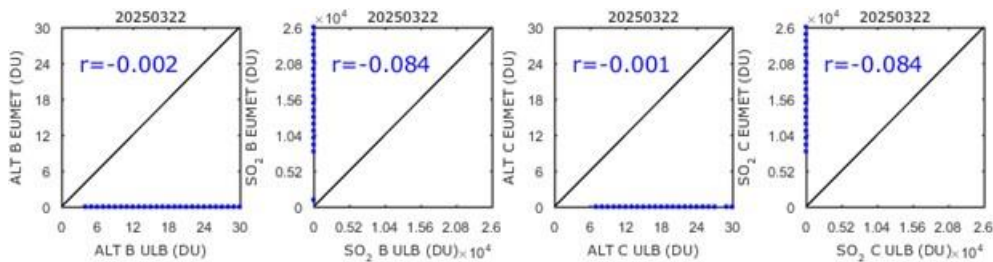


Figure 7.41. Same as Figure 7.40 but for 22/03/2025.

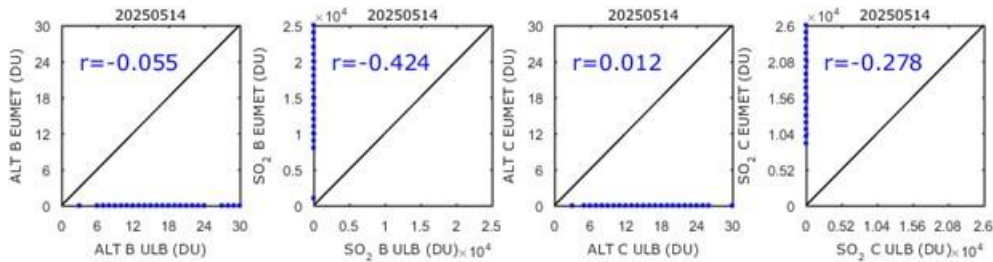


Figure 7.42. Same as Figure 7.40 but for 14/05/2025.

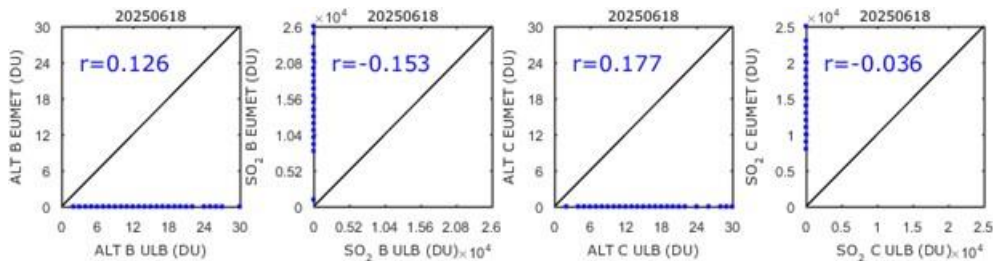


Figure 7.43. Same as Figure 7.40 but for 18/06/2025.

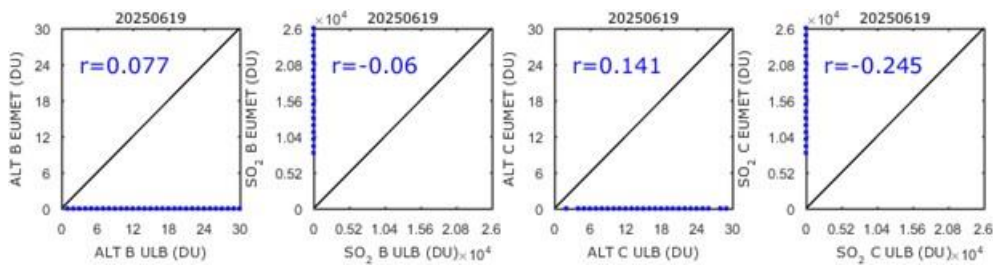


Figure 7.44. Same as Figure 7.40 but for 19/06/2025.

IASI O3:

The IASI NRT O₃ product (v6.5) has been declared operational on 18 May 2022. Here we present statistical results when comparing the EUMETSAT product disseminated by EUMETCast in BUFR format (OZO, called “bufr” hereinafter) with the native product produced at ULB (FORLI-O3 v20191122, called “native” hereinafter) for six days representative of six months: January 15th, February 15th, March 15th, April 15th, May 15th and June 15th, 2025, for Metop-B and Metop-C. This allows monitoring if any discrepancy occurs between the two, EUMETSAT and native, products. The data have been filtered following the recommendations of the Product User Manual. Furthermore, data associated with DOFS > 2 have also been filtered out.

Total and 0 – 6 km ozone column are investigated. Detailed statistics for total column between bufr and native data for each of the six days are presented in Table 7.22 – Table 7.27. No critical deviation was found for these dates.

The difference between individual pixels in the native and BUFR formats is due to the fact that the NRT EUMETSAT version is still based on v2015. It is worth mentioning that, since June 2024, approximately 3.5 out of 10 pixels are now processed in the BUFR product (compared to only 1 out of 10 previously), resulting in about 80 % of pixels being common between the two products (up from only 25 % before), significantly reducing the gap.

Table 7.22. Statistics for total ozone column between bufr and native data for January 15th 2025

O3 - 15 January 2025	IASI-B		IASI-C	
	Native	Bufr	Native	Bufr
Individual Pixels	405390	396013	354149	349434
Common Pixels	349139 (86.12 %)		308076 (86.99 %)	
Correlation	0.9990		0.9991	
Total Column Diff - Mean (DU)	2.3509 ± 2.5953		2.3525 ± 2.5902	
Total Column Diff - Max (DU)	71.7404		92.1714	
Total Column Diff - Min (DU)	-98.8843		-65.7821	
Total Column Rel. Diff - Mean (%)	0.8602 ± 0.8241		0.8706 ± 0.7864	
Total Column Rel. Diff - Max (%)	20.5980		16.5307	
Total Column Rel. Diff - Min (%)	-15.7432		-11.1047	

Table 7.23. Same as Table 7.22, but for February 15th 2025

O3 - 15 February 2025	IASI-B		IASI-C	
	Native	Bufr	Native	Bufr
Individual Pixels	372787	365302	398945	394123
Common Pixels	321532 (86.25 %)		343599 (86.13 %)	
Correlation	0.9994		0.9994	
Total Column Diff - Mean (DU)	2.9204 ± 2.1584		2.4594 ± 2.6296	
Total Column Diff - Max (DU)	98.1030		93.8797	
Total Column Diff - Min (DU)	-69.1622		-52.5826	
Total Column Rel. Diff - Mean (%)	1.0525 ± 0.6903		0.9167 ± 0.8142	
Total Column Rel. Diff - Max (%)	20.2850		17.0116	
Total Column Rel. Diff - Min (%)	-11.7482		-11.3211	

Table 7.24. Same as Table 7.22, but for March 15th 2025

O3 - 15 March 2025	IASI-B		IASI-C	
	Native	Bufr	Native	Bufr
Individual Pixels	356258	344196	394357	387996
Common Pixels	302787 (84.99 %)		339538 (86.10 %)	
Correlation	0.9992		0.9991	
Total Column Diff - Mean (DU)	2.6146 ± 3.2405		2.3665 ± 4.1072	
Total Column Diff - Max (DU)	123.1605		81.9025	
Total Column Diff - Min (DU)	-90.9428		-104.3992	
Total Column Rel. Diff - Mean (%)	1.0018 ± 0.8712		0.9633 ± 1.0340	
Total Column Rel. Diff - Max (%)	32.7388		22.1290	
Total Column Rel. Diff - Min (%)	-20.3731		-15.7442	

Table 7.25. Same as Table 7.22, but for April 15th 2025

03 - 15 April 2025	IASI-B		IASI-C	
	Native	Bufr	Native	Bufr
Individual Pixels	387243	374459	389670	376847
Common Pixels	332677 (85.91 %)		333966 (85.70 %)	
Correlation	0.9998		0.9998	
Total Column Diff - Mean (DU)	3.0721 ± 1.6538		3.0748 ± 1.6547	
Total Column Diff - Max (DU)	26.6007		37.3164	
Total Column Diff - Min (DU)	-51.5701		-39.0478	
Total Column Rel. Diff - Mean (%)	1.0573 ± 0.5692		1.0580 ± 0.5733	
Total Column Rel. Diff - Max (%)	8.6371		7.6963	
Total Column Rel. Diff - Min (%)	-13.7061		-7.8169	

Table 7.26. Same as Table 7.22, but for May 15th 2025

03 - 15 May 2025	IASI-B		IASI-C	
	Native	Bufr	Native	Bufr
Individual Pixels	380262	371443	387207	378168
Common Pixels	326643 (85.90 %)		331963 (85.73 %)	
Correlation	0.9996		0.9996	
Total Column Diff - Mean (DU)	3.0445 ± 1.4520		3.0599 ± 1.4617	
Total Column Diff - Max (DU)	35.9215		58.9288	
Total Column Diff - Min (DU)	-39.1238		-36.8461	
Total Column Rel. Diff - Mean (%)	1.0535 ± 0.5181		1.0597 ± 0.5204	
Total Column Rel. Diff - Max (%)	7.4037		13.3949	
Total Column Rel. Diff - Min (%)	-8.8038		-11.1379	

Table 7.27. Same as Table 7.22, but for June 15th 2025

O3 - 15 June 2025	IASI-B		IASI-C	
	Native	Bufr	Native	Bufr
Individual Pixels	367684	358959	381437	371928
Common Pixels	317833 (86.44 %)		328855 (86.21 %)	
Correlation	0.9993		0.9993	
Total Column Diff - Mean (DU)	3.0023 ± 1.5134		3.0011 ± 1.5434	
Total Column Diff - Max (DU)	29.3210		24.1093	
Total Column Diff - Min (DU)	-26.3669		-23.9599	
Total Column Rel. Diff - Mean (%)	1.0472 ± 0.5426		1.0457 ± 0.5535	
Total Column Rel. Diff - Max (%)	10.5455		9.3006	
Total Column Rel. Diff - Min (%)	-7.6301		-7.7005	

Figure 7.45 and Figure 7.46 present the correlation plots of bufr and native total ozone column for IASI/Metop-B and IASI/Metop-C, respectively. Similarly, Figure 7.45 – Figure 7.48 show the correlation plots of bufr and native 0 – 6 km ozone column for IASI/Metop-B and IASI/Metop-C, respectively. Correlation coefficients (in blue) are ~1.

So far, the discrepancies are found within the numerical errors inherent to the use of different IT infrastructure.

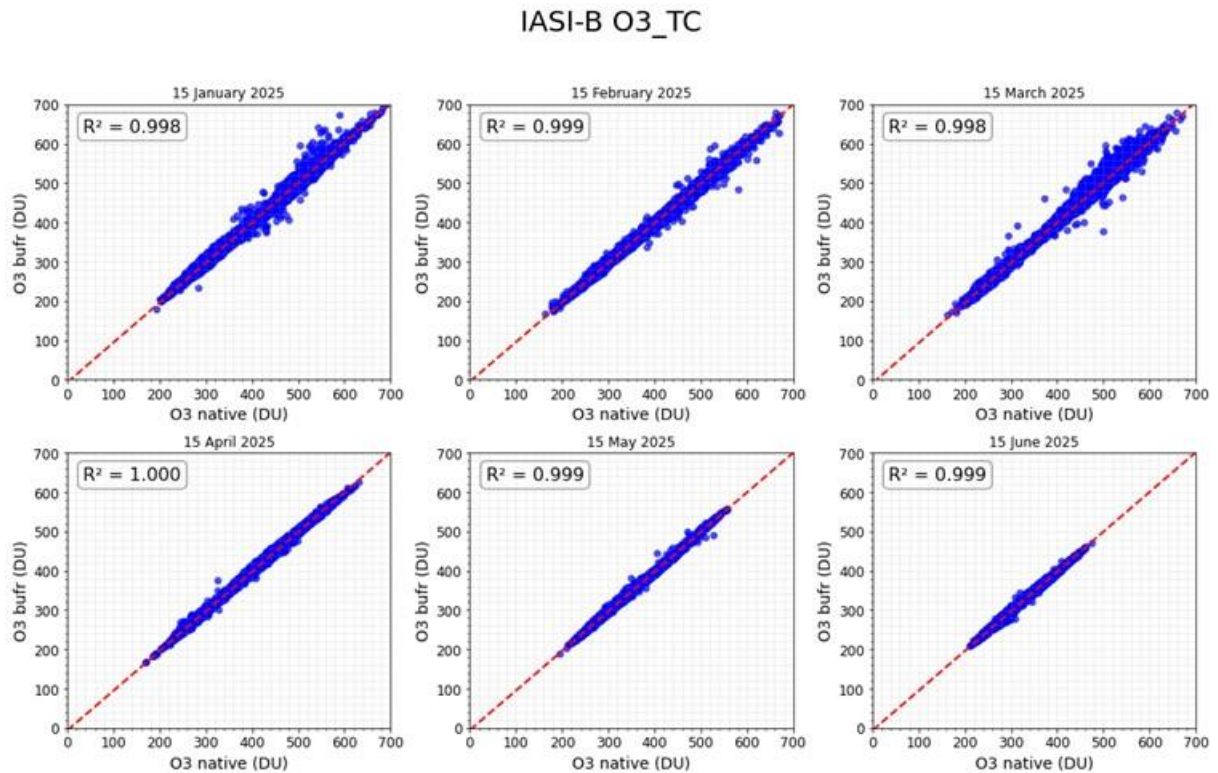


Figure 7.45. Correlation plots of bufr and native total ozone column for IASI/Metop-B for 6 days: January 15th, February 15th, March 15th, April 15th, May 15th and June 15th, 2025. X-axis corresponds to native data (DU) and Y-axis corresponds to bufr data (DU).

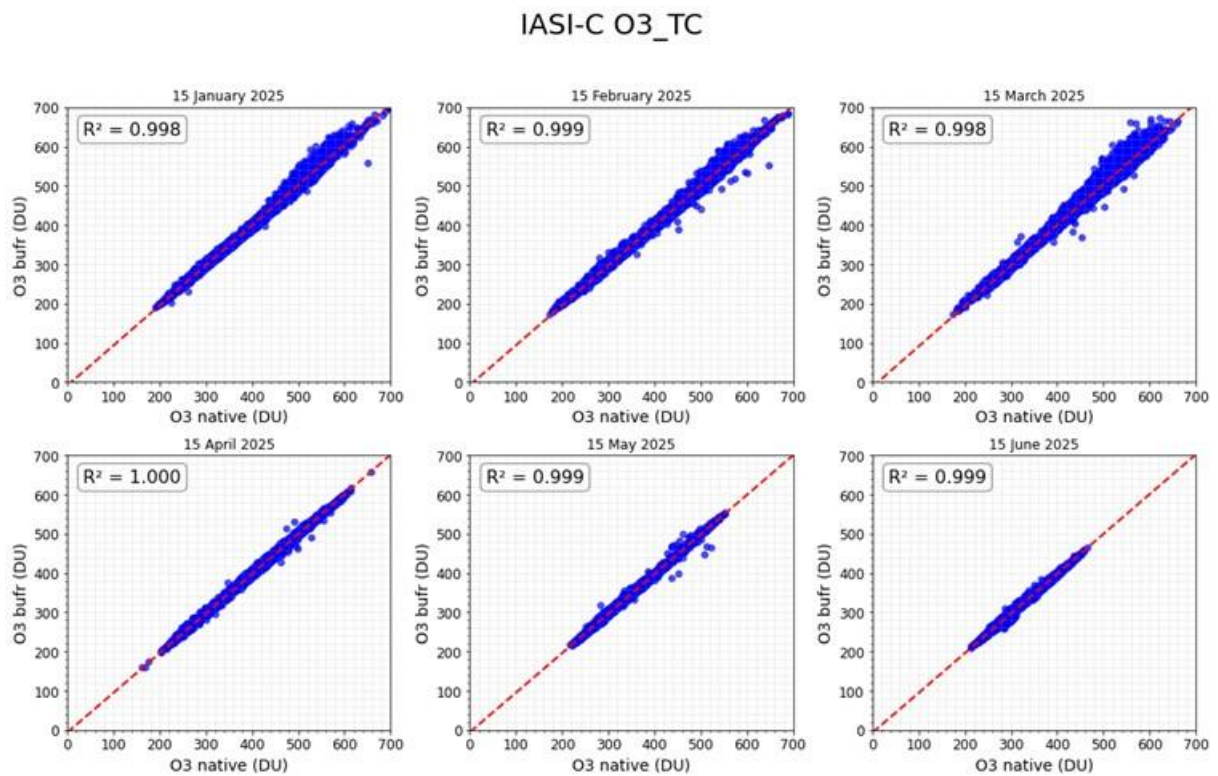


Figure 7.46. Same as Figure 7.45, but for IASI/Metop-C.

IASI-B O3_06

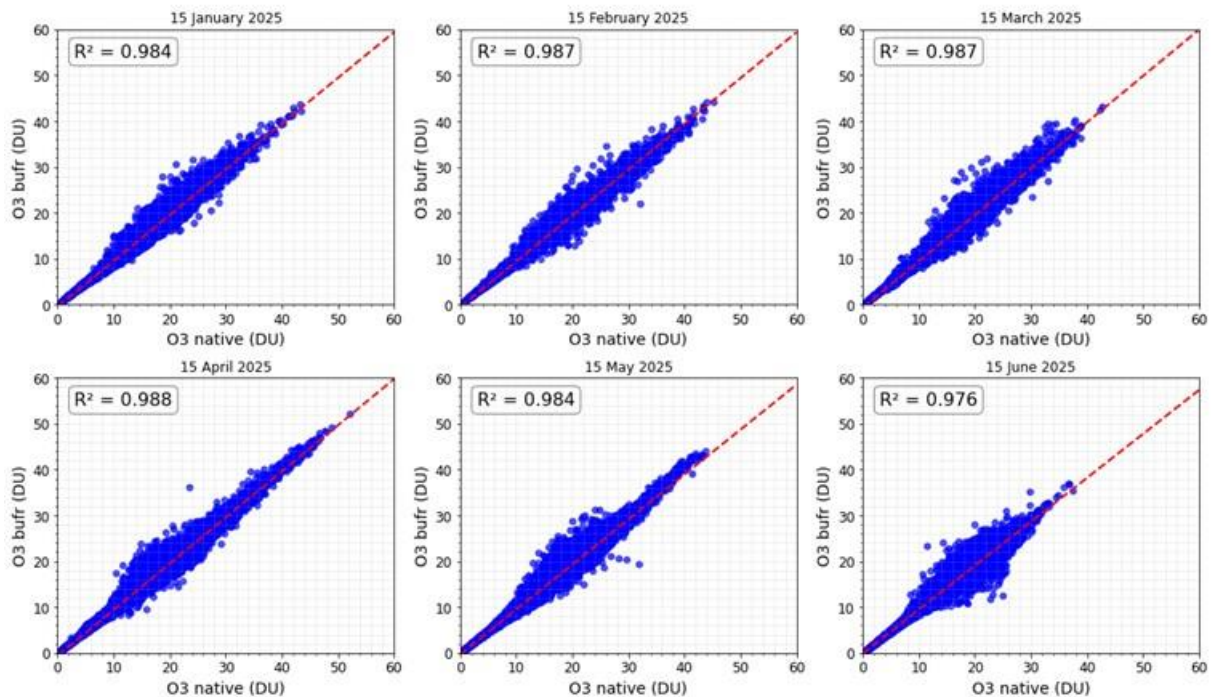


Figure 7.47. Correlation plots of bufr and native 0 – 6 km ozone column for IASI/Metop-B for six days: January 15th, February 15th, March 15th, April 15th, May 15th and June 15th, 2025. X-axis corresponds to native data (DU) and Y-axis corresponds to bufr data (DU).

IASI-C O3_06

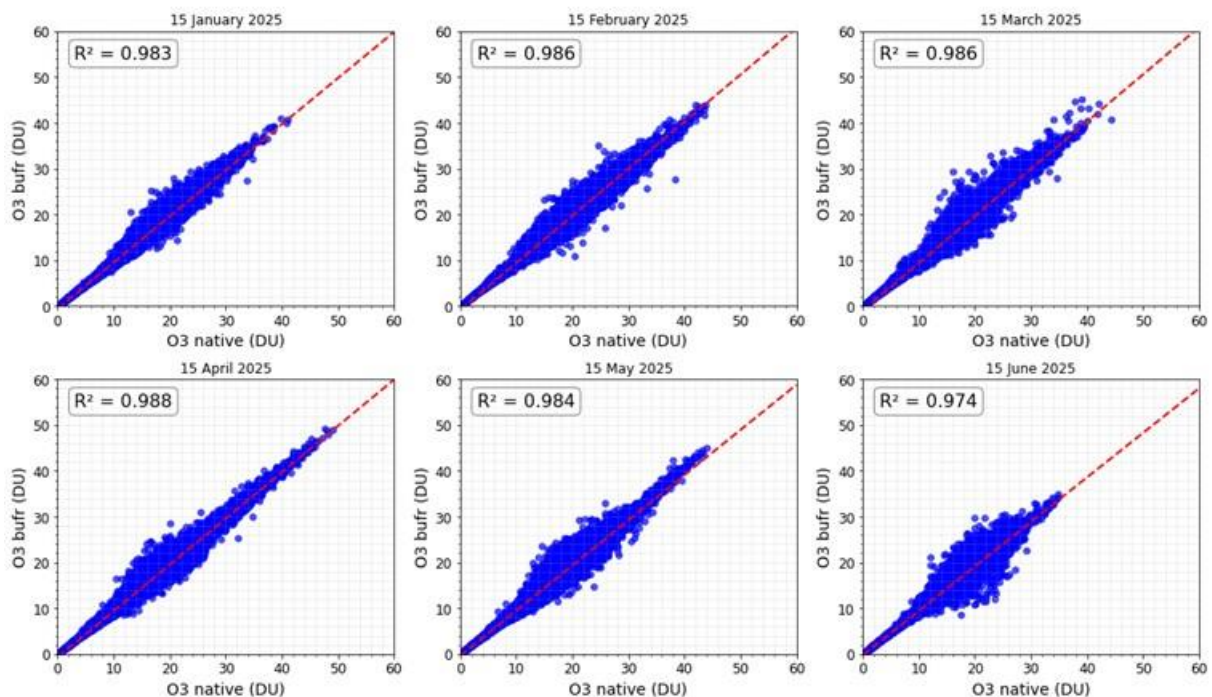


Figure 7.48. Same as Figure 7.47, but for IASI/Metop-C.

IASI HNO₃:

The IASI NRT HNO₃ product (v6.5) has been declared operational on 18 May 2022. Here we present statistical results when comparing the EUMETSAT product disseminated by EUMETCast in BUFR format (NAC, called “buf” hereinafter) with the native product produced at ULB (FORLI-HNO₃ v20191122, called “native” hereinafter) for six days representative of six months: January 15th, February 15th, March 16th, April 15th, May 15th and June 15th, 2025, for Metop-B and Metop-C. This allows monitoring if any discrepancy occurs between the two, EUMETSAT and native, products. The data have been filtered following the recommendations of the Product User Manual.

HNO₃ total column is investigated. Detailed statistics for total column between buf and native data for each of the six days are presented in Table 7.28 - Table 7.33. No critical deviation was found for these dates.

The difference between individual pixels in the native and BUFR formats is due to the fact that the NRT EUMETSAT version is still based on v2015. It is worth mentioning that, since June 2024, approximately 3.5 out of 10 pixels are now processed in the BUFR product (compared to only 1 out of 10 previously), resulting in about 80 % of pixels being common between the two products (up from only 25 % before), significantly reducing the gap.

Table 7.28. Statistics for total HNO₃ column between buf and native data for January 15th 2025

HNO ₃ - 15 January 2025	IASI-B		IASI-C	
	Native	Buf	Native	Buf
Individual Pixels	269578	255597	234834	226970
Common Pixels	225462 (83.64 %)		199280 (84.86 %)	
Correlation	0.9997		0.9991	
Total Column Diff - Mean (x10 ¹⁶ molec cm ⁻²)	0.0095 ± 0.0217		0.0077 ± 0.0350	
Total Column Diff - Max (x10 ¹⁶ molec cm ⁻²)	1.3077		13.7419	
Total Column Diff - Min (x10 ¹⁶ molec cm ⁻²)	-1.4988		-0.9367	
Total Column Rel. Diff - Mean (%)	1.0691 ± 1.5578		0.9410 ± 1.3714	
Total Column Rel. Diff - Max (%)	29.8851		34.1660	
Total Column Rel. Diff - Min (%)	-16.7032		-18.9749	

Table 7.29. Same as Table 7.28, but for February 15th 2025

HNO₃ - 15 February 2025	IASI-B		IASI-C	
	Native	Bufr	Native	Bufr
Individual Pixels	270897	261250	271813	264349
Common Pixels	225631 (83.29 %)		222992 (82.04 %)	
Correlation	0.9998		0.9996	
Total Column Diff - Mean (x10 ¹⁶ molec cm ⁻²)	0.0096 ± 0.0165		0.0074 ± 0.0237	
Total Column Diff - Max (x10 ¹⁶ molec cm ⁻²)	0.6303		1.4372	
Total Column Diff - Min (x10 ¹⁶ molec cm ⁻²)	-0.5574		-6.6068	
Total Column Rel. Diff - Mean (%)	1.1387 ± 1.4614		1.0074 ± 1.5470	
Total Column Rel. Diff - Max (%)	29.7747		17.3228	
Total Column Rel. Diff - Min (%)	-30.3918		-62.0606	

Table 7.30. Same as Table 7.28, but for March 15th 2025

HNO₃ - 15 March 2025	IASI-B		IASI-C	
	Native	Bufr	Native	Bufr
Individual Pixels	259506	229691	283007	254357
Common Pixels	203228 (78.31 %)		226089 (79.89 %)	
Correlation	0.9935		0.9997	
Total Column Diff - Mean (x10 ¹⁶ molec cm ⁻²)	0.0105 ± 0.0957		0.0094 ± 0.0191	
Total Column Diff - Max (x10 ¹⁶ molec cm ⁻²)	1.3016		0.6796	
Total Column Diff - Min (x10 ¹⁶ molec cm ⁻²)	-34.9688		-1.7258	
Total Column Rel. Diff - Mean (%)	1.2879 ± 1.8083		1.1406 ± 1.5609	
Total Column Rel. Diff - Max (%)	35.8263		27.1202	
Total Column Rel. Diff - Min (%)	-95.0566		-36.9413	

Table 7.31. Same as Table 7.28, but for April 15th 2025

HNO₃ - 15 April 2025	IASI-B		IASI-C	
	Native	Bufr	Native	Bufr
Individual Pixels	307218	246702	308678	248186
Common Pixels	222054 (72.28 %)		223476 (72.40 %)	
Correlation	0.9999		0.9998	
Total Column Diff - Mean (x10 ¹⁶ molec cm ⁻²)	0.0083 ± 0.0159		0.0085 ± 0.0168	
Total Column Diff - Max (x10 ¹⁶ molec cm ⁻²)	0.5090		0.5186	
Total Column Diff - Min (x10 ¹⁶ molec cm ⁻²)	-0.5977		-1.8430	
Total Column Rel. Diff - Mean (%)	0.9167 ± 1.3627		0.9679 ± 1.4437	
Total Column Rel. Diff - Max (%)	26.7950		40.8557	
Total Column Rel. Diff - Min (%)	-19.0231		-24.3360	

Table 7.32. Same as Table 7.28, but for May 15th 2025

HNO₃ - 15 May 2025	IASI-B		IASI-C	
	Native	Buf	Native	Buf
Individual Pixels	300787	277439	306143	282679
Common Pixels	250007 (83.12 %)		254602 (83.16 %)	
Correlation	0.9956		0.9983	
Total Column Diff - Mean (x10 ¹⁶ molec cm ⁻²)	0.0076 ± 0.0714		0.0078 ± 0.0443	
Total Column Diff - Max (x10 ¹⁶ molec cm ⁻²)	22.2749		17.7489	
Total Column Diff - Min (x10 ¹⁶ molec cm ⁻²)	-2.8686		-1.1795	
Total Column Rel. Diff - Mean (%)	0.8099 ± 5.4095		0.8513 ± 3.5309	
Total Column Rel. Diff - Max (%)	1663.7287		1277.7251	
Total Column Rel. Diff - Min (%)	-21.0297		-28.7401	

Table 7.33. Same as Table 7.28, but for June 15th 2025

HNO₃ - 15 June 2025	IASI-B		IASI-C	
	Native	Buf	Native	Buf
Individual Pixels	288922	278597	305083	295250
Common Pixels	250718 (86.78 %)		265757 (87.11 %)	
Correlation	0.9991		0.9996	
Total Column Diff - Mean (x10 ¹⁶ molec cm ⁻²)	0.0076 ± 0.0450		0.0074 ± 0.0276	
Total Column Diff - Max (x10 ¹⁶ molec cm ⁻²)	2.7875		1.2111	
Total Column Diff - Min (x10 ¹⁶ molec cm ⁻²)	-15.2418		-2.9403	
Total Column Rel. Diff - Mean (%)	0.7772 ± 1.4832		0.7957 ± 1.5097	
Total Column Rel. Diff - Max (%)	40.0146		44.7238	
Total Column Rel. Diff - Min (%)	-93.2316		-34.9719	

Figure 7.49 and Figure 7.50 present the correlation plots of buf and native total HNO₃ column, for IASI/Metop-B and IASI/Metop-C, respectively. Correlation coefficients (in blue) are ~1.

So far, the discrepancies are found within the numerical errors inherent to the use of different IT infrastructure.

IASI-B HNO₃

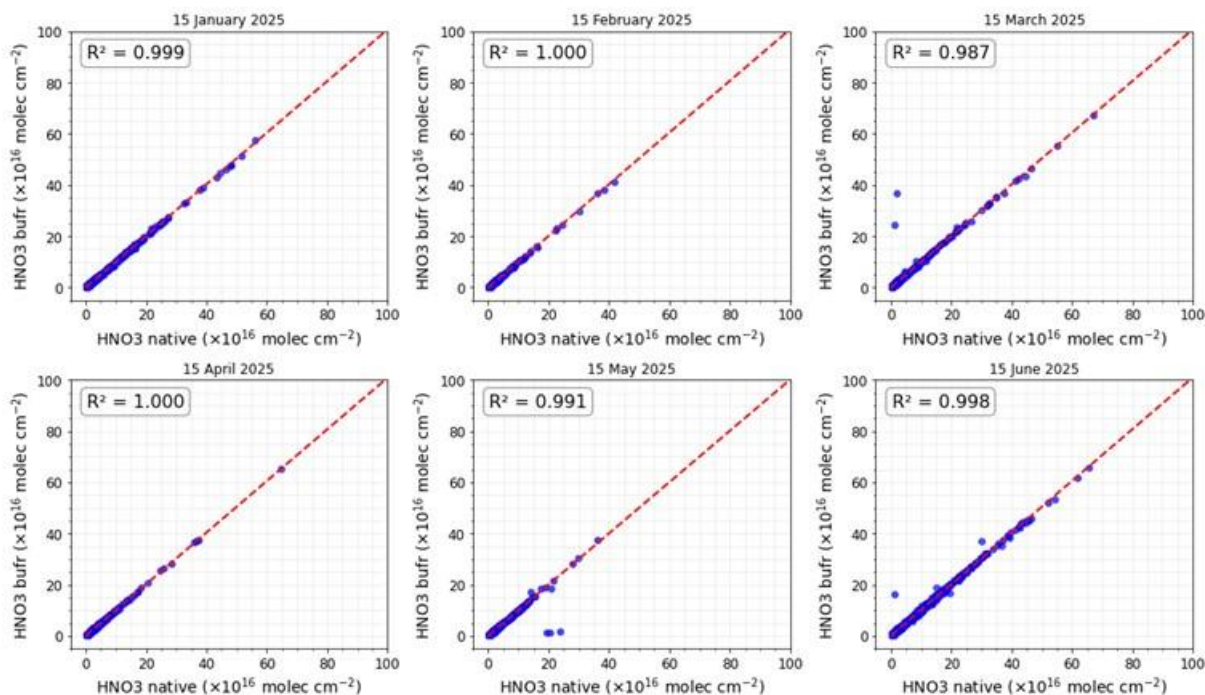


Figure 7.49. Correlation plots of bufr and native total HNO₃ column for IASI/Metop-B for six days: January 15th, February 15th, March 15th, April 15th, May 15th and June 15th, 2025. X-axis corresponds to native data (molec. cm⁻²) and Y-axis corresponds to bufr data (molec. cm⁻²).

IASI-C HNO₃

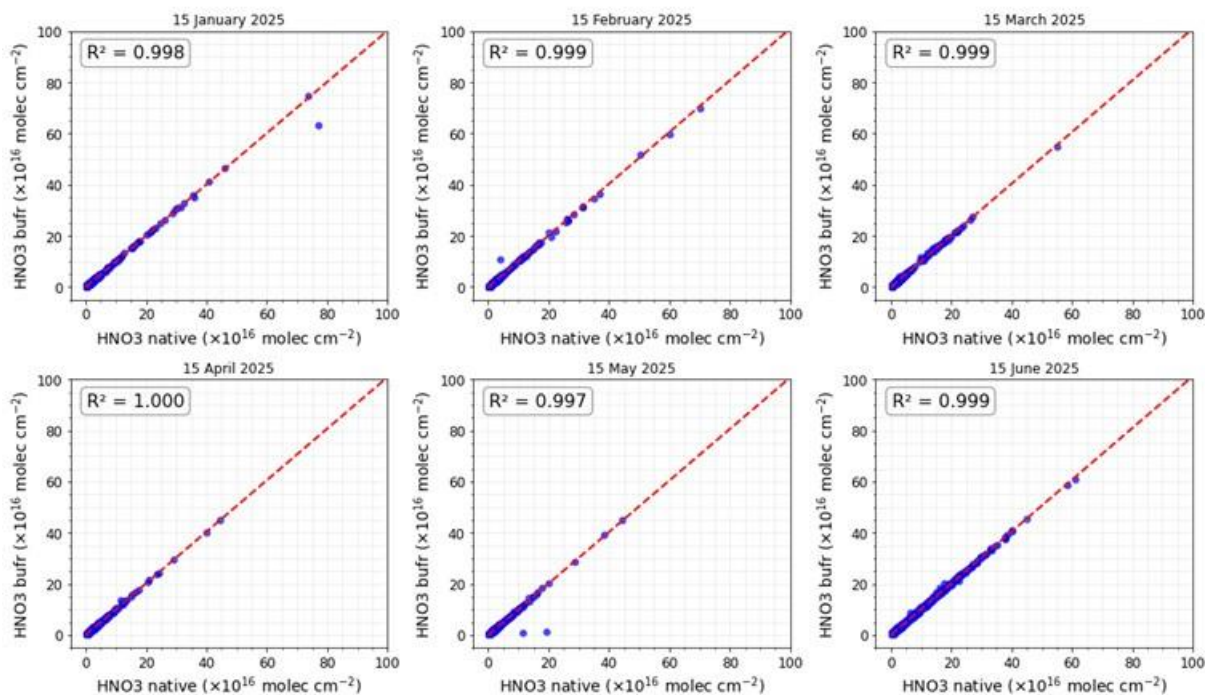


Figure 7.50. Same as Figure 7.49, but for IASI/Metop-C.

Validation with CO FTIR ground-based data

This section presents a comparison between the Metop-B/C IASI CO data and FTIR measurement data available from the NDACC (Network for the Detection of Atmospheric Composition Change) network. The Copernicus Atmosphere Monitoring Service (CAMS) projects supports selected NDACC instruments and PIs for rapid delivery of quality measurements to the NDACC data host ([contract CAMS27](#)). Recent FTIR measurement data is now available for many more sites (in this study data from 25 sites is used).

These ground-based, remote-sensing instruments are sensitive to the CO abundance in the troposphere and lower stratosphere, i.e. between the surface and up to 20 km altitude. CO total columns are validated (from surface to 100 km). A description of the FTIR instruments and retrieval methodology can be found at <https://nors.aeronomie.be>. The typical uncertainty on the FTIR CO column is approximately 3 %, which is also used in the colour scale in Figure 7.52.

In this comparison each FTIR measurement is co-located to all IASI measurements within a time difference of 3 hours and within a distance of 50 km to the effective location of the FTIR measurement (this effective location is calculated along the line of sight of the FTIR measurement). The IASI *a priori* is substituted in the FTIR retrieval and subsequently the FTIR retrieved profile with the IASI *a priori* is smoothed using the IASI averaging kernel, as described in Rodgers *et al.*, 2003. In the plots the relative differences are calculated using the latter FTIR columns (smoothed with the IASI averaging kernels). This validation methodology is described in more detail in Ronsmans *et al.*, 2016.

Table 7.34. Statistics between IASI-B/C and FTIR CO smoothed total columns for the entire time period January 2017 – September 2025 (the column “std” is the standard deviation of the local FTIR columns relative to the standard deviation of the IASI columns)

	Metop-B					Metop-C				
	# meas.	Std.	R	rel. Diff.	Std. Rel. Diff.	# meas.	Std.	R	rel. Diff.	Std. Rel. Diff.
Eureka	928	0.7	0.87	18.2	16.3	33	0.3	0.00	12.3	21.2
Ny Ålesund	233	0.9	0.88	19.5	9.34	178	0.9	0.90	19.0	9.36
Thule	7825	0.8	0.84	5.84	12.0	4917	0.8	0.85	7.28	11.5
Kiruna	1176	1.1	0.82	-2.96	7.37	720	1.1	0.83	-2.61	6.96
Harestua	217	0.7	0.80	4.80	8.87	215	0.8	0.87	3.29	6.62
St. Petersburg	1329	0.8	0.88	8.45	7.42	652	0.8	0.92	9.44	6.55
Bremen	551	0.8	0.85	8.75	7.57	297	0.9	0.82	8.42	7.38
Garmisch	4705	0.8	0.82	3.10	8.51	3108	0.8	0.85	3.53	7.85
Zugspitze	4873	0.9	0.89	-1.02	7.07	3224	0.9	0.91	-1.35	6.22
Jungraujoch	2721	0.9	0.88	-0.72	6.51	2436	0.9	0.90	-1.05	5.42
Toronto	2235	0.7	0.81	23.4	15.0	1716	0.6	0.84	24.0	14.6
Rikubetsu	113	0.9	0.84	4.68	8.22	78	1.0	0.82	2.75	8.31
Boulder	7536	0.9	0.86	-1.55	7.90	6951	0.9	0.86	-1.28	8.58
Xianghe	2680	0.6	0.84	12.0	14.7	2321	0.7	0.84	10.1	12.9
Tsukuba	519	0.8	0.81	7.22	9.94	355	0.9	0.88	5.22	6.99
Hefei	453	0.6	0.72	19.6	14.7	547	0.6	0.79	18.4	13.5
Izana	1137	1.0	0.95	-0.47	4.21	573	0.9	0.96	0.80	4.41
Mauna Loa	1526	1.1	0.99	-0.80	2.81	632	1.1	0.99	-0.71	2.76
Altzomoni	1579	1.1	0.96	4.38	4.30	1027	1.1	0.96	4.17	4.53

Paramaribo	119	0.9	0.92	9.00	4.57	35	0.8	0.83	7.89	5.91
Porto Velho	278	0.9	0.98	9.82	6.64	0	-	-	-	-
La Reunion Mado	4136	1.0	0.99	5.07	3.73	2341	1.0	0.99	5.55	3.56
Wollongong	3026	0.8	0.93	7.61	8.11	2234	0.8	0.94	7.39	8.09
Lauder	4092	0.8	0.93	10.4	7.17	2992	0.9	0.96	10.2	6.51
Arrival Heights	700	0.9	0.93	16.7	8.48	559	0.9	0.93	15.6	8.54
Average for all sites		0.85	0.88	7.64	8.45		0.85	0.85	7.02	8.26

The correlation coefficients of the Taylor diagrams (Figure 7.51 and Table 7.34) are generally ranging from ~0.8 to nearly 1, showing a very good agreement between the IASI and FTIR data, for Metop-B and Metop-C. However, some sites are special:

1. Rikubetsu, Ny Ålesund, Paramaribo and Harestua have only a few co-located measurements and are statistically less relevant
2. Toronto has a lower correlation although the site has many co-locations. This may be due to some co-locations where the IASI concentration is much higher than observed by the FTIR and probably related to false co-locations during fire events. The FTIR time-series seems to suffer from outliers being too low.
3. At Kiruna, Thule and Eureka the satellite underestimates the CO columns by up to 30 % during the early spring weeks and is related to a reduced sensitivity of the IASI CO product during local spring.

The Taylor diagrams in Figure 7.51 and statistics in Table 7.34 also show that the standard deviations of the FTIR columns values are smaller compared the satellite standard deviation probably due to higher noise on the satellite time-series. Almost all site points are shifted left of the satellite reference, typically with a factor of 0.8 to 1 of the standard deviation of the satellite CO columns.

Figure 7.52 shows the time-series of bi-weekly mean relative differences for the time period January 2017 – September 2025. Red indicates a positive bias (IASI > NDACC) while blue indicates an underestimation of the satellite retrievals. The chosen colour scale is based on the FTIR typical uncertainty. The IASI retrieval uncertainty should be added (typically around 4 %), so only biases above 5 % are to be considered significant. In the Northern Hemisphere a seasonal changing bias is observed: overestimation during summer and underestimation during winter months. A similar seasonal dependence but less pronounced is observed in the Southern Hemisphere. A longer time period is required to study this seasonal dependence in more detail.

We can conclude that for most of the 25 stations included in the comparison, mean relative differences, or biases, are less than 10 % (see the individual station plots at <https://cdop.aeronomie.be> under Validation Results). For the Eureka, Ny Ålesund and Arrival Heights stations, located at high latitudes, biases are larger. A similar bias is found by Buchholz *et al.* (2017) when comparing with MOPITT data. When looking at the stations between -60° and 60°, the Toronto station shows the largest biases (mean bias ± 20 %) which seems to be due to outliers.

The IASI data are generally overestimating with the overall bias of approx. 7 % being off the same order as the reported combined total uncertainty of 5 % (Table 7.34).

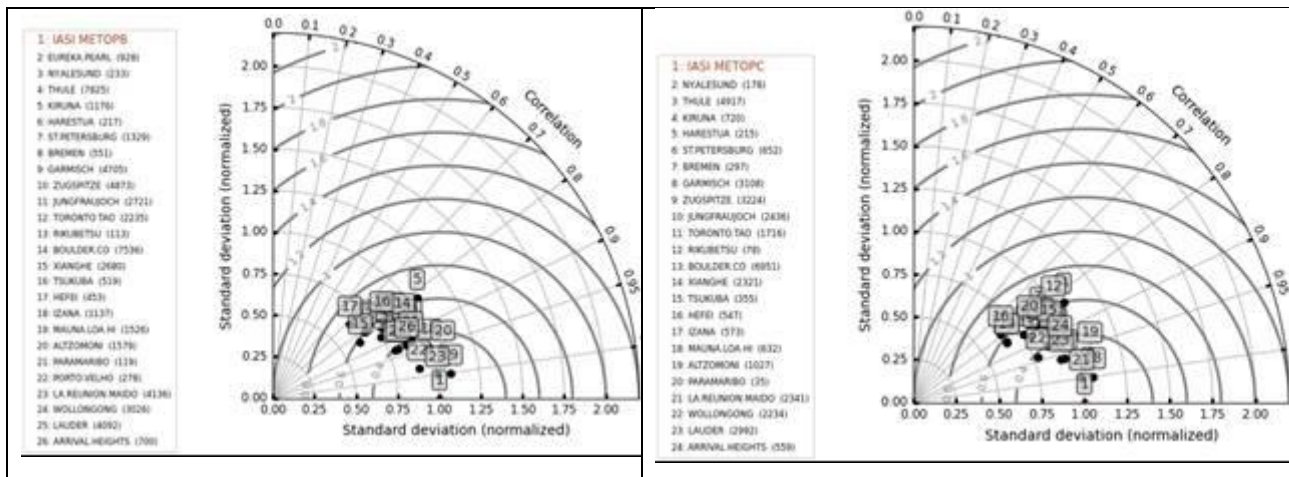


Figure 7.51. Correlation plots for IASI-B (left) and IASI-C (right) CO total columns against 25 NDACC FTIR sites (Eureka is left out due to low measurement count for Metop-C). The stations are slightly shifted to the left, indicating that the satellite time-series has a higher standard deviation (more noisy).

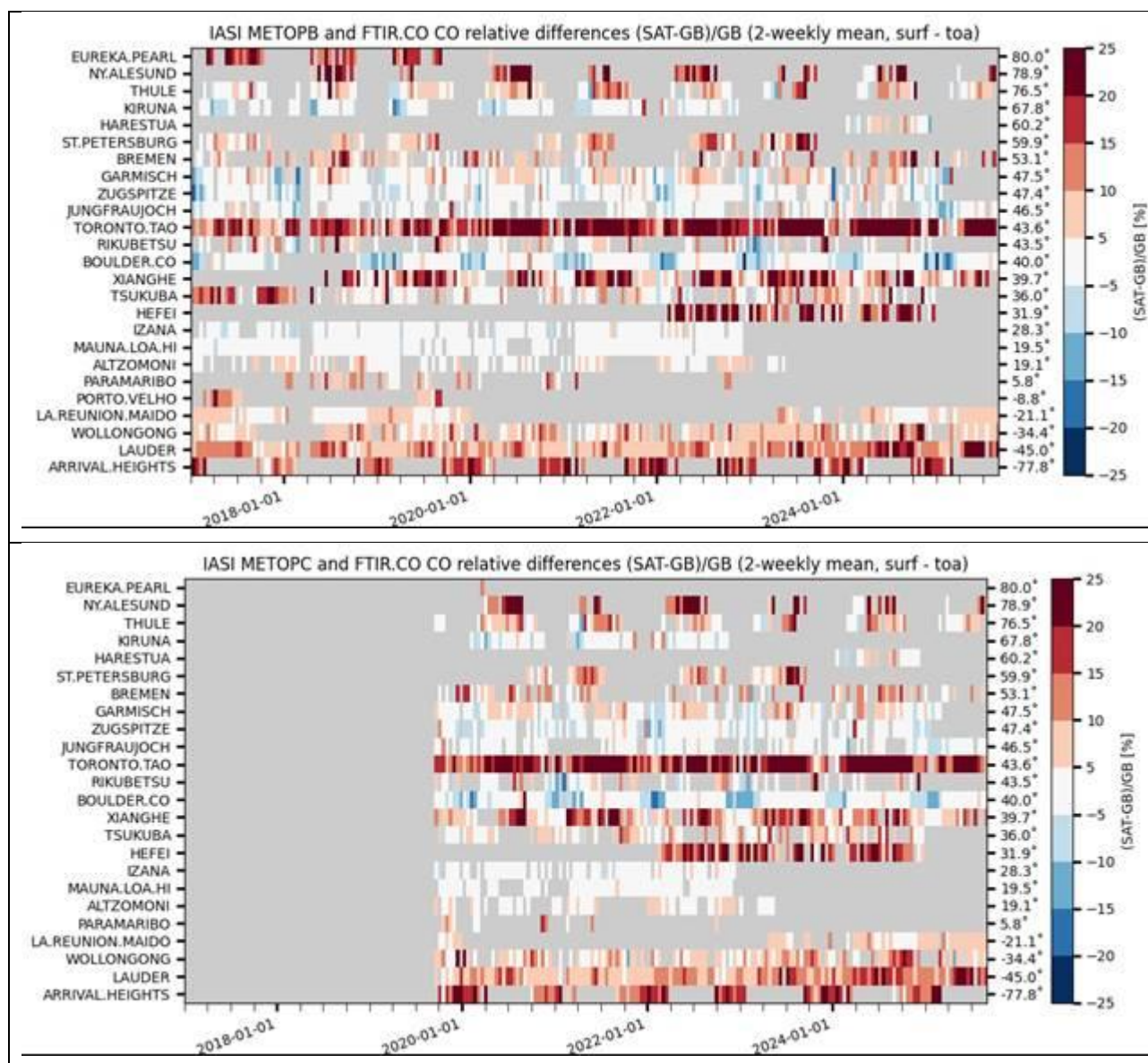


Figure 7.52. Time-series of bi-weekly relative difference for IASI-B (top) and IASI-C (bottom). The Metop-C relative bias time-series seems to correspond closely to the Metop-B time-series.

Acknowledgements: The data used in this publication were obtained as part of the Network for the Detection of Atmospheric Composition Change (NDACC) and are publicly available. Rapid delivery of NDACC data is partly supported by the CAMS-27 data procurement service contracted by ECMWF for the validation of the Copernicus Atmospheric Monitoring Service (CAMS).

References:

Buchholz, R. R., Deeter, M. N., Worden, H. M., Gille, J., Edwards, D. P., Hannigan, J. W., Jones, N. B., Paton-Walsh, C., Griffith, D. W. T., Smale, D., Robinson, J., Strong, K., Conway, S., Sussmann, R., Hase, F., Blumenstock, T., Mahieu, E., and Langerock, B.: Validation of MOPITT carbon monoxide using ground-based Fourier transform infrared spectrometer data from NDACC, *Atmos. Meas. Tech.*, 10, 1927-1956, 2017.

<https://doi.org/10.5194/amt-10-1927-2017>

Rodgers, C. D., and Connor, B. J.: Intercomparison of remote sounding instruments, *J. Geophys. Res.*, 108, 4116-4129, 2003.

<https://doi.org/10.1029/2002JD002299>

Ronsmans, G., Langerock, B., Wespes, C., Hannigan, J. W., Hase, F., Kerzenmacher, T., Mahieu, E., Schneider, M., Smale, D., Hurtmans, D., De Mazière, M., Clerbaux, C., and Coheur, P.-F.: First characterization and validation of FORLI-HNO₃ vertical profiles retrieved from IASI/Metop, *Atmos. Meas. Tech.*, 9, 4783-4801, 2016.

<https://doi.org/10.5194/amt-9-4783-2016>

Validation with HNO₃ FTIR ground-based data

This section presents a comparison between the Metop-B/C IASI HNO₃ data (released Dec 2019) and FTIR measurement data available from the NDACC (Network for the Detection of Atmospheric Composition Change) network.

These ground-based, remote-sensing instruments are sensitive to the HNO₃ abundance in the stratosphere. A description of the FTIR instruments and retrieval methodology can be found at <https://nors.aeronomie.be>. and in <https://www2.acom.ucar.edu/irwg/links> (IRWG retrieval guidelines). The typical uncertainty on the FTIR columns is of the order of 10%, which is also used in the color scale in Figure 7.54. More details on the comparison methodology can be found in the dedicated validation report with reference

[SAF/AC/IASB/VR/HNO3/ValidationReport_HNO3_ORR_MetopB/C](#).

Table 7.35. Statistics between IASI-B/C and FTIR HNO₃ smoothed total columns for the entire time period Dec 2019 – Dec 2024 (the column “std” is the standard deviation of the local FTIR columns relative to the standard deviation of the IASI columns)

	Metop-B					Metop-C				
	# meas.	Std.	R	rel. Diff.	Std. Rel. Diff.	# meas.	Std.	R	rel. Diff.	Std. Rel. Diff.
Eureka	112	1.1	0.9	2.38	11.4	103	1.1	0.91	-1.30	10.3
Ny Ålesund	14	1.2	0.8	-11.1	6.97	14	1.0	0.46	-13.0	11.8
Thule	2259	1.0	0.89	-2.26	9.01	2245	1.1	0.88	-2.86	9.29
Kiruna	1142	1.0	0.95	11.0	8.59	1138	1.0	0.95	10.2	8.30
Harestua	258	0.8	0.95	16.8	7.38	255	0.9	0.95	16.8	6.95
St. Petersburg	830	0.9	0.95	16.2	8.16	825	1.0	0.96	14.3	8.00
Bremen	74	0.9	0.87	23.6	10.4	3905	1.0	0.89	25.2	13.0
Zugspitze	3917	1.0	0.88	26.5	12.9	1428	0.8	0.92	17.2	8.16
Jungraujoch	1415	0.9	0.92	19.3	8.32	2668	0.8	0.89	17.8	12.6
Toronto	2723	0.8	0.89	19.5	12.1	82	0.9	0.92	9.41	9.61
Rikubetsu	78	0.9	0.91	11.6	9.74	463	0.8	0.94	18.3	10.2
Tsukuba	473	0.9	0.93	18.6	10.5	807	0.9	0.85	13.8	11.1
Izana	837	0.9	0.83	16.0	10.8	968	1.0	0.85	17.9	11.1
Mauna Loa	957	1.1	0.84	19.2	11.8	139	0.7	0.71	21.8	12.7
Altzomoni	90	0.5	0.51	29.2	19.3	110	0.6	0.70	20.1	21.0
Maido	31	0.7	0.68	19.2	8.13	28	1.3	0.71	16.0	6.23
Wollongong	551	0.8	0.92	22.6	9.85	542	0.9	0.90	20.7	9.43
Lauder	3012	0.8	0.89	25.4	11.4	2961	0.8	0.88	23.5	11.3
Arrival Heights	851	1.0	0.92	-4.59	13.4	842	1.0	0.92	-5.99	12.6
		0.91	0.86	14.69	10.52		0.92	0.85	12.62	10.72

The correlation coefficients of the Taylor diagrams (Figure 7.53 and Table 7.35) are generally ranging from ~0.8 to nearly 1, showing a very good agreement between the IASI and FTIR data, for Metop-B and Metop-C. However, some sites are special:

1. Ny Ålesund, Toronto and Maido have only a few co-located measurements and are statistically less relevant.
2. Higher biases are observed in the Southern hemisphere (Wollongong and Lauder).
3. High latitude sites have a nearly vanishing bias (compared to the FTIR uncertainties) while mid-latitude sites have a positive bias of the order of 20 %, which confirms the conclusions from the validation report revealing a dependence of the bias on the absolute column values.

The Taylor diagrams in Figure 7.53 and statistics in Table 7.35 also show that the standard deviations of the FTIR columns values are smaller compared the satellite standard deviation probably due to higher noise on the satellite time-series. Almost all site points are shifted left of the satellite reference, typically with a factor of 0.75 to 1 of the standard deviation of the satellite columns.

Figure 7.54 shows the time-series of bi-weekly mean relative differences for the time period Dec 2019 – Dec 2024. Red indicates a positive bias (IASI > NDACC) while blue indicates an underestimation of the satellite retrievals. The chosen color scale is based on the FTIR typical uncertainty.

The statistics reveal an overall bias of approx. 20 % for mid-latitudes and tropical sites (the combined total uncertainty on the bias is of the order of 15 %) and nearly vanishing bias at high latitude sites (Table 7.35). For all of the 19 stations included in the comparison, mean relative differences, or biases, are less than the target threshold of 35 % but larger than the optimal threshold of 10 %.

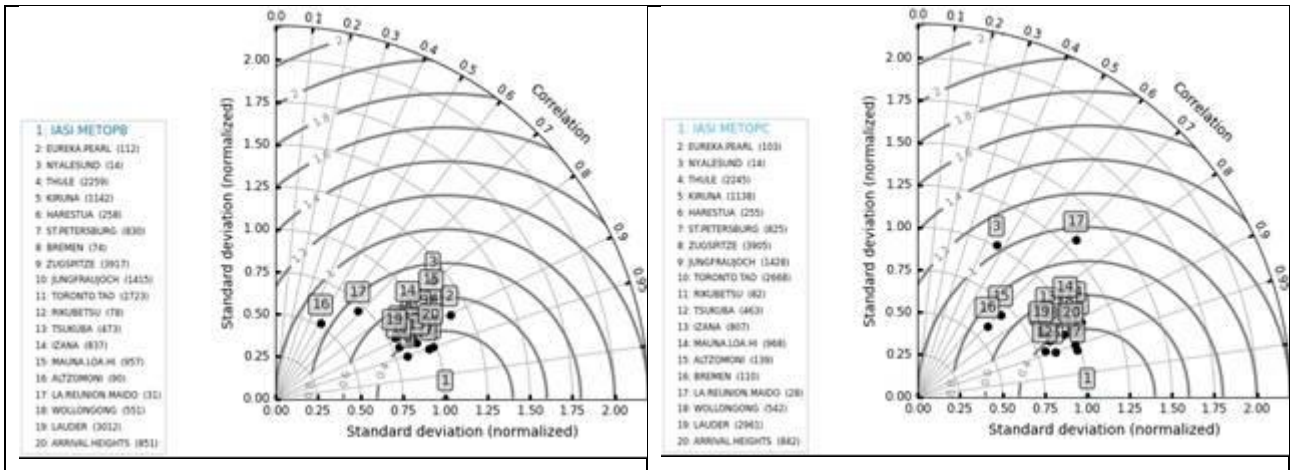
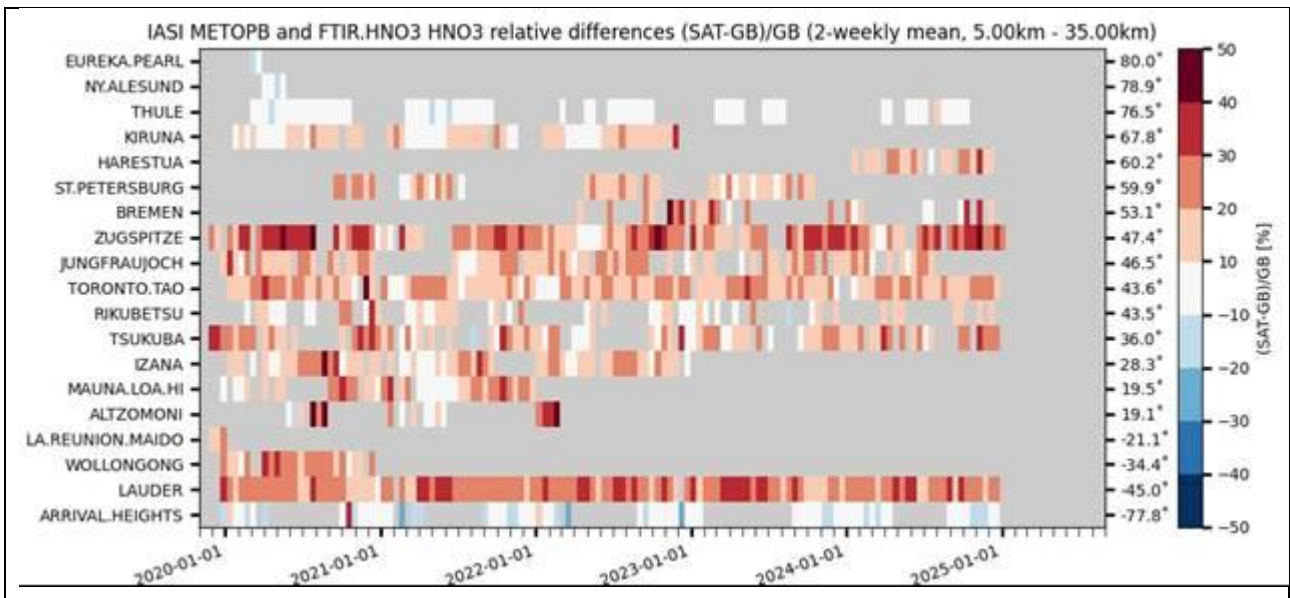


Figure 7.53. Correlation plots for IASI-B (left) and IASI-C (right) HNO₃ total columns against 19 NDACC FTIR sites. The stations are slightly shifted to the left, indicating that the satellite time-series has a higher standard deviation (more noisy).



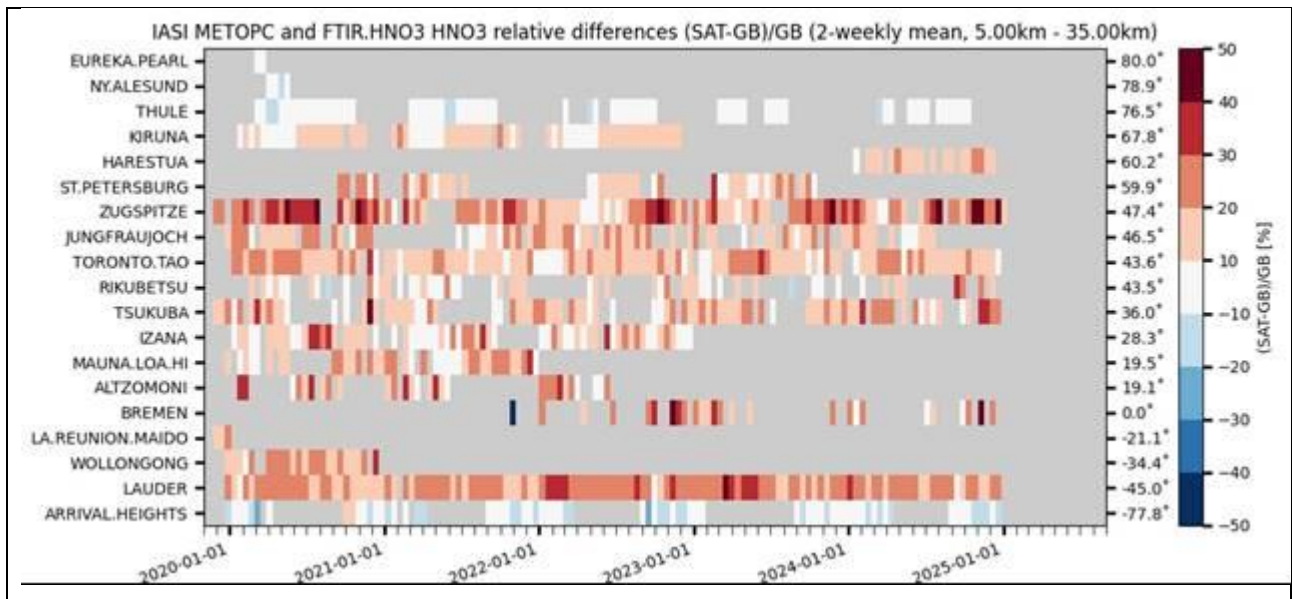


Figure 7.54. Time-series of bi-weekly relative difference for IASI-B (top) and IASI-C (bottom). The Metop-C relative bias time-series seems to correspond closely to the Metop-B time-series.

Acknowledgements: The data used in this publication were obtained as part of the Network for the Detection of Atmospheric Composition Change ([NDACC](#)) and are publicly available.

8. List of AC SAF users

The institutes of registered users of AC SAF products are listed below.

8.1. FMI archive

Europe:

Armenia:

- ICHD

Austria:

- Central Institute for Meteorology and Geodynamics
- Private individual
- Sistema GmbH
- University of Veterinary Medicine
- University of Vienna (2 users)

Belarus:

- National Academy of Sciences
- State University

Belgium:

- BIRA-IASB (2 users)
- Flanders Marine Institute
- Ghent University (16 users)
- Karel de Grote University College
- KMI (4 users)
- KU Leuven
- Novigo+
- Private individual
- ULB (3 users)
- Unknown

Bulgaria:

- Bulgarian Academy of Science
- Space Research and Technology Institute (2 users)

Croatia:

- J. J. Strossmayer University of Osijek

Czech Republic:

- Czech Hydrometeorological Institute (4 users)
- Global Change Research Institute

Denmark:

- Aarhus University (2 users)
- DMI (3 users)
- DTU Compute

Estonia:

- Estonian Environment Agency

- Intertrust

Finland:

- FMI (11 users)
- Häme University of Applied Sciences
- University of Helsinki (3 users)

France:

- AERIS/ICARE
- Aix-Marseille University
- CNRS (3 users)
- Grenoble Alpes University
- Laboratory of Atmospheric Optics
- Lasem
- LATMOS
- LISA (2 users)
- LISA-CNRS
- LSCE-IPSL-CNRS
- Météo France (6 users)
- Mines Paristech
- ONERA
- Open University
- Private Individual (2 users)
- Reuniwatt
- Sistema
- Sorbonne University
- Université Claude Bernard
- University of Reunion (2 users)
- University of Lille
- University of Paris Est Creteil

Germany:

- Brandenburg University of Technology
- DLR (5 users)
- DWD (4 users)
- EUMETSAT (25 users)
- Federal Office for Radiation Protection
- Forschungszentrum Jülich GmbH (5 users)
- Fraunhofer Institute
- Fraunhofer IOSB
- Gymnasium Olching (2 users)
- Oldenburg University
- Potsdam Institute for Climate Impact Research
- Private Individual (2 users)
- Max Planck Institute for Chemistry (5 users)
- Sabrina Szeto Consulting
- Synwer GmbH
- Technical University of Munich

- University of Bremen (6 users)
- University of Cologne
- University of Hildesheim
- University of Konstanz
- University of Münster
- University of Potsdam

Greece:

- AUTH (5 users)
- Eratosthenes Centre of Excellence
- Hellenic Centre for Marine Research
- IESL/FORTH
- National and Kapodistrian University of Athens
- National Technical University of Athens (2 users)
- Private Individual
- Technical University of Crete
- University of Athens (2 users)
- University of the Aegean
- University of Crete (2 users)

Hungary:

- Eötvös Loránd University (2 users)
- Hungarian Academy of Sciences
- Hungarian Meteorological Service (2 users)
- Individual
- University of Szeged

Ireland:

- Trinity College Dublin

Italy:

- ARPA Valle d'Aosta
- B-Open Solutions S.r.l. (2 users)
- CNR (3 users)
- European Space Agency
- fabbricadigitale
- IFAC-CNR (2 users)
- Julia Wagemann Consulting
- LaMMA Consortium (2 users)
- MEEO (3 users)
- National Institute for Astrophysics
- Private Individual (2 users)
- Regional Environmental Protection Agency Calabria
- University of Bologna (2 users)
- University of Milan
- University of Modena and Reggio Emilia
- University of Venice

Latvia:

- Latvian Environment, Geology and Meteorology Centre

Lithuania:

- Lithuanian National Meteorological Service
- Vilnius University

Malta:

- University of Malta

The Netherlands:

- BESSR
- Delft University of Technology
- ESA
- KNMI (6 users)
- Leiden University
- S[&]T Corporation (2 users)
- Wageningen University & Research (2 users)

Norway:

- Norwegian Institute for Air Research (2 users)
- UiT The Arctic University of Norway

Poland:

- CloudFerro
- IMGW
- Institute of Environmental Protection (2 users)
- Institute of Geodesy and Cartography
- Military University of Technology
- O3Lab
- University of Warsaw

Portugal:

- Instituto Dom Luiz
- Instituto Português do Mar e da Atmosfera (4 users)
- University of Aveiro
- University of Lisbon
- University of Trás-os-Montes and Alto Douro (2 users)

Republic of North Macedonia:

- Hydrometeorological Service

Romania:

- Babes-Bolyai University (3 users)
- Global Top Systems
- INCAS
- INOE (2 users)
- National Meteorological Administration (2 users)
- University of Galați (3 users)
- Politehnica University of Bucharest

Russia:

- Altai State University
- Daghestan Scientific Centre of Russian Academy of Sciences
- Federal Research Center Krasnoyarsk Scientific Center of the Siberian Branch of the RAS (2 users)
- Federal State Budget Educational Institution of Higher Education
- Fedorov Institute of Applied Geophysics
- IG RAS
- Institute of Atmospheric Physics
- Institute of Computational Modeling of the Siberian Branch of the RAS
- Institute of Global Climate and Ecology
- Irkutsk State Transport University
- Moscow State University
- Planeta (3 users)
- Research Center of Ecological Safety
- Roscosmos
- St. Petersburg State University
- Tomsk State University of Control Systems and Radioelectronics
- V.E. Zuev Institute of Atmospheric Optics

Serbia:

- Geographical institute “Jovan Cvijic”, SASA

Slovakia:

- Private Individual

Slovenia:

- Bide-san, s.p.

Spain:

- Autonomous University of Barcelona
- Barcelona Supercomputing Center
- Basque Meteorology Agency
- Central University of Catalonia
- Complutense University of Madrid
- CREAM-CSIC-UAB
- GREA
- I.E.S. Punta del Verde
- Modeliza
- NAITEC (2 users)
- Pablo de Olavide University
- Polytechnic University of Catalonia (2 users)
- Private Individual
- San Cernin
- State Meteorological Agency (2 users)
- University of Alicante
- University of Barcelona (3 users)
- University of the Basque Country
- University of Extremadura

- University of Granada (2 users)
- University of Málaga
- University of Oviedo
- University of Valencia (3 users)
- University of Valladolid (2 users)

Sweden:

- Blackebergs Gymnasium
- NBI/Handelsakademin
- SMHI (5 users)

Turkey:

- Cukurova University
- Hacettepe University
- Istanbul University
- Middle East Technical University
- Turkish State Meteorological Service (2 users)
- Van Yüzüncü Yıl University

Ukraine:

- Batata LLC
- Scientific Centre for Aerospace Research of the Earth
- Taras Shevchenko National University of Kyiv
- UHE LED LLC
- UHMC
- Ukrainian Hydrometeorological Institute (3 users)

United Kingdom:

- Aggreko
- Atheras Analytics
- ECMWF (2 users)
- ESA
- IDEMS International
- London School of Economics and Political Science
- Office of National Statistics
- Private individual
- Rutherford Appleton Lab (2 users)
- Satavia Ltd.
- Satellite Applications Catapult
- Science and Technology Facilities Council (2 users)
- siHealth Ltd.
- University College London
- University of Cambridge
- University of Edinburgh
- University of Hertfordshire
- University of Leeds (2 users)
- University of Leicester
- University of Manchester
- University of Oxford

- University of Sheffield
- University of York

Asia:

Afghanistan:

- Vortil Co. Ltd.

Bangladesh:

- Institute of Forestry and Environmental Sciences
- Stamford University
- University of Dhaka

China:

- Anhui Institute of Optics and Fine Mechanics (2 users)
- Anhui Institute of Meteorological Sciences
- Anhui Normal University
- Beijing Municipal Environmental Monitoring Center
- Beijing Normal University (4 users)
- Beijing Zhixin Remote Sensing Geographic Information Co., Ltd
- Chengdu University of Information Technology
- China Academy of Sciences (8 users)
- China Meteorological Administration
- China University of Geosciences
- China University of Mining and Technology (6 users)
- Chinese Academy of Meteorological Sciences (3 users)
- East China University of Science and Technology
- Fudan University
- Guangzhou University
- Hebei University of Engineering (2 users)
- HTHJ
- Institute of Atmospheric Physics (3 users)
- Institute of Desert Meteorology
- Institute of Earthquake Forecasting
- Institute of Remote Sensing and Digital Earth (3 users)
- Jiangsu Meteorological Observatory
- Jiangsu Normal University (2 users)
- Jilin University
- Lanzhou University (2 users)
- Lanzhou Jiaotong University
- Nanjing University (2 users)
- Nanjing University of Information Science & Technology (8 users)
- National Satellite Meteorological Center
- National Space Science Center
- National University of Defense Technology
- Northeast Normal University
- Northwest Normal University
- Peking University (6 users)
- Private Individual

- “School”
- Shanghai University (2 users)
- Shandong University
- Shenzhen University
- Southern University of Science and Technology (4 users)
- State Environmental Protection Key Lab of Satellite Remote Sensing
- Sun Yat-Sen University (2 users)
- The Chinese University of Hong Kong (2 users)
- The Institute of Atmospheric Physics (3 users)
- Tsinghua University (2 users)
- (unknown) (4 users)
- University of Science and Technology (6 users)
- Wuhan University (9 users)
- Xiamen University
- Zhejiang University (3 users)

India:

- Anna University
- ARIES
- Aryabhata Research Institute of Observational Sciences
- Banaras Hindu University
- Birla Institute of Technology
- Bose Institute
- Council of Scientific and Industrial Research
- CSIR-NIO
- CSIR-NPL
- Dibrugarh University
- “Education”
- EY
- IIT KGP
- Indian Institute of Remote Sensing
- Indian Institute of Science
- Indian Institute of Technology Delhi
- Indian Institute of Technology Kharagpur (4 users)
- Indian Institute of Technology Roorkee (2 users)
- Indian Institute of Tropical Meteorology (3 users)
- Indian Space Research Organization (3 users)
- Jawaharlal Nehru Technological University, Kakinada
- Jawaharlal Nehru University
- Malaviya National Institute of Technology Jaipur
- Mangalore University
- Manipal Center for Natural Sciences
- MSRIT
- National Atmospheric Research Laboratory (2 users)
- National Centre for Medium Range Weather Forecasting
- National Institute of Technology
- National Remote Sensing Centre

- Savitribai Phule Pune University (2 users)
- School of Planning and Architecture, Bhopal
- SIG
- Sriram Engineering College
- SRM Institute of Science and Technology
- University of Calcutta
- University of Hyderabad
- University of Kalyani
- Vikram Sarabhai Space Centre (2 users)
- Vindhyan Ecology and Natural History Foundation

Indonesia:

- Bandung Institute of Technology (2 users)
- Meteorological, Climatological, and Geophysical Agency (3 users)
- National Institute for Aeronautics and Space
- Sumatera Institute of Technology

Iran:

- Sepehr Payesh

Japan:

- Chiba University
- Ibaraki University
- Japan Meteorological Agency
- Kyoto University
- Kyushu University
- National Institute for Environmental Studies
- Waseda University

Malaysia:

- Malaysian Meteorological Department
- Malaysian Space Agency
- National University of Malaysia (5 users)
- University of Science Malaysia

Myanmar:

- Yangon Technological University

Nepal:

- International Centre for Integrated Mountain Development (2 users)
- Institute for Advanced Sustainability Studies
- Institute of Tibetan Plateau Research
- Institute of Engineering

Pakistan:

- University of the Punjab
- National University of Sciences & Technology

Philippines:

- Manila Observatory

Singapore:

- National University of Singapore (2 users)

South Korea:

- Chungnam National University (3 users)
- Gwangju Institute of Science and Technology (5 users)
- Hankuk University of Foreign Studies
- Korea Meteorological Administration (2 users)
- Korea Polar Research Institute
- National Institute of Environmental Research (2 users)
- National Meteorological Satellite Center (4 users)
- Pukyong National University
- Yonsei University (3 users)
- Kongju National University
- Seoul National University

Sri Lanka:

- Central Environmental Authority
- Private Individual

Taiwan:

- Academia Sinica
- Garmin
- National Central University (3 users)
- National Taipei University
- National Taiwan University
- Research Center for Environmental Changes

Thailand:

- Asian Institute of Technology
- King Mongkut's Institute of Technology Ladkrabang

Vietnam:

- University of Science (2 users)

Middle East:

Iran:

- Atmospheric Science & Meteorological Research Center
- Islamic Azad University
- Tabriz Islamic Art University
- Tabriz University
- "University"
- University of Tehran
- Unknown

Iraq:

- Al Iraqia University
- Mustansiriyah University

Israel:

- Israel Institute for Biological Research

- University of Tel Aviv (2 users)

Oman:

- Sultan Qaboos University

Saudi Arabia:

- King Abdullah University of Science and Technology (2 users)
- Private individual

United Arab Emirates:

- Amity University
- Khalifa University
- Uruk Engineering & Contracting

North America:

Canada:

- Canadian Space Agency
- Dalhousie University
- Environment and Climate Change Canada
- Environment Canada
- University of Saskatchewan

United States of America:

- Caltech
- Colorado State University (2 users)
- Department of Defence
- EMDO Lab
- Florida State University
- Harvard-Smithsonian Center for Astrophysics
- Intertek
- Joint Center for Satellite Data Assimilation
- Michigan Technological University (5 users)
- Mote Marine Laboratory
- NASA (3 users)
- Naval Research Laboratory
- NOAA
- Northeastern University
- Northern Arizona University
- Princeton University
- Private Individual
- SpaceKnow Inc.
- Texas A&M University
- The Aerospace Corporation
- Trinity Consultants Inc.
- University of Alabama in Huntsville
- University of Alaska (2 users)
- University of Arizona
- University of California (4 users)
- University of Central Florida

- University of Colorado Boulder
- University of Kansas
- University of Maryland (2 users)
- University of North Carolina at Chapel Hill
- University of Tennessee
- University of Washington (2 users)
- Unknown
- USGS
- U.S. Environmental Protection Agency

South America:

Argentina:

- National Space Activities Commission
- Universidad Nacional de Córdoba
- Universidad Nacional de Rosario

Brazil:

- Agência Pernambucana de Águas e Clima
- APAC
- Federal University of Pernambuco (2 users)
- Federal University of Viçosa
- LAPIS
- Universidade Federal de Alagoas

Chile:

- MAP Agro Asesorías
- National Forest Corporation
- University of the Americas

Colombia:

- International Center for Tropical Agriculture
- Universidad EAFIT

Ecuador:

- Universidad San Francisco de Quito (2 users)

Guatemala:

- ASEFOR
- INSIVUMEH

Mexico:

- Ibero Puebla
- Instituto Politecnico Nacional

Paraguay:

- Universidad San Carlos

Peru:

- Servicio Nacional de Meteorología e Hidrología del Perú
- Talsa

Uruguay:

- Universidad de la República

Australia / New Zealand:

- Bureau of Meteorology
- Massey University
- University of Canterbury (3 users)
- University of Melbourne (2 users)
- University of Southern Queensland (2 users)
- University of Sydney

Africa:

Algeria:

- CTS/ASAL
- Meteo Algeria

Cameroon:

- African Institute for Mathematical Sciences

Democratic Republic of the Congo:

- University of Kinshasa

Egypt:

- Egyptian Meteorological Authority (3 users)
- National Research Institute of Astronomy and Geophysics

Eritrea:

- Department of Environment

Ethiopia:

- Addis Ababa University
- Bahir Dar University

Ghana:

- Ghana Meteorological Agency
- Kwame Nkrumah University of Science and Technology
- University of Energy and Natural Resources

Morocco:

- Abdelmalek Essaadi University
- EM5D
- Maroc Météo
- Mohammed VI Polytechnic University
- University of Hassan II Casablanca

Nigeria:

- Abdou Moumouni University
- Federal University Lafia
- Federal University of Technology Akure

South Africa:

- National Chemical Emergency Centre

- North-West University
- South African Weather Service (2 users)
- Stellenbosch University
- University of KwaZulu-Natal
- University of Pretoria (2 users)
- University of the Witwatersrand

Registered users: **757**

8.2. DLR archive

Europe:

Austria:

- University of Veterinary Medicine
- University of Vienna

Belarus:

- National Academy of Sciences

Belgium:

- Antea Group
- BIRA-IASB (6 users)
- Flanders Marine Institute
- Ghent University (12 users)
- KMI (3 users)
- Novigo+
- ULB (4 users)

Bulgaria:

- Space Research and Technology Institute (2 users)

Cyprus:

- The Cyprus Institute

Czech Republic:

- Charles University
- Czech Hydrometeorological Institute (5 users)
- Global Change Research Institute

Denmark:

- Aarhus University (2 users)
- DTU Compute

Estonia:

- Estonian Environment Agency
- Intertrust

Finland:

- FMI (10 users)
- Häme University of Applied Sciences

France:

- AERIS/ICARE
- Aix-Marseille University
- CNRS (3 users)
- Grenoble Alpes University
- Institute of Environmental Geosciences
- Laboratory of Atmospheric Optics
- Lasem
- LATMOS (3 users)
- LISA
- LISA-CNRS
- LSCE-IPSL-CNRS
- Météo France (4 users)
- Mines Paristech
- Open University
- Reuniwatt
- Sistema
- Sorbonne University
- Université Claude Bernard
- University of Reunion (2 users)

Germany:

- Brandenburg University of Technology
- DLR (6 users)
- DWD (2 users)
- EUMETSAT (22 users)
- Forschungszentrum Jülich GmbH (3 users)
- Fraunhofer Institute
- Gymnasium Olching (2 users)
- Heidelberg University
- Karlsruhe Institute of Technology (3 users)
- Max Planck Institute for Chemistry (4 users)
- Potsdam Institute for Climate Impact Research
- Private Individual (2 users)
- Sabrina Szeto Consulting
- Technical University of Munich
- University of Augsburg
- University of Bremen (8 users)
- University of Cologne (2 users)
- University of Hildesheim
- University of Münster

Greece:

- AUTH (4 users)
- Eratosthenes Centre of Excellence
- Hellenic Centre for Marine Research
- IESL/FORTH

- National and Kapodistrian University of Athens
- National Technical University of Athens (2 users)
- Private Individual
- Technical University of Crete
- University of Athens (2 users)
- University of Crete (2 users)

Hungary:

- Hungarian Meteorological Service (3 users)
- Individual
- University of Szeged

Ireland:

- Trinity College Dublin

Italy:

- B-open Solutions S.r.l. (2 users)
- Ca' Foscari University of Venice
- CNR (2 users)
- fabbricadigitale
- IFAC-CNR
- Italian National Research Council
- Julia Wagemann Consulting
- LaMMA Consortium
- MEEO (3 users)
- National Institute of Geophysics and Volcanology
- Private Individual
- Regional Environmental Protection Agency Calabria
- University of Bologna
- University of Modena and Reggio Emilia
- University of Venice

Latvia:

- Latvian Environment, Geology and Meteorology Centre

Lithuania:

- Lithuanian National Meteorological Service

Malta:

- University of Malta

The Netherlands:

- BESSR
- Delft University of Technology
- KNMI (7 users)
- Leiden University
- S[&]T Corporation (2 users)
- Wageningen University & Research (2 users)

Norway:

- Norwegian Institute for Air Research

- UiT The Arctic University of Norway

Poland:

- CloudFerro
- Institute of Environmental Protection (2 users)
- Institute of Geodesy and Cartography
- Institute of Meteorology and Water Management-NRI
- Military University of Technology
- O3Lab
- University of Warsaw

Portugal:

- Instituto Dom Luiz (2 users)
- Instituto Português do Mar e da Atmosfera (3 users)
- University of Trás-os-Montes and Alto Douro

Romania:

- Babes-Bolyai University (3 users)
- Global Top Systems
- INOE (3 users)
- University of Galați (3 users)
- Politehnica University of Bucharest

Russia:

- Altai State University
- Federal State Budget Educational Institution of Higher Education
- Institute of Computational Modeling of the Siberian Branch of the RAS
- Institute of Global Climate and Ecology
- Irkutsk State Transport University
- Planeta

Serbia:

- Geographical institute “Jovan Cvijic”, SASA

Slovakia:

- Private Individual

Slovenia:

- Bide-san, s.p.

Spain:

- Autonomous University of Barcelona
- Barcelona Supercomputing Center
- Complutense University of Madrid
- GREA
- Modeliza
- NAITEC
- Pablo de Olavide University
- Polytechnic University of Catalonia (2 users)
- Private Individual
- San Cernin

- State Meteorological Agency (2 users)
- Universitat Politècnica de València
- University of Alicante
- University of Barcelona (3 users)
- University of Granada (3 users)
- University of Extremadura (2 users)
- University of Oviedo (2 users)
- University of Valencia (3 users)
- University of Valladolid

Sweden:

- SMHI (4 users)
- The Swedish Defence Research Agency (2 users)

Switzerland:

- BGC

Turkey:

- Cukurova University
- Hacettepe University
- Kastamony University
- Middle East Technical University
- Turkish State Meteorological Service (2 users)
- Van Yüzüncü Yıl University

Ukraine:

- Batata LLC
- Scientific Centre for Aerospace Research of the Earth
- UHE LED LLC
- UHMC
- Ukrainian Hydrometeorological Institute (2 users)

United Kingdom:

- Aggreko
- ECMWF (4 users)
- ESA
- IDEMS International
- Hibarcus
- Lancaster University
- London School of Economics and Political Science
- Private individual
- Rutherford Appleton Lab
- Satavia Ltd.
- Satellite Applications Catapult
- Science and Technology Facilities Council (2 users)
- siHealth Ltd.
- University of Cambridge
- University of Hertfordshire
- University of Leeds (2 users)

- University of Leicester (2 users)
- University of Manchester
- University of York (2 users)

Asia:

Bangladesh:

- Institute of Forestry and Environmental Sciences
- University of Dhaka

China:

- Anhui Normal University
- Anhui Institute of Meteorological Sciences University of Dhaka
- Anhui Institute of Optics and Fine Mechanics (3 users)
- Anhui University (3 users)
- Beijing Municipal Environmental Monitoring Center
- Beijing Normal University
- Beijing Zhixin Remote Sensing Geographic Information Co., Ltd
- Chinese Academy of Meteorological Sciences (2 users)
- China Academy of Sciences (8 users)
- China Meteorological Administration
- China University of Mining and Technology (8 users)
- Chinese University of Hong Kong
- East China Normal University
- East China University of Science and Technology
- Fudan University
- Guangzhou University
- Hebei University of Engineering (3 users)
- Hong Kong University of Science and Technology
- HTHJ
- Institute of Atmospheric Physics
- Institute of Geographic Sciences and Natural Resources Research, China Academy of Sciences
- Institute of Remote Sensing and Digital Earth
- Jiangsu Meteorological Observatory
- Jiangsu Normal University (2 users)
- Jinan University
- Lanzhou University
- Nanjing University (4 users)
- Nanjing University of Information Science & Technology (7 users)
- National Satellite Meteorological Center
- National Space Science Center
- Ningbo University
- Northeast Normal University
- Northwest Normal University
- Ocean University of China
- Peking University (5 users)
- PIE
- Piesat Information Technology Co. ,Ltd.

- Private Individual
- “School”
- Shandong University (4 users)
- Shanghai University
- Shenzhen University
- South China Agricultural University
- Southern University of Science and Technology (3 users)
- State Environmental Protection Key Lab of Satellite Remote Sensing
- The Chinese University of Hong Kong (2 users)
- The Institute of Atmospheric Physics (2 users)
- Tsinghua University (3 users)
- University of Science and Technology (8 users)
- (unknown) (5 users)
- Wuhan University (9 users)
- Wuhan University of Technology (2 users)
- Zhejiang Academy of Agricultural Sciences
- Zhejiang University (2 users)

India:

- Anna University
- ARIES
- Aryabhata Research Institute of Observational Sciences
- Banaras Hindu University
- Birla Institute of Technology
- Bose Institute
- Central University of Hyderabad
- Central University of Rajasthan
- CSIR-NIO
- Dibrugarh University (2 users)
- “Education”
- EY
- Heritage Institute of Technology (2 users)
- IIT KGP
- Indian Institute of Remote Sensing
- Indian Institute of Science
- Indian Institute of Technology Delhi
- Indian Institute of Technology Kharagpur (3 users)
- Indian Institute of Technology Roorkee (2 users)
- Indian Institute of Tropical Meteorology (3 users)
- Indian Space Research Organization (3 users)
- Jawaharlal Nehru University
- Malaviya National Institute of Technology Jaipur
- Manipal Center for Natural Sciences
- MSRIT
- National Atmospheric Research Laboratory
- National Centre for Medium Range Weather Forecasting
- National Institute of Technology

- Savitribai Phule Pune University (2 users)
- School of Planning and Architecture, Bhopal
- SIG
- Sriram Engineering College
- SRM Institute of Science and Technology
- University of Calcutta
- University of Hyderabad
- University of Kalyani
- Vikram Sarabhai Space Centre

Indonesia:

- Bandung Institute of Technology
- Meteorological, Climatological, and Geophysical Agency (3 users)
- National Institute for Aeronautics and Space
- Sumatera Institute of Technology

Japan:

- Chiba University
- Fukuoka University
- Ibaraki University
- Japan Meteorological Agency
- Kyushu University (2 users)
- Nagoya University
- National Institute for Environmental Studies
- Remote Sensing Technology Center of Japan
- Waseda University

Malaysia:

- Malaysian Meteorological Department
- Malaysian Space Agency
- National University of Malaysia (4 users)
- University of Science Malaysia

Myanmar:

- Yangon Technological University

Nepal:

- Institute for Advanced Sustainability Studies
- Institute of Engineering
- International Centre for Integrated Mountain Development (2 users)

Pakistan:

- National University of Sciences and Technology
- University of the Punjab

Singapore:

- National University of Singapore (2 users)

South Korea:

- Chungnam National University (3 users)
- Gwangju Institute of Science and Technology (4 users)

- Korea Meteorological Administration
- Korea Polar Research Institute
- National Institute of Environmental Research (2 users)
- National Meteorological Satellite Center (3 users)
- Seoul National University (4 users)
- Ulsan National Institute of Science and Technology
- University of Suwon
- Yonsei University (6 users)

Sri Lanka:

- Central Environmental Authority

Taiwan:

- National Central University (2 users)

Thailand:

- King Mongkut's Institute of Technology Ladkrabang

Vietnam:

- University of Science (2 users)

Middle East:

Iran:

- Khavaran Institute of Higher Education
- Sepehr Payesh
- Tabriz University
- "University"
- University of Tehran (2 users)

Iraq:

- Al Iraqia University
- Mustansiriyah University

Saudi Arabia:

- King Abdulaziz City for Science and Technology
- King Abdullah University of Science and Technology
- Private individual

United Arab Emirates:

- Amity University (2 users)
- Khalifa University
- Uruk Engineering & Contracting

North America:

Canada:

- Environment and Climate Change Canada (5 users)
- Environment Canada
- University of Saskatchewan (2 users)

USA:

- Arizona State University

- Caltech (2 users)
- Colorado State University (3 users)
- Department of Defence
- Florida State University
- Johns Hopkins University
- Harvard University (3 users)
- Intertek
- Joint Center for Satellite Data Assimilation
- Michigan Technological University (3 users)
- NASA (7 users)
- NOAA (4 users)
- Northern Arizona University
- Princeton University
- Private Individual
- Smithsonian Astrophysical Observatory
- SpaceKnow Inc.
- Texas A&M University
- Trinity Consultants Inc.
- University of Alabama in Huntsville
- University of Alaska (2 users)
- University of Arizona
- University of California (5 users)
- University of Central Florida
- University of Colorado Boulder
- University of Houston
- University of Illinois
- University of Maryland (3 users)
- University of North Carolina at Chapel Hill (2 users)
- University of Washington (3 users)
- University of Wisconsin-Madison
- Unknown
- USGS
- U.S. Environmental Protection Agency
- Utah State University
- Woods Hole Oceanographic Institution

South America:

Argentina:

- Argentine Air Force
- National Space Activities Commission
- Universidad Nacional de Rosario

Brazil:

- Agência Pernambucana de Águas e Clima
- APAC
- Federal University of Pernambuco
- LAPIS

- Universidade Federal de Alagoas
- University of São Paulo (2 users)

Chile:

- National Forest Corporation
- University of the Americas

Colombia:

- International Center for Tropical Agriculture
- Universidad EAFIT

Ecuador:

- Universidad San Francisco de Quito

Guatemala:

- INSIVUMEH

Mexico:

- Ibero Puebla
- Instituto Politecnico Nacional

Paraguay:

- Universidad San Carlos

Peru:

- Servicio Nacional de Meteorología e Hidrología del Perú

Uruguay:

- Universidad de la República

Australia / New Zealand:

- Environmental Systems & Services
- University of Canterbury (2 users)
- University of Melbourne (2 users)
- University of Southern Queensland

Africa:

Algeria:

- CTS/ASAL
- Meteo Algeria

Cameroon:

- African Institute for Mathematical Sciences

Democratic Republic of the Congo:

- University of Kinshasa

Egypt:

- Egyptian Meteorological Authority (3 users)
- National Research Institute of Astronomy and Geophysics

Eritrea:

- Department of Environment

Ghana:

- Ghana Meteorological Agency
- Kwame Nkrumah University of Science and Technology

Morocco:

- Abdelmalek Essaadi University
- EM5D
- Maroc Météo
- Mohammed VI Polytechnic University
- National Center for Meteorological Research
- University of Hassan II Casablanca

Nigeria:

- Federal University Lafia
- Federal University of Technology Akure

South Africa:

- North-West University
- South African Weather Service
- Stellenbosch University
- University of Pretoria
- University of the Witwatersrand
- Ware Jacob Enterprises

Registered users: **684**

8.3. DMI (NUV product via FTP)

- Meteorological Institute of Romania
⇒ Several commercial companies obtain the data from MIR
- Danish Meteorological Institute, Denmark
- TrygFonden, Denmark
- Department for Health, Greenland Homerule
- The Danish Cancer Society, Denmark
- Libraries of Hjørring Community
- SunSense AS, Norway
- Richard McKenzie, New Zealand
- Elian Wolfram, Laser Research Center and Applications, Argentina
- KMI, Belgium
- By & Havn I/S, Denmark
- Municipality of Aarhus

Registered users: **12**

8.4. KNMI (unofficial NRT AAI via FTP)

- FMI, Finland
- William B. Hanson Center for Space Science, USA
- University of Leicester, UK

Registered users: 3

8.5. Known international projects that use EUMETCast or WMO/GTS

- MACC project
- SACS service
- Temis WWW service
- ESA GlobVapour
- ESA CCI Ozone project

8.6. EUMETCast

Albania	6	Hungary	13	Poland	14
Algeria	4	Iceland	1	Portugal	7
Angola	1	India	2	Qatar	3
Armenia	1	Iran, Islamic Republic of	35	Reunion	2
Austria	22	Iraq	2	Romania	10
Azerbaijan	3	Ireland	8	Russian Federation	7
Belgium	12	Israel	5	Rwanda	2
Benin	1	Italy	290	San Marino	1
Bosnia and Herzegovina	1	Jordan	1	Saudi Arabia	2
Botswana	4	Kazakhstan	6	Senegal	6
Brazil	4	Kenya	6	Serbia	2
Bulgaria	6	Kuwait	2	Seychelles	1
Burkina Faso	1	Kyrgyzstan	1	Slovakia	7
Cameroon	3	Latvia	1	Slovenia	1
Canada	1	Lebanon	3	South Africa	7
Cape Verde	1	Lesotho	2	South Sudan	1
China	4	Liberia	1	Spain	43
Congo	2	Libya	1	Sudan	1
Congo, Democratic Republic of	1	Lithuania	2	Sweden	5
Croatia	1	Luxembourg	2	Switzerland	15
Cyprus	1	Madagascar	4	Tajikistan	1
Czech Republic	22	Malawi	2	Tanzania, United Republic of	3
Denmark	6	Mali	1	Togo	1
Egypt	3	Malta	2	Tunisia	3
Equatorial Guinea	1	Mauritania	3	Türkiye	7
Estonia	3	Mauritius	2	Turkmenistan	1
Eswatini	2	Moldova, Republic of	1	Uganda	3
Ethiopia	6	Morocco	5	Ukraine	3
Finland	5	Mozambique	2	United Arab Emirates	3
France	64	Namibia	1	United Kingdom	115
Gabon	1	The Netherlands	24	United States	2
Georgia	1	Niger	3	Uzbekistan	1
Germany	112	Nigeria	7	Vietnam	1
Ghana	6	Norway	5	Yemen	1
Greece	20	Oman	1	Zambia	3
Guinea-Bissau	2	Pakistan	2	Zimbabwe	2
Hong Kong	1	Palestine	1		
TOTAL (December 2024)	1074				

9. Updates during the reporting period

Listed below are the major configuration updates concerning operational data processing and archiving. If new versions of relevant AC SAF documents are released during the reporting period, they should be listed here also.

9.1. Software updates

Nothing to report.

9.2. Hardware updates

Nothing to report.

9.3. Documentation updates

28 January	FMI: AC SAF Operations Report 2/2023 rev. 3
28 January	FMI: AC SAF Operations Report 1/2024 rev. 3
7 February	DMI: Algorithm Theoretical Basis Document for Global 1-day UV Index Forecast (issue 1.13)
7 February	DMI: Product User Manual for Global 1-day UV Index Forecast (issue 1.12)
7 February	DMI: AC SAF Validation Report for Global 1-day UV Index Forecast (issue 6.3)
28 February	FMI: AC SAF Service Specification (issue 1.9)
6 June	FMI: AC SAF Operations Report 2/2024 rev. 1

10. Changes in appearance and content of the web portal

Listed below are the major changes in the appearance and content on the [AC SAF main web pages](#).

Table 10.1. Changes in appearance and content of the main AC SAF web pages during the reporting period

Date	Description
5 February	<i>products/iasi_dust_demo.php</i> published, <i>datarecord_access.php</i> updated to include IASI dust optical depth product
14 March	<i>datarecords/ler.php</i> updated due to release of LER v4.1, <i>datarecord_access.php</i> updated with LER v4.1 to replace the previous versions
13 May	<i>products/nuv.php</i> published, replacing <i>nuv_clear.php</i> and <i>nuv_cloud.php</i> . <i>nrt_access.php</i> updated accordingly.
14 May	Link to AC SAF account on Bluesky added to page footer

In addition to updates above, following routine updates are conducted whenever necessary:

- The links to public AC SAF user documents are updated whenever new documents or new versions of existing documents become available
- The “top story” on the front page is updated
- News list on the front page is updated

APPENDIX 1

Table A.1 presents the overall summary of orders from AC SAF archive at FMI, by product type, during the reporting period.

Table A.2 presents a detailed summary of product orders from AC SAF archive at FMI during the reporting period.

Table A.1. Overall summary of product orders, by product type, during the reporting period

Product type	Number of orders	Number of distinct users	Number of files	Total size
O3MARP				
O3MARS				
O3MOHP	23	8	1723	507 GB
O3MOUV subset				
O3MOUV time-series				
LER-MS				
LER-PMD				

Table A.2. More detailed summary of product orders during the reporting period

JANUARY			
Product type	Number of products	Order size	Institute / company
OUV-A OUV-AB OUV-B OUV-BC	Time series for 6423 days Selected subset: ERYDD, DNADD, VITDD, UVADD, UVBDD, ERYDR, DNADR, VITDR, UVADR, UVBDR, UVI Location: 0.37W, 41.93N (2.65 MB in total)		University of Barcelona, Spain
ARP-C	1	6.85 GB	EY, India
OUV-BC	366 Selected subset: UVADD, UVBDD, UVI Region: 18.0E – 29.0E, 53.0N – 61.0N (10.9 MB in total)		Latvian Environment, Geology and Meteorology Centre
OUV-A OUV-AB OUV-B OUV-BC	Time series for 6423 days Selected subset: ERYDD, DNADD, VITDD, UVADD, UVBDD, ERYDR, DNADR, VITDR, UVADR, UVBDR, UVI Location: 35.51W, 33.89N (1.09 MB in total)		University of Barcelona, Spain

OUV-A OUV-AB OUV-B OUV-BC	Time series for 6423 days Selected subset: ERYDD, DNADD, VITDD, UVADD, UVBDD, ERYDR, DNADR, VITDR, UVADR, UVBDR, UVI Location: 36.0W, 34.23N (1.09 MB in total)		University of Barcelona, Spain
OUV-A OUV-AB OUV-B OUV-BC	Time series for 6423 days Selected subset: ERYDD, DNADD, VITDD, UVADD, UVBDD, ERYDR, DNADR, VITDR, UVADR, UVBDR, UVI Location: 35.84W, 33.5N (1.09 MB in total)		University of Barcelona, Spain
OHP-B	1	1.09 MB	V.E. Zuev Institute of Atmospheric Optics, Russia
FEBRUARY			
Product type	Number of products	Order size	Institute / company
ARS-B ARS-C	425 423	871 MB	AUTH, Greece
ARS-B ARS-C	438 438	901 MB	AUTH, Greece
ARS-B ARS-C	439 433	896 MB	AUTH, Greece
ARS-B ARS-C	422 422	869 MB	AUTH, Greece
ARS-B ARS-C	439 439	905 MB	AUTH, Greece
OUV-B OUV-BC	Time series for 2191 days Selected subset: ERYDD, DNADD, UVADD, UVBDD, ERYDR, UVADR, UVBDR, UVI Location: 16.43W, 48.26N (687 kB in total)		University of Vienna, Austria
LER-MS-AB LER-MS-ABC LER-PMD-AB LER-PMD-ABC	1 1 1 1	8.06 GB	University of Vienna, Austria
MARCH			
Product type	Number of products	Order size	Institute / company
OUV-BC	2 Selected subset: VITDR, JO1D, JNO2 Region: global (3.58 MB in total)		EUMETSAT, Germany

OUV-BC	2 Selected subset: UVBDD Region: global (1.33 MB in total)		Tabriz Islamic Art University, Iran
OHP-A	15	5.57 GB	IFAC-CNR, Italy
OHP-A	14	5.21 GB	IFAC-CNR, Italy
OHP-A	14	5.22 GB	IFAC-CNR, Italy
OHP-A	14	5.21 GB	IFAC-CNR, Italy
OHP-A	14	5.23 GB	IFAC-CNR, Italy
OHP-A	14	5.21 GB	IFAC-CNR, Italy
OHP-A	14	5.24 GB	IFAC-CNR, Italy
OHP-A	14	5.25 GB	IFAC-CNR, Italy
OHP-A	15	5.61 GB	IFAC-CNR, Italy
OHP-A	11	4.10 GB	IFAC-CNR, Italy
OUV-A OUV-AB OUV-B OUV-BC	Time series for 2022 days Selected subset: ERYDD Location: 40.70W, 23.14N (390 kB in total)		Central University of Catalonia, Spain
OHP-C	14	3.49 GB	Wuhan University, China
OHP-A	14	5.22 GB	IFAC-CNR, Italy
OHP-A	14	5.02 GB	IFAC-CNR, Italy
OHP-A	15	5.57 GB	IFAC-CNR, Italy
OUV-BC	366 Selected subset: DNADD, PLADD, UVADD, UVBDD, DNADR, PLADR, UVADR, UVBDR Region: 78.0W – 79.0W, 6.0S – 9.0S (16.5 MB in total)		MAP Agro Asesorías, Chile
OUV-BC	366 Selected subset: DNADD, PLADD, UVADD, UVBDD, DNADR, PLADR, UVADR, UVBDR Region: 65.0W – 67.0W, 7.0S – 34.0S (18.5 MB in total)		MAP Agro Asesorías, Chile

OUV-BC	<p>366 Selected subset: DNADD, PLADD, UVADD, UVBDD, DNADR, PLADR, UVADR, UVBDR Region: 67.0W – 81.5W, 5.0S – 32.0S (31.4 MB in total)</p>	MAP Agro Asesorías, Chile
OUV-BC	<p>366 Selected subset: DNADD, PLADD, UVADD, UVBDD, DNADR, PLADR, UVADR, UVBDR Region: 42.0W – 110.0W, 0.0S – 36.0S (103 MB in total)</p>	MAP Agro Asesorías, Chile
OUV-BC	<p>366 Selected subset: DNADD, PLADD, UVADD, UVBDD Region: global (857 MB in total)</p>	MAP Agro Asesorías, Chile
OUV-BC	<p>366 Selected subset: DNADD, PLADD, UVADD, UVBDD Region: 40.0W – 90.0W, 0.0S – 40.0S (46.7 MB in total)</p>	MAP Agro Asesorías, Chile
OUV-BC	<p>366 Selected subset: DNADD, PLADD, UVADD, UVBDD Region: 32.0W – 90.0W, 12.0S – 57.0S (77.1 MB in total)</p>	MAP Agro Asesorías, Chile
OUV-BC	<p>366 Selected subset: DNADD, PLADD, UVADD, UVBDD Region: 50.0W – 90.0W, 1.0S – 37.0S (37.3 MB in total)</p>	MAP Agro Asesorías, Chile
OUV-BC	<p>366 Selected subset: DNADD, PLADD, UVADD, UVBDD Region: 40.0W – 90.0W, 10.0N – 40.0S (55.8 MB in total)</p>	MAP Agro Asesorías, Chile

OUV-BC	366 Selected subset: DNADD, PLADD, UVADD, UVBDD Region: 60.0W – 86.0W, 4.0S – 34.0S (25.8 MB in total)		MAP Agro Asesorías, Chile
OHP-B	439	163 GB	University Of Hertfordshire, UK
OUV-BC	366 Selected subset: DNADD, PLADD, UVADD, UVBDD Region: 46.0W – 85.0W, 2.0S – 54.0S (44.7 MB in total)		Talsa, Peru
OUV-BC	1 Selected subset: DNADD, PLADD, UVADD, UVBDD Region: 46.0W – 85.0W, 2.0S – 54.0S (132 kB in total)		Talsa, Peru
OUV-BC	366 Selected subset: DNADD, PLADD, UVADD, UVBDD Region: 46.0W – 85.0W, 2.0S – 54.0S (44.7 MB in total)		MAP Agro Asesorías, Chile
OUV-BC	366 Selected subset: DNADD, PLADD, UVADD, UVBDD Region: global (857 MB in total)		MAP Agro Asesorías, Chile
OUV-BC	366 Selected subset: DNADD, PLADD, UVADD, UVBDD Region: global (1.76 GB in total)		Talsa, Peru
OUV-BC	366 Selected subset: DNADD, PLADD, UVADD, UVBDD Region: global (857 MB in total)		MAP Agro Asesorías, Chile
OUV-BC	Time series for 366 days Selected subset: DNADD, PLADD, UVADD, UVBDD Location: 78.6W, 8.6S (34.7 kB in total)		MAP Agro Asesorías, Chile

OUV-BC	1 Selected subset: DNADD, PLADD, UVADD, UVBDD Region: global (4.79 MB in total)	Talsa, Peru
OUV-BC	Time series for 366 days Selected subset: DNADD, PLADD, UVADD, UVBDD Location: 71.3W, 32.9S (34.7 kB in total)	MAP Agro Asesorías, Chile
OHP-B	877 220 GB	University Of Hertfordshire, UK
OUV-BC	1 Selected subset: UVI Region: 33.0W – 83.0W, 14.0S – 70.0S (51.8 kB in total)	FMI, Finland
OUV-BC	Time series for 365 days Selected subset: DNADD, PLADD, UVADD, UVBDD, DNADR, PLADR, UVADR, UVBDR Location: 78.7W, 8.6S (116 kB in total)	MAP Agro Asesorías, Chile
OUV-BC	Time series for 364 days Selected subset: DNADD, PLADD, UVADD, UVBDD, DNADR, PLADR, UVADR, UVBDR Location: 78.7W, 8.6S (50.7 kB in total)	MAP Agro Asesorías, Chile
OUV-BC	Time series for 365 days Selected subset: DNADD, PLADD, UVADD, UVBDD, DNADR, PLADR, UVADR, UVBDR Location: 78.7W, 8.6S (50.8 kB in total)	MAP Agro Asesorías, Chile
OUV-BC	Time series for 366 days Selected subset: DNADD, PLADD, UVADD, UVBDD, DNADR, PLADR, UVADR, UVBDR Location: 78.7W, 8.6S (50.9 kB in total)	MAP Agro Asesorías, Chile

OUV-BC	Time series for 365 days Selected subset: DNADD, PLADD, UVADD, UVBDD, DNADR, PLADR, UVADR, UVBDR Location: 78.7W, 8.6S (46.8 kB in total)		MAP Agro Asesorías, Chile
OUV-BC	Time series for 86 days Selected subset: DNADD, PLADD, UVADD, UVBDD, DNADR, PLADR, UVADR, UVBDR Location: 78.7W, 8.6S (12.6 kB in total)		MAP Agro Asesorías, Chile
APRIL			
Product type	Number of products	Order size	Institute / company
OHP-B OHP-C	14 14	7.05 GB	University of Science and Technology, China
OHP-C	10	2.50 GB	Federal State Budget Educational Institution of Higher Education, Russia
OUV-BC	Time series for 1548 days Selected subset: DNADD, PLADD, UVADD, UVBDD, DNADR, PLADR, UVADR, UVBDR Location: 71.3W, 32.9S (213 kB in total)		MAP Agro Asesorías, Chile
ARP-B	439	3.19 GB	AUTH, Greece
ARP-C	439	3.22 GB	AUTH, Greece
ARP-B	439	3.18 GB	AUTH, Greece
ARP-C	439	3.21 GB	AUTH, Greece
OUV-BC	Time series for 824 days Selected subset: ERYDD, DNADD, PLADD, VITDD, UVADD, UVBDD, ERYDR, DNADR, PLADR, VITDR, UVADR, UVBDR, JO1D, JNO2, UVI Location: 78.7W, 8.6S (450 kB in total)		FMI, Finland
ARP-B ARP-C	71 71	1.04 GB	FMI, Finland
ARP-C	17	125 MB	Federal State Budget Educational Institution of Higher Education, Russia

OUV-BC	Time series for 1 day Selected subset: UVI Location: 118.0E, 2.5S (636 B in total)		Bandung of Institute Technology, Indonesia
OUV-BC	1 Selected subset: UVADD, UVBDD, UVI Region: 18.0E – 29.0E, 53.0N – 61.0N (952 kB in total)		Latvian Environment, Geology and Meteorology Centre
MAY			
Product type	Number of products	Order size	Institute / company
OUV-BC	30 Selected subset: UVADD, UVBDD, UVI Region: 18.0E – 29.0E, 53.0N – 61.0N (919 kB in total)		Latvian Environment, Geology and Meteorology Centre
OUV-BC	21 Selected subset: UVADD, UVBDD, UVI Region: global (36.4 MB in total)		Manipal Center for Natural Sciences, India
OUV-BC	1 Selected subset: UVI Region: global (611 kB in total)		University of Science Malaysia
OUV-BC	Time series for 315 days Selected subset: UVI Location: 1.4E, 43.6N (26.5 kB in total)		Météo France
OUV-BC	Time series for 315 days Selected subset: UVI Location: 61.0W, 14.6N (26.5 kB in total)		Météo France
OUV-BC	Time series for 315 days Selected subset: UVI Location: 149.6W, 17.5S (26.5 kB in total)		Météo France
LER-PMD-ABC	1	1.69 GB	University of Science and Technology, China
LER-MS-ABC	1	2.38 GB	University of Science and Technology, China
OUV-A OUV-B OUV-AB OUV-BC	Time series for 4521 days Selected subset: UVI Location: 40.3W, 20.3S (371 kB in total)		Federal University of Viçosa, Brazil

OUV-A OUV-B OUV-AB OUV-BC	Time series for 5479 days Selected subset: ERYDD, DNADD, UVADD, UVBDD, UVI Location: 35.3W, 5.8S (1.17 MB in total)		Federal University of Viçosa, Brazil
ARS-B ARS-C	433 437	903 MB	AUTH, Greece
ARS-B ARS-C	426 424	875 MB	AUTH, Greece
ARS-B ARS-C	438 439	904 MB	AUTH, Greece
ARS-B ARS-C	424 424	878 MB	AUTH, Greece
ARS-B ARS-C	424 425	874 MB	AUTH, Greece
ARS-B ARS-C	439 439	906 MB	AUTH, Greece
ARS-B ARS-C	425 424	880 MB	AUTH, Greece
ARS-B ARS-C	426 424	883 MB	AUTH, Greece
ARS-B ARS-C	397 396	817 MB	AUTH, Greece
ARS-B ARS-C	440 439	905 MB	AUTH, Greece
ARS-B ARS-C	424 424	881 MB	AUTH, Greece
ARS-B ARS-C	438 439	911 MB	AUTH, Greece
OUV-A OUV-B OUV-AB OUV-BC	Time series for 5479 days Selected subset: UVI Location: 35.3W, 5.8S (450 kB in total)		Federal University of Viçosa, Brazil
OUV-A OUV-B OUV-AB OUV-BC	Time series for 5479 days Selected subset: UVI Location: 38.5W, 3.7S (450 kB in total)		Federal University of Viçosa, Brazil
OUV-A OUV-B OUV-AB OUV-BC	Time series for 5479 days Selected subset: UVI Location: 49.3W, 25.4S (450 kB in total)		Federal University of Viçosa, Brazil
OUV-A OUV-B OUV-AB OUV-BC	Time series for 5479 days Selected subset: UVI Location: 44.3W, 2.5S (450 kB in total)		Federal University of Viçosa, Brazil

OUV-A OUV-B OUV-AB OUV-BC	Time series for 5479 days Selected subset: UVI Location: 46.6W, 20.7S (450 kB in total)	Federal University of Viçosa, Brazil
OUV-A OUV-B OUV-AB OUV-BC	Time series for 5479 days Selected subset: UVI Location: 37.3W, 5.2S (450 kB in total)	Federal University of Viçosa, Brazil
OUV-A OUV-B OUV-AB OUV-BC	Time series for 5479 days Selected subset: UVI Location: 51.2W, 23.3S (450 kB in total)	Federal University of Viçosa, Brazil
OUV-A OUV-B OUV-AB OUV-BC	Time series for 5479 days Selected subset: UVI Location: 37.3W, 5.2S (450 kB in total)	Federal University of Viçosa, Brazil
OUV-A OUV-B OUV-AB OUV-BC	Time series for 5843 days Selected subset: UVI Location: 35.3W, 5.8S (480 kB in total)	Federal University of Viçosa, Brazil
OUV-A OUV-B OUV-AB OUV-BC	Time series for 5843 days Selected subset: UVI Location: 38.5W, 3.7S (480 kB in total)	Federal University of Viçosa, Brazil
OUV-A OUV-B OUV-AB OUV-BC	Time series for 5843 days Selected subset: UVI Location: 49.3W, 25.4S (480 kB in total)	Federal University of Viçosa, Brazil
OUV-A OUV-B OUV-AB OUV-BC	Time series for 5843 days Selected subset: UVI Location: 44.3W, 2.5S (480 kB in total)	Federal University of Viçosa, Brazil
OUV-A OUV-B OUV-AB OUV-BC	Time series for 5843 days Selected subset: UVI Location: 37.3W, 5.2S (480 kB in total)	Federal University of Viçosa, Brazil
OUV-A OUV-B OUV-AB OUV-BC	Time series for 5843 days Selected subset: UVI Location: 46.6W, 20.7S (480 kB in total)	Federal University of Viçosa, Brazil
OUV-A OUV-B OUV-AB OUV-BC	Time series for 5843 days Selected subset: UVI Location: 51.2W, 23.3S (480 kB in total)	Federal University of Viçosa, Brazil

<p>OUV-A OUV-B OUV-AB OUV-BC</p>	<p>Time series for 5843 days Selected subset: UVI Location: 37.1W, 6.5S (480 kB in total)</p>	<p>Federal University of Viçosa, Brazil</p>
<p>OUV-A OUV-B OUV-AB OUV-BC</p>	<p>Time series for 5843 days Selected subset: UVI Location: 52.4W, 28.3S (480 kB in total)</p>	<p>Federal University of Viçosa, Brazil</p>
<p>OUV-A OUV-B OUV-AB OUV-BC</p>	<p>Time series for 5843 days Selected subset: UVI Location: 40.8W, 20.0S (480 kB in total)</p>	<p>Federal University of Viçosa, Brazil</p>
<p>OUV-A OUV-B OUV-AB OUV-BC</p>	<p>Time series for 5478 days Selected subset: ERYDD, DNADD, PLADD, VITDD, UVADD, UVBDD, UVI Location: 35.2W, 5.7S (691 kB in total)</p>	<p>Federal University of Viçosa, Brazil</p>
<p>OUV-A OUV-B OUV-AB OUV-BC</p>	<p>Time series for 5478 days Selected subset: ERYDD, DNADD, UVADD, UVBDD, UVI Location: 52.6W, 28.5S (1.17 MB in total)</p>	<p>Federal University of Viçosa, Brazil</p>
<p>OUV-A OUV-B OUV-AB OUV-BC</p>	<p>Time series for 5478 days Selected subset: ERYDD, DNADD, UVADD, UVBDD, UVI Location: 52.6W, 28.5S (1.17 MB in total)</p>	<p>Federal University of Viçosa, Brazil</p>
<p>OUV-A OUV-B OUV-AB OUV-BC</p>	<p>Time series for 5478 days Selected subset: ERYDD, DNADD, UVADD, UVBDD, UVI Location: 52.9W, 28.6S (570 kB in total)</p>	<p>Federal University of Viçosa, Brazil</p>
<p>OUV-A OUV-B OUV-AB OUV-BC</p>	<p>Time series for 6543 days Selected subset: ERYDD, UVADD, UVBDD, ERYDR, UVADR, UVBDR, UVI Location: 48.3E, 16.4N (825 kB in total)</p>	<p>Federal University of Viçosa, Brazil</p>
<p>OUV-A OUV-B OUV-AB OUV-BC</p>	<p>Time series for 5478 days Selected subset: ERYDD, DNADD, UVADD, UVBDD, UVI Location: 52.2W, 28.1S (570 kB in total)</p>	<p>Federal University of Viçosa, Brazil</p>

OUV-A OUV-B OUV-AB OUV-BC	Time series for 5478 days Selected subset: ERYDD, DNADD, UVADD, UVBDD, UVI Location: 54.3W, 27.8S (570 kB in total)		Federal University of Viçosa, Brazil
OUV-A OUV-B OUV-AB OUV-BC	Time series for 5478 days Selected subset: ERYDD, DNADD, UVADD, UVBDD, UVI Location: 52.7W, 28.5S (570 kB in total)		Federal University of Viçosa, Brazil
OUV-A OUV-B OUV-AB OUV-BC	Time series for 5478 days Selected subset: ERYDD, DNADD, UVADD, UVBDD, UVI Location: 51.7W, 27.9S (570 kB in total)		Federal University of Viçosa, Brazil
JUNE			
Product type	Number of products	Order size	Institute / company
OUV-A OUV-B OUV-AB OUV-BC	Time series for 5478 days Selected subset: ERYDD, DNADD, UVADD, UVBDD, UVI Location: 53.6W, 29.6S (570 kB in total)		Federal University of Viçosa, Brazil
OUV-A OUV-B OUV-AB OUV-BC	Time series for 5478 days Selected subset: ERYDD, DNADD, UVADD, UVBDD, UVI Location: 52.5W, 28.6S (570 kB in total)		Federal University of Viçosa, Brazil
OUV-A OUV-B OUV-AB OUV-BC	Time series for 5478 days Selected subset: ERYDD, DNADD, UVADD, UVI Location: 54.2W, 29.5S (510 kB in total)		Federal University of Viçosa, Brazil
OUV-A OUV-B OUV-AB OUV-BC	Time series for 5478 days Selected subset: ERYDD, DNADD, UVADD, UVBDD, UVI Location: 35.2W, 5.8S (570 kB in total)		Federal University of Viçosa, Brazil
ARB-B ARP-C	97 93	1.37 GB	FMI, Finland
OHP-A OHP-C	1 1	624 MB	San Cernin, Spain

<p>OUV-A OUV-B OUV-AB OUV-BC</p>	<p>20 Selected subset: DNADD, PLADD, UVBDD, DNADR, PLADR, UVBDR, JO1D, JNO2 Region: global (90.7 MB in total)</p>		<p>San Cernin, Spain</p>
<p>ARB-B ARP-C</p>	<p>14 12</p>	<p>189 MB</p>	<p>FMI, Finland</p>
<p>ARS-B ARS-C</p>	<p>14 15</p>	<p>30.4 MB</p>	<p>FMI, Finland</p>
<p>ARS-B ARS-C</p>	<p>439 440</p>	<p>914 MB</p>	<p>AUTH, Greece</p>
<p>ARS-B ARS-C</p>	<p>27 25</p>	<p>54.5 MB</p>	<p>AUTH, Greece</p>
<p>OUV-A OUV-B OUV-AB OUV-BC</p>	<p>Time series for 5478 days Selected subset: UVI Location: 53.3W, 27.1S (329 kB in total)</p>		<p>Federal University of Viçosa, Brazil</p>
<p>OUV-A OUV-B OUV-AB OUV-BC</p>	<p>Time series for 5478 days Selected subset: UVI Location: 53.0W, 26.7S (329 kB in total)</p>		<p>Federal University of Viçosa, Brazil</p>
<p>OUV-A OUV-B OUV-AB OUV-BC</p>	<p>Time series for 5478 days Selected subset: UVI Location: 49.4W, 27.4S (329 kB in total)</p>		<p>Federal University of Viçosa, Brazil</p>
<p>OUV-A OUV-B OUV-AB OUV-BC</p>	<p>Time series for 5478 days Selected subset: UVI Location: 53.0W, 26.7S (329 kB in total)</p>		<p>Federal University of Viçosa, Brazil</p>
<p>OUV-A OUV-B OUV-AB OUV-BC</p>	<p>Time series for 5478 days Selected subset: UVI Location: 51.5W, 29.1S (329 kB in total)</p>		<p>Federal University of Viçosa, Brazil</p>
<p>OUV-A OUV-B OUV-AB OUV-BC</p>	<p>Time series for 5478 days Selected subset: UVI Location: 51.7W, 30.3S (329 kB in total)</p>		<p>Federal University of Viçosa, Brazil</p>
<p>OUV-A OUV-B OUV-AB OUV-BC</p>	<p>Time series for 5478 days Selected subset: UVI Location: 51.1W, 28.7S (329 kB in total)</p>		<p>Federal University of Viçosa, Brazil</p>

OUV-A OUV-B OUV-AB OUV-BC	Time series for 5478 days Selected subset: UVI Location: 52.4W, 24.0S (329 kB in total)	Federal University of Viçosa, Brazil
OUV-A OUV-B OUV-AB OUV-BC	Time series for 5478 days Selected subset: UVI Location: 48.9W, 27.2S (329 kB in total)	Federal University of Viçosa, Brazil
OUV-A OUV-B OUV-AB OUV-BC	Time series for 5478 days Selected subset: UVI Location: 25.7W, 52.1S (329 kB in total)	Federal University of Viçosa, Brazil
OUV-A OUV-B OUV-AB OUV-BC	Time series for 5478 days Selected subset: UVI Location: 50.7W, 27.1S (329 kB in total)	Federal University of Viçosa, Brazil
OUV-A OUV-B OUV-AB OUV-BC	Time series for 5478 days Selected subset: UVI Location: 51.2W, 29.1S (329 kB in total)	Federal University of Viçosa, Brazil
OUV-A OUV-B OUV-AB OUV-BC	Time series for 5478 days Selected subset: UVI Location: 35.1W, 7.8S (329 kB in total)	Federal University of Viçosa, Brazil
OUV-A OUV-B OUV-AB OUV-BC	Time series for 5478 days Selected subset: UVI Location: 42.4W, 3.8S (329 kB in total)	Federal University of Viçosa, Brazil
OUV-A OUV-B OUV-AB OUV-BC	Time series for 5478 days Selected subset: UVI Location: 39.2W, 6.3S (329 kB in total)	Federal University of Viçosa, Brazil
OUV-A OUV-B OUV-AB OUV-BC	Time series for 5478 days Selected subset: UVI Location: 38.4W, 6.1S (329 kB in total)	Federal University of Viçosa, Brazil
OUV-A OUV-B OUV-AB OUV-BC	Time series for 5478 days Selected subset: UVI Location: 35.9W, 5.9S (329 kB in total)	Federal University of Viçosa, Brazil
OUV-A OUV-B OUV-AB OUV-BC	Time series for 5478 days Selected subset: UVI Location: 38.3W, 10.7S (329 kB in total)	Federal University of Viçosa, Brazil

OUV-A OUV-B OUV-AB OUV-BC	Time series for 5478 days Selected subset: UVI Location: 39.2W, 12.7S (329 kB in total)	Federal University of Viçosa, Brazil
OUV-A OUV-B OUV-AB OUV-BC	Time series for 5478 days Selected subset: UVI Location: 35.5W, 8.6S (329 kB in total)	Federal University of Viçosa, Brazil
OUV-A OUV-B OUV-AB OUV-BC	Time series for 5478 days Selected subset: UVI Location: 45.4W, 2.6S (329 kB in total)	Federal University of Viçosa, Brazil
OUV-A OUV-B OUV-AB OUV-BC	Time series for 5478 days Selected subset: UVI Location: 41.9W, 4.5S (329 kB in total)	Federal University of Viçosa, Brazil
OUV-A OUV-B OUV-AB OUV-BC	Time series for 5478 days Selected subset: UVI Location: 41.9W, 6.4S (329 kB in total)	Federal University of Viçosa, Brazil
OUV-A OUV-B OUV-AB OUV-BC	Time series for 5478 days Selected subset: UVI Location: 19.8W, 40.8S (329 kB in total)	Federal University of Viçosa, Brazil
OUV-A OUV-B OUV-AB OUV-BC	Time series for 5478 days Selected subset: UVI Location: 20.8W, 42.0S (329 kB in total)	Federal University of Viçosa, Brazil
OUV-A OUV-B OUV-AB OUV-BC	Time series for 5478 days Selected subset: UVI Location: 40.9W, 19.8S (329 kB in total)	Federal University of Viçosa, Brazil
OUV-A OUV-B OUV-AB OUV-BC	Time series for 5478 days Selected subset: UVI Location: 42.0W, 20.8S (329 kB in total)	Federal University of Viçosa, Brazil
OUV-A OUV-B OUV-AB OUV-BC	Time series for 5478 days Selected subset: UVI Location: 40.7W, 15.6S (329 kB in total)	Federal University of Viçosa, Brazil
OUV-A OUV-B OUV-AB OUV-BC	Time series for 5478 days Selected subset: UVI Location: 44.4W, 15.2S (329 kB in total)	Federal University of Viçosa, Brazil

OUV-A OUV-B OUV-AB OUV-BC	Time series for 5478 days Selected subset: UVI Location: 40.4W, 19.2S (329 kB in total)	Federal University of Viçosa, Brazil
OUV-A OUV-B OUV-AB OUV-BC	Time series for 5478 days Selected subset: UVI Location: 41.7W, 20.6S (329 kB in total)	Federal University of Viçosa, Brazil
OUV-A OUV-B OUV-AB OUV-BC	Time series for 5478 days Selected subset: UVI Location: 49.1W, 19.6S (329 kB in total)	Federal University of Viçosa, Brazil
OUV-A OUV-B OUV-AB OUV-BC	Time series for 5478 days Selected subset: UVI Location: 50.1W, 18.8S (329 kB in total)	Federal University of Viçosa, Brazil
OUV-A OUV-B OUV-AB OUV-BC	Time series for 5478 days Selected subset: UVI Location: 42.4W, 21.9S (329 kB in total)	Federal University of Viçosa, Brazil
OUV-A OUV-B OUV-AB OUV-BC	Time series for 5418 days Selected subset: UVI Location: 46.6W, 23.5S (326 kB in total)	Federal University of Viçosa, Brazil
OUV-A OUV-B OUV-AB OUV-BC	Time series for 5478 days Selected subset: UVI Location: 44.1W, 44.0S (329 kB in total)	Federal University of Viçosa, Brazil
OUV-A OUV-B OUV-AB OUV-BC	Time series for 5478 days Selected subset: UVI Location: 40.3W, 17.7S (329 kB in total)	Federal University of Viçosa, Brazil
OUV-A OUV-B OUV-AB OUV-BC	Time series for 5478 days Selected subset: UVI Location: 50.0W, 7.8S (329 kB in total)	Federal University of Viçosa, Brazil
OUV-A OUV-B OUV-AB OUV-BC	Time series for 5478 days Selected subset: UVI Location: 47.7W, 7.7S (329 kB in total)	Federal University of Viçosa, Brazil
OUV-A OUV-B OUV-AB OUV-BC	Time series for 5478 days Selected subset: UVI Location: 48.3W, 10.1S (329 kB in total)	Federal University of Viçosa, Brazil

OUV-A OUV-B OUV-AB OUV-BC	Time series for 5478 days Selected subset: UVI Location: 55.4W, 14.5S (329 kB in total)		Federal University of Viçosa, Brazil
OUV-A OUV-B OUV-AB OUV-BC	Time series for 5478 days Selected subset: UVI Location: 49.3W, 8.3S (329 kB in total)		Federal University of Viçosa, Brazil
OUV-A OUV-B OUV-AB OUV-BC	Time series for 5478 days Selected subset: UVI Location: 48.3W, 5.7S (329 kB in total)		Federal University of Viçosa, Brazil
OUV-A OUV-B OUV-AB OUV-BC	Time series for 5478 days Selected subset: UVI Location: 55.9W, 4.8S (329 kB in total)		Federal University of Viçosa, Brazil
OUV-A OUV-B OUV-AB OUV-BC	Time series for 5478 days Selected subset: UVI Location: 47.9W, 5.5S (329 kB in total)		Federal University of Viçosa, Brazil
OUV-A OUV-B OUV-AB OUV-BC	Time series for 5478 days Selected subset: UVI Location: 58.1W, 3.1S (329 kB in total)		Federal University of Viçosa, Brazil
OUV-A OUV-B OUV-AB OUV-BC	Time series for 5478 days Selected subset: UVI Location: 72.7W, 7.7S (329 kB in total)		Federal University of Viçosa, Brazil
OUV-A OUV-B OUV-AB OUV-BC	Time series for 5478 days Selected subset: UVI Location: 67.7W, 10.5S (329 kB in total)		Federal University of Viçosa, Brazil
OUV-A OUV-B OUV-AB OUV-BC	Time series for 5478 days Selected subset: UVI Location: 51.4W, 20.3S (329 kB in total)		Federal University of Viçosa, Brazil
ARP-B ARP-C	84 80	1.19 GB	FMI, Finland
OUV-BC	31 Selected subset: UVADD, UVBDD, UVI Region: 18.0E – 29.0E, 53.0N – 61.0N (948 kB in total)		Latvian Environment, Geology and Meteorology Centre

OUV-A OUV-B OUV-AB OUV-BC	Time series for 5478 days Selected subset: UVI Location: 55.0W, 19.5S (329 kB in total)		Federal University of Viçosa, Brazil
OUV-A OUV-B OUV-AB OUV-BC	Time series for 5478 days Selected subset: UVI Location: 58.4W, 9.9S (329 kB in total)		Federal University of Viçosa, Brazil
OUV-A OUV-B OUV-AB OUV-BC	Time series for 5478 days Selected subset: UVI Location: 54.2W, 23.1S (329 kB in total)		Federal University of Viçosa, Brazil
OUV-A OUV-B OUV-AB OUV-BC	Time series for 5478 days Selected subset: UVI Location: 52.7W, 10.8S (329 kB in total)		Federal University of Viçosa, Brazil
OUV-A OUV-B OUV-AB OUV-BC	Time series for 5478 days Selected subset: UVI Location: 56.5W, 15.2S (329 kB in total)		Federal University of Viçosa, Brazil
OUV-A OUV-B OUV-AB OUV-BC	Time series for 5478 days Selected subset: UVI Location: 56.4W, 20.2S (329 kB in total)		Federal University of Viçosa, Brazil
OUV-A OUV-B OUV-AB OUV-BC	Time series for 5478 days Selected subset: UVI Location: 54.6W, 20.4S (329 kB in total)		Federal University of Viçosa, Brazil
OUV-A OUV-B OUV-AB OUV-BC	Time series for 5478 days Selected subset: UVI Location: 48.0W, 16.1S (329 kB in total)		Federal University of Viçosa, Brazil
OHP-B	42	21.4 GB	Shandong University, China
OHP-C	43		
OHP-B	43	10.8 GB	Shandong University, China
OHP-C	42	10.5 GB	Shandong University, China
OUV-BC	24 Selected subset: UVADD, UVADR Region: 49.0E – 51.0E, 3.0N – 5.0N (589 kB in total)		Private Individual, Belgium

APPENDIX 2

Table A.3 presents a detailed summary of failed product orders from AC SAF archive at FMI during the reporting period. The middle column indicates whether the failure was related to problems with AC SAF archive and/or ordering system or was the problem on the user's side.

Table A.3. Summary of failed product orders during the reporting period

Date	Error type	Failure description and details
		Order ID: User institute: Order contents: Ordering log error message: Failure description: Corrective action: Final outcome: